ACTA TECHNICA

ACADEMIAE SCIENTIARUM HUNGARICAE

EDITOR: M. MAJOR

VOLUME 96
NUMBERS 1–4

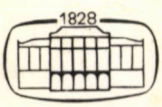

AKADÉMIAI KIADÓ, BUDAPEST 1983

ACTA TECHNICA

A JOURNAL OF THE HUNGARIAN ACADEMY OF SCIENCES

Acta Technica publishes original papers, preliminary reports and reviews in English, which contribute to the advancement of engineering sciences.
Acta Technica is published by

AKADÉMIAI KIADÓ
Publishing House of the Hungarian Academy of Sciences
H-1450 Budapest, Alkotmány u. 21.

Subscription information

Orders should be addressed to

KULTURA Foreign Trading Company
H-1389 Budapest P.O. Box 149

or to its representatives abroad

Acta Technica is indexed in Current Contents

ACTA TECHNICA

VOLUME 96 NOS 1 - 4

BOOK REVIEW

CONTENTS

BOOK REVIEW

ACTA TECHNICA

ACADEMIAE SCIENTIARUM HUNGARICAE

VOLUME 96

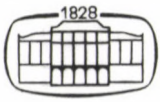

AKADÉMIAI KIADÓ, BUDAPEST 1983

Acta Technica Academiae Scientiarum Hungaricae, 96 (1—4) pp. 3—17 (1983)

A SPECIAL MIXING-TYPE PULVERIZED COAL BURNER

K. REMÉNYI*

[Received 27 September 1983]

For the purpose of starting with coal dust the boilers fired with pulverized coal and for the partly open circuit firings a special pulverized coal mixing burner had been developed in the Villamosenergiaipari Kutató Intézet (Institute for Electrical Power Research). The pulverized coal burner designed by taking into consideration the effects of various factors in the fundamental equations of burning and flow, ensures the separation of the coal dust being ground in the pulverizing mill and dried by the drying inert gases, as well as the efficient mixing before starting the burning with primary air of any proportion and temperature. By means of that burner it can be achieved that the inert gases do not enter into the combustion chamber, the combustion temperature is high, owing to the high temperature the primary air ignition is stable, there is no risk of coal dust explosion, and so the firing scheme is simple.

Notations

ρ — Time-mean density
t — time
v — time-mean velocity
V — vector differential operator
F — body force per unit volume
P — time-mean pressure
T — turbulent stress tensor
h — average enthalpy
J_h; j — turbulent flux vector
m_j — time-mean chemical species' mass fraction
R_j — mass rate of creation per unit volume
R — universal gas constant
M — molecular weight
T — temperature
c_p — specific heat
H_j — combustion heat
E_j — activation energy
μ — turbulent viscosity
d — mean flow rate of deformation tensor
Γ — turbulent exchange coofficient
u — relative combustible content during burning of the coal particle
e_x — instantaneous combustible content
e_0 — ignition combustible content
w_t — tangential velocity in the cyclone
w_r — radial velocity in the cyclone

* K. Reményi, H-1014 Budapest, Uri u. 38, Hungary

Acta Technica Academiae Scientiarum Hungaricae, 96 1983
Akadémiai Kiadó, Budapest

r — radius
m — exponent
d — diameter of limit particle
C — constant

1. Introduction, definition of the task

Because of the heavy rise in oil prices possibilities had to be found in fuel engineering that facilitate the reduction of power oil consumption. In power engineering significant oil consumption is required for starting the boilers and stabilizing the firing. This is a particular problem in countries like Hungary where the power engineering fuels are of very low quality because of the considerable ash and moisture content. Above all in the course of starting cold boilers a large quantity of oil has to be used until the pulverizing, firing system and the boiler plant are warmed up to a temperature where the pulverized coal burners can be put into operation. It is obvious that firing should take place by means of pulverized coal during the entire course of starting or at least as soon as possible. For that purpose a coal dust system independent of the boilers coal preparation system has to be presented. In that case a large quantity of pulverized coal has to be stored. In case of less explosive hard coals this can be solved, but with younger brown coals, lignition problems arise. The dried coal dust is explosive, it can only be transported from the warehouse to the boiler by means of inert materials, e.g. steam, which in turn impairs the conditions of ignition. Taking into consideration the fundamental equations of combustion theory and flowing, a burner design had been realized that creates favourable conditions for the ignition and burning of pulverized coal, furthermore the condition required for operation with power engineering facilities is available. The system can be used in case of central storage—with transport by means of inert gases—and of other external sources of pulverized coal. A plant had been implemented for a lignite fired boiler having an output of 620 t/h. The operative implementation had been preceded by model tests in 1 : 10 scale.

2. Theoretical basis

Then designing the burner the effects of the factors in the fundamental equations of combustion and fluid flow had been analyzed, that may be influenced by means of design and operation. As realization was planned for lignite fired boilers, also the concrete tests and calculations for Hungarian lignites were carried out.

3. Firing considerations

The equations of conservation of mass, pulse, energy and chemical elements served by taking into account the firing considerations. These fundamental equations [1–7] are:

$$\frac{D\rho}{Dt} + \rho(V \cdot v) = 0\,, \tag{1}$$

$$\rho \cdot \frac{Dh}{Dt} = \rho F - Vp + V\tau\,, \tag{2}$$

$$\rho \cdot \frac{Dh}{Dt} = -VJ_h - p(Vv) + Vv : \tau \tag{3}$$

$$\rho \cdot \frac{Dm_j}{Dt} = -VJ_j + R_j \tag{4}$$

It is known from thermodynamics

$$p = \rho \frac{R}{M} T, \tag{5}$$

$$h = c_p T + \Sigma(H_j m_j)\,, \tag{6}$$

$$R_j = -F_j \exp(-E_j/RT) \tag{7}$$

from fluid mechanics

$$\tau = 2\mu d\,, \tag{8}$$

$$J_h = -\Gamma_h V h\,, \tag{9}$$

$$J_j = -\Gamma_j V m_j\,, \tag{10}$$

and for a given chemical component

$$\Sigma m_j = 1\,. \tag{11}$$

Equations (1) and (2) chiefly characterize the flow conditions of the materials departing from the burner. Good mixing conditions may be achieved by means of swirl burners. Therefore, when developing the design we aimed at achieving a turbulent flow.

In equations (3) and (4) the physical-chemical characteristics of the fuel as well as the conditions of burning, play an important role. The physico-chemical circumstances formed after leaving the burner determine ignition and combustion. According to equations (6) and (7) the most significant part is played by the quality, reactivity of the fuel, the temperature and in the combustible mixture the concentration of the fuel and the reacting material. During firing obviously the individual factors are in close interaction. However, the role played will be analyzed for the point of view of designing the heating plant.

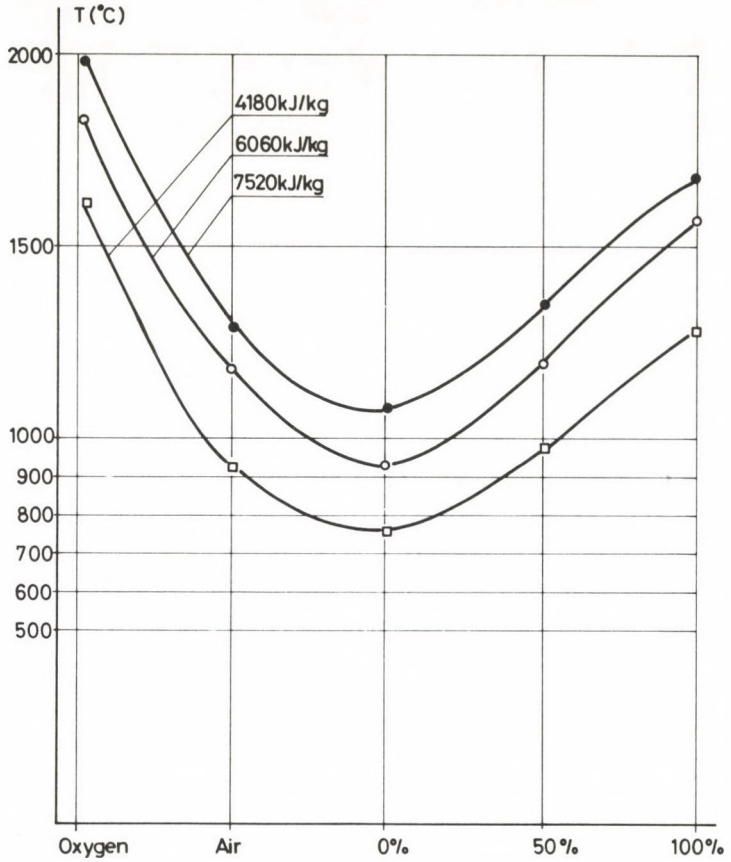

Fig. 1. Change of adiabatic combustion temperature in case of changing combustion environment, for coals with different calorific power (on the horizontal axis the extent of drying gas removal, in per cent)

Burning up of fuels of different qualities, particularly of lignites with high humidity content by means of drying gas, drawn from the combustion chamber after drying and grinding in the mill, takes place by direct injection into the chamber. In that case a significant quantity of inert gas gets into the combustion chamber, reducing oxygen concentration, pulverized coal concentration and combustion temperature. Below an oxygen concentration depending on the fuel no ignition can take place. The effect of injecting the drying gas into the combustion chamber is shown in Fig. 1. The curves of the figure indicate the change in the adiabatic combustion temperature of the lignites having different calorific powers if the raw coal is burned up in oxygen, in ambient air or by removing the drying combustion gas by some method (parameters of the average quality of the given coal are: 6060 KJ/kg, humidity 44%, ash content 25%. Even 50 per cent removal of the drying results as an important rise of the combustion temperature. This is particularly significant for the stability of firing, and also to the

starting period of the boiler when it is needed to bring about pulverized coal firing in a cold combustion chamber, as soon as possible. The essential difference between firing with the theoretical combustion air and the 100 per cent separation of the drying, as is given by the fact, that while with the first one the humidity content of the coal reduces the temperature of combustion, with the second one an important part of the humidity is removed by means of the drying gas. An important parameter in the process of combustion is the concentration of combustible matter. The role of concentration in the course of burning up the pulverized coal—air mixture in a "detonating bomb" is evaluated on the basis of pressure change rates. The detonating bomb is a pirotechnically fired vessel of 70 dm^3 volume. The experimental results for lignites of

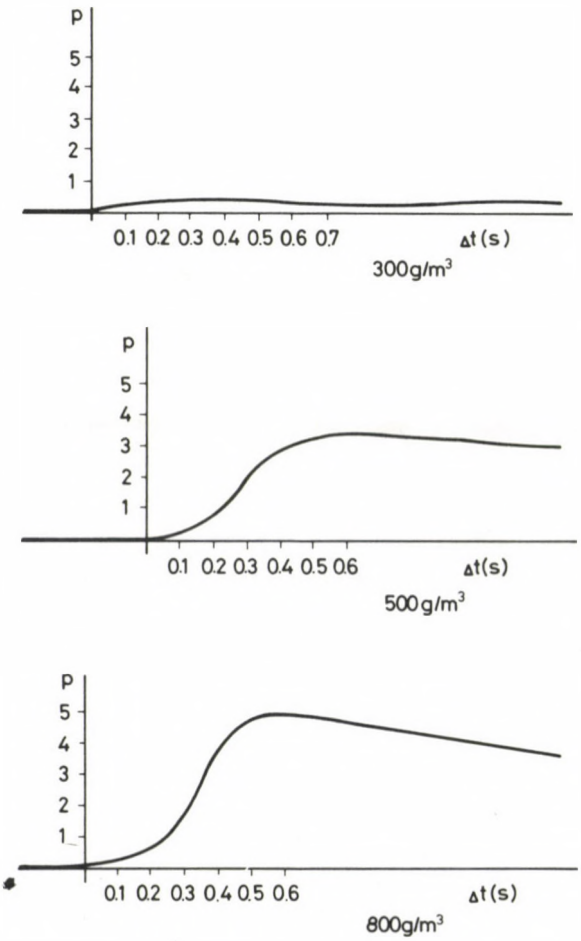

Fig. 2. (a) Explosion pressure change curves for lignite from "Gyöngyös", with different coal dust concentrations.

Gyöngyös and Bükkábrány (mines in Hungary) are indicated in figure series 2 and 3. From Figs 2 and 3 the average pressure change rate ($\Delta P_{max}/\Delta t$) and the maximum pressure change rate $(dP/dt)_{max}$ are shown by Fig. 4. In the examined concentration range it can be established that with low concentrations the pressure change decreases essentially, that is to say, the velocity of combustion, and in the case of lignite from Bükkábrány with 300 g/m^3 concentration at a very low value burning is greatly protracted.

The effect of oxygen concentration was studied in a laboratory-type combustion chamber of 2100 mm length and 57 mm internal diameter, being vertical, and suitable for carrying out reaction kinetical examinations. The section of the combustion chamber is shown in Fig. 5. As an example for measurements carried out in the

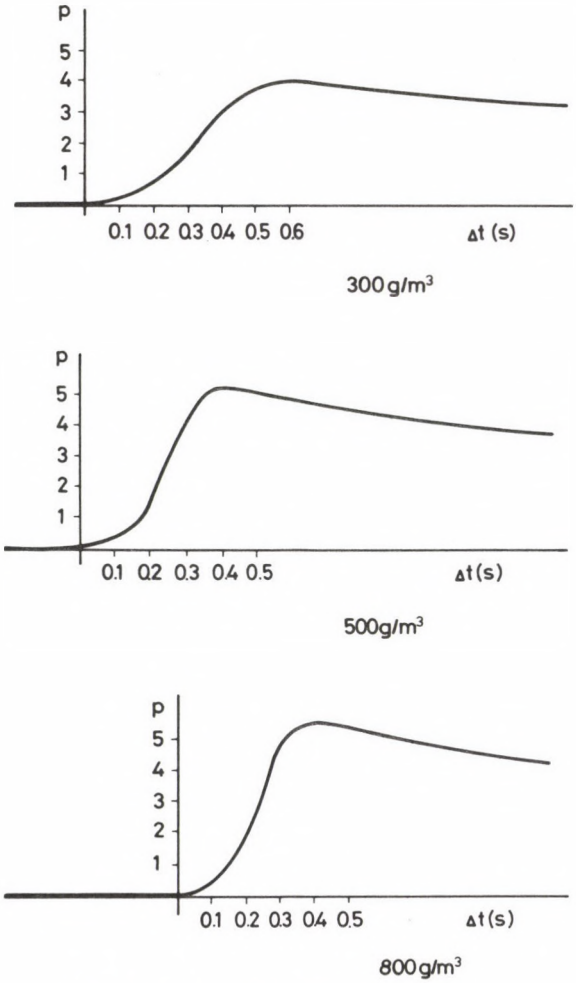

(b) The same for lignite from "Bükkábrány"

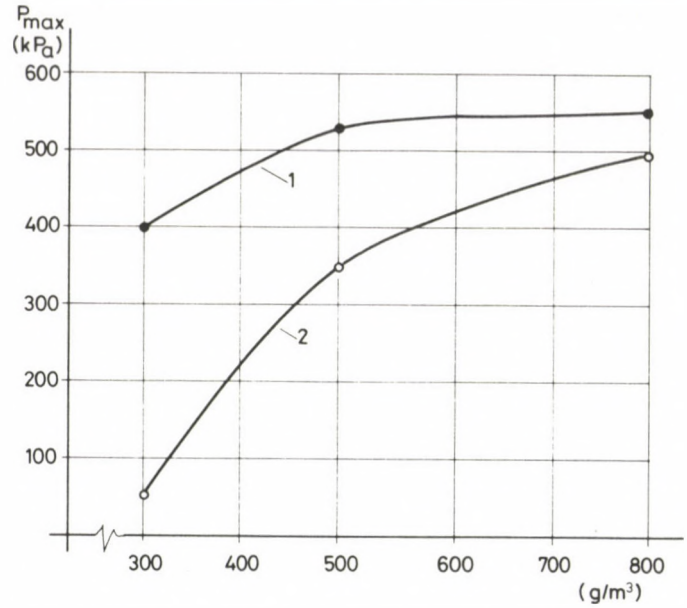

Fig. 3. Maximum explosion pressure values for different coal dust concentrations: 1 — lignite from "Gyöngyös", 2 — lignite from "Bükkábrány"

experimental plant Fig. 6 shows the combustion velocity tests accomplished with the 0.6 ÷ 0.8 mm fraction of the lignite from Gyöngyös. On the horizontal axis of the figure there is the combustion time, on the vertical one the relative combustible content "u", calculated on the basis of the following formula, in the knowledge of the e_x combustible content measured in some instant of the reaction and of the initial e_0 combustible content:

$$u = \frac{e_x}{e_0}.$$

The curves numerically show that with rising oxygen content the velocity of combustion is essentially higher.

In addition to the effect on the velocity of combustion the oxygen concentration influences the ignition temperature of the pulverized coal as well. The ignition temperatures were measured with the method of Goldbert–Greenwald. When carrying out measurements with 21% and 10.5% oxygen concentration it was experienced that with Hungarian lignites that the extent of change in oxygen concentration resulted in 155 ÷ 165 °C change in the temperature of ignition in case of lower oxygen concentrations.

Thus, on the basis of the theoretical fundamental equations of combustion and of the experiments being carried out, the requirements concerning the burner can be defined

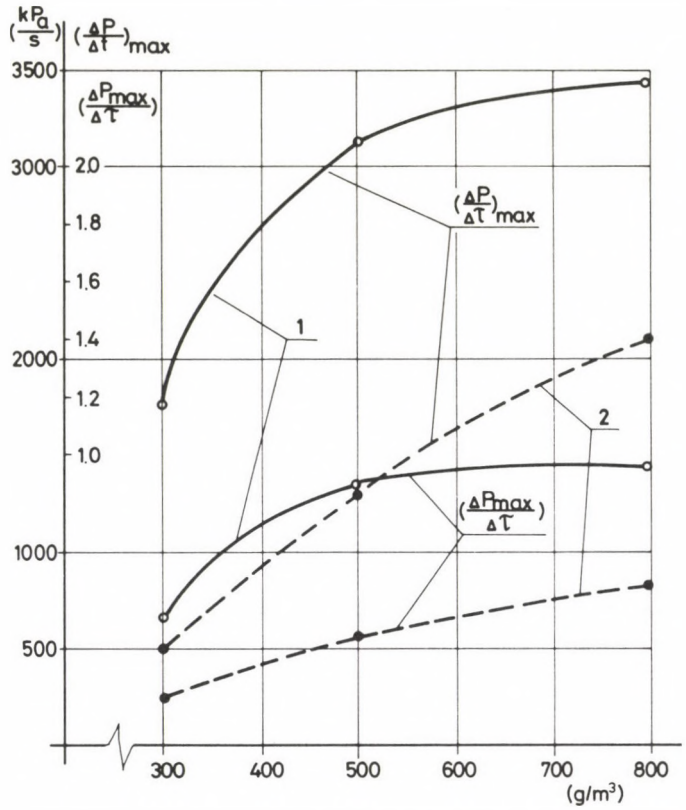

Fig. 4. $(\Delta p_{max}/\Delta t)$ average and $(\Delta p/\Delta t)_{max}$ maximum pressure change values with different coal dust concentrations: 1 lignite from "Gyöngyös", 2 lignite from "Bükkábrány"

— high combustion temperature,
— pulverized coal with humidity content as low as possible,
— small quantity of inert gas in the combustion zone,
— oxygen concentration as high as possible,
— favourable ignition and combustion conditions,
— good mixing conditions,
— adequate pulverized coal concentration,
— safe operation
should be ensured for the burner.

In the case of the usual, open circuit firings with intermediate coal dust storage the task can be solved in principle, however, with younger brown coals the storage and the transport of the coal dust by means of air bears there might be the risk of explosion. But in that case the harmful, coal dust drying inert gas does not go into the firing process. Thus, the burner should be designed so as to separate the drying inert gas and

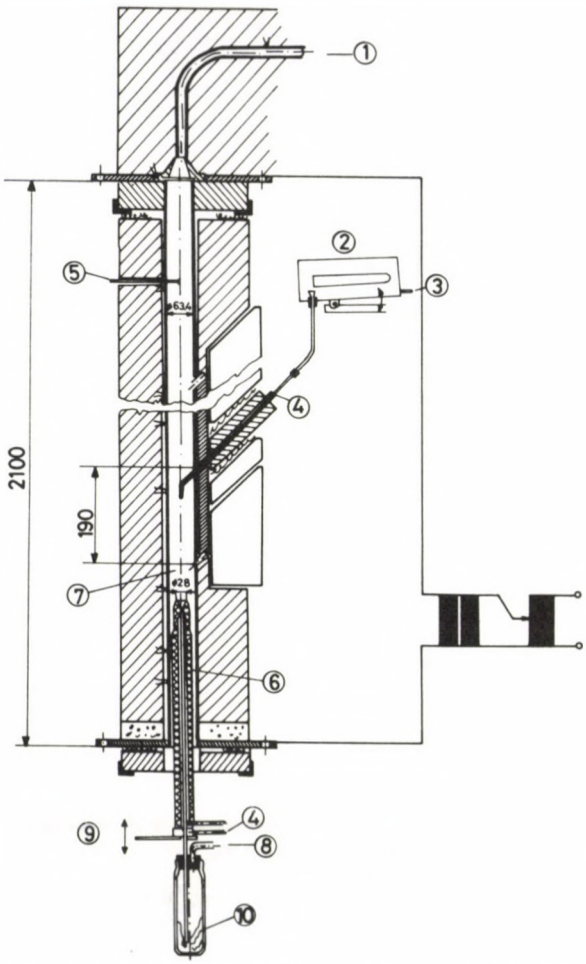

Fig. 5. The section of the equipment serving for reaction kinetical examinations

the vapour, and to ensure possibly favourable mixing before ignition, excluding the risk of explosion. Such a solution can be implemented by means of a specially designed cyclone burner. For the right design of the burner one has to go back to the analysis of flow taking place in the cyclones. In the dust separating cyclone the centrifugal field of force separates the dust from the gas stream; the flow pattern being indicated in Fig. 7. On the turbulent flow the effect of gas on the offtake pipe is superimposed as a vortex sink. For describing the turbulent flow the equation

$$w_t r^m = \text{const}$$

serves, being valid for potential turbulent flow. Fig. 8 shows the change in velocity of the turbulent flow for the theoretical $m = 1$ and for the real value $m < 1$. If on the vortex

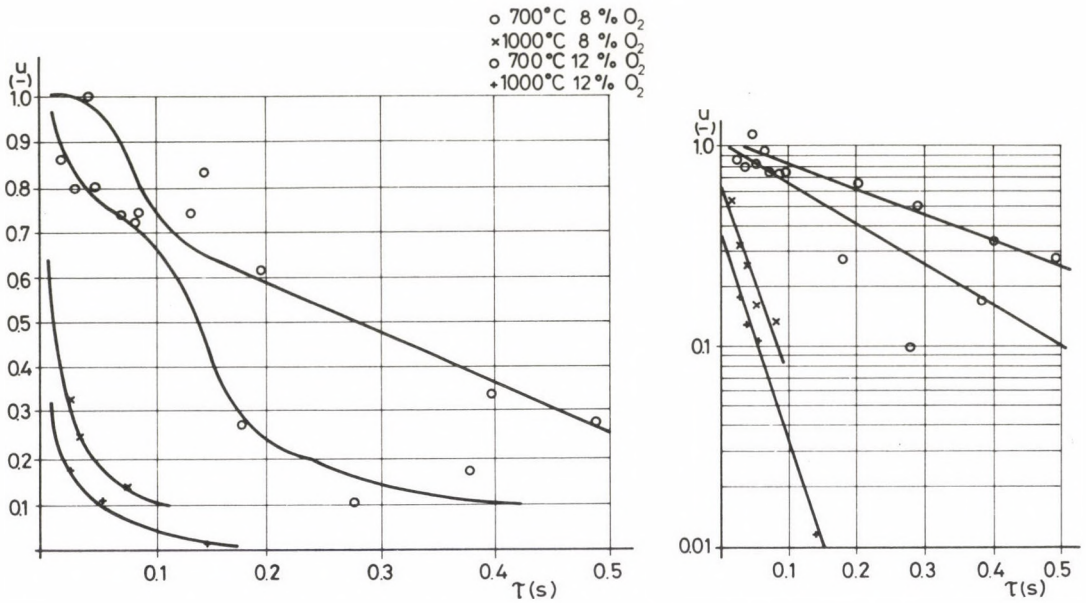

Fig. 6. Changing in the relative combustible content of the lignite from "Gyöngyös" in the course of burn-out time, at different temperatures and oxygen concentrations

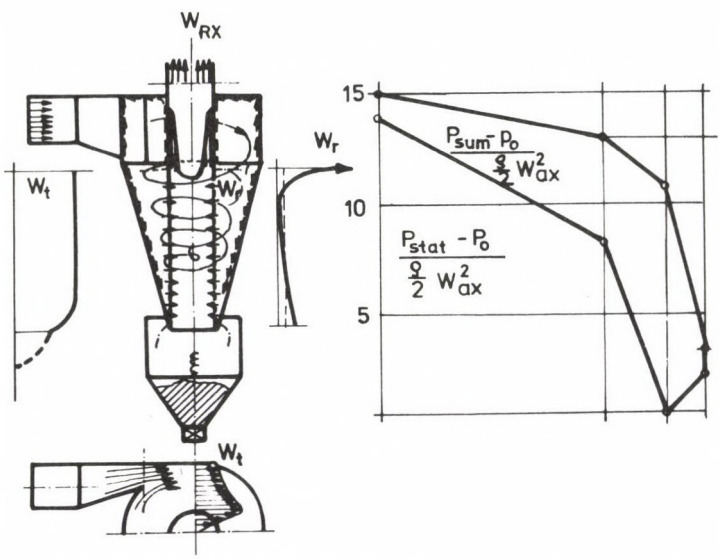

Fig. 7. Section of a dust separating cyclone, showing the characteristic velocity and pressure circumstances [10]

also a sink is superimposed, a radial secondary motion also takes place. The flow pattern of the vortex sink is a logarithmic spiral, i.e.

$$rw_r = \text{const}.$$

As resultant of both motions the dust particle carries out the motion seen in Fig. 9. In such a flow pattern to the radii r, in case of ρ_g, ρ_p, η_p gas, dust material and shape characterises the limit particle that already does not carry out radial motion

$$d = \frac{3}{4} \mathrm{Cr} \frac{\rho_g}{\rho_p} \left(\frac{w_r}{w_t} \right)^2.$$

Thus, by means of the design solution the quantity of the departing dust can be controlled. In this case that coal dust also means a loss if it does not get into the

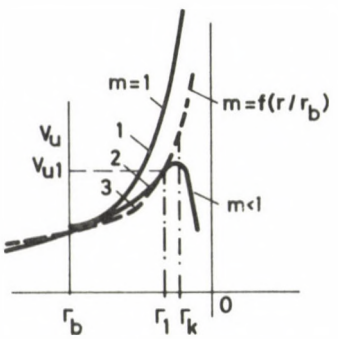

Fig. 8. Velocity variation of the turbulent flow [11]

Fig. 9. Flow lines of the vortex sink, and motion of the coal dust particle in a turbulent flow:
1 vortex line, 2 flow line of the vortex sink

combustion chamber. With the usual dust collecting cyclones the entire gas quantity leaves through the exhaust pipe. If a small quantity of transport gas with the cyclone, used as burner, is led together with the pulverized coal into the combustion chamber, the loss of coal dust can be significantly reduced. If the pulverized coal burner is used for starting up, then coal loss can be reduced too, however, it is not significant as compared with the high oil price.

If the burner is used for partly open circuit firing, then after the pre-separating burner as a secondary current, it can be used for the separation of pulverized coal from a gas stream having such low coal dust concentration that incidentally presents only 5 per cent of the entire quantity burnt up, thus the pulverized coal loss is a low value even with a not very high efficiency of separation. The reduction of the losses in the departing flue gas is essentially higher than the said loss.

For designing the cyclone burner one can depart from the flow pattern of Fig. 7. By removing the dust collecting lock tank the possibility of pulverized coal outflow has been created. Inlet of the combustion air can be achieved by means of the pipe coaxially placed into the cyclone. By examining the flow pattern it can be established that in the axis of the cyclone at the outlet pipe also a secondary current can be created, being in the core opposite to the direction of the outflowing gas. If that flowing current is filled up with the inlet channel of the primary air, also the flow conditions of the cyclone will be improved.

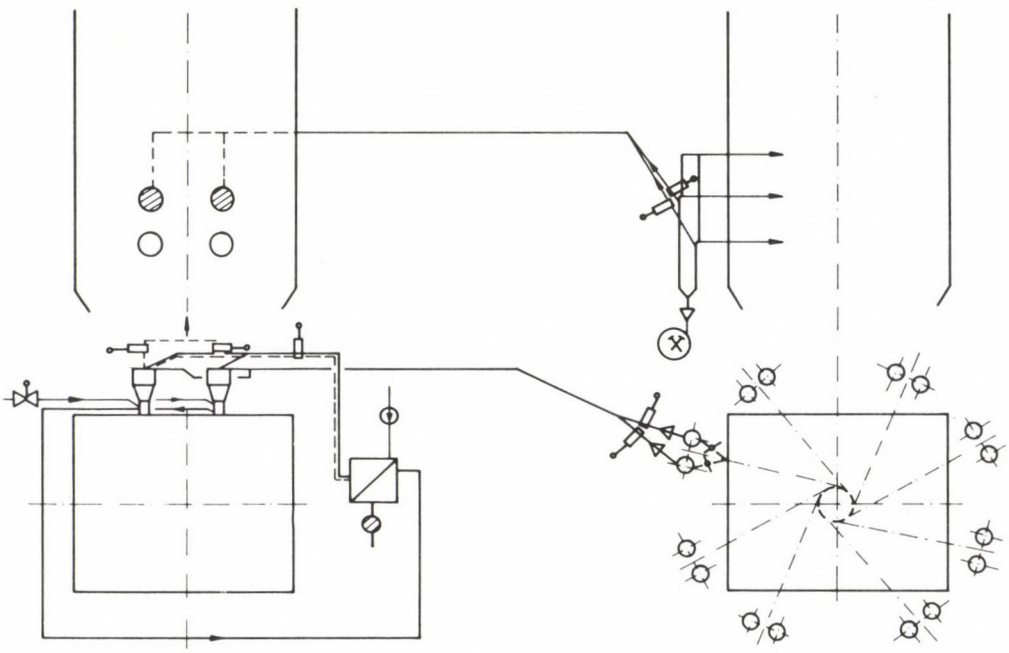

Fig. 10. Scheme of the pulverized coal ignition system

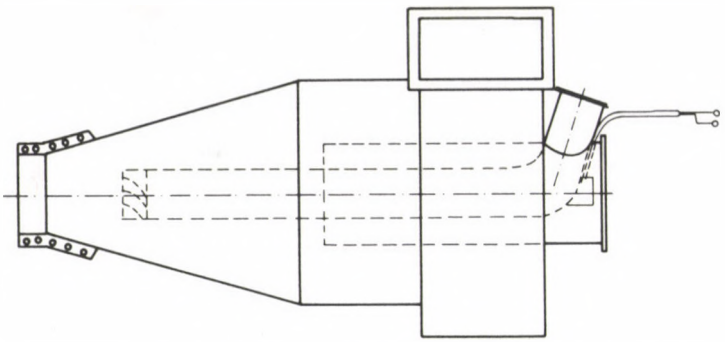

Fig. 11. Mixing-type burner with 30 MW heat output

Based on the previous theoretical combustion and flow considerations a pulverized coal igniting burner has been designed and mounted for starting a lignite fired steam boiler of 62 0 t/h steam output (590 MW heat output). The pulverized coal necessary for ignition was ensured from one of the mills of a boiler operating, beside the boiler to be started, in order to avoid storage. The scheme of the principle for the ignition system is indicated in Fig. 10. Main characteristics of the system are:

— boiler output	590 MW
— quantity of the gas transporting the pulverized coal to the cyclone burners	120000 m^3/h
— dust concentration	177 g/m^3
— calorific power of the pulverized coal	12040 KJ/kg
— final humidity of the pulverized coal	12 per cent
— individual heat output of the two cyclones	30 MW
— at the starter the primary air makes out of the theoretically required combustion air	50 per cent
— temperature of the primary air	150 °C

The section of the cyclone-type burner of 30 MW heat output is shown Fig. 11.

Prior to the operative implementation measurements carried out on a warm model of 1:10 scale in order to get acquainted with the flow, separation and combustion circumstances were obtained. The photo of the experimental burner can be seen in Fig. 12. Based on the experimental results the operative implementation has been carried out. The experiments permitted optimum determination of the most important dimensions (cyclone dimensions, layout of gas outlet pipe and primary air conduit, etc.) decisively influencing the operation of the burner. The most important means for the operative control of the burner is the intensity of exhaustion of the separated transport gas. With it also the extent of separation and the position of the flame can be well set. Thus, the burner ensures that the dried dust coal is separated from the transporting gases, then mixed with the combustion air into a pulverized coal—air mixture suitable for firing.

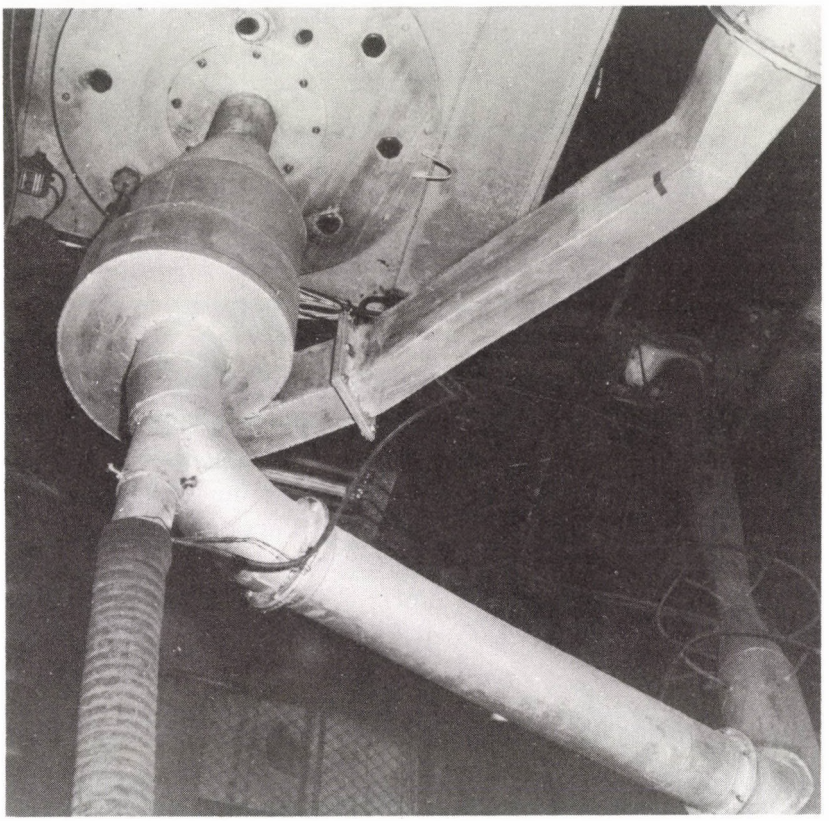

Fig. 12. Photo of the experimental burner

Summarizing: the special burner solution described possesses advantages that cannot be offered by any of the burners made thus far, in particular:

— the inert gases serving for the purpose of drying are separated from the pulverized coal, and do not impair the ignition and combustion circumstances,
— if necessary, the entire combustion air demand and the pulverized coal can be introduced into the combustion chamber this being well mixed,
— the temperature of the combustion air may even achieve the ignition temperature, creating favourable conditions for igniting,
— with the favourable ignition and combustion conditions there is no risk of coal dust explosion,
— the burner permits the creation of a simple firing system.

References

1. Beér, J. M., Chigier, N. A.: Combustion Aerodynamics. Applied Science Publishers Ltd., London 1972
2. Williams, A. F.: Combustion Theory. Addison-Weslex Publishing Company, Reading, Massachusetts, Palo Alto, London
3. Jones, W. P., Whitelaw, J. H.: Calculation methods for reacting turbulent flows. Combustion and Flame 48 (1982)
4. Rajan, S., Strehlow, R. A.: Effects of chemical reactions in the shocked gas on the propagation characteristics of cylindrical detonation waves. Combustion and Flame 49 (1983)
5. Sibulkin, M. Kulkarni, A. K. Annamalai, K.: Burning on a vertical fuel surface with finite chemical reaction rate. Combustion and Flame 44 (1982)
6. Hertzberg, M., Cashdollar, K. L., Lazzara, Ch. P.: The limits of flammability of pulverized coals and other dusts. Eighteenth Symposium (International) on Combustion 1981
7. Hertzberg, M. Cashdollar, K. L., Daniel, L. NG., Conti, R. S.: Domains of flammability and thermal iquitability for pulverized coals and other dusts: particle size dependences and microscopic residue analyses. Nineteenth Symposium (International) on Combustion 1982
8. Reményi, K.: Combustion Stability. Akadémiai Kiadó, Budapest 1980
9. Barth, W.: Berechnung und Auslegung von Zyklonabscheidern. Brennstoff–Wärme–Kraft (1956), Nr. 1.
10. Muschelknantz, E.: Auslegung von Zyklonabscheidern in der Technischen Praxis. Staub (1970), Nr. 5.
11. Koncz, I.: Portalanítás és porleválasztás (Dedusting and Dust Separation). Műszaki Könyvkiadó, Budapest 1982

Acta Technica Academiae Scientiarum Hungaricae, 96 (1—4) pp. 19—57 (1983)

INCREMENTAL VARIATIONAL PRINCIPLES IN CONTACT PROBLEMS

I. PÁCZELT*

[Received 14 May 1983]

The finite element incremental variational principles examined by T. H. H. Pian have been generalized for cases where there is a discontinuity in part of the interface between elements concerning both the displacement and the stress fields. By modifying the arising principles, variational principles have been established for the analysis of frictionless contact problems of unilateral connection, followed by the analysis of the solution process of the contact problem of elasto-plastic solids by the incremental variational principle relying on modified complementary and potential energy.

1. Introduction

As it is known, for the solution of materially and/or geometrically nonlinear boundary problems combined (iterations an loading increasing) linearised methods are generally applied. An essential feature of this solution process is that it is generally incorrect at the beginning of the load increment, satisfying neither the equilibrium equation nor the compatibility conditions.

The building up of various finite element incremental methods on the variational principle has been concerned with by T. H. H. Pian [1]. The principles, however, do not take into consideration discontinuities of an effectively given value in part of element interfaces in the fields of displacements and of stresses. These are the cases e.g. of solids joining with overlapping, as well as of thin-walled plate, shell, diaphragm problems where the stress (internal force) discontinuity is due to a linearly distributed external load. Neither is the case of contact conditions with unilateral connection considered in [1].

To simplify the discussion, the variational principles have been formulated for three-dimensional solids but the obtained results are valid for two- and one-dimensional problems as well.

Assumptions made in establishing variational principles involve:

1. mutual independence of the examined fields element by element, or for some principles, inside the element;
2. *a priori* fulfilment of boundary conditions, field equations and fitting conditions depending on the selected principle;

* I. Páczelt, H-3531 Miskolc, Győri kapu u. 37 III 3, Hungary

Acta Technica Academiae Scientiarum Hungaricae, 96 1983
Akadémiai Kiadó, Budapest

3. symmetry of stress and strain tensors;
4. small displacements and strains due to load increments, hence validity of the linearized theory;
5. negligible dynamic (inertia) effects;
6. the examined system to be in isothermal condition.

A field satisfying the proper field equation FE, boundary condition BC and fitting condition FC is called *fixed* from these aspects, otherwise it is *free*.

For the sake of conciseness, field equations, boundary and fitting conditions other than *a priori* satisfied will be called free equations.

2. Stating the boundary value problem

Let the magnitude at the beginning of the load increment be marked with $(\ )_0$, its icrement with $\Delta(\ )$, and its value specified at the boundary of the given system with $\bar{(\ )}$.

Let us take a structure of N elements (Fig. 1). Element e of volume V^e is bounded by surface S^e. Volume V^e is acted upon throughout by distributed load of density $\mathbf{q}^e$;

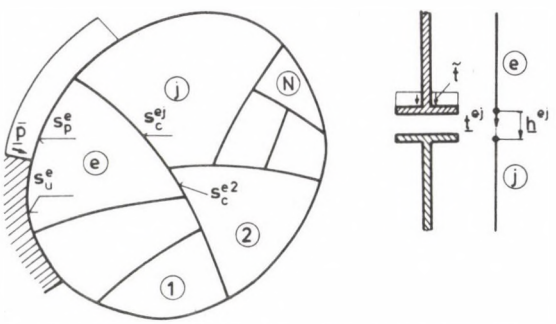

Fig. 1. Elastic structure of N elements. Interpretation of discontinuities $\mathbf{t}$ in the stress field between the elements, and $\mathbf{h}$ in the displacement field

surface S_p^e by surface load of given density $\bar{\mathbf{p}}$; and surface S_u^e is subject to known displacement $\bar{\mathbf{u}}$. In the remaining part S_c^e of surface S^e, element e contacts adjacent elements.

Be $\mathbf{T}$ and $\mathbf{A}$ the stress and the strain tensor resp., $\mathbf{u}$ the field of displacement, $\mathbf{C}$ the fourth-order tensor of material constants, $\mathbf{n}^e$ the outer normal to surface S^e, $\mathbf{h}$ and $\mathbf{t}$ specified discontinuities in the displacement and the stress field, resp. Symbols ". ." and "." signify double and simple scalar multiplication, resp., V is the Hamiltonian differential operator.

Now, for the element surface V^e:

1. the equilibrium equation:

$$V \cdot (\mathbf{T}_0 + \Delta\mathbf{T}) + \mathbf{q}_0 + \Delta\mathbf{q} = \mathbf{0} \tag{2.1}$$

2. the geometry equation:

$$\mathbf{A}_0 + \Delta\mathbf{A} = \frac{1}{2}(V(\mathbf{u}_0 + \Delta\mathbf{u}) + (\mathbf{u}_0 + \Delta\mathbf{u})V) \tag{2.2}$$

3. the material equation between stress and strain increments:

$$\Delta\mathbf{T} = \mathbf{D}\,..\,\Delta\mathbf{A};\ \ \mathbf{A} = \mathbf{C}\,..\,\Delta\mathbf{T};\ \ \mathbf{D} = \mathbf{C}^{-1} \tag{2.3a–c}$$

4. the boundary condition of stress on surface S_p^e:

$$\mathbf{n}\cdot(\mathbf{T}_0 + \Delta\mathbf{T}) = \bar{\mathbf{p}} + \Delta\bar{\mathbf{p}} \tag{2.4}$$

5. the boundary condition of geometry on surface S_u^e:

$$\mathbf{u}_0 + \Delta\mathbf{u} = \bar{\mathbf{u}}_0 + \Delta\bar{\mathbf{u}} \tag{2.5}$$

and at last, the dynamic and kinematic fitting conditions between elements j adjacent to element e. In writing the fitting conditions, parts S_c^{ej} and S_c^{je} of surfaces S_c^e and S_c^j of adjacent elements e and j, resp., are assumed to be about similar in form when unloaded, points on element surfaces S_c^{ej} and S_c^{je} form pairs of points. (The pair of points is composed of a surface point of coordinate x of one solid, and the crossing point of the normal at that point with the other solid.)

Formula for FC will make a distinction between the following cases:

2.1 Bilateral connection

$$\mathbf{n}^e\cdot(\mathbf{T}_0 + \Delta\mathbf{T})^e + \mathbf{n}^j\cdot(\mathbf{T}_0 + \Delta\mathbf{T})^j - (\mathbf{t}_0 + \Delta\mathbf{t})^{ej} = \mathbf{0} \tag{2.6}$$

$$(\mathbf{u}_0 + \Delta\mathbf{u})^j - (\mathbf{u}_0 + \Delta\mathbf{u})^e + (\mathbf{h}_0 + \Delta\mathbf{h})^{ej} = \mathbf{0} \tag{2.7}$$

on surface S_c^{ej}, hence

$$\left.\begin{aligned}\mathbf{n}^e\cdot\mathbf{T}^e + \mathbf{n}^j\cdot\mathbf{T}^j - \mathbf{t}^{ej} &= \mathbf{0} \\ \mathbf{u}^j - \mathbf{u}^e + \mathbf{h}^{ej} &= \mathbf{0}\end{aligned}\right\}\ x\in S_c^{ej}. \qquad \begin{matrix}(2.6)'\\(2.7)'\end{matrix}$$

2.2 Bilateral connection without friction

In this case, for $\mathbf{t}^{ej}\cdot\boldsymbol{\tau} = 0$, the shear stress in the tangential plane of surface S_c has to vanish, that is:

$$\tau^e = \mathbf{n}^e\cdot\mathbf{T}^e\cdot\boldsymbol{\tau}^e = 0;\quad \tau^j = \mathbf{n}^j\cdot\mathbf{T}^j\cdot\boldsymbol{\tau}^j = 0 \tag{2.8}$$

where $\boldsymbol{\tau}$ is the unit vector along the surface, furthermore, taking $\mathbf{n}^e = -\mathbf{n}^j$ into consideration, and defining normal stresses

$$\sigma_N^e = \mathbf{n}^e\cdot\mathbf{T}^e\cdot\mathbf{n}^e;\quad \sigma_N^j = -\mathbf{n}^j\cdot\mathbf{T}^j\cdot\mathbf{n}^e$$

displacements in direction $\mathbf{n}^e$ of matched points on surfaces S_c^{ej} and S_c^{je}, their initial gaps and loads:

$$u_N^e = \mathbf{n}^e \cdot \mathbf{u}^e; \quad u_N^j = \mathbf{n}^e \cdot \mathbf{u}^j; \quad \mathrm{h}^{ej} = \mathbf{n}^e \cdot \mathbf{h}^{ej}; \quad \mathrm{t}_N^{ej} = \mathbf{t}^{ej} \cdot \mathbf{n}^e$$

permits to write fitting conditions:

$$\sigma_N^e - \sigma_N^j = t_N^{ej} \tag{2.9}$$

$$u_N^j - u_N^e + h_N^{ej} = 0\,. \tag{2.10}$$

2.3 Unilateral connection

In a bilateral connection, element e contacts adjacent elements throughout its surface part S_c^e. In unilateral connection, normal component of the contact stress points inside the solid, but it cannot be stated *a priori* to be non-zero at all points of range S_c^e. At points of zero normal stress, the solids are in no interaction, so they are separated from each other.

Assumptions allow contact at any point of range S_c^e, to be called thus potential contact range. Points in surface parts S_c^{ej} and S_c^{je} of adjacent elements e and j being congruent, to simplify notations, these surfaces will be denoted by Ω^{ej}.

After deformation, elements e and j will be spaced in direction $\mathbf{n}^e$ at:

$$y \overset{\text{def}}{=} u_N^j - u_N^e + h^{ej} \quad x \in \Omega^{ej} \tag{2.11}$$

There is a contact for geometry condition

$$y = 0 \quad x \in \Omega_p^{ej} \tag{2.12}$$

and there is a gap for

$$y > 0 \quad x \in \Omega_0^{ej}\,. \tag{2.13}$$

A priori unknown contact and gap ranges Ω_p^{ej} and Ω_0^{ej} satisfy condition $\Omega^{ej} = \Omega_p^{ej} \cup \Omega_0^{ej}$.

Contact stress interpreted on element e is in the gap range:

$$\mathbf{p}(x) = \mathbf{0} \quad x \in \Omega_0^{ej} \tag{2.14}$$

while at contact:

$$\mathbf{p}(x) = -p_N \mathbf{n}^e + \mathbf{p}_\tau \quad x \in \Omega_p^{ej} \tag{2.15}$$

where $p_N \geqq 0$ is the contact pressure, $\mathbf{p}_\tau$ is tangential component of vector $\mathbf{p}$.

For

$$\mathbf{p}_\tau \equiv \mathbf{0} \quad x \in \Omega^{ej} \tag{2.16}$$

the problem is that of frictionless (normal) contact.

3. Analysis of a system of a single element (solid)

In conformity with the assumptions, the state before the load increment is known and the system behaviour is considered to be linear during minor load increments. Thus, in writing incremental variational principles, those of linear elasticity may be started from.

For a structure of a single element, computed on the basis of free, independent fields $\mathbf{T}$ and $\mathbf{u}$, stationarity of the Reissner functional

$$H_R = H_R(\mathbf{T}, \mathbf{u}) = \int_V [\mathbf{T}..\mathbf{A}(\mathbf{u}) - B(\mathbf{T}) - \mathbf{q}\cdot\mathbf{u}]\,\mathrm{d}V - \int_{S_p} \mathbf{p}\cdot\mathbf{u}\,\mathrm{d}S - \int_{S_u} \mathbf{n}\cdot\mathbf{T}\cdot(\mathbf{u}-\bar{\mathbf{u}})\,\mathrm{d}S \tag{3.1}$$

is known to be a necessary and sufficient condition of the establishment and truth of the corresponding free equations (2.1) through (2.5).

Here $B = \frac{1}{2}\mathbf{T}..\mathbf{C}..\mathbf{T}$ is the specific complementary strain energy, that is:

$$\mathbf{A} = \frac{\partial B}{\partial \mathbf{T}}.$$

Substituting linearized relationships $\mathbf{T} = \mathbf{T}_0 + \Delta\mathbf{T}$, $\mathbf{u} = \mathbf{u}_0 + \Delta\mathbf{u}$ into (3.1), and omitting invariable, subsequently useless magnitudes, we arrive at the functional

$$\begin{aligned} H_R &= H_R(\Delta\mathbf{T}, \Delta\mathbf{u}) \\ &= \int_V [(\mathbf{T}_0 + \Delta\mathbf{T})..\tfrac{1}{2}(V(\Delta\mathbf{u}) + (\Delta\mathbf{u})V) \\ &+ \Delta\mathbf{T}..(\mathbf{A}_0(\mathbf{u}_0) - \mathbf{A}_0(\mathbf{T}_0)) \\ &- \frac{1}{2}\Delta\mathbf{T}..\mathbf{C}..\Delta\mathbf{T} - (\mathbf{q}_0 + \Delta\mathbf{q})\cdot\Delta\mathbf{u}]\,\mathrm{d}V \\ &- \int_{S_p} (\bar{\mathbf{p}}_0 + \Delta\bar{\mathbf{p}})\cdot\Delta\mathbf{u}\,\mathrm{d}S \\ &- \int_{S_u} [\mathbf{n}\cdot\Delta\mathbf{T}\cdot(\mathbf{u}_0 + \Delta\mathbf{u} - (\bar{\mathbf{u}}_0 + \Delta\bar{\mathbf{u}})) + \mathbf{n}\cdot\mathbf{T}_0\cdot\Delta\mathbf{u}]\,\mathrm{d}S, \end{aligned} \tag{3.2}$$

where

$\mathbf{A}_0(\mathbf{T}_0)$ is the initial strain tensor field,

$$B = \Delta\mathbf{T}..\mathbf{A}_0(\mathbf{T}_0) + \frac{1}{2}\Delta\mathbf{T}..\mathbf{C}..\Delta\mathbf{T}$$

the specific complementary strain energy increment, interpreted according to

$$\mathbf{A} = \partial B/\partial\Delta\mathbf{T} = \mathbf{A}_0(\mathbf{T}_0) + \mathbf{C}..\Delta\mathbf{T}$$

$$\mathbf{A}_0(\mathbf{u}_0) \overset{\text{def}}{=} \frac{1}{2}(V\mathbf{u}_0 + \mathbf{u}_0 V).$$

Transforming the first integral in the obtained functional and the integral $\int_V \Delta\mathbf{T}..\mathbf{A}_0(\mathbf{u}_0)\mathrm{d}V$ according to the Gauss-Ostrogradsky theorem, we can write Π_R in another form:

$$\Pi_R^C = \Pi_R^C(\Delta\mathbf{T}, \Delta\mathbf{u})$$

$$= \int_V \{-\frac{1}{2}\Delta\mathbf{T}..\mathbf{C}..\Delta\mathbf{T} - \Delta\mathbf{T}..\mathbf{A}_0(\mathbf{T}_0) - V\cdot(\Delta\mathbf{T})\cdot\mathbf{u}_0\}\,\mathrm{d}V$$

$$- \int_V [V\cdot(\mathbf{T}_0+\Delta\mathbf{T}) + (\mathbf{q}_0+\Delta\mathbf{q})]\cdot\Delta\mathbf{u}\,\mathrm{d}V$$

$$+ \int_{S_p} \{[\mathbf{n}\cdot(\mathbf{T}_0+\Delta\mathbf{T}) - (\bar{\mathbf{p}}_0+\Delta\bar{\mathbf{p}})]\cdot\Delta\mathbf{u} + \mathbf{n}\cdot\Delta\mathbf{T}\cdot\mathbf{u}_0\}\,\mathrm{d}S$$

$$+ \int_{S_u} \mathbf{n}\cdot\Delta\mathbf{T}\cdot(\bar{\mathbf{u}}_0+\Delta\bar{\mathbf{u}})\,\mathrm{d}S \tag{3.3a}$$

or, transforming integral $\int_V (V\cdot\mathbf{T}_0)\cdot\Delta\mathbf{u}\,\mathrm{d}V$ in the obtained functional, we arrive at

$$\Pi_R^I = \Pi_R^I(\Delta\mathbf{T}, \Delta\mathbf{u})$$

$$= \int_V \left\{-\frac{1}{2}\Delta\mathbf{T}..\mathbf{C}..\Delta\mathbf{T} - \Delta\mathbf{T}..\mathbf{A}_0(\mathbf{T}_0) - \mathbf{T}_0..\Delta\mathbf{A}(\Delta\mathbf{u})\right.$$

$$\left. - V\cdot(\Delta\mathbf{T})\cdot\mathbf{u}_0 - \mathbf{q}_0\cdot\Delta\mathbf{u}\right\}\mathrm{d}V$$

$$- \int_V [V\cdot(\Delta\mathbf{T}) + \Delta\mathbf{q}]\cdot\Delta\mathbf{u}\,\mathrm{d}V$$

$$+ \int_{S_p} \{[\mathbf{n}\cdot\Delta\mathbf{T} - \Delta\bar{\mathbf{p}}]\cdot\Delta\mathbf{u} + \mathbf{n}\cdot\Delta\mathbf{T}\cdot\mathbf{u}_0 - \bar{\mathbf{p}}_0\cdot\Delta\mathbf{u}\}\,\mathrm{d}S$$

$$+ \int_{S_u} \{\mathbf{n}\cdot\Delta\mathbf{T}\cdot(\bar{\mathbf{u}}_0+\Delta\bar{\mathbf{u}}) - \mathbf{n}\cdot\mathbf{T}_0\cdot\Delta\mathbf{u}\}\,\mathrm{d}S \tag{3.3b}$$

Requiring $\mathbf{T}$ in Π_R to satisfy equilibrium equation (2.1) and dynamic BC (2.4), variational stipulations $\delta(\Delta\mathbf{T})\,|_{S_p} = \mathbf{0}$, $\delta(V\cdot\Delta\mathbf{T})\,|_V = \mathbf{0}$ may lead to the "complete" complementary energy

$$\Pi_R^C \Rightarrow \Pi_c^C = \Pi_c^C(\Delta\mathbf{T})$$

$$= \int_V \left\{\frac{1}{2}\Delta\mathbf{T}..\mathbf{C}..\Delta\mathbf{T} + \Delta\mathbf{T}..\mathbf{A}_0(\mathbf{T}_0)\right\}\mathrm{d}V$$

$$- \int_{S_u} \mathbf{n}\cdot\Delta\mathbf{T}\cdot(\bar{\mathbf{u}}_0+\Delta\bar{\mathbf{u}})\,\mathrm{d}S \tag{3.4}$$

Satisfying only the incremental parts in the equilibrium equation and in the dynamic BC

$$\begin{aligned} V\cdot(\Delta\mathbf{T})+\Delta\mathbf{q}&=\mathbf{0} \qquad x\in V\\ \mathbf{n}\cdot\Delta\mathbf{T}&=\Delta\bar{\mathbf{p}} \qquad x\in S \end{aligned} \tag{3.5a, b}$$

Π_R^I would yield the "incomplete" complementary energy:

$$\Pi_R^I\Rightarrow\Pi_c^I=\Pi_c^I(\Delta\mathbf{T},\Delta\mathbf{u})$$

$$=\int_V\left\{\frac{1}{2}\Delta\mathbf{T}\,..\,\mathbf{C}\,..\,\Delta\mathbf{T}+\Delta\mathbf{T}\,..\,\mathbf{A}_0(\mathbf{T}_0)-\mathbf{T}_0\,..\,\Delta\mathbf{A}(\Delta\mathbf{u})+\mathbf{q}_0\cdot\Delta\mathbf{u}\right\}\mathrm{d}V$$

$$+\int_{S_p}\bar{\mathbf{p}}_0\cdot\Delta\mathbf{u}\,\mathrm{d}S+\int_{S_u}\{\mathbf{n}\cdot\Delta\mathbf{T}\cdot(\bar{\mathbf{u}}_0+\Delta\bar{\mathbf{u}})-\mathbf{n}\cdot\mathbf{T}_0\cdot\Delta\mathbf{u}\}\,\mathrm{d}S \tag{3.6}$$

The incremental potential energy is obtained by requiring (3.2) to contain relationship $\Delta\mathbf{T}=\mathbf{C}^{-1}\,..\,\Delta\mathbf{A}(\Delta\mathbf{u})$ and to *a priori* satisfy the kinematic BC.

Introducing notation $\mathbf{D}=\mathbf{C}^{-1}$, we find

$$\Pi_p=\Pi_p(\Delta\mathbf{u})$$

$$=\int_V\left\{\frac{1}{2}\Delta\mathbf{A}\,..\,\mathbf{D}\,..\,\Delta\mathbf{A}+\mathbf{T}_0\,..\,\Delta\mathbf{A}-(\mathbf{q}_0+\Delta\mathbf{q})\cdot\Delta\mathbf{u}\right\}\mathrm{d}V$$

$$-\int_{S_p}(\bar{\mathbf{p}}_0+\Delta\bar{\mathbf{p}})\cdot\Delta\mathbf{u}\,\mathrm{d}S\,. \tag{3.7}$$

4. Analysis of a system of several elements and bilateral connection

The considered boundary value problem is the system of partial differential equations (2.1)–(2.7). At first, the variational principles will be formulated so as to satisfy *a priori* the FC (2.6) to (2.7) between elements.

4.1. The discontinuity potential

For the approximation of fields $\mathbf{T}$ and $\mathbf{u}$ taken for separate elements having derivatives at least once continuous, it is often hard to require the *a priori* fulfilment of the dynamic and kinematic fitting conditions.

Kinematic FC may be taken into consideration by applying a Lagrangian multiplier. Thus, for adjacent elements e and j, vector $\boldsymbol{\lambda}_1=(\boldsymbol{\lambda}_0+\Delta\boldsymbol{\lambda})_1$ in integral

$$\Pi_1^{ej}=\int_{S_c^{ej}}\boldsymbol{\lambda}_1\cdot(\mathbf{u}^j-\mathbf{u}^e+\mathbf{h}^{ej})\,\mathrm{d}S \tag{4.1}$$

is the Lagrangian factor, while concerning all the system,

$$\Pi_1 = \sum_{e=1}^{N-1} \sum_{j>e}^{N} \Pi_1^{ej} = \sum_{e,j} \Pi_1^{ej} \tag{4.2}$$

will be the term containing the kinematic FC.

Here and in the following, complete value of any mechanical magnitude will be understood as sum of values at the beginning of load increment, and that of the increment, e.g. $\mathbf{u} = \mathbf{u}_0 + \Delta\mathbf{u}$, $\mathbf{h} = \mathbf{h}_0 + \Delta\mathbf{h}$, etc.

Summation in (4.2) is understood as taking integral Π_1^{ej} for elements $j > e$ adjacent to element e of the smaller subscript.

Thereby a single integration at the element interface is sufficient, along the contact surface between elements of the lower and the higher subscript. Subsequently, double summing in (4.2) will be replaced by a simplified notation.

Stress discontinuity of a given value at the contact range S_c of the elements is due to load $\mathbf{t}$ applied at that point (Fig. 1).

Assuming load $\mathbf{t}^{ej}$ to be distributed according to load factor γ between arbitrary adjacent elements e and j, interface load potential for the entire system becomes:

$$\Pi_{t_1} = -\sum_{e,j} \int_{S_c^{ej}} \mathbf{t}^{ej} \cdot (\mathbf{u}^j + (1-\gamma)\mathbf{u}^e)\, \mathrm{d}S\,. \tag{4.3a}$$

For zero initial gap $\mathbf{h}^{ej}$ along S_c^{ej}, γ may assume any value in interval (0, 1).

For $\mathbf{h}^{ej} = \mathbf{0}$, $\gamma = 0$ or $\gamma = 1$, depending on whether the load acts on element e or j. For $\gamma = 0.5$, the load is exactly halved between elements.

Depending on the γ value, let us interpret potentials

$$\Pi_{t2} = \Pi_{t1}(\gamma = 1); \qquad \Pi_{t3} = \Pi_{t1}(\gamma = 0); \qquad \Pi_{t4} = \Pi_{t1}(\gamma = 0.5)\,. \tag{4.3b}$$

Discontinuity potential is understood as:

$$J_1 = \Pi_1 + \Pi_{t1}\,. \tag{4.4}$$

4.2 Variational principle type I

4.2.1 Principle involving a complementary stress multiplier

The variation principle involving free fields $\mathbf{T}$ and $\Delta\mathbf{u}$, taking discontinuities into consideration, may rely on functional

$$\begin{aligned} L_{R_1} &= \sum_e \Pi_R^e(\Delta\mathbf{T}^e, \Delta\mathbf{u}^e) + J_1(\Delta\mathbf{u}; \Delta\boldsymbol{\lambda}_1) \\ &= \Pi_R(\Delta\mathbf{T}, \Delta\mathbf{u}) + \mathbf{J}_1(\Delta\mathbf{u}, \Delta\boldsymbol{\lambda}_1) = \text{stationary}\,, \end{aligned} \tag{4.5}$$

sum of Reissner's functional (3.2) written for N elements of the system, and of discontinuity potential (4.4).

It is easy to demonstrate that variational equation $\delta_{\Lambda \mathbf{T}} L_{R_1} = 0$ obtained from stationarity condition $\delta L_{R_1} = 0$ yields

$$\begin{aligned} \Lambda \mathbf{A}(\Lambda \mathbf{T}) &\overset{\text{def}}{=} \mathbf{C} \,..\, \Lambda \mathbf{T} = \Lambda \mathbf{A}(\Lambda \mathbf{u}) \\ \mathbf{A}_0(\mathbf{T}_0) &\overset{\text{def}}{=} \mathbf{C} \,..\, \mathbf{T}_0 = \mathbf{A}_0(\mathbf{u}_0) \end{aligned} \qquad x \in V$$

and the kinematic BC

$$\mathbf{u}_0 + \Lambda \mathbf{u} = \bar{\mathbf{u}}_0 + \Lambda \bar{\mathbf{u}} \quad x \in S_u ,$$

equation $\delta_{\Lambda \mathbf{u}} I_{R_1} = 0$ yields equilibrium equation (2.1), stress boundary condition (2.4), and dynamic FC

$$\begin{aligned} \mathbf{n}^e \cdot (\mathbf{T}_0 + \Lambda \mathbf{T})^e - (\boldsymbol{\lambda}_0 + \Lambda \boldsymbol{\lambda})_1 - (\mathbf{t}_0 + \Lambda \mathbf{t})^{ej}(1-\gamma) &= \mathbf{0} \\ \mathbf{n}^j \cdot (\mathbf{T}_0 + \Lambda \mathbf{T})^j + (\boldsymbol{\lambda}_0 + \Lambda \boldsymbol{\lambda})_1 - (\mathbf{t}_0 + \Lambda \mathbf{t})^{ej}\gamma &= \mathbf{0} \end{aligned} \qquad \text{(4.6a, b)}$$

for surface S_c^{ej}, while equation $\delta_{\Lambda \boldsymbol{\lambda}_1} L_{R_1} = 0$ leads to kinematic FC (2.7), in conformity with the mutual independence and arbitrariness of field variations. Here δ_x denotes first variation with respect to variable x. Letting γ take different values, (4.6) lends different physical purports to multiplier $\boldsymbol{\lambda}_1$, namely:

$$\begin{aligned} &\text{for} \quad \gamma = 1, \qquad \text{stress} \qquad \boldsymbol{\lambda}_1 = \mathbf{n}^e \cdot (\mathbf{T}_0 + \Lambda \mathbf{T})^e \\ &\text{for} \quad \gamma = 0, \qquad \text{stress} \qquad \boldsymbol{\lambda}_1 = -\mathbf{n}^j \cdot (\mathbf{T}_0 + \Lambda \mathbf{T})^j \\ &\text{for} \quad \gamma = 0.5, \qquad \text{stress} \qquad \boldsymbol{\lambda}_1 = \frac{1}{2} [\mathbf{n}^e \cdot (\mathbf{T}_0 + \Lambda \mathbf{T})^e - n^j \cdot (\mathbf{T}_0 + \Lambda \mathbf{T})^j] \end{aligned} \qquad \text{(4.7a–c)}$$

4.2.2 Use of multipliers deduced from stress tensor fields

Eqs (4.7a–c) directly involve the possibility to assume as Lagrangian factors their real physical purports, i.e. stresses

$$\begin{aligned} \boldsymbol{\lambda}_2 = \boldsymbol{\lambda}_2(\mathbf{T}^e) &\overset{\text{def}}{=} \mathbf{n}^e \cdot \mathbf{T}^e \\ \boldsymbol{\lambda}_3 = \boldsymbol{\lambda}_3(\mathbf{T}^j) &\overset{\text{def}}{=} -\mathbf{n}^j \cdot \mathbf{T}^j \\ \boldsymbol{\lambda}_4 = \boldsymbol{\lambda}_4(\mathbf{T}^e, \mathbf{T}^j) &\overset{\text{def}}{=} \frac{1}{2} (\mathbf{n}^e \cdot \mathbf{T}^e - \mathbf{n}^j \cdot \mathbf{T}^j) \end{aligned}$$

$$e = 1, \ldots, N-1; \qquad j > e \qquad \text{(4.8a–c)}$$

Now, replacing vectors $\boldsymbol{\lambda}_1$ by $\boldsymbol{\lambda}_i (i = 2, 3, 4)$ in (4.5), we arrive at functionals containing only fields $\Lambda \mathbf{T}$ and $\Lambda \mathbf{u}$. Now, free equations arising from the stationarity of functional

$$\begin{aligned} L_{Ri} &= L_{Ri}(\Lambda \mathbf{T}, \Lambda \mathbf{u}) \\ &= H_R(\Lambda \mathbf{T}, \Lambda \mathbf{u}) + J_i(\Lambda \mathbf{u}, \Lambda \mathbf{T}) \end{aligned} \qquad \text{(4.9)}$$

correspond to Eqs (2.1) to (2.7), where

$$J_i = H_i + H_{ti} \ (i = 2, 3, 4) \qquad \text{(4.10)}$$

4.2.3 Application of stress multipliers and additional displacements

An attempt to solve boundary value problem (2.1) to (2.7) may be realized where stress multiplier λ_i $(i=1, 2, 3)$ is complemented by a field of displacements satisfying the kinematic boundary condition interpreted at element interfaces. Additional fields $\tilde{\mathbf{u}}$ and $\tilde{\tilde{\mathbf{u}}}$ will be assumed to belong to elements of lower and higher subscripts e and j, respectively, at the element interface (inner) S_c^{ej}, while additional fields at boundaries S_u and S_p will be $\tilde{\mathbf{u}}$ and $\tilde{\tilde{\mathbf{u}}}$, respectively. Three main cases will be distinguished, involving respective fields $\tilde{\mathbf{u}}$, $\tilde{\tilde{\mathbf{u}}}$, and both, respectively boundaries S_c^{ej}.

Functionals for the quoted cases are:

$$L_{Rk}=\tilde{\Pi}_{R,k-4}+\sum_{e,j}\int_{S_c^{ej}}[\lambda_{k-4}^{e}\cdot(\tilde{\mathbf{u}}-\mathbf{u}^{e}+\mathbf{h}^{ej})-\mathbf{t}^{ej}\cdot\tilde{\mathbf{u}}-$$

$$-\lambda_{k-4}^{j}\cdot(\tilde{\mathbf{u}}-\mathbf{u}^{j})]\,\mathrm{d}S\quad(k=5,6 \tag{4.11a}$$

$$L_{Rl}=\tilde{\Pi}_{R,l-6}+\sum_{e,j}\int_{S_c^{ej}}[\lambda_{l-6}^{j}\cdot(\mathbf{u}^{j}-\tilde{\tilde{\mathbf{u}}}+\mathbf{h}^{ej})-\mathbf{t}^{ej}\cdot\tilde{\tilde{\mathbf{u}}}+$$

$$+\lambda_{l-6}^{e}\cdot(\tilde{\tilde{\mathbf{u}}}-\mathbf{u}^{e})]\,\mathrm{d}S\quad(l=7,8 \tag{4.11b}$$

$$L_{Rm}=\tilde{\Pi}_{R,m-8}+\sum_{e,j}\int_{S_c^{ej}}\left\{\frac{1}{2}[(\lambda_{m-8}^{e}+\lambda_{m-8}^{j})\cdot(\tilde{\mathbf{u}}-\tilde{\tilde{\mathbf{u}}}+\mathbf{h}^{ej})-\mathbf{t}^{ej}\cdot(\tilde{\mathbf{u}}+\tilde{\tilde{\mathbf{u}}})]\right.$$

$$\left.+\lambda_{m-8}^{e}\cdot(\tilde{\tilde{\mathbf{u}}}-\mathbf{u}^{e})+\lambda_{m-8}^{j}\cdot(\mathbf{u}^{j}-\tilde{\mathbf{u}})\right\}\mathrm{d}S\quad(m=9,10 \tag{4.11c}$$

where

$$\tilde{\Pi}_{R,s}=\sum_{e}\left\{\int_{V^e}\left[-\frac{1}{2}\Delta\mathbf{T}\,..\,\mathbf{C}\,..\,\Delta\mathbf{T}-\mathbf{q}\cdot\Delta\mathbf{u}+\mathbf{T}\,..\,\Delta\mathbf{A}(\Delta\mathbf{u})+\right.\right.$$

$$\left.+\Delta\mathbf{T}\,..\,(\mathbf{A}_0(\mathbf{u}_0)-\mathbf{A}_0(\mathbf{T}_0))\right]\mathrm{d}V-$$

$$-\int_{S_p^e}[\bar{\mathbf{p}}\cdot\Delta\tilde{\mathbf{u}}-\lambda_1^{e}\cdot(\tilde{\mathbf{u}}-\mathbf{u})]\,\mathrm{d}S+$$

$$\left.+\int_{S_u^e}\lambda_s^{e}\cdot(\tilde{\mathbf{u}}-\mathbf{u})\,\mathrm{d}S\right\} \tag{4.12}$$

λ_1^e, λ_1^j are independent of each other, $\lambda_2^e=\mathbf{n}^e\cdot\mathbf{T}^e$; $\lambda_2^j=-\mathbf{n}^j\cdot\mathbf{T}^j$ are fields computed from stress tensors.

Integrals in functionals $L_{Ri}(i=5, \ldots, 10)$ involve full field values for the sake of conciseness. Of course, in computations based on the variational principle, the computations of integrals which can be considered constants from the point of view of variation can be omitted.[1]

[1] Multipliers in the above functionals may be recognized from Fig. 2. Stress and displacement fields have been traced in thick, and in dashed line, resp. Those at element boundaries arise from the original field $\mathbf{T}$, while fields between elements are additional ones.

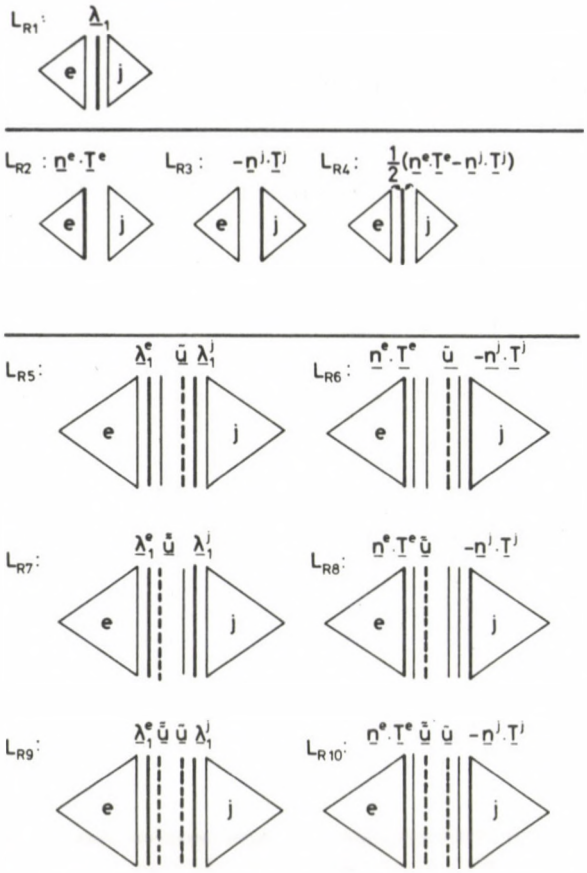

Fig. 2. Combinations of stress multipliers $\boldsymbol{\lambda}_i$, $\mathbf{n}^e \cdot \mathbf{T}^e$, $-\mathbf{n}^j \cdot \mathbf{T}^j$ in functionals L_{Ri} and of additionaly fields $\tilde{\mathbf{u}}$, $\bar{\mathbf{u}}$ assumed at element boundaries

4.2.4. C-type transformation of functionals L_{Ri}

The transformation of integral $\int_V [\mathbf{T}..\Delta\mathbf{A}(\Delta\mathbf{u}) + \Delta\mathbf{T}..\mathbf{A}_0(\mathbf{u}_0)]\,dV$ in $L_{Ri}(i=1, \ldots, 10)$ permits us to write L_{Ri} as:

$$L_{Ri} \Rightarrow L_{Ri}^C = -\Pi_c^C + \Pi_E^C + J_i^C \quad (i=1, \ldots, 4) \tag{4.13}$$

where for $-\Pi_c^C$ see (3.4)

$$\Pi_E^C = \Pi_{EV}^C + \Pi_{ES}^C \tag{4.14a}$$

$$\Pi_{EV}^C = -\int_V [(V \cdot \mathbf{T} + \mathbf{q}) \cdot \Delta\mathbf{u} - V \cdot (\Delta\mathbf{T}) \cdot \mathbf{u}_0]\,dV \tag{4.14b}$$

$$\Pi_{ES}^C = \int_{S_p} [(\mathbf{n} \cdot \mathbf{T} - \bar{\mathbf{p}}) \cdot \Delta\mathbf{u} + \mathbf{n} \cdot \Delta\mathbf{T} \cdot \mathbf{u}_0]\,dS \tag{4.14c}$$

furthermore

$$J_i^C = J_i + \sum_e \int_{S_c^e} (\mathbf{n} \cdot \mathbf{T} \cdot \Lambda\mathbf{u} + \mathbf{n} \cdot \Lambda\mathbf{T} \cdot \mathbf{u}_0)\, \mathrm{d}S \tag{4.15}$$

or, in detail:

$$\begin{aligned} J_1^C = \sum_{e,j} \int_{S_c^{ej}} \{ & \boldsymbol{\lambda}_1 \cdot \mathbf{h}^{ej} + (\boldsymbol{\lambda}_1 + \mathbf{n}^j \cdot \mathbf{T}^j - \mathbf{t}^{ej}{}_{\gamma}) \cdot \Lambda\mathbf{u}^j + \\ & + (\mathbf{n}^e \cdot \mathbf{T}^e - \boldsymbol{\lambda}_1 - (1-\gamma)\mathbf{t}^{ej}) \cdot \Lambda\mathbf{u}^e + \\ & + (\mathbf{n}^e \cdot \Lambda\mathbf{T}^e - \Lambda\boldsymbol{\lambda}_1 - (1-\gamma)\Lambda\mathbf{t}^{ej}) \cdot \mathbf{u}_0^e + \\ & + (\mathbf{n}^j \cdot \Lambda\mathbf{T}^j + \Lambda\boldsymbol{\lambda}_1 - \Lambda\mathbf{t}^{ej}{}_{\gamma}) \cdot \mathbf{u}_0^j \}\, \mathrm{d}S\,, \end{aligned}$$

$$\begin{aligned} J_2^C = \sum_{e,j} \int_{S_c^{ej}} \{ & \mathbf{n}^e \cdot \mathbf{T}^e \cdot \mathbf{h}^{ej} + (\mathbf{n}^e \cdot \mathbf{T}^e + \mathbf{n}^j \cdot \mathbf{T}^j - \mathbf{t}^{ej}) \cdot \Lambda\mathbf{u}^j \\ & + (\mathbf{n}^j \cdot \Lambda\mathbf{T}^j + \mathbf{n}^e \cdot \Lambda\mathbf{T}^e - \Lambda\mathbf{t}^{ej}) \cdot \mathbf{u}_0^j \}\, \mathrm{d}S \end{aligned}$$

etc.

For additional disceplacement fields:

$$L_R \begin{bmatrix} k \\ l \\ m \end{bmatrix} \Rightarrow L_R^C \begin{bmatrix} k \\ l \\ m \end{bmatrix} = -\tilde{\Pi}_c^C \begin{bmatrix} k-4 \\ l-6 \\ m-8 \end{bmatrix} + \Pi_{EV}^C + \tilde{\Pi}_{ES}^C + J^C \begin{bmatrix} k \\ l \\ m \end{bmatrix}$$

$$k = 5,6; \qquad l = 7,8; \qquad m = 9,10$$

where:

$$\begin{aligned} -\tilde{\Pi}_{c,S}^C = \sum_e \Bigg\{ & \int_{V^e} \left[-\frac{1}{2}\, \Lambda\mathbf{T} \,..\, \mathbf{C} \,..\, \Lambda\mathbf{T} - \Lambda\mathbf{T} \,..\, \mathbf{A}_0(\mathbf{T}_0) \right] \mathrm{d}V + \\ & + \int_{S^e} [\boldsymbol{\lambda}_s \cdot (\tilde{\mathbf{u}} - \mathbf{u}) + \mathbf{n} \cdot \mathbf{T} \cdot \Lambda\mathbf{u} + \mathbf{n} \cdot \Lambda\mathbf{T} \cdot \mathbf{u}_0]\, \mathrm{d}S \end{aligned}$$

$$(s = 1, 2) \tag{4.17}$$

$$\tilde{\Pi}_{ES}^C = \sum_e \int_{S_p^e} [\boldsymbol{\lambda}_s \cdot (\tilde{\mathbf{u}} - \mathbf{u}) + \mathbf{n} \cdot \mathbf{T} \cdot \Lambda\mathbf{u} + \mathbf{n} \cdot \Lambda\mathbf{T} \cdot \mathbf{u}_0 - \tilde{\mathbf{p}} \cdot \Lambda\tilde{\mathbf{u}}]\, \mathrm{d}S$$

$$(s = 1, 2) \tag{4.18}$$

$$\begin{aligned} J_k^C = \sum_{e,j} \int_{S_c^{ej}} \{ & \boldsymbol{\lambda}_{k\ 4}^e \cdot \mathbf{h}^{ej} + (\mathbf{n}^e \cdot \mathbf{T}^e - \boldsymbol{\lambda}_{k\ 4}^e) \cdot \Lambda\mathbf{u}^e + \\ & + (\mathbf{n}^j \cdot \mathbf{T}^j + \boldsymbol{\lambda}_{k\ 4}^j) \cdot \Lambda\mathbf{u}^j + (\boldsymbol{\lambda}_{k\ 4}^e - \boldsymbol{\lambda}_{k\ 4}^j - \mathbf{t}^{ej}) \cdot \tilde{\mathbf{u}} + \\ & + (\mathbf{n}^e \cdot \Lambda\mathbf{T}^e - \Lambda\boldsymbol{\lambda}_{k\ 4}^e) \cdot \mathbf{u}_0^e + (\mathbf{n}^j \cdot \Lambda\mathbf{T}^j + \Lambda\boldsymbol{\lambda}_{k\ 4}^j) \cdot \mathbf{u}_0^j \}\, \mathrm{d}S \end{aligned}$$

$$(k = 5, 6) \tag{4.19}$$

4.2.5. I-type transformation of functionals L_{Ri}

The transformation of integral $\int_V \Lambda\mathbf{T} \cdot \cdot (\mathbf{A}(\mathbf{u}_0 + \Lambda\mathbf{u}))\,\mathrm{d}V$ in L_{Ri} yields functional L_{Ri} equivalent to L_{Ri} $(i = 1, \ldots, 10)$:

$$L_{Ri} \Rightarrow L^I_{Ri} = \Pi^I_R + J^I_i + \sum_e \int_{S^e_\sigma} \mathbf{n} \cdot \Lambda\mathbf{T} \cdot \mathbf{u}\,\mathrm{d}S$$

For sub-cases $i = 1, \ldots, 4$:

$$L^I_{Ri} = -\Pi^I_c + \Pi^I_E + J^I_i \quad (i = 1, \ldots, 4) \tag{4.20}$$

where for Π^I_c see (3.6),

$$\Pi^I_E = \Pi^I_{EV} + \Pi^I_{ES} \tag{4.21a}$$

$$\Pi^I_{EV} = -\int_V \{[V \cdot (\Lambda\mathbf{T})] \cdot \mathbf{u}_0 + [V \cdot (\Lambda\mathbf{T}) + \Lambda\mathbf{q}] \cdot \Lambda\mathbf{u}\}\,\mathrm{d}V \tag{4.21b}$$

$$\Pi^I_{ES} = \int_{S_p} \{\mathbf{n} \cdot \Lambda\mathbf{T} \cdot \mathbf{u}_0 + (\mathbf{n} \cdot \Lambda\mathbf{T} - \Lambda\bar{\mathbf{p}}) \cdot \Lambda\mathbf{u}\}\,\mathrm{d}S \tag{4.21c}$$

furthermore:

$$J^I_i = J_i + \sum_e \int_{S^e_\sigma} \mathbf{n} \cdot \Lambda\mathbf{T} \cdot \mathbf{u}\,\mathrm{d}S \tag{4.22}$$

or, in detail:

$$\begin{aligned}
J^I_1 = \sum_{e,j} \int_{S^{ej}_\sigma} \{&(\Lambda\boldsymbol{\lambda}_1 + \mathbf{n}^j \cdot \Lambda\mathbf{T}^j - \Lambda\mathbf{t}^{ej}_\gamma) \cdot \mathbf{u}^j + \Lambda\boldsymbol{\lambda} \cdot \mathbf{h}^{ej} + \\
&+ (\mathbf{n}^e \cdot \Lambda\mathbf{T}^e - \Lambda\boldsymbol{\lambda}_1 - (1-\gamma)\Lambda\mathbf{t}^{ej}) \cdot \mathbf{u}^e + \\
&+ \boldsymbol{\lambda}_{1,0} \cdot (\Lambda\mathbf{u}^j - \Lambda\mathbf{u}^e + \Lambda\mathbf{h}^{ej}) + \\
&+ \mathbf{t}^{ej}_0 \cdot (\Lambda\mathbf{u}^j \cdot \gamma + \Lambda\mathbf{u}^e \cdot (1-\gamma)\}\,\mathrm{d}S\,, \\
J^I_2 = J^I_1(\boldsymbol{\lambda}_1 = \mathbf{n}^e \cdot \mathbf{T}^e,\ \gamma = 1) \\
= \sum_{e,j} \int_{S^{ej}_\sigma} \{&(\mathbf{n}^e \cdot \Lambda\mathbf{T}^e + \mathbf{n}^j \cdot \Lambda\mathbf{T}^j - \Lambda\mathbf{t}^{ej}) \cdot \mathbf{u}^j + \mathbf{n}^e \cdot \Lambda\mathbf{T}^e \cdot \mathbf{h}^{ej} + \\
&+ \mathbf{n}^e \cdot \mathbf{T}^e_0 \cdot (\Lambda\mathbf{u}^j - \Lambda\mathbf{u}^e + \Lambda\mathbf{h}^{ej}) - \mathbf{t}^{ej}_0 \cdot \Lambda\mathbf{u}^j\}\,\mathrm{d}S.
\end{aligned}$$

Involving complementary displacement fields, we arrive at functionals

$$L_R\begin{bmatrix} k \\ l \\ m \end{bmatrix} \Rightarrow L^I_R\begin{bmatrix} k \\ l \\ m \end{bmatrix} = -\tilde{\Pi}^I_c\begin{bmatrix} k & 4 \\ l & 6 \\ m & 8 \end{bmatrix} + \Pi^I_{EV} + \tilde{\Pi}^I_{ES} + J^I\begin{bmatrix} k \\ l \\ m \end{bmatrix}$$

$$k = 5, 6;\ l = 7, 8;\ m = 9, 10$$

where

$$-\tilde{\Pi}^I_{c,s} = -\sum_e \left\{ \int_{V^e} \left[\frac{1}{2} \Delta\mathbf{T} \,..\, \mathbf{C} \,..\, \Delta\mathbf{T} + \Delta\mathbf{T} \,..\, \mathbf{A}_0(\mathbf{T}_0) - \right.\right.$$

$$\left. - \mathbf{T}_0 \,..\, \Delta\mathbf{A}(\Delta\mathbf{u}) + \mathbf{q}_0 \cdot \Delta\mathbf{u} \right] \mathrm{d}V$$

$$+ \int_{S^e_u} [\boldsymbol{\lambda}_s \cdot (\tilde{\mathbf{u}} - \mathbf{u}) + \mathbf{n} \cdot \Delta\mathbf{T} \cdot \mathbf{u}] \, \mathrm{d}S$$

$$(s = 1, 2) \tag{4.24}$$

$$\tilde{\Pi}^I_s = \sum_e \int_{S^e_p} [\boldsymbol{\lambda}_s \cdot (\tilde{\mathbf{u}} - \mathbf{u}) + \mathbf{n} \cdot \Delta\mathbf{T} \cdot \mathbf{u} - \bar{\mathbf{p}} \cdot \Delta\tilde{\mathbf{u}}] \, \mathrm{d}S \tag{4.25}$$

$$J^I_k = \sum_{e,j} \int_{S^{ej}_c} \{\mathbf{u}^e \cdot (\Delta\mathbf{T}^e \cdot \mathbf{n}^e - \Delta\boldsymbol{\lambda}^e_{k-4}) + \tilde{\mathbf{u}} \cdot (\boldsymbol{\lambda}^e_{k-4} - \boldsymbol{\lambda}^j_{k-4} - \mathbf{t}^{ej})$$

$$+ \mathbf{u}^j \cdot (\Delta\mathbf{T}^j \cdot \mathbf{n}^j + \Delta\boldsymbol{\lambda}^j_{k-4}) + \boldsymbol{\lambda}^j_{k\ 4,0} \cdot \Delta\mathbf{u}^j$$

$$- \boldsymbol{\lambda}^e_{k\ 4,0} \cdot \Delta\mathbf{u}^e + \boldsymbol{\lambda}^e_{k\ 4} \cdot \mathbf{h}^{ej}\} \, \mathrm{d}S$$

$$(k = 5, 6) \tag{4.26}$$

etc.

4.3. Variational principle type II

The obtained functionals L^C_{Ri}, L^I_{Ri} permit easy deduction of other principles depending on stipulations for tensor **T**. Two sub-cases will be distinguished. Stipulations concerning the equilibrium equation and the dynamical boundary condition will be made either for the full field **T** or for the increment field $\Delta\mathbf{T}$ alone. These stipulations together with the functionals assignable to variational principles have been compiled in Table II. For example, in the first case, L^C_{ci} may be obtained from L^C_{Ri}, taking into consideration that Π^C_E may be considered as constant from the aspect of variation.

Consideration of J^C_i, $\Pi^C_{c,s}$ and $\tilde{\Pi}^C_{ES}$ shows field **u** to be needed only at element surfaces, thus a field **u** approximated independently of **T** may be considered as a Lagrangian multiplier. Thus, obviously, in cases $i = 5, \ldots, 10$, fields $\tilde{\mathbf{u}}$, $\tilde{\tilde{\mathbf{u}}}$ assumed independently of **T** and $\tilde{\mathbf{u}}$ are irrelevant, needless to apply. This is why case 1 comprise $i = 1, \ldots, 4$ sub-classes.

Cases 2 and 3 in Table II permit us to omit Π^C_{EV}, case 4 Π^C_{ES} and case 5 $\tilde{\Pi}^C_{ES}$, in view of stipulations on field **T**.

Similar considerations may lead to functionals from L^I_{Ri} for further variational principles in Table II.

4.4. *Variational principle type III*

In this variational principle, field **u** is required to satisfy the kinematic BC, and relationship $\Delta\mathbf{T}=\mathbf{D}\,..\,\Delta\mathbf{A}(\Delta\mathbf{u})$ is assumed to hold, permitting us to formulate the principle of stationarity of modified potential energy, relying on functional

$$L_{P_i}=\Pi_p(\Delta\mathbf{u})+J_i \quad (i=1,\ldots,4) \tag{4.27a}$$

$$L_p\begin{bmatrix}k\\l\\m\end{bmatrix}=\tilde{\Pi}_p\begin{bmatrix}k & 4\\l & 6\\m & 8\end{bmatrix}+J\begin{bmatrix}k\\l\\m\end{bmatrix} \tag{4.27b}$$

$$k=5,6;\ l=7,8;\ m=9,10$$

where

$$\tilde{\Pi}_{p,s}=\Pi_p+\sum_e\int_{S_p^e+S_u^e}\boldsymbol{\lambda}_s\cdot(\tilde{\mathbf{u}}-\mathbf{u})\,\mathrm{d}S \tag{4.28}$$

derived from L_{Ri} [(4.5), (4.9)] with respect to (3.7).

4.5. *Variational principles for a continuous displacement field*

If there are no prescribed discontinuities at the element boundaries, then the displacement field is continuous.

Since no mention has been made concerning the sizes of the elements the case may be realized where the elastic system is mentally decomposed to elementary parts, finite elements, approximating the stress tensor field, displacement field in the solid by element-wise interpreted functions. There is a possibility to locally approximate the fields needed, hence, the described principles involve variational principles of the finite element method.

Also for functionals obtained by substituting $\mathbf{h}=\mathbf{0}$, kinematic and dynamic FC—not *a priori* satisfied—arise as part of free equations at element boundaries. Now, multipliers continue to provide for satisfying—in the integral sense—not *a priori* satisfied dynamic or kinematic FC. (Of course, a way may be chosen where some FC is *a priori* satisfied by the assumed fields.)

In conformity with considerations in Appendix 1, because of $\mathbf{h}=\mathbf{0}$, multiplier terms involving kinematic FC may be written in a simpler form. For instance, in conformity with (A.1.2), Π_1 in (4.4) becomes:

$$\Pi_1=-\sum_e\int_{S_u^e}\boldsymbol{\lambda}_1^e\cdot\mathbf{u}^e\,\mathrm{d}S \tag{4.29a}$$

Exemptness of discontinuity in components $\mathbf{u}'$ in approximating displacement field **u** permits us to replace (4.29a) by summation

$$\Pi_1''=-\sum_e\int_{S_u^e}\boldsymbol{\lambda}_1^e\cdot\mathbf{u}^{e\prime\prime}\,\mathrm{d}S \tag{4.29b}$$

affecting only components with a discontinuity in field **u** by scalar multiplication.

Element models related to variational principles involving also fields beyond those in the original boundary value problem are termed *hybrid* models. Those involving both fields $\mathbf{T}$ and $\mathbf{u}$ are termed *mixed field* models.

After these introductory ideas let us take in order the most important principles from the point of view of practical applications.

4.5.1. Modified Hellinger–Reissner principles

4.5.1.1. Mixed field model

The substitution of $\boldsymbol{\lambda}_2 = \mathbf{n}^e \cdot \mathbf{T}^e$ for $\boldsymbol{\lambda}_1$ in (4.29) permits us, for $\mathbf{h} = \mathbf{0}$, to derive functional Π_{MM} in Table I from functional L_{R2} in (4.9). Now, at interfaces only components $\mathbf{u}''$ are discontinuous, though, with continuous stress fields. Thereby in load potential $\Pi_{t2} = \Pi_{t3}$ load $\mathbf{t}$ causing discontinuity of stress field may only be non-zero for continuous displacement components $\mathbf{u}'$.

For a safe continuity of field $\mathbf{u}$, integral for S_c^e vanishes, to yield the functional for the Reissner variational principle suiting analysis of the structural problem.

4.5.1.2. Model of hybrid mixed fields

Taking $\mathbf{h} = \mathbf{0}$ in $L_{Rk} (k = 5,6)$ and making simple transformations, we find functional Π_{HMM} in Table I. This functional contains unknown fields $\Delta\mathbf{T}$, $\Delta\mathbf{u}$, $\Delta\boldsymbol{\lambda}_1$, $\Delta\tilde{\mathbf{u}}$

Table I. Modified Reissner variational principles for discontinuous fields

Stipulation	Functional	
	$\mathbf{h} \neq \mathbf{0}$	$\mathbf{h} = \mathbf{0}$
	$L_{Ri}(L_{Ri}^C, L_{Ri}^I)$ $i = 1, \ldots, 4$ if kin. is met $L_R = \Pi_R + \Pi_{t1}$ if dyn. is met $L_R^C = -\Pi_c^C + \Pi_E^C + \sum_{e,j} \int_{S_c^{ej}} \boldsymbol{\lambda}_i \cdot \mathbf{h}^{ej} \, dS$	$\Pi_{MM} = \Pi_R - \sum_e \int_{S_c^e} \mathbf{n} \cdot \mathbf{T} \cdot \mathbf{u}'' \, dS +$ $+ \Pi_{t3}(\mathbf{u}')$ $(i = 2)$
	$L_{Rk}(L_{Rk}^C, L_{Rk}^I)$ $k = 5,6$ $L_{Rl}(L_{Rl}^C, L_{Rl}^I)$ $l = 7,8$ $L_{Rm}(L_{Rm}^C, L_{Rm}^I)$ $m = 9,10$	$\Pi_{HMM} = \int_V \Big\{ \mathbf{T} \,..\, \Delta\mathbf{A}(\Delta\mathbf{u}) - \frac{1}{2} \Delta\mathbf{T} \,..\, \mathbf{C} \,..\, \Delta\mathbf{T} + \Delta\mathbf{T} \,..\, [\mathbf{A}_0(\mathbf{u}_0) - \mathbf{A}_0(\mathbf{T}_0)] - \mathbf{q} \cdot \Delta\mathbf{u} \Big\} dV - \int_{S_p} \bar{\mathbf{p}} \cdot \Delta\tilde{\mathbf{u}} \, dS - \Pi_t(\tilde{\mathbf{u}}) +$ $+ \sum_e \int_{S_e} \boldsymbol{\lambda}_k^e \cdot (\tilde{\mathbf{u}} - \mathbf{u}^e) \, dS \quad (k = 5.6)^*$

* Here and in the following $\Pi_t(\tilde{\mathbf{u}}) = -\sum_{e,j} \int_{S_c^{ej}} \mathbf{t}^{ej} \cdot \tilde{\mathbf{u}} \, dS$

for $k=5$ and $\Delta\mathbf{T}$, $\Delta\mathbf{u}$, $\Delta\tilde{\mathbf{u}}$ for $k=6$. $\tilde{\mathbf{u}}$ satisfies kinematic BC. Functionals obtained from $L_{RI}(l=7,8)$ for $\mathbf{h}=\mathbf{0}$ equal those for $k=5,6$. Finally, for $m=9,10$, λ^e_{k-4} in Table I has to be replaced by $(1/2)\,(\lambda^e_{m-8}+\lambda^j_{m-8})$, and $\tilde{\mathbf{u}}$ Π_t by $(\tilde{\mathbf{u}}+\tilde{\tilde{\mathbf{u}}})/2$.

Table II. Principles of stationarity of modified complementary energy in the case of discontinuous fields

Case	Stipulation	Functional	
		$\mathbf{h}\neq\mathbf{0}$	$\mathbf{h}=\mathbf{0},\ \mathbf{t}=\mathbf{0}$
1	$V\cdot\mathbf{T}+\mathbf{q}=\mathbf{0}$ $x\in V$ $\mathbf{n}\cdot\mathbf{T}=\bar{\mathbf{p}}$ $x\in S_p$	$L^C_{ci}=-\Pi^C_c+J^C_i$ $(i=1,\ldots,4)$	$\Pi^C_{H\ 1}=-\Pi^C_c(\Delta T)+\sum_e\int_{S^e_p}\mathbf{u}\cdot$ $\cdot(\mathbf{T}^e\cdot\mathbf{n}^e-\lambda_1)\,dS=-\Pi^C_c(\Delta\mathbf{T})+$ $+\sum_e\int_{S^e_p}\mathbf{n}^e\cdot\mathbf{T}^e\cdot\mathbf{u}\,dS\quad(i=2)$
2	$V\cdot\mathbf{T}+\mathbf{q}=\mathbf{0}$ $x\in V$	$L^C_{ci}=-\Pi^C_c+\Pi^C_{ES}+J^C_i$ $(i=1,\ldots,4)$	
3	$V\cdot\mathbf{T}+\mathbf{q}=\mathbf{0}$ $x\in V$ $\tilde{\mathbf{u}}=\mathbf{u}$ $x\in S_u$	$L^C_{ck}=-\tilde{\Pi}^C_{c,k-4}+J^C_k+\Pi^C_{ES}$ $(k=5,6)$	$\Pi^C_{H\ 2}=\sum_e\Big\{-\int_{V^e}\Big[\frac{1}{2}\Delta\mathbf{T}\,..\,\mathbf{C}\,..\,\Delta\mathbf{T}+$ $+\Delta\mathbf{T}\,..\,\mathbf{A}_0(\mathbf{T}_0)\Big]dV+\int_{S^e}\mathbf{n}^e\cdot\mathbf{T}^e\cdot\tilde{\mathbf{u}}\,dS-$ $\int_{S^e_p}\bar{\mathbf{p}}\cdot\Delta\tilde{\mathbf{u}}\,dS\Big\}\quad(k=6)$
4	$\mathbf{n}\cdot\mathbf{T}=\mathbf{p}$ $x\in S_p$	$L^{C'}_{ci}=-\Pi^C_c+\Pi^C_{EV}+J^C_i$ $(i=1,\ldots,4)$	
5	$\mathbf{n}\cdot\mathbf{T}=\mathbf{p}$ $\tilde{\mathbf{u}}\in S_p$ $\tilde{\mathbf{u}}=\bar{\mathbf{u}}$ $x\in S_u$	$L^{C'}_{ck}=-\tilde{\Pi}^C_{c,k-4}+\Pi^C_{EV}+J^C_k$ $k=6$	$\Pi^C_{HS\ 3}=\sum_e\Big\{-\int_{V^e}\Big[\frac{1}{2}\Delta\mathbf{T}\,..\,\mathbf{C}\,..\,\Delta\mathbf{T}+$ $+\Delta\mathbf{T}\,..\,\mathbf{A}_0(\mathbf{T}_0)\Big]dV-\int_{V^e}[(V\cdot\mathbf{T}+\mathbf{q})\cdot$ $\cdot\Delta\mathbf{u}-V\cdot(\Delta\mathbf{T})\cdot\mathbf{u}_0]\,dV+\int_{S^e}\mathbf{n}^e\cdot\mathbf{T}^e\cdot$ $\cdot\tilde{\mathbf{u}}\,dS-\int_{S^e_p}\bar{\mathbf{p}}\cdot\Delta\tilde{\mathbf{u}}\,dS\Big\}$
6	$V\cdot(\Delta\mathbf{T})+\Delta\mathbf{q}=\mathbf{0}$ $x\in V$ $\mathbf{n}\cdot\Delta\mathbf{T}=\Delta\bar{\mathbf{p}}$ $x\in S_p$ continuity of $\mathbf{u}$ between the elements	$L^I_{ci}=-\Pi^I_c+J^I_i$ $(i=1,\ldots,4)$	$\Pi^I_{HS\ 1}=-\Pi^I_c+\sum_e\int_{S^e_p}\mathbf{u}\cdot$ $\cdot(\Delta\mathbf{T}^e\cdot\mathbf{n}^e-\Delta\lambda_1)\,dS\quad(i=1)$ $\Pi^I_{HS}=-\Pi^I_c+\sum_e\int_{S^e_p}\mathbf{n}^e\cdot\Delta\mathbf{T}^e\cdot\mathbf{u}\,dS$ $(i=2)$

Table II. cont.

Case	Stipulation	Functional	
		$\mathbf{h} \neq \mathbf{0}$	$\mathbf{h} = \mathbf{0}, \mathbf{t} = \mathbf{0}$
7	$V \cdot (\Delta\mathbf{T}) + \Delta\mathbf{q} = \mathbf{0}$ $x \in V$	$L^I_{ci} = -\Pi^I_c + \Pi^I_{ES} + J^I_i$ $(i = 1, \ldots, 4)$	$\Pi^I_{HS\,2} = -\sum_e \left\{ \int_{V_e} \left[\frac{1}{2} \Delta\mathbf{T} \,..\, \mathbf{C} \,..\, \Delta\mathbf{T} + \right.\right.$ $+ \Delta\mathbf{T} \,..\, \mathbf{A}_0(\mathbf{T}_0) + \mathbf{q}_0 \cdot \Delta\mathbf{u} -$ $\left. - \mathbf{T}_0 \,..\, \Delta\mathbf{A}(\Delta\mathbf{u}) \right] \mathrm{d}V - \int_{S_e} \mathbf{n} \cdot \Delta\mathbf{T} \cdot \mathbf{u} \,\mathrm{d}S +$ $+ \int_{S_p} \bar{\mathbf{p}} \cdot \Delta\mathbf{u} \,\mathrm{d}S \quad (i = 2)$ $\mathbf{u} = \bar{\mathbf{u}} \quad x \in S_u$ continuity of $\mathbf{u}$ between the elements
8	$V \cdot (\Delta\mathbf{T}) + \Delta\mathbf{q} = \mathbf{0}$ $x \in V$ $\tilde{\mathbf{u}} = \bar{\mathbf{u}}$ $x \in S_u$	$L^{I'}_{ck} = -\tilde{\Pi}^I_{c,k-4} + \tilde{\Pi}^I_{ES} + J^I_k$ $(k = 5,6)$	$\Pi^I_{HS-3} = -\sum_e \left\{ \int_{V_e} \left[\frac{1}{2} \Delta\mathbf{T} \,..\, \mathbf{C} \,..\, \Delta\mathbf{T} - \right.\right.$ $- \mathbf{T}_0 \,..\, \Delta\mathbf{A}(\Delta\mathbf{u}) + \mathbf{q}_0 \cdot \Delta\mathbf{u} + \Delta\mathbf{T} \,..$ $\left. .. \mathbf{A}_0(\mathbf{T}_0) \right] \mathrm{d}V + \int_{S^p_T} \bar{p} \cdot \Delta\tilde{\mathbf{u}} \,\mathrm{d}S$ $- \int_{S_e} [\mathbf{n} \cdot \Delta\mathbf{T} \cdot \tilde{\mathbf{u}} + \mathbf{n} \cdot \mathbf{T}_0 \cdot (\Delta\tilde{\mathbf{u}} - \Delta\mathbf{u})] \,\mathrm{d}S$
9	$\mathbf{n} \cdot (\Delta\mathbf{T}) = \Delta\bar{\mathbf{p}}$ $x \in S_p$	$L^{I'}_{ci} = \Pi^I_c + \Pi^I_{EV} + J^I_i$ $(i = 1, \ldots, 4)$	
10	$\mathbf{n} \cdot (\Delta\mathbf{T}) = \Delta\bar{\mathbf{p}}$ $x \in S_p$ $\tilde{\mathbf{u}} = \bar{\mathbf{u}}$ $x \in S_u$	$L^{I'}_{c.}\begin{bmatrix} k \\ l \\ m \end{bmatrix} = -\Pi^I_{c.}\begin{bmatrix} k-4 \\ l-6 \\ m-8 \end{bmatrix} + \Pi^I_{EV} + J^I\begin{bmatrix} k \\ l \\ m \end{bmatrix}$ $k = 5,6;\ l = 7,8;\ m = 9,10$	

4.5.2. Stationarity principles of modified complementary energy

Functionals of principles on condition $\mathbf{h} = \mathbf{t} = \mathbf{0}$ are seen in Table II, taking integral transformations according to Appendix 1 into consideration.

Principles relying on functionals $\Pi^C_{HS\,1}$, $\Pi^C_{HS\,2}$ and $\Pi^C_{HS\,3}$ correspond to the generalizations of hybrid stress models applied in the theory of linear elasticity by S. Atluri [2], T. H. H. Pian [3] and S. P. Wolf [4].

Among variational principles involving stipulations on stress increments $\Pi^I_{HS\,2}$, Π^I_{HS-3} suggested by T. H. H. Pian excel. $\Pi^I_{HS\,2}$ is obtained by assuming continuity of field $\mathbf{u}$ between elements, and kinematic BC to be satisfied, while $\Pi^I_{HS\,3}$ relies on the identity of $\tilde{\mathbf{u}}$ between elements.

Table III. Principles of stationarity of modified potential energy in the case of discontinuous fields

Stipulation		Functional	
		$\mathbf{h} \neq \mathbf{0}$	$\mathbf{h} = \mathbf{0}$
$\mathbf{A}_0 = \frac{1}{2}(\nabla \mathbf{u}_0 + \mathbf{u}_0 \nabla)$; $\Delta\mathbf{A} = \frac{1}{2}[\nabla(\Delta\mathbf{u}) + (\Delta\mathbf{u})\nabla]$ $x \in V$	$\mathbf{u} = \bar{\mathbf{u}}$ $x \in S_u$	L_{P1} L_{Pi} $(i = 2, \ldots, 4)$ if $\mathbf{u}^j - \mathbf{u}^e + \mathbf{h}^{ej} = \mathbf{0}$ then $L_P = \Pi_p + \Pi_{t2}$	$\Pi_{HD-1} = \Pi_p - \sum_e \int_{S_c^e} \boldsymbol{\lambda}_1 \cdot \mathbf{u}'' \, dS + \Pi_{t3}(\mathbf{u}')$ $\Pi_{NCD} = \Pi_p + \Pi_{t3}(\mathbf{u}') + \sum_{e,j} \int_{S_c^{ej}} \mathbf{n}^e \cdot \mathbf{T}^e \cdot (\mathbf{u}^j - \mathbf{u}^e)'' \, dS \quad (i = 2)$
	$\tilde{\mathbf{u}} = \bar{\mathbf{u}}$ $x \in S_u$	L_{Pk} $(k = 5, 6)$	$\Pi_{HD-2} = \Pi_p + \Pi_t(\tilde{\mathbf{u}}) + \sum_e \int_{S^e} \boldsymbol{\lambda}_1 \cdot (\tilde{\mathbf{u}} - \mathbf{u}^e) \, dS \quad (k = 5)$ $\Pi_{HD-3} = \Pi_p + \Pi_t(\tilde{\mathbf{u}}) + \sum_e \int_{S^e} \mathbf{n}^e \cdot \mathbf{T}^e \cdot (\tilde{\mathbf{u}} - \mathbf{u}^e) \, dS \quad (k = 6)$
	$\tilde{\mathbf{u}} = \bar{\mathbf{u}}$ $x \in S_u$	L_{Pl} $(l = 7, 8)$ L_{Pm} $(m = 9, 10)$	

4.5.3. Stationarity principles of modified potential energy

Substituting $\mathbf{h} = \mathbf{0}$, variational principles under 4.4 simple yield functionals of Table III

5. Analysis of non-frictional contact problems with unilateral connection

For the sake of simplicity, boundary value problem under 2 will be considered for $e = 1,2$. The contact range will be assumed to be exempt from outside load, to have a potential $\Pi_{t1} = 0$.

With notations in (2.6) to (2.16), fitting conditions are: Solids 1 and 2 may contact in range $S_c^{12} = S_c^{21} = \Omega$. Solids cannot interpenetrate in preferential direction $\mathbf{n}^1$ (Fig. 3), that is:

$$y \overset{\text{def}}{=} u_N^2 - u_N^1 + h \geqq 0 \qquad x \in \Omega \tag{5.1}$$

while the normal stress is:

$$\begin{aligned} &\sigma_N^1 \overset{\text{def}}{=} \mathbf{n}^1 \cdot \mathbf{T}^1 \cdot \mathbf{n}^1 = -p_N \leqq 0 && x \in S_c^1 \\ &\sigma_N^2 \overset{\text{def}}{=} -\mathbf{n}^1 \cdot \mathbf{T}^2 \cdot \mathbf{n}^2 = -p_N \leqq 0 && x \in S_c^2 \\ &\sigma_N^1 = \sigma_N^2 && x \in \Omega \end{aligned} \tag{5.2a–c}$$

and the shear stress because of exemptness of friction assumes the form

$$\tau^e = |\mathbf{p}_\tau^e| = |\mathbf{T}^e \cdot \mathbf{n}^e \mp \sigma_N^e \mathbf{n}^1| = 0 \quad e = \begin{cases} 1 \\ 2 \end{cases} \tag{5.3}$$

(Subsequently, contact pressure p_N will be denoted by p.)

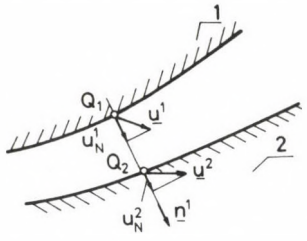

Fig. 3. Geometrical condition of contact. For $y \overset{\text{def}}{=} u_N^2 - u_N^1 + h = 0$ there is a contact, for $y > 0$, there is a gap, where $u_N^i = \mathbf{u}^i \cdot \mathbf{n}^1$ is the projection along normal $\mathbf{n}^1$ of the pair of points Q_1, Q_2; $\overline{Q_1 Q_2} = h$ — initial gap

At contact, at an arbitrary point of range Ω we have

$$y(x) \geq 0, \quad p(x) > 0 \quad x \in \Omega_p \tag{5.4}$$

with a gap:

$$y(x) \geqq 0, \quad p(x) \geq 0 \quad x \in \Omega_0 \tag{5.5}$$

that is:

$$yp = 0 \qquad x \in \Omega \tag{5.6}$$

Or else, for

$$y(x) < 0, \quad p(x) \geqq 0 \quad x \in \Omega'_p \tag{5.7}$$

there is a contact range, and for

$$y(x) > 0, \quad p(x) = 0 \quad x \in \Omega'_0 \tag{5.8}$$

there is a gap range.

Relationships $\Omega = \Omega_0 \cup \Omega_p$, $\Omega = \Omega'_0 \cup \Omega'_p$ hold, where Ω_0 and Ω_p, as well as Ω'_0 and Ω'_p are still unknown.

5.1. Discontinuity potentials for taking the unilateral connection into consideration

Obviously, in case of a non-frictional, bilateral connection along $\mathbf{n}^1$, $\boldsymbol{\lambda}_1(\mathbf{u}^2 - \mathbf{u}^1 + \mathbf{h})$ may be replaced by

$$(\lambda \mathbf{n}^1) \cdot (\mathbf{u}^2 - \mathbf{u}^1 + \mathbf{h}) = \lambda \cdot (u_N^2 - u_N^1 + h) = \lambda \cdot y$$

hence, in conformity with the discontinuity potential providing for kinematic FC:

$$\int_{\Omega} \lambda y \, dS \tag{5.9}$$

normal stress $\lambda = \mathbf{n}^1 \cdot \mathbf{T}^1 \cdot \mathbf{n}^1$.

For a unilateral connection, λ can only be a compressive stress, hence:

$$\lambda = -p \leqq 0 \quad (\boldsymbol{\lambda}_1 = -p\mathbf{n}^1).$$

Thus, in a frictionless contact problem, the discontinuity potential becomes:

$$J_1 \Rightarrow J^p = -\int_{\Omega} py \, dS \quad p \geqq 0 \quad x \in \Omega. \tag{5.10}$$

First variation of (5.9) under condition $p \geqq 0$:

$$-\int_{\Omega} \delta p \cdot y \, dS \leqq 0 \tag{5.11}$$

namely in range Ω_0, $\delta p \geqq 0$, while in range Ω_p, δp is arbitrary (under condition $p + \delta p \geqq 0$).

Another interpretation may be made of the discontinuity potential. Namely, let us approximate gap function y by a special field $\tilde{y}$.

Since $\tilde{y} \geqq 0$, $x \in \Omega$, in the contact range, because of $\delta\tilde{y} \geqq 0$, $-\int_{\Omega_p} \lambda \delta\tilde{y} \, dS \geqq 0$, and in the gap range, because of the arbitrary value of $\delta\tilde{y}$ (under condition $\tilde{y} + \delta\tilde{y} \geqq 0$), $\int_{\Omega_0} \lambda \delta\tilde{y} \, dS = 0$, that is:

$$-\int_{\Omega} \lambda \delta\tilde{y} \, dS \geqq 0, \quad \tilde{y} \geqq 0 \quad x \in \Omega. \tag{5.13}$$

Now, let us consider every variational principle in turn. Functionals involved in the principles are easy to produce by assigning bilateral connection functionals to discontinuity functionals (5.10) or (5.12).

5.2. Modified Reissner's variational principles for solving non-frictional contact problems

5.2.1. First principle:

In conformity with the variational principle relying on functional

$$L_R^p = \Pi_R(\Delta\mathbf{T}, \Delta\mathbf{u}) - \int_{\Omega} py(\mathbf{u}) \, dS = \Pi_R + J^p \tag{5.14}$$

obtained from L_{R1} by replacing J_1 according to (5.10), all fields $\Delta\mathbf{T}$, $\Delta\mathbf{u}$ and p meeting variational equation—inequality

$$\delta_{\Delta\mathbf{T}} L_R^p = 0, \quad \delta_{\Delta\mathbf{u}} L_R^p = 0, \quad \delta_p L_R^p \leqq 0 \tag{5.15a–c}$$

for $p \geqq 0$, correspond to real fields. Functionals equivalent to L_R^p may be produced by C- and I-type transformations of L_{Ri}.

Since in frictionless unilateral connections we have

$$\boldsymbol{\lambda}_1 = -p\mathbf{n}^1, \quad p \geqq 0, \quad x \in \Omega \tag{5.16}$$

substituting $\mathbf{t}^{ej} = \mathbf{0}$ into L_{R1}^C in (4.13) for $e=1$, $j=2$ and reminding (4.15) where $J_1 = J^p$, the new functional becomes

$$\begin{aligned} L_{R1}^C \Rightarrow L_R^{Cp} &= -\Pi_c^C + \Pi_E^C + J^p + \sum_e \int_{S_c^e} (\mathbf{n} \cdot \mathbf{T} \cdot \Delta\mathbf{u} + \mathbf{n} \cdot \Delta\mathbf{T} \cdot \mathbf{u}_0)\, dS = \\ &= -\Pi_c^C + \Pi_E^C - \int_\Omega \{ph + (p+\sigma_N^2)\Delta u_N^2 - (\sigma_N^1 + p)\Delta u_N^1 \\ &\quad + (p + \Delta\sigma_N^2)u_{N,0}^2 - (p + \Delta\sigma_N^1)u_{N,0}^1\}\, dS \\ &\quad + \sum_e \int_{S_c^e} (\mathbf{n}^e \cdot \mathbf{T}^e \cdot \Delta\mathbf{u}_\tau^e + \mathbf{n}^e \cdot \Delta\mathbf{T}^e \cdot \mathbf{u}_{\tau,0}^e)\, dS \end{aligned} \tag{5.17a}$$

where decomposition $\mathbf{u}^e = u_N^e \mathbf{n}^1 + \mathbf{u}_\tau^e$ of the displacement field has also been used.

Introducing notation $\mathbf{n}^e \cdot \mathbf{T}^e \cdot \mathbf{u}_\tau^e = \tau^e u_\tau^e$ (work density of shear stress τ along tangential displacement normal to $\mathbf{n}^1$) and adding a term to be considered as constant for variation, the obtained functional may be written more concisely:

$$\begin{aligned} L_R^{Cp} &= -\Pi_c^C + \Pi_E^C + \sum_e \int_{S_c^e} \tau^e u_\tau^e\, dS - \\ &\quad - \int_\Omega \{ph + (p+\sigma_N^2)u_N^2 - (p+\sigma_N^1)u_N^1\}\, dS \end{aligned} \tag{5.17b}$$

showing fields u_N^e to act as Lagrangian factors to satisfy condition $p = -\sigma_N^e$.

Transformations similar to that for functional L_{R1}^I lead—omitting details—to the form:

$$L_{R1}^I \Rightarrow L_R^{Ip} = -\Pi_c^I + \Pi_E^I + \sum_e \int_{S_c^e} \mathbf{n} \cdot \Delta\mathbf{T} \cdot \mathbf{u}\, dS + J^p \tag{5.18}$$

Variational equations—inequalities assignable to functionals L_R^{Cp}, L_R^{Ip} are the same as for L_R^p.

Solution of variational equation (5.15b) being $-p = \sigma_N^1$, $-p = \sigma_N^2$, replacement of $-p$ by σ_N^1 or σ_N^2 permits us to formulate the following principle, also derivable from L_{R2}.

5.2.2. Second principle:

Fields satisfying variational equation—inequality $\delta_{\mathbf{u}} L_R^{\sigma} = 0$, $\delta_{\Delta \mathbf{T}} L_R^{\sigma} \leqq 0$ obtained from functional

$$L_{R2} \Rightarrow L_R^{\sigma} = \Pi_R(\Delta \mathbf{T}, \Delta \mathbf{u}) + \begin{Bmatrix} \int_{\Omega} \sigma_N^1 y \, \mathrm{d}S \\ \int_{\Omega} \sigma_N^2 y \, \mathrm{d}S \end{Bmatrix} \tag{5.19}$$

under condition

$$\sigma_N^1 \leqq 0 \quad \text{or} \quad \sigma_N^2 \leqq 0 \quad x \in \Omega \tag{5.20a, b}$$

correspond to real fields.

Just like for the first principle, functionals belonging to C- or I-type transformations are of the form:

$$\left.\begin{matrix} L_{R2}^C \\ L_{R3}^C \end{matrix}\right\} \Rightarrow L_R^{C\sigma} = -\Pi_E^C + \Pi_c^C + \sum_e \int_{S_c^e} (\mathbf{n} \cdot \mathbf{T} \cdot \Delta \mathbf{u} + \mathbf{n} \cdot \Delta \mathbf{T} \cdot \mathbf{u}_0) \, \mathrm{d}S +$$

$$+ \begin{Bmatrix} \int_{\Omega} \sigma_N^1 y \, \mathrm{d}S \\ \int_{\Omega} \sigma_N^2 y \, \mathrm{d}S \end{Bmatrix} =$$

$$= -\Pi_c^C + \Pi_E^C + \begin{Bmatrix} \int_{\Omega} [\sigma_N^1 h + (\sigma_N^1 - \sigma_N^2) u_N^2] \, \mathrm{d}S \\ \int_{\Omega} [\sigma_N^2 h + (\sigma_N^1 - \sigma_N^2) u_N^1] \, \mathrm{d}S \end{Bmatrix} +$$

$$+ \sum_e \int_{S_c^e} \tau^e u_\tau^e \, \mathrm{d}S + \text{const} \qquad \left(5.21 \begin{Bmatrix} \text{a} \\ \text{b} \end{Bmatrix}\right)$$

$$\left.\begin{matrix} L_{R2}^I \\ L_{R3}^I \end{matrix}\right\} \Rightarrow L_R^{I\sigma} = -\Pi_c^I + \Pi_E^I + \sum_e \int_{S_c^e} \mathbf{n} \cdot \Delta \mathbf{T} \cdot \mathbf{u} \, \mathrm{d}S$$

$$+ \begin{Bmatrix} \int_{\Omega} \sigma_N^1 y \, \mathrm{d}S \\ \int_{\Omega} \sigma_N^2 y \, \mathrm{d}S \end{Bmatrix} = -\Pi_c^I + \Pi_E^I +$$

$$+ \begin{Bmatrix} \int_{\Omega} [\Delta \sigma_N^1 h + \sigma_{N,0}^1 (u_N^2 - u_N^1 + h) + u_N^2 (\Delta \sigma_N^1 - \Delta \sigma_N^2)] \, \mathrm{d}S \\ \int_{\Omega} [\Delta \sigma_N^2 h + \sigma_{N,0}^2 (u_N^2 - u_N^1 + h) + u_N^1 (\Delta \sigma_N^1 - \Delta \sigma_N^2)] \, \mathrm{d}S \end{Bmatrix} +$$

$$+ \sum_e \int_{S_c^e} \tau^e u_\tau^e \, \mathrm{d}S \qquad \left(5.22 \begin{Bmatrix} \text{a} \\ \text{b} \end{Bmatrix}\right)$$

Correct results are preconditioned by the *a priori* satisfying of conditions $\sigma_N^1 \leqq 0$, and $\sigma_N^2 \leqq 0$, in cases a), and b), respectively.

5.2.3. Third principle:

Obviously, if conddition $\sigma_N^1 = \sigma_N^2 = \sigma_N \; x \in \Omega$ holds, functional $L_R^{C\sigma}$ (5.21) yields functional

$$L_R^{C\sigma'} = -\Pi_c^C(\Lambda\mathbf{T}) + \Pi_E^C + \sum_{e=1}^{2} \int_{\Omega} \tau^e u_\tau^e \, \mathrm{d}S + \int_{\Omega} \sigma_N h \, \mathrm{d}S \tag{5.23}$$

In conformity with the variational principle, equation—inequality

$$\delta_{\Lambda\mathbf{u}} L_R^{C\sigma'} = 0, \quad \delta_{\Lambda\mathbf{T}} L_R^{C\sigma'} \leqq 0$$

holds only, alongside with condition $\sigma_N \leqq 0 \; x \in \Omega$ if the fields are real ones.

5.2.4. Fourth principle.

Above, positivity of stresses p or $-\sigma_N^e$ provided for contact – gap conditions inside range Ω. Provided fulfilment of condition $y = u_N^2 - u_N^1 + h \geqq 0 \; x \in \Omega$ is required, it is sufficient to take variation of functional $\Pi_R(\Lambda\mathbf{T}, \Lambda\mathbf{u})$ according to:

$$\delta_{\Lambda\mathbf{T}} \Pi_R = 0, \quad \delta_{\Lambda\mathbf{u}} \Pi_R \geqq 0, \quad y \geqq 0, \quad x \in \Omega \tag{5.25a, b}$$

(5.25) being satisfied by the real fields.

5.2.5. Fifth principle.

In addition to the first principle, further hybrid variational principles may be set up, namely, by assuming one or two fields missing from the original boundary value problem. Let the positivity of one of the fields *a priori* provided, the other be a simple Lagrangian factor. Let the former be gap $\tilde{y}$ arising in deformation, the other the normal stress in range Ω. The new functional to be varied becomes:

$$L_R^{y\lambda} = \Pi_R(\Lambda\mathbf{T}, \Lambda\mathbf{u}) + \int_{\Omega} \lambda \cdot (u_N^2 - u_N^1 + h - \tilde{y}) \, \mathrm{d}S \tag{5.26}$$

yielding all free equations according to the variational equation—inequality:

$$\begin{aligned} &\delta_{\Lambda\mathbf{T}, \Lambda\mathbf{u}, \lambda} \, L_R^{y\lambda} = 0 \\ &\delta_{\tilde{y}} L_R^{y\lambda} \geqq 0, \quad \tilde{y} \geqq 0 \quad x \in \Omega \end{aligned} \tag{5.27a, b}$$

Upon C- and I-type transformations, functionals equivalent to $L_R^{y\lambda}$ become:

$$L_R^{Cy\lambda} = -\Pi_c^C + \Pi_E^C + \int_\Omega \lambda(y-\tilde{y})\,\mathrm{d}S + \\ + \sum_e \int_{S_c^e} (\mathbf{n}\cdot\mathbf{T}\cdot\Delta\mathbf{u} + \mathbf{n}\cdot\Delta\mathbf{T}\cdot\mathbf{u}_0)\,\mathrm{d}S \tag{5.28}$$

$$L_R^{Iy\lambda} = -\Pi_c^I + \Pi_E^I + \int_\Omega \lambda(y-\tilde{y})\,\mathrm{d}S + \\ + \sum_e \int_{S_c^e} \mathbf{n}\cdot\Delta\mathbf{T}\cdot\mathbf{u}\,\mathrm{d}S \tag{5.29}$$

In conformity with the variational principle, real fields satisfy (5.27).

5.2.6. *Sixth principle*

This principle results from the former one by substituting $\sigma_N^e (e=1,\ 2)$ for λ. Functionals to be varied are:

$$L_R^y = \Pi_R(\Delta\mathbf{T}, \Delta\mathbf{u}) + \begin{Bmatrix} \int_\Omega \sigma_N^1(u_N^2 - u_N^1 + h - \tilde{y})\,\mathrm{d}S \\ \int_\Omega \sigma_N^2(u_N^2 - u_N^1 + h - \tilde{y})\,\mathrm{d}S \end{Bmatrix} \qquad \left(5.30\left\{\begin{matrix}\mathrm{a} \\ \mathrm{b}\end{matrix}\right\}\right)$$

$$L_R^{Cy} = L_R^{Cy\lambda}(\lambda=\sigma_N^2); \quad L_R^{Iy} = L_R^{Iy\lambda}(\lambda=\sigma_N^e) \tag{5.31a, b}$$

Fields satisfying variational equation—inequality

$$\delta_{\Delta\mathbf{T},\,\Delta\mathbf{u}} L_R^{Ay} = 0; \quad \delta_{\tilde{y}} L_R^{Ay} \geqq 0, \quad \tilde{y} \geqq 0 \quad x \in \Omega \tag{5.32a, b}$$

correspond to real fields. ($A = C,\ I$).

5.2.7. *Some comments*

5.2.7.1. According to the variational principles above, a non-negativity condition is prescribed for full-valued contact pressure or gap in range S_c^e, although values marked $(\ )_0$ in the state before load increment are known. One point of importance is that contact and gap conditions refer to the full value rather than to the increments (see (5.4) to (5.8)).

Provided with increasing load the contact range extends:

$$\int_\Omega py\,\mathrm{d}S = \int_\Omega (p_0 + \Delta p)(y_0 + \Delta y)\,\mathrm{d}S = \int_\Omega \Delta py\,\mathrm{d}S \tag{5.32}$$

since $p_0 y_0 = 0\ x \in \Omega$, $p_0 \Delta y = 0\ x \in (\Omega_0)_0$ thus, $\Delta p = p$ in range $\Omega_p - (\Omega_p)_0 = \Delta\Omega_p$ (see Fig. 4).

Thus, for an extending contact range, $\Delta p \geqq 0$ may be assumed, hence it is sufficient to take the contact pressure increment.

On the other hand, non-negativity of fields y and $\tilde{y}$ in principle 4 to 6 cannot be replaced by inequalities $\Delta y \geqq 0$ and $\Delta \tilde{y} \geqq 0$; they unfortunately do not hold for extending Ω_p.

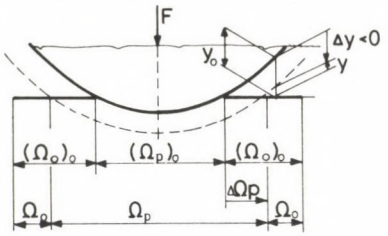

Fig. 4. Illustration of an "extending" contact range

5.2.7.2. In practical computations, approximation of contact pressure safeguarding its non-negativity is simplest made according to the first principle by finite element approximation of field p, and according to the fourth principle, by checking condition $y \geqq 0$ in a finite number of points.

5.3. Stationary principles of modified complementary energy for the analysis of frictionless contact problems

Functionals belonging to the respective variational principles are easy to derive from functionals L_R^C and L_R^I under item 5.2, taking stipulations on tensor fields $\mathbf{T}$ and $\Delta\mathbf{T}$ into consideration. Stipulations and their consequences have been compiled in Table IV.

Table IV

Field	Stipulation		Consequence
$\mathbf{T}^e$	$V \cdot \mathbf{T}^e + \mathbf{q}^e = \mathbf{0}$	$x \in V^e$	$II_{EV}^C = 0$
	$\mathbf{n}^e \cdot \mathbf{T}^e = \bar{\mathbf{p}}$	$x \in S_p^e$	$II_{ES}^C = 0$
	$\tau^e = 0$	$x \in S_c^e$	$\int_\Omega \tau^e u_t^e \, dS = 0$
$\Delta\mathbf{T}^e$	$V \cdot (\Delta\mathbf{T}^e) + \Delta\mathbf{q}^e = \mathbf{0}$	$x \in V^e$	$II_{EV}^I = 0$
	$\mathbf{n}^e \cdot \Delta\mathbf{T}^e = \Delta\bar{\mathbf{p}}$	$x \in S_p^e$	$II_{ES}^I = 0$
	$\tau^e = 0$	$x \in S_c^e$	$\int_\Omega \tau^e u_t^e \, dS = 0$

Now, no difficulties arise in producing functionals $L_c^{C\cdot}$ and $L_c^{I\cdot}$ from functionals $L_R^{C\cdot}$ and $L_R^{I\cdot}$, respectively. For instance, **T** meets stipulations in Table IV for functional

$$L_R^{Cp} \Rightarrow L_c^{Cp} = -\Pi_c^C - \int_\Omega [ph + (p+\sigma_N^2)u_N^2 - (p+\sigma_N^1)u_N^1]\,\mathrm{d}S \tag{5.33}$$

Writing of the other functionals will be dispensed with.

5.4. Stationary principles of the modified potential energy for the analysis of frictionless contact problems

Requiring field **u** to satisfy the kinematic boundary condition, and considering relationship between **T** and **A** to hold through Hooke's law, simple transformations of the modified Reissner principles yield the following functionals.

5.4.1. First principle

Fields meeting the variational equation-inequality

$$\delta_{\Delta\mathbf{u}} L_P^p = 0, \quad \delta_p L_P^p \leqq 0, \quad p \geqq 0 \quad x \in \Omega \tag{5.34a, b}$$

assigned to functional

$$L_R^p \Rightarrow L_P^p = \Pi_p(\Delta\mathbf{u}) - \int_\Omega py\,\mathrm{d}S \tag{5.35}$$

are real fields.

5.4.2. Second principle

Provided condition $y \geqq 0 \quad x \in \Omega$ is satisfied, all fields $\mathbf{u}^e$ meeting variational inequality $\delta_{\Delta\mathbf{u}} \Pi_p \geqq 0$ correspond to real fields.

5.4.3. Third principle

In conformity with the principle based on functional

$$L_P^{y\lambda} = \Pi_p(\Delta\mathbf{u}) - \int_\Omega \lambda(y - \tilde{y})\,\mathrm{d}S \tag{5.36}$$

derived from functional $L_R^{y\lambda}$, variational equations-inequalities

$$\delta_{\Delta\mathbf{u},\lambda} L_P^{y\lambda} = 0, \quad \delta_{\tilde{y}} L_P^{y\lambda} \geqq 0, \quad \tilde{y} \geqq 0 \quad x \in \Omega \tag{5.37a, b}$$

hold for real fields.

5.4.4. Fourth principle

For functional

$$L_P^y = \Pi_p(\Delta \mathbf{u}) - \int_\Omega \sigma_N^e(\mathbf{u}^e) \cdot (y - \tilde{y})\, \mathrm{d}S \tag{5.37}$$

obtained from the former one by substituting $\lambda = \sigma_N^e(\mathbf{u}^e)$, we have

$$\delta_{\Delta \mathbf{u}} L_P^y = 0, \quad \delta_{\tilde{y}} L_P^y \geqq 0, \quad \tilde{y} \geqq 0 \quad x \in \Omega\,. \tag{5.38a, c}$$

5.4.5. Remark.
5.2.7.1 and 5.2.7.2 are valid for the above in principle.

6. Solution of the contact problem of a system of elasto-plastic solids by the method of initial stresses

Examination of incremental variational principles in preceding chapters aimed at the analysis of a system of elasto-plastic solids.

In the finite element method applied for solving non-linear problems, the incremental procedure (step-wise load applications) is known to be applied by determining (1) tangential rigidities, (2) initial deformations, or (3) initial stresses. In the first case, rigidity matrix of the system is modified in conformity with the elastoplastic condition developing in the load increment, while in both latter cases, only the complementary, fictitious load corresponding to the developing plastic range has to be determined, without modifying the rigidity matrix for the elastic system. Zienkiewicz, O. C. et al. [5] were the first who suggested the method of incremental initial stresses in analyses relying on the principle of virtual work. Computation based on modified complementary energy has been presented by Spilker, R. L. and Pian, T. H. H. [6], and by Spilker, R. L. and Munir, N. I. [7], with favourable computational findings.

Non-linear stress-strain function $\sigma - \varepsilon$ for a one-dimensional case is seen in Fig. 5. Point P representing the stress state would proceed along a straight line of slope E starting from point K at load step $(i-1)$ if the system could be considered as elastic. Since, in fact, an elasto-plastic condition develops, stress at P differs from that of Q belonging to increment $\Delta\varepsilon$. Hence a fictitious stress σ_f between them has to be reckoned with, namely the real stress increment corresponds to stress increment $\Delta\sigma_{ep}$ in the elasto-plastic condition. Thereby, generalizing the one-dimensional case in the figure, by the end of load increment, the stress tensor becomes:

$$\mathbf{T} = \mathbf{T}_0 + \Delta\mathbf{T}' - \mathbf{T}_f$$

that is, for functionals belonging to subsequent variational principles,

$$\mathbf{T}_0 \Rightarrow \mathbf{T}_0 - \mathbf{T}_f \tag{6.1}$$

$$\Delta\mathbf{T} \Rightarrow \Delta\mathbf{T}' \tag{6.2}$$

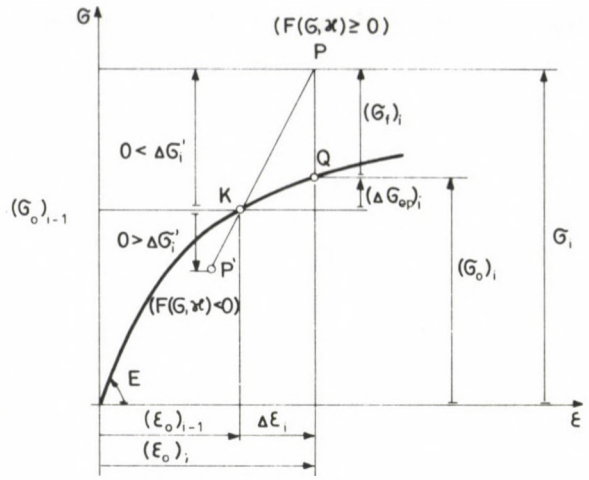

Fig. 5. Description of the initial stress method in a linear case. $(\ )_i$ is the value determined in load increment i

have to be substituted, because in variational principles the increment effect has been considered linear. Substitutions also imply $\mathbf{T}_0$ and $\mathbf{T}_f$ to be considered as given within the load increment, and only $\Lambda\mathbf{T}'$ to be subject to variation.

Two of the discussed variational principles will be examined in detail for practical applications.

6.1. Frictionless contact problem solved by a computation method based on modified complementary energy

Let us start from functional L_R^{Ip} in (5.18) substituting(6.1) and (6.2) into (5.18) and satisfying equilibrium equation

$$V \cdot (\Lambda\mathbf{T}) + \Lambda\mathbf{q} = \mathbf{0} \quad x \in V \tag{6.3}$$

and taking the field $\mathbf{u}$ which fulfils the kinematic boundary condition, we arrive at

$$\begin{aligned} L_R^{Ip} \Rightarrow L_C^{Ip} = \sum_e \Bigg\{ & - \int_{V^e} \left(\frac{1}{2}\, \Lambda\mathbf{T}' \,..\mathbf{C}\,..\Lambda\mathbf{T}' + \mathbf{T}_f \,..\Lambda\mathbf{A}(\Lambda\mathbf{u}) \right) \mathrm{d}V \\ & + \int_{V^e} \Lambda\mathbf{T}' \,..[\mathbf{A}_0(\mathbf{u}_0) - \mathbf{A}_0(\mathbf{T}_0)]\, \mathrm{d}V \\ & - - - - - - - - - - - - - - - - - - \\ & + \int_{S^e} \mathbf{n} \cdot \Lambda\mathbf{T}' \cdot \Lambda\mathbf{u}\, \mathrm{d}S - \int_{S_p^e} \Lambda\bar{\mathbf{p}} \cdot \Lambda\mathbf{u}\, \mathrm{d}S \\ & + \int_{V^e} [\mathbf{T}_0 \,..\Lambda\mathbf{A}(\Lambda\mathbf{u}) - \mathbf{q}_0 \cdot \Lambda\mathbf{u}]\, \mathrm{d}V - \int_{S_p^e} \bar{\mathbf{p}}_0 \cdot \Lambda\mathbf{u}\, \mathrm{d}S \Bigg\} \\ & - \int_{\Omega} p \cdot (u_N^2 - u_N^1 + h)\, \mathrm{d}S \end{aligned} \tag{6.4}$$

Since according to the variational principle, load increment

$$\Delta\mathbf{A}(\Delta\mathbf{u})=\mathbf{C}\,..\,\Delta\mathbf{T}'$$

at the beginning of load increment i,

$$\begin{aligned}\mathbf{A}_0(\mathbf{u}_0)_i &= \mathbf{A}_0(\mathbf{u}_0)_{i-1}+\Delta\mathbf{A}(\Delta\mathbf{u})_i \\ &= \mathbf{A}_0(\mathbf{T}_0)_{i-1}+(\mathbf{C}\,..\,\Delta\mathbf{T}')_i=\mathbf{A}_0(\mathbf{T}_0)_i \qquad i=1,2,\ldots \\ \mathbf{A}_0(\mathbf{u}_0)_{i=0} &= \mathbf{A}_0(\mathbf{T}_0)_{i=0}=0\,,\end{aligned}$$

that is, $\mathbf{A}_0(\mathbf{u}_0)_i$ and $\mathbf{A}_0(\mathbf{T}_0)_i$ are identical, causing integral underlined in dash line to vanish. The obtained functional without an integral over range is denoted as Π^{II}_{mc} in [1], and considered, according to computational observations confronting accuracies and running times, as superior to results obtained either with a model for

$$\Delta\mathbf{T}'-\mathbf{T}_f=\Delta\mathbf{T}$$

satisfying equilibrium equation

$$\nabla\cdot(\Delta\mathbf{T})+\Delta\mathbf{q}=\mathbf{0}\quad x\in V$$

or by the finite element model applying compatible elements.

6.1.1. Stating the problem of finite dimensions

Local approximation by applying the finite element method is convenient for fields arising in a system of two solids.

Assuming a spatial problem, vector $\boldsymbol{\sigma}$ type (6, 1) comprising stress tensor $\mathbf{T}$ in solid α is approximated as:

$$\mathbf{T}^{\alpha}\Rightarrow\boldsymbol{\sigma}^{\alpha}(x)=\sum_{i=1}^{n_\alpha}\mathbf{S}^{\alpha}_i(x)\mathbf{s}^{\alpha}_i=\underset{(6,\,n_\alpha)}{\mathbf{S}^{\alpha}(x)}\ \underset{(n_\alpha,\,1)}{\mathbf{s}^{\alpha}} \tag{6.5}$$

where $\mathbf{S}^{\alpha}(x)$—approximation matrix, and $\mathbf{s}^{\alpha}$—vector of constants. The adopted approximation has to satisfy equilibrium equation (6.3). Approximation (6.5) is composed of approximations separately interpreted of each of the E_α elements making up solid α. An element α_e may be approximated as:

$$\boldsymbol{\sigma}^{\alpha_e}(x)=\mathbf{S}^{\alpha_e}(x)\mathbf{s}^{\alpha_e}. \tag{6.6}$$

Element surface stresses are approximated as:

$$\mathbf{n}^{\alpha_e}\cdot\mathbf{T}^{\alpha_e}\Rightarrow\mathbf{R}^{\alpha_e}(x)\mathbf{s}^{\alpha_e}. \tag{6.7}$$

The remaining fields in the event of a displacement field are approximated as:

$$\mathbf{u}^{\alpha}(x)=\sum_{i=1}^{m_\alpha}\mathbf{U}^{\alpha}_i(x)\mathbf{u}^{\alpha}_i=\underset{(3,\,m_\alpha)}{\mathbf{U}^{\alpha}(x)}\ \underset{(m_\alpha,\,1)}{\mathbf{u}^{\alpha}}+\delta^{\alpha}_1\mathbf{U}_R(x)\mathbf{u}_R \tag{6.8a}$$

or for element α_e:

$$\mathbf{u}^{\alpha_e}(x)=\mathbf{U}^{\alpha_e}(x)\mathbf{u}^{\alpha_e}+\delta^{\alpha}_1\mathbf{U}^{\alpha_e}_R(x)\mathbf{u}_R \tag{6.8b}$$

its value at the boundary of finite element e being:

$$\mathbf{u}^{\alpha_e}(x)=\mathbf{L}^{\alpha_e}(x)\mathbf{u}^e+\delta_1^\alpha\,\mathbf{L}_R^{\alpha_e}(x)\mathbf{u}_R \tag{6.9}$$

and normal displacement imposed on range Ω:

$$u_N^\alpha=u_N^\alpha(x)=\hat{\mathbf{N}}^\alpha(x)\mathbf{u}^\alpha+\delta_1^\alpha\hat{\mathbf{N}}_R^\alpha(x)\mathbf{u}_R \tag{6.10}$$

δ_1^α being the Kronecker symbol ($\alpha=1,\ \delta_1^1=1;\ \alpha=2,\ \delta_1^2=0$).

Vector $\boldsymbol{\varepsilon}(x)$ type (6, 1) composed of the strain tensor field belonging to the displacement field is:

$$\mathbf{A}^\alpha\Rightarrow\underset{(6,1)}{\boldsymbol{\varepsilon}^\alpha(x)}=\mathbf{D}_\varepsilon\mathbf{u}^\alpha(x)=\mathbf{D}_\varepsilon\mathbf{U}^\alpha(x)\mathbf{u}^\alpha=\underset{(6,\,m_\alpha\,(m_\alpha,\,1)}{\mathbf{B}(x)}\ \mathbf{u}^\alpha \tag{6.11}$$

The contact pressure is approximated as:

$$p=p(x)=\mathbf{P}^t(x)\mathbf{p}\quad x\in\Omega$$

In conformity with assumptions, solid 2 cannot, but solid 1 can do rigid-body motion. Skew symmetrical parts of field $\hat{\mathbf{u}}^1(x)=\mathbf{U}^1(x)\mathbf{u}^1$ and of the pertaining derivate tensor field $(\nabla\hat{\mathbf{u}}^1(x))$ in (6.8) have to be zero at an arbitrary point $x=x_0$ of the solid, at the same time displacement and angular rotation at x_0 correspond to elements of vector $\mathbf{u}_R$ in term $\mathbf{U}_R^1(x)\mathbf{u}_R$ describing rigid-body motion. Now, the number of coordinates describing displacement of solid 1 is m_1+d_1 where d_1 is the degree of freedom of the rigid-body motion of solid 1.

Fictitious stresses $\mathbf{T}_f$ and $\mathbf{T}_0$ are replaced by (6, 1)-type vectors $\boldsymbol{\sigma}_f$ and $\boldsymbol{\sigma}_0$, respectively; while fourth-order tensor of material constants $\mathbf{C}$ is interpreted as a matrix type (6, 6).

Making use of matrices and vectors (t sign of transpose)

$$\tilde{\mathbf{H}}^{\alpha_e}=\int_{V^{\alpha_e}}\mathbf{S}^t\mathbf{C}\mathbf{S}\,\mathrm{d}V,\ 1_e=1,\ldots,E_1;\ 2_e=1,\ldots,E_2,$$

$$\mathbf{G}_1^{\alpha_e}=\int_{S^{\alpha_e}}\mathbf{R}^t\mathbf{L}\,\mathrm{d}S,\ \mathbf{G}_2^{1_e}=\int_{S^{1_e}}\mathbf{R}^t\mathbf{L}_R\,\mathrm{d}S=\mathbf{0}$$

$$\mathbf{F}_0^{\alpha_e}=\int_{V^{\alpha_e}}\mathbf{B}^t\boldsymbol{\sigma}_0\,\mathrm{d}V,\ \mathbf{F}_f^{\alpha_e}=\int_{V^{\alpha_e}}\mathbf{B}^t\boldsymbol{\sigma}_f\,\mathrm{d}V$$

$$\Delta\mathbf{Q}^{\alpha_e}=\int_{S_p^{\alpha_e}}\mathbf{L}^t\Delta\bar{\mathbf{p}}\,\mathrm{d}S,\ \Delta\mathbf{Q}_R^{1_e}=\int_{S_p^{1_e}}\mathbf{L}_R^t\Delta\bar{\mathbf{p}}\,\mathrm{d}S$$

$$\mathbf{Q}_{R,0}^{1_e}=\int_{S_p^{1_e}}\mathbf{L}_R^t\bar{\mathbf{p}}_0\,\mathrm{d}S+\int_{V^{1_e}}\mathbf{U}_R^t\mathbf{q}_0\,\mathrm{d}V$$

$$\mathbf{N}=[\mathbf{N}^2,-\mathbf{N}^1],\ \mathbf{h}=\int_\Omega\mathbf{P}h\,\mathrm{d}S,\ \mathbf{u}^t=[\mathbf{u}^{1t},\mathbf{u}^{2t}]$$

$$\mathbf{N}^\alpha=\int_{\substack{\Omega\\(S_c^\alpha)}}\mathbf{P}\hat{\mathbf{N}}\,\mathrm{d}S,\ \mathbf{G}_R=\int_\Omega\mathbf{P}\hat{\mathbf{N}}_R^1\,\mathrm{d}S,$$

we arrive at

$$L_C^{Ip} \Rightarrow L_1 = \sum_{e=1}^{E_1+E_2} \left\{ -\frac{1}{2} \Delta \mathbf{s}^{e,t} \tilde{\mathbf{H}}^e \Delta \mathbf{s}^e - \Delta \mathbf{u}^{e,t} \mathbf{F}_f^e + \right.$$

$$\left. + \Delta \mathbf{s}^{e,t} \mathbf{G}_1^e \Delta \mathbf{u}^e + \Delta \mathbf{u}^{e,t} (\mathbf{F}_0^e - \Delta \mathbf{Q}^e - \mathbf{Q}_0^2) \right\} -$$

$$- \mathbf{p}^t [\mathbf{N}\mathbf{u} - \mathbf{G}_R \mathbf{u}_R + \mathbf{h}] - \sum_{e=1}^{E_1} \Delta \mathbf{u}_R^t (\Delta \mathbf{Q}_R + \mathbf{Q}_{R,0})^e \tag{6.13}$$

In conformity with equation $\delta_{\Delta \mathbf{T}}$, $L_C^{Ip} = 0$, substituting derivative with respect to element-wise independent $\Delta \mathbf{s}^e$:

$$\Delta \mathbf{s}^e = (\tilde{\mathbf{H}}^e)^{-1} \mathbf{G}_1^e \Delta \mathbf{u}^e \tag{6.14}$$

into (6.13) we find

$$L_1 = \sum_{e=1}^{E_1+E_2} \left\{ \frac{1}{2} \Delta \mathbf{u}^{e,t} \tilde{\mathbf{K}}^e \Delta \mathbf{u}^e + \Delta \mathbf{u}^{e,t} (\mathbf{F}_0 - \mathbf{Q}_0 - \mathbf{F}_f - \Delta \mathbf{Q})^e \right\}$$

$$- \mathbf{p}^t [\mathbf{N}\mathbf{u} - \mathbf{G}_R \mathbf{u}_R + \mathbf{h}] - \Delta \mathbf{u}_R^t \sum_{e=1}^{E_1} (\Delta \mathbf{Q}_R + \mathbf{Q}_{R,0})^e \tag{6.15}$$

where $\tilde{\mathbf{K}}^e = (\mathbf{G}_1^t \tilde{\mathbf{H}}^{-1} \mathbf{G}_1)^e$ is rigidity matrix of element e; $\Delta \mathbf{Q}$ is the load increment on the element; $\Delta \mathbf{Q}_R$, $\mathbf{Q}_{R,0}$ are vectors composed of the pair of vectors of external load increment, and of the initial value of load increment reduced to point x_0; $\mathbf{R}_0 = \mathbf{Q}_0 - \mathbf{F}_0$ is (residual) load to correct disequilibrium. Connecting elements in the usual way—field $\mathbf{u}(x)$ is continuous throughout the solid—results in the function of the form:

$$L_1 = \frac{1}{2} \Delta \mathbf{u}^t \mathbf{K} \Delta \mathbf{u} - \Delta \mathbf{u}^t (\mathbf{R}_0 + \mathbf{F}_f + \Delta \mathbf{Q})$$

$$- \mathbf{p}^t (\mathbf{N}\mathbf{u} - \mathbf{G}_R \mathbf{u}_R + \mathbf{h}) - \Delta \mathbf{u}_R^t (\Delta \mathbf{Q}_R + \mathbf{Q}_{R,0}) \tag{6.16}$$

where $\mathbf{K}$ is rigidity matrix of the composed system. The two solids being independent, $\mathbf{K} = \langle \mathbf{K}^1, \mathbf{K}^2 \rangle$ is a quasi-diagonal matrix.

In conformity with variational equation—inequality (5.15b, c) referring to functional $L_R^{Ip} \Rightarrow L_C^{Ip}$ (5.18)⇒(6.4) we have

$$\delta_{\Delta \mathbf{u}} L_C^{Ip} = 0 \Rightarrow \delta (\Delta \mathbf{u})^t \frac{\partial L_1}{\partial \Delta \mathbf{u}} = \mathbf{0} \Rightarrow \frac{\partial L_1}{\partial \Delta \mathbf{u}} = 0 \tag{6.17a}$$

$$\delta (\Delta \mathbf{u}_R)^t \frac{\partial L_1}{\partial \Delta \mathbf{u}_R} = 0 \Rightarrow \frac{\partial L_1}{\partial \Delta \mathbf{u}_R} = \mathbf{0} \tag{6.17b}$$

$$\mathbf{K} \Delta \mathbf{u} - (\mathbf{R}_0 + \mathbf{F}_f + \Delta \mathbf{Q}) - \mathbf{N}^t \mathbf{p} = \mathbf{0} \tag{6.18}$$

$$\mathbf{G}_R^t \mathbf{p} - (\Delta \mathbf{Q}_R + \mathbf{Q}_{R,0}) = \mathbf{0} \tag{6.19}$$

hence:

$$\Delta\mathbf{u} = \mathbf{K}^{-1}(\mathbf{R}_0 + \Delta\mathbf{Q} + \mathbf{F}_f) + \mathbf{K}^{-1}\mathbf{N}^t\mathbf{p} \tag{6.20}$$

In conformity with variational inequality

$$\delta_p L_C^{Ip} \leqq 0 \Rightarrow \delta\mathbf{p}^t \frac{\partial L_1}{\partial \mathbf{p}} = -\delta\mathbf{p}^t(\mathbf{N}\mathbf{u} - \mathbf{G}_R\mathbf{u}_R + \mathbf{h}) = \delta\mathbf{p}^t\mathbf{y} \leqq 0 \tag{6.21}$$

for $\mathbf{p} \geqq \mathbf{0}$, $\delta\mathbf{p}$ is arbitrary, thus $\mathbf{y} = \mathbf{0}$, while for $\mathbf{p} = \mathbf{0}$, $\delta\mathbf{p} \geqq \mathbf{0}$, that is, $\mathbf{y} \geqq \mathbf{0}$, hence $\mathbf{p}^t\mathbf{y} = 0$,

$$\mathbf{y} = \mathbf{N}\mathbf{u}_0 + \mathbf{N}\Delta\mathbf{u} - \mathbf{G}_R(\mathbf{u}_{R,0} + \Delta\mathbf{u}_R) + \mathbf{h} \geqq \mathbf{0} \tag{6.22}$$

Substituting (6.20) into (6.22), we arrive at inequality

$$\begin{aligned}\mathbf{y} = &-\mathbf{G}_R\mathbf{u}_R + \mathbf{H}\mathbf{p} + [\mathbf{N}\mathbf{u}_0 - \mathbf{G}_R\mathbf{u}_{R,0} + \mathbf{h} + \\ &+ \mathbf{N}\mathbf{K}^{-1}(\mathbf{R}_0 + \Delta\mathbf{Q} + \mathbf{F}_f)] \geqq \mathbf{0}\end{aligned} \tag{6.23}$$

where

$$\mathbf{H} = \mathbf{N}\mathbf{K}^{-1}\mathbf{N}^t$$

is an influence matrix.

The solution of inequality system (6.19) and (6.23) under condition $\mathbf{p}^t\mathbf{y} = 0$ resulting from the contact-gap condition yields solution of the contact problem for the i-th load increment.

In the solution setup, quantities $(\ )_0$ are loads at the end of the precedent load increment, and $\boldsymbol{\sigma}_f$ is the value computed under the plasticity condition assigned to the problem.

To inequality system (6.19) and (6.23) the following quadratic programming may be assigned:

$$\min_{\Delta\mathbf{u}, \Delta\mathbf{u}_R} \max_{\mathbf{p} \geqq \mathbf{0}} \{L_1 = \Pi - \mathbf{p}^t(\mathbf{N}\mathbf{u} + \mathbf{h} - \mathbf{G}_R\mathbf{u}_R)\} \tag{6.24}$$

hence, minimizing

$$\Pi = \frac{1}{2}\Delta\mathbf{u}^t\mathbf{K}\Delta\mathbf{u} - \Delta\mathbf{u}^t(\mathbf{R}_0 + \Delta\mathbf{Q} + \mathbf{F}_f) - \Delta\mathbf{u}_R^t(\mathbf{Q}_{R,0} + \Delta\mathbf{Q}_R) \tag{6.25}$$

while maximizing with respect to $\mathbf{p}$:

$$\min \{\Pi \mid -(\mathbf{N}\mathbf{u} - \mathbf{G}_R\mathbf{u}_R + \mathbf{h}) \leqq \mathbf{0}\} \tag{6.26}$$

In conformity with relationship

$$L_1 = L_1(\mathbf{u}, \mathbf{p} \geqq \mathbf{0}) + \delta L_1 + \delta^2 L_1$$

function L_1 is subject to inequality relationship

$$L_1(\mathbf{u}, \mathbf{p}^* \geqq \mathbf{0}) \leqq L_1(\mathbf{u}, \mathbf{p} \geqq \mathbf{0}) \leqq L_1(\mathbf{u}^*, \mathbf{p} \geqq \mathbf{0}) \tag{6.27}$$

where $\mathbf{p}^*$, $\mathbf{u}^*$ are possible values, $\mathbf{u}$ and $\mathbf{p}$ are exact solutions.

Both necessary and sufficient condition of the min—max. characteristics of L_1 according to (6.27) is to fulfil the Kuhn–Tucker local conditions [8], actually

$$\frac{\partial L_1}{\partial \mathbf{u}} = \mathbf{0}, \quad \frac{\partial L_1}{\partial \mathbf{p}} \leqq \mathbf{0}, \quad \mathbf{p}^t \frac{\partial L_1}{\partial \mathbf{p}} = 0 \tag{6.28a–c}$$

identical to relationships (6.17), (6.21) established on the "physical" side of the contact problem.

6.1.2. The law of elasto-plastic materials

Determination of initial stresses $\boldsymbol{\sigma}_f$ requires knowledge of the real elastic-plastic stress increment $\Delta \mathbf{T}_{ep} \Rightarrow \Delta \boldsymbol{\sigma}_{ep}$. In knowledge of the material law,

$$\Delta \boldsymbol{\sigma}_{ep} = \mathbf{D}_{ep} \Delta \boldsymbol{\varepsilon} \tag{6.29}$$

where $\mathbf{D}_{ep}$ is matrix of material constants obeying the elasto-plastic law.

According to the theory of plastic yield, $\mathbf{D}_{ep}$ is obtained from surface $F(\boldsymbol{\sigma}, \kappa) = 0$ and the associated law as [9]:

$$\mathbf{D}_{ep} = \mathbf{D} - \mathbf{D}\left(\frac{\partial F}{\partial \boldsymbol{\sigma}}\right)\left(\frac{\partial F}{\partial \boldsymbol{\sigma}}\right)^t \mathbf{D}\left[E_t^p + \left(\frac{\partial F}{\partial \boldsymbol{\sigma}}\right)^t \mathbf{D}\left(\frac{\partial F}{\partial \boldsymbol{\sigma}}\right)\right]^{-1} \tag{6.30}$$

where $\mathbf{D}$ is the matrix of elasticity ($\boldsymbol{\sigma} = \mathbf{D}\boldsymbol{\varepsilon}$), E_t^p is tangent to the equivalent stress-strain function. $\mathbf{D}_{ep}$ is a symmetric, positive definite matrix, valid also for elastic-ideally plastic materials ($E_t^p = 0$).

$\mathbf{D}_{ep}$ being dependent on the current stress state, hence on the load history, it has to be determined again and again in each load increment.

Under the Huber–Mises–Hencky yield condition we have

$$F(\boldsymbol{\sigma}, \kappa) = \frac{1}{\sqrt{2}}[(\sigma_x - \sigma_y)^2 + (\sigma_x - \sigma_z)^2 + (\sigma_y - \sigma_z)^2 + 6(\tau_{xy}^2 + \tau_{xz}^2 + \tau_{yz}^2)]^{1/2} - \sigma_F = 0 \tag{6.31}$$

and

$$\frac{\partial F}{\partial \boldsymbol{\sigma}} = \frac{1}{\sigma_F} \begin{bmatrix} 1 & -0.5 & -0.5 & & & \\ -0.5 & 1 & -0.5 & & & \\ -0.5 & -0.5 & 1 & & & \\ & & & 3 & & \\ & & & & 3 & \\ & & & & & 3 \end{bmatrix} \boldsymbol{\sigma} \tag{6.32}$$

where σ_F is the yield point.

6.1.3. Steps of solving problem (6.24) under yield conditions

Vectors $\mathbf{F}_f$ and $\mathbf{F}_0$ arising from $\boldsymbol{\sigma}_f$ and $\boldsymbol{\sigma}_0$, resp., may be determined by numerical integration. Namely, integrand values are determined in the Gaussian points of integration, then multiplied by the Gaussian weight factors W^n of integration and summed.

Assume to be at load increment i. $\boldsymbol{\sigma}_{0,i-1}$ by the end of increment $(i-1)$ will be considered as $\boldsymbol{\sigma}_0$, while $\boldsymbol{\sigma}_f$ will be determined by iteration from $\Delta\mathbf{u}_i$ [6].

In the following, subscript i will refer to values determined in load increment i.

Computation involves the following iteration:

1. In knowledge of $(\mathbf{F}_f)_i^{k-1}$, contact problem described by inequality system

$$\mathbf{y} = -\mathbf{G}_R\mathbf{u}_{R,i}^k + \mathbf{H}\mathbf{p}_i^k + (\mathbf{N}\mathbf{u}_{0,i-1} + \mathbf{h}) + \\ + \mathbf{N}\mathbf{K}^{-1}(\mathbf{R}_{0,i-1} + \Delta\mathbf{Q}_i) + \mathbf{N}\mathbf{K}^{-1}(\mathbf{F}_f)_i^{k-1} \geqq \mathbf{0} \tag{6.33a}$$

$$\mathbf{G}_R^t\mathbf{p}_i^k - [(\mathbf{Q}_{R,0})_{i-1} + \Delta\mathbf{Q}_{R,i}] = \mathbf{0} \tag{6.33b}$$

$$\mathbf{p}_i^k \geqq \mathbf{0}, \quad \mathbf{y}^t\mathbf{p}_i^k = 0 \tag{6.34a, b}$$

is solved, taking a value $(\mathbf{F}_f)_i^0 = 0$.

2. $(\Delta\mathbf{u})_i^k$ is expressed from (6.20):

$$(\Delta\mathbf{u})_i^k = \mathbf{K}^{-1}(\mathbf{R}_{0,i-1} + \Delta\mathbf{Q}_i + (\mathbf{F}_f)_i^{k-1}) - \mathbf{K}^{-1}\mathbf{N}^t\mathbf{p}_i^k \tag{6.35}$$

3. then, knowing the displacement field, the $(\mathbf{F}_f)_i^k$ value is determined by steps indicated for the hybrid stress model in Fig. 6.

4. In possession of $(\mathbf{F}_f)_i^k$, return to step 1 $(k = k+1)$ if

$$|\mathbf{p}_i^k| - |\mathbf{p}_i^{k-1}| \leqq \delta \tag{6.36}$$

where δ is a low number, else computation of load increment $i = i+1$ begins with increasing the load if $i \leqq ISTEP$ where $ISTEP$ is the number of load increments. Computation ends at full load value.

6.2. Computation method of modified potential energy for solving frictionless contact problems

The computation is based on the variational principle involving functional L_p^p (5.34).

Again, a contact between two solids is examined. Solids are decomposed into $E_\alpha(\alpha = 1, 2)$ finite elements with compatible displacement fields. Displacement fields, strain tensor fields and contact pressure are invariably approximated by (6.8) to (6.12). The elasto-plastic material law is assumed in the form (6.29) to (6.32).

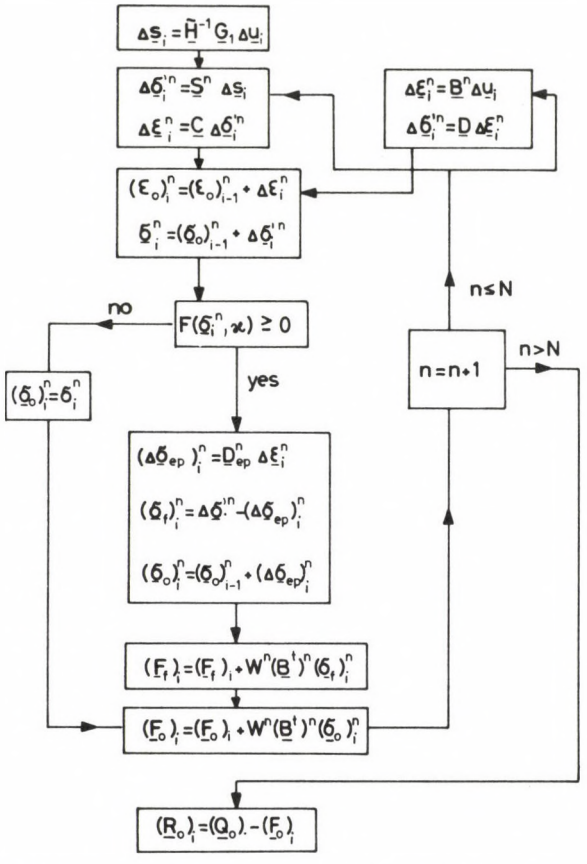

Fig. 6. Algorithm for determining nodal force $(\mathbf{F}_f)_i^k$ from initial stresses, and residual load $(\mathbf{R}_0)_i$ in case of a hybrid stress and compatible displacement model. To simplify notation, element subscript e and symbol of k-th iteration have been omitted. Gaussian points of numerical integration number N

Making use of potential energy Π_p (3.7) and taking substitution (6.1)–(6.2) into consideration:

$$L_P^p = \sum_{e=1}^{E_1+E_2} \left\{ \int_{V^e} \left[\frac{1}{2}\,\Delta\mathbf{A}\,..\mathbf{D}\,..\Delta\mathbf{A} + (\mathbf{T}_0 - \mathbf{T}_f)\,..\Delta\mathbf{A} - \right.\right.$$

$$\left. - (\mathbf{q}_0 + \Delta\mathbf{q})\cdot\Delta\mathbf{u} \right] \mathrm{d}V - \int_{S_p^e} (\bar{\mathbf{p}}_0 + \Delta\bar{\mathbf{p}})\cdot\Delta\mathbf{u}\,\mathrm{d}S -$$

$$\left. - \int_{\Omega} p\cdot(u_N^2 - u_N^1 + h)\,\mathrm{d}S \right\} \tag{6.37}$$

Applying symbols under 6.1.1, the function for problems of finite dimensions is:

$$L_P^p \Rightarrow L_2 = \sum_{e=1}^{E_1+E_2} \left\{ \frac{1}{2} \Delta \mathbf{u}^{e,t} \mathbf{K}^e \Delta \mathbf{u}^e + \Delta \mathbf{u}^{e,t} (\mathbf{F}_0 - \mathbf{F}_f)^e - \right.$$

$$\left. - \Delta \mathbf{u}^{e,t} (\mathbf{Q}_0 + \Delta \mathbf{Q})^e \right\} - \sum_{e=1}^{E_1} \Delta \mathbf{u}_R^t (\mathbf{Q}_{R,0} + \Delta \mathbf{Q}_R)^e$$

$$+ \mathbf{p}^t (\mathbf{G}_R \mathbf{u}_R - \mathbf{N}\mathbf{u} - \mathbf{h}) \tag{6.38}$$

where

$$\mathbf{K}^e = \int_{V_e} \mathbf{B}^t \mathbf{D} \mathbf{B} \, \mathrm{d}V \tag{6.39a}$$

$$\Delta \mathbf{Q}^{\alpha_e} = \int_{S_p^{\alpha_e}} \mathbf{L}^t \Delta \bar{\mathbf{p}} \, \mathrm{d}S + \int_{V^{\alpha_e}} \mathbf{U}^t \Delta \mathbf{q} \, \mathrm{d}V \tag{6.39b}$$

$$\Delta \mathbf{Q}_R^{1,e} = \int_{S_p^{1,e}} \mathbf{L}_R^t \Delta \bar{\mathbf{p}} \, \mathrm{d}S + \int_{V^{1,e}} \mathbf{U}^t \Delta \mathbf{q} \, \mathrm{d}V \tag{6.39c}$$

other magnitudes being those in (6.13).

The connection of the elements leads to a function of the form (6.16):

$$L_2 = \frac{1}{2} \Delta \mathbf{u}^t \mathbf{K} \Delta \mathbf{u} - \Delta \mathbf{u}^t (\mathbf{Q}_0 - \mathbf{F}_0 + \mathbf{F}_f + \Delta \mathbf{Q}) -$$

$$- \Delta \mathbf{u}_R^t (\mathbf{Q}_{R,0} + \Delta \mathbf{Q}) - \mathbf{p}^t (\mathbf{N}\mathbf{u} - \mathbf{G}_R \mathbf{u}_R + \mathbf{h})$$

Making use of (6.18) and (6.19), variational equation—inequality (5.35) may lead to inequality (6.23) replacing (6.22), defining again a quadratic programming problem of the form (6.24). Steps of solving the elasto-plastic contact problem set up are the same as those under 6.1.3. In determining the fictitious load, iteration has to be made like that for the compatible displacement model in Fig. 6.

7. Variational principles for linear systems of elements in bilateral or unilateral connection

Variational principles for linear systems with bilateral and unilateral connections may be derived from those under items 4 and 5, respectively, with zero initial values $(\ )_0 \equiv \mathbf{0}$, and replacing the variation by the full value $\Delta(\ ) = (\ )$

$$\text{e.g. } \mathbf{T}_0 = \mathbf{0}, \quad \Delta \mathbf{T} = \mathbf{T} \quad \text{etc.}$$

Writing of functionals and variational equations—inequalities will here be omitted. Obviously, distinction between C- and I-type transformations would be meaningless. The involved principles, as well as the variational principles applying field $\mathbf{T}$ meeting the basic equation for the stress tensor, see in [10].

APPENDIX 1

Transformation of integrals relating to discontinuous fields

A.1.1. For zero initial gap, discontinuity in the displacement field on an element surface S_c^{ej} hence, the kinematic fitting condition can be handled by involving a term:

$$\int_{S_c^{ej}} \boldsymbol{\lambda} \cdot (\mathbf{u}^j - \mathbf{u}^e)\, \mathrm{d}S$$

On the surface S_c of a structure of N elements, integral

$$I_u = \sum_{e,j} \int_{S_c^{ej}} \boldsymbol{\lambda} \cdot (\mathbf{u}^j - \mathbf{u}^e)\, \mathrm{d}S \tag{A.1.1}$$

holds. Multiplier $\boldsymbol{\lambda}$ as a stress has to belong to some normal to the surface. In the following, in writing integrals containing $\boldsymbol{\lambda}$, $\boldsymbol{\lambda}$ is assumed to belong to the element of the lower subscript.

Integral (A.1.1) transformed to involve element e joined by those $e-1, j$ and $j+1$ becomes:

$$\begin{aligned} I_u = \ldots + \int_{S_c^{e-1,e}} \boldsymbol{\lambda}^{e-1} \cdot (\mathbf{u}^e - \mathbf{u}^{e-1})\, \mathrm{d}S + \int_{S_c^{ej}} \boldsymbol{\lambda}^e \cdot (\mathbf{u}^j - \mathbf{u}^e)\, \mathrm{d}S + \\ + \int_{S_c^{e,j+1}} \boldsymbol{\lambda}^e \cdot (\mathbf{u}^{j+1} - \mathbf{u}^e)\, \mathrm{d}S + \ldots = \ldots - \int_{S_c^e} \boldsymbol{\lambda}^e \cdot \mathbf{u}^e\, \mathrm{d}S \ldots \\ = - \sum_{e=1}^{N} \int_{S_c^e} \boldsymbol{\lambda}^e \cdot \mathbf{u}^e\, \mathrm{d}S \end{aligned} \tag{A.1.2}$$

namely

$$S_c^e = S_c^{e-1,e} \cup S_c^{e,j} \cup S_c^{e,j+1}$$

$$\boldsymbol{\lambda}^{e-1} = -\boldsymbol{\lambda}^e$$

in range $S_c^{e-1,e}$.

A.1.2. In some of the variational principles, the technique of multipliers is applied to make the stress field continuous, giving rise to integral

$$I_t = \sum_{e,j} \int_{S_c^{ej}} \tilde{\mathbf{u}} \cdot (\mathbf{t}^j + \mathbf{t}^e)\, \mathrm{d}S \tag{A.1.3}$$

where $\tilde{\mathbf{u}}$—displacement multiplier; $\mathbf{t}^e$, $\mathbf{t}^j$—stress vectors belonging to external normals of elements e and j, respectively. Again, assuming element e to be joined by those $e-1, j$, $j+1$:

$$\begin{aligned} I_t = \ldots + \int_{S_c^{e-1,e}} \tilde{\mathbf{u}} \cdot (\mathbf{t}^{e-1} + \mathbf{t}^e)\, \mathrm{d}S + \int_{S_c^{e,j}} \tilde{\mathbf{u}} \cdot (\mathbf{t}^j + \mathbf{t}^e)\, \mathrm{d}S + \\ + \int_{S_c^{e,j+1}} \tilde{\mathbf{u}} \cdot (\mathbf{t}^{j+1} + \mathbf{t}^e)\, \mathrm{d}S + \ldots = \ldots + \int_{S_c^e} \tilde{\mathbf{u}} \cdot \mathbf{t}^e\, \mathrm{d}S + \ldots = \\ = \sum_{e=1}^{N} \int_{S_c^e} \tilde{\mathbf{u}} \cdot \mathbf{t}^e\, \mathrm{d}S \end{aligned} \tag{A.1.4}$$

A.1.3. In cases with discontinuity only in terms $\mathbf{u}''$ of displacement field $\mathbf{u}$, I_u may be replaced by integral

$$I_u'' = \sum_{e,j} \int_{S_c^{ej}} \boldsymbol{\lambda} \cdot (\mathbf{u}^{j''} - \mathbf{u}^{e''}) \, dS = - \sum_{e} \int_{S_c^e} \boldsymbol{\lambda} \cdot \mathbf{u}^{e''} \, dS \tag{A.1.5}$$

imposing, for a real discontinuity in the stress field, to compute integral

$$I_t' = \sum_{e,j} \int_{S_c^{ej}} \tilde{\mathbf{u}} \cdot (\mathbf{t}^{j'} + \mathbf{t}^{e'}) \, dS = \sum_{e} \int_{S_c^e} \tilde{\mathbf{u}} \cdot \mathbf{t}^{e'} \, dS \tag{A.1.6}$$

where $\mathbf{t}'$ is the stress vector part involving discontinuity.

References

1. Pian, T. H. H.: Variational principles for incremental finite element methods. Journal of The Franklin Institute 302 (1976) No. 5 & 6, 473–488
2. Atluri, S.: A new assumed stress hybrid finite element model for solid continua, AIAA J. 9 (1971), No 8, 1647–1649
3. Pian, T. H. H.: Derivation of element stiffness matrices by assumed stress distributions. AIAA J. 2 (1964), No 7, 1333–1336
4. Wolf, S. P.: Generalized hybrid stress finite element models. AIAA J. 11 (1973), No. 3, 386–388
5. Zienkiewicz, O. C., Vallappan, S., King, I. P.: Elastic-plastic solutions of engineering problems. "Initial Stress" finite element approach. Int. J. Num. Meth. Engng. 1 (1969), 75–100
6. Spilker, R. L., Pian, T. H. H.: Hybrid—stress models for elastic-plastic analysis by the initial-stress approach. Int. J. Num. Meth. Engng. 14 (1979), 359–378
7. Spilker, R. L., Munir, N. I.: Elastic-plastic analysis of plates by the hybrid-stress model and initial-stress approach. Int. J. Num. Meth. Engng. 17 (1981), 1791–1810
8. Künzi, H. P.—Krelle, W.: Nichtlineare Programmierung. Springer-Verlag, Berlin 1962
9. Zienkiewicz, O. C.: The Finite Element Method in Engineering Science. McGraw-Hill, London 1977
10. Páczelt, I.: Analysis of the Contact Problem of Elastic Systems. (In Hungarian) Dr. Sci. Techn. Thesis, Miskolc 1981

Acta Technica Academiae Scientiarum Hungaricae, 96 (1—4) pp. 59—85 (1983)

EXISTENCE AND UNIQUENESS CRITERIA OF THE MEMBRANE STATE OF SHELLS

III. ELLIPTIC SHELLS

T. TARNAI*

[Received 1 June 1977]

In this paper the problem is analysed what kind of support is needed or is allowed in order to ensure that the shell be in a statically determinate membrane state. Previous two parts of this paper have been concerned with criteria of existence and uniqueness of the solution of the membrane shell equation in connection with hyperbolic and parabolic shells. This Part III presents the analysis of elliptic shells.

1. Introduction

The equilibrium of membrane shells is described in the orthogonal coordinate system xyz as:

$$\mathscr{L}F = \frac{\partial^2 z}{\partial y^2}\frac{\partial^2 F}{\partial x^2} - 2\frac{\partial^2 z}{\partial x\,\partial y}\frac{\partial^2 F}{\partial x\,\partial y} + \frac{\partial^2 z}{\partial x^2}\frac{\partial^2 F}{\partial y^2} = -g \tag{1}$$

where $z = z(x, y)$ is the equation of the middle surface of the shell,

$$\mathscr{L} = \frac{\partial^2 z}{\partial y^2}\frac{\partial^2}{\partial x^2} - 2\frac{\partial^2 z}{\partial x\,\partial y}\frac{\partial^2}{\partial x\,\partial y} + \frac{\partial^2 z}{\partial x^2}\frac{\partial^2}{\partial y^2}$$

is the Pucher operator, $g = g(x, y)$ is the intensity function of an external load parallel to the z-axis (vertical), and $F(x, y)$ is the unknown stress function yielding the reduced internal forces as follows:

$$n_x = \frac{\partial^2 F}{\partial y^2}, \quad n_{xy} = n_{yx} = -\frac{\partial^2 F}{\partial x\,\partial y}, \quad n_y = \frac{\partial^2 F}{\partial x^2}.$$

The first and second parts [22], [23] of this paper examined the existence and uniqueness criteria of the solution of Eq. (1) of membrane shells hyperbolic and parabolic, resp., at all points of the domain of definition, and subjected to vertical loads. This part will be concerned with the criteria of existence of a unique solution of Eq. (1) for a shell elliptic at any point of its floor plan configuration, that is, if discriminant

$$D = \frac{\partial^2 z}{\partial x^2}\frac{\partial^2 z}{\partial y^2} - \left(\frac{\partial^2 z}{\partial x\,\partial y}\right)^2$$

is positive everywhere in the domain.

* T. Tarnai, H-1037, Budapest, Kolostor u. 17, Hungary

Features of elliptic equations are rather different from those of hyperbolic and parabolic ones, especially the two ones below:

1. Initial-value problem of hyperbolic and parabolic equations is a properly posed problem. It has a unique solution continuously depending on initial values, and the domain of solution may be exactly delimited by means of the characteristics. In contrast, the initial-value problem is not always correct for elliptic equations. It may have no solution, and if it has one, it is not always continuously depending on initial values. Furthermore, if there exists a solution of the problem, the domain where the solution is determined cannot in general be predicted.

2. Boundary-value problems for hyperbolic equations have a unique solution for an open boundary curve. For a closed boundary curve, problems are usually overdeterminate, and so insoluble. Also boundary-value problems of parabolic equations have unique solutions primarily for open boundary curves but often can also be—uniquely—solved for closed boundary curves [23]. Boundary-value problems of elliptic equations cannot have a unique solution else but for closed boundaries. Open boundary curves make the problem indeterminate, the solution non-unique.

Boundary will be understood below as groundplan projection of the real shell edge on plane xy. The real shell edge line will be denoted by $\bar{S}$, its ground-plan projection by S.

2. Initial-value problem in an elliptic case (Cauchy problem)

The Cauchy problem for elliptic equations has much less been considered in mathematic publications than different boundary-value problems. Namely, partly the Cauchy problem of elliptic equations—as mentioned—is not a properly posed problem, and partly there is a restricted range of physical problems leading to the Cauchy problem for elliptic equations. Among membrane shells, however, there is an important group of free-edged apse-like formed shells, internal stress patterns of which are known to be determinable by solving a Cauchy type problem. This is why existence, uniqueness, and continuous dependence on initial conditions of the Cauchy problem have to be closer looked at.

Let us first define the term of analytic functions. Two-variable function $u(x, y)$ is called analytic with respect to x, y at a point (x_0, y_0) of some domain if in the neighbourhood of (x_0, y_0) it can be expanded into a power series according to $(x-x_0)$, $(y-y_0)$. Function $u(x, y)$ is analytic in a domain if it is analytic in every point of the domain. As a consequence of this definition, $u(x, y)$ can be infinite times differentiated at the point where it is analytic. The term of analytic functions may be similarly defined also in the single-variable case.

Let us consider now the generalized Cauchy problem for the elliptic partial differential equation (1).

Let a direction i (unit vector) be given at any point of boundary curve S in the plane xy (Fig. 1). Also, let value φ of stress function F be given on boundary S, and value ψ of the directional derivative of function F in direction i.

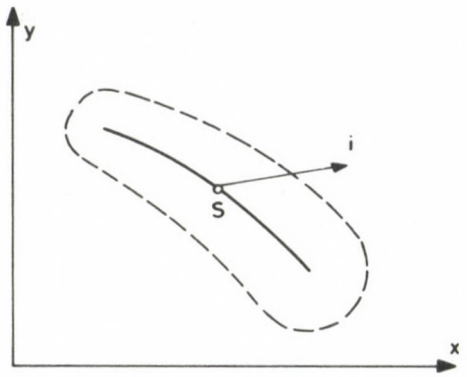

Fig. 1. The domain of solutions of the initial-value problem

Let the following conditions be satisfied:

(a) boundary curve S lies in the domain of definition of Eq. (2a);
(b) boundary curve S is "smooth enough" so that its transformation mapping curve S to straight line $\xi_0 = 0$, and direction i to the normal of straight line $\xi_0 = 0$, yields the original variables as analytic functions of the new variables; that is, curve S is an analytic one (p.43 in [18]);
(c) direction i varies "smoothly enough" along curve S so that transformation under (b) exists, that is, direction function i is an analytic one (p. 43 in [18]);
(d) direction i assigned to a given point of curve S is not tangential to curve S at that point;
(e) $g(x, y)$ is analytic;
(f) both φ and ψ are analytic;
(g) $z(x, y)$ is analytic.

Now, in conformity with the Cauchy–Kovalevskaya theorem, initial-value problem

$$\mathscr{L}F = -g\,, \tag{2a}$$

$$F|_S = \varphi, \quad \left.\frac{\partial F}{\partial i}\right|_S = \psi \tag{2b}$$

has a unique analytic solution in some neighbourhood of curve S (Fig. 1) (p. 44 in [18]). No size of this neighbourhood is defined by the theorem.

We should mention that if functions in problem (2a, b) are not required to be analytic, the existence of a solution for problem (2a, b) generally fails, but its unicity

prevails for a rather wide class of functions. If the problem has a solution so that the middle surface function $z(x, y)$ is twice differentiable, and the second partial derivatives are Lipschitz-continuous, as well as boundary curve S is differentiable and the derivative is Lipschitz-continuous, then the solution is unique (Theorem II, p. 19 in [16]). A two-variable function $u(x, y)$ is called Lipschitz-continuous in a domain if there is a constant c such that inequality

$$|u(x_1, y_1) - u(x_2, y_2)| \leqq c[(x_1 - x_2)^2 + (y_1 - y_2)^2]^{1/2}$$

is satisfied for any pair of points (x_1, y_1), (x_2, y_2) of the domain. The Lipschitz continuity may be similarly defined also in the single-variable case.

Let the normal (unit vector) of curve S in plane xy be denoted by n. Be $i \equiv n$, and let

$$F|_S = 0, \quad \left.\frac{\partial F}{\partial n}\right|_S = 0$$

hold in condition (2b).

This is to specify edge S to be free. Thus, elliptic shells may be provided with a free boundary curve by specifying the shell middle surface, the load function and the boundary curve to be analytic. For an open curve S, neither the right nor the left bank

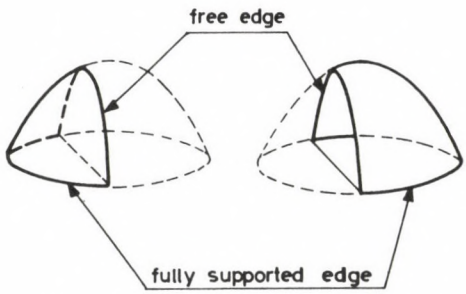

Fig. 2. Apse-like formed shells with edges in the vertical plane

of the curve is preferential, thus, the solution is defined both to the right and to the left of curve S. If S is a straight line, apse-like formed shells both to the right and to the left of the vertical plane containing S are known to be in membrane state ([5], p. 98 in [19], p. 207 in [21]). Such an application of the generalized Cauchy problem for problem (2a, b) permits to extend the range of apse-like formed shells in membrene state. Apse-like formed shells may be in unique membrane state not only if the free edge is a curve of vertical plane in the middle surface (Fig. 2) but also if the real edge of the shell is an arbitrary spatial surface curve, with analytic projection on plane xy. Such a generalized apse-like formed shell is illustrated in Fig. 3.

We mention here that for a rectilinear curve S, also normal and shear force values may be specified along S [22]. Of course, also these need to be analytic functions.

The edge section physically closing the shell ground plan joining S has to lie in the domain of solution of the problem. No condition may be specified here but edge beams must bear any internal force arising at the edge.

Thus, if the elliptic shell has already a free edge section, no condition may be specified for the other shell edge sections, as seen from an analysis independent of the mathematical theory. An elliptic shell will be seen below to be in membrane state if the

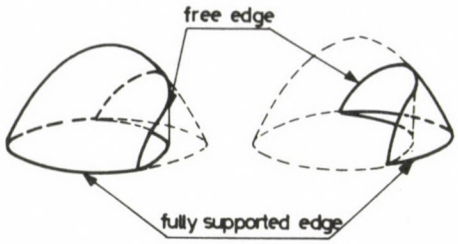

Fig. 3. Apse-like formed shells with spatial curve edge

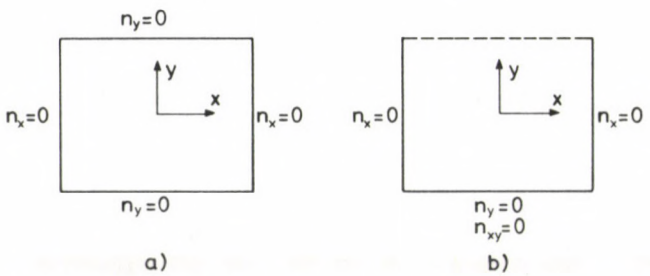

Fig. 4. Ground plan and boundary conditions of elliptic shells (a) all four sides are exempt from lateral pressure; (b) one side is free, two sides are exempt from lateral pressure, one side is fully supported

stress function value is specified all around its boundary, e.g. to be continuous and linearly varying boundary section-wise. For straight boundary sections this is known to mean exemptness from lateral thrust. Thus, in the case seen in Fig. 4a, an elliptic paraboloid shell over a rectangular ground plan is always in membrane state. For any side of the rectangle, one condition has been specified. Beles and Soare [2] examined the case of transferring the condition from one side to the other, without changing the total number of conditions. Exemptness of lateral thrust having been specified for the opposite side, to compensate for the similar condition here, also exemptness of shear force will be specified for the opposite edge, making the edge to be free (Fig. 4a). In final account, for one side of the rectangle, conditions $F=0$, $\partial F/\partial n=\partial F/\partial y=0$ have been specified, and condition $F=0$ for the two joining sides, while no condition has been specified for the side opposite to the free edge. A hyperbolic paraboloid shell of e.g. saddle shape is known [22] to be in unique memberane state under these conditions. In

this problem, the authors found the shell not to be in membrane state. The infinite series used for the analysis were divergent.

In conformity with the condition of analycity of functions in (2a, b), if a section of boundary curve S is straight, boundary S has to be straight all along, and if functions φ and ψ vanish in a section of boundary S, that is, this section of boundary S is free, then values of functions φ and ψ have to be zero all along boundary S. Opposite to hyperbolic and parabolic shells, boundary S of elliptic shells cannot consist of alternating boundary sections with zero and non-zero edge forces.

If the full shell edge is a single, non-self-intersecting curve, then it seems that the share of free edge in the full edge length is not restricted. Beyond of needing to be an open curve, the extension of the free edge is restricted solely by strength aspects. Namely, theoretically, the fully supported edge section of the shell may be infinitesimal, and the shell equilibrium to be provided by infinite forces acting at this infinitesimal length. In a similar case for hyperbolic and parabolic shells the ratio of free to total edge length cannot be arbitrarily great. The extension of the free edge is restricted by characteristics [22, 23].

If conditions (a) to (g) are satisfied, the Chauchy problem (2a, b) has a unique solution in the neighbourhood of boundary S if it is a non-self-intersecting closed curve [17]. Let Ω be a bounded domain limited by boundary S. The neighbourhood of boundary S where the solution exists has two parts, one outside, and the other inside domain Ω. The part of the neighbourhood inside domain Ω cannot embrace the full domain Ω.

The problem has generally no solution in the full domain Ω since there it is overdeterminate. Namely for the existence and uniqueness of a solution of (2a) in the full domain Ω, it is sufficient to specify a single condition on boundary S, e.g. the value of stress function F, or of the directional derivative $\partial F/\partial i$. It follows that an elliptic shell with a free edge all around, over a bounded, simply connected domain, cannot in general be in membrane state even if, as a rigid body, it would be in equilibrium. However, it can be in membrane state over an unbounded domain outside curve S. In compliance with the physicality of the problem, in the latter case only a finite part of the unbounded domain is taken into consideration.

Applying cylindrical coordinates r, ϑ, Tolotti [25] proved the existence of a solution of the Cauchy problem

$$\Lambda F(r, \vartheta) = 0\,, \tag{3a}$$

$$F\,|_{r=R} = f_1(\vartheta)\,, \quad \left.\frac{\partial F}{\partial r}\right|_{r=R} = f_2(\vartheta) \tag{3b}$$

for the case where f_1 and f_2 are periodic analytic functions with a period 2π, and Λ is the Laplacian operator

$$\Lambda = \frac{\partial^2}{\partial r^2} + \frac{1}{r}\frac{\partial}{\partial r} + \frac{1}{r^2}\cdot\frac{\partial^2}{\partial \vartheta^2}\,.$$

The proof referred to polyharmonic functions, of a more general form. Initial value problem (3a, b) refers to a homogeneous equation, with inhomogeneous initial conditions. The counterpart of this problem refers to an inhomogeneous equation with homogeneous initial conditions:

$$\Delta F(r, \vartheta) = -g(r, \vartheta), \tag{4a}$$

$$F|_{r=R} = 0, \quad \left.\frac{\partial F}{\partial r}\right|_{r=R} = 0, \tag{4b}$$

where $g(r, \vartheta)$ is a periodic analytic function with period 2π. No mathematical publication concerned with this problem in itself has been found. In compliance with the analyticity of the functions, the Cauchy–Kovalevskaya theorem provides for the

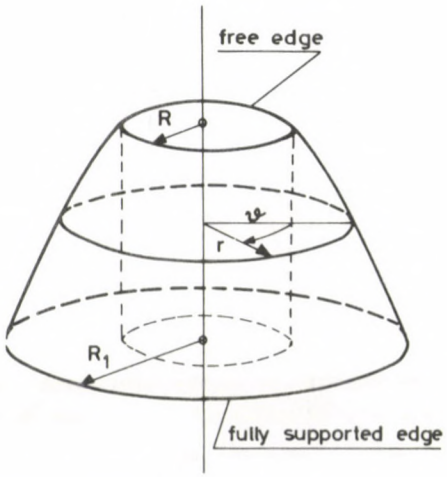

Fig. 5. Paraboloid shell of revolution with free edge

existence and uniqueness of the solution of problem (4a, b). Solution of the initial-value problem (4a, b) describes membrane state of a shell of paraboloid of revolution with a central circular opening of free edge. The case where the superior edge of smaller radius R is free, and the lower edge of greater radius R_1 is fully supported, is seen in Fig. 5. The opposite case with a fully supported edge of smaller radius R and free edge of greater radius R_1 is also possible, where R has to be replaced by R_1 in (4b).

Load function g needs not be circular symmetric. Thereby problem (4a, b) is more general than the known one where also load function g is circular symmetric [6]. The free-edged opening may be anywhere on the shell surface. For instance, Eibl [11] developed an example of the case of eccentric circular free-edged opening on a spherical shell.

A shell with two or more free-edged openings cannot, in general, be in membrane state. Namely, there is no analytic one-to-one transformation such as to map two or more closed curves with no point in common to a single straight line.

We mention here that if the free edge of the shell is a closed curve, then the other edge physically closing the shell has to be a non-self-intersecting closed curve lying in the domain of solution and not crossing the free edge line. The two edge lines together have to delimit a bounded, doubly connected domain.

Let us consider now the problem of the continuous dependence of the solution on the initial values. Only cases where functions in the Cauchy problem are analytic, hinting to the existence and uniqueness of solution, will be considered. If, in addition, the solution is a continuous function of the initial values, then the Cauchy problem is a properly posed one. Introductorily, however, the possibility of the Cauchy problem for elliptic partial differential equations to be ill-posed was mentioned.

In the actual case of the existence of a unique solution, improper setting of the problem appears by the discontinuous dependence of the solution on the initial values. This occurrence will be demonstrated on an example due to Hadamard (p. 40 in [13]), referred to by several authors (e.g. [1]; p. 84 in [18]).

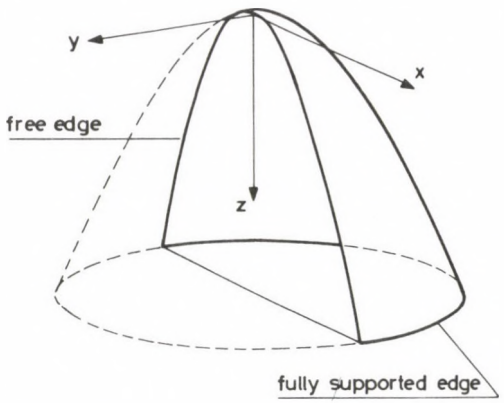

Fig. 6. Apse-like formed paraboloid shell of revolution

Let us consider an apse-like formed paraboloid shell of revolution with no surface load (Fig. 6) where the middle surface of the shell results from cutting surface

$$z=\frac{1}{2}(x^2+y^2)$$

by plane $y=0$. Let the cutting line be the free edge of the shell. The state of stress in the shell may be determined by solving the Cauchy problem (2a, b), actually of the form:

$$\frac{\partial^2 F}{\partial x^2}+\frac{\partial^2 F}{\partial y^2}=0\,, \tag{5a}$$

$$F(x,0)=0\,,\quad \frac{\partial F(x,0)}{\partial y}=0\,. \tag{5b}$$

Due to the Cauchy–Kovalevskaya theorem, problem (5a, b) has a unique solution, i.e.: $F(x, y)=0$. Hence, the reduced normal forces are

$$n_x=\frac{\partial^2 F}{\partial y^2}=0\,,\quad n_{xy}=-\frac{\partial^2 F}{\partial x\partial y}=0\,,\quad n_y=\frac{\partial^2 F}{\partial x^2}=0$$

obviously, namely unloaded shells do not develop internal forces.

Now, let us approximate the first condition in (5b) by an expression of the form:

$$F(x, 0)=\frac{1}{m^a}\sin mx\,, \tag{6}$$

where $a\geqq 2$ is constant, and $m>0$ is an integer. For $m\to\infty$, (6) uniformly tends to $F(x, 0)=0$. Thus, for an arbitrarily small $\varepsilon>0$, there is a number M so that for $m>M$ inequality

$$\frac{1}{m^a}|\sin mx|<\varepsilon \tag{7}$$

holds.

Let us fix the value of ε and choose a number m so that (7) is satisfied. Now, let us find the solution of Laplace's equation (5a) under conditions

$$F(x, 0)=\frac{1}{m^a}\sin mx\,,\quad \frac{\partial F(x, 0)}{\partial y}=0\,. \tag{8}$$

Due to the Cauchy–Kovalevskaya theorem, a unique solution exists:

$$F(x, y)=\frac{1}{m^a}\sin mx\cdot\cosh my\,. \tag{9}$$

Stress function (9) yields the reduced normal forces:

$$n_x=\frac{\partial^2 F}{\partial y^2}=\frac{1}{m^{a-2}}\sin mx\cdot\cosh my\,,$$

$$n_{xy}=-\frac{\partial^2 F}{\partial x\partial y}=\frac{1}{m^{a-2}}\cos mx\cdot\sinh my\,,$$

$$n_y=\frac{\partial^2 F}{\partial x^2}=-\frac{1}{m^{a-2}}\sin mx\cdot\cosh my\,.$$

Although initial conditions (8) slightly differ from (5b) (less than by ε), solution (9) and the resulting reduced normal forces are seen to differ significantly from zero in any arbitrary small neighbourhood of the x-axis. Thus, somewhat changing the initial values in problem (5a, b), the solution will significantly change. Thus, the problem is ill-posed.

This example is little conclusive since no stress analysis of unloaded, free-edged apse-like formed shells occurs in practice. The example becomes conclusive from the

possibility to demonstrate the improper setting of the Cauchy problem by the same considerations for an apse-like formed shell subjected to surface loads, or for an apse-like formed shell with no surface load, with an edge subjected to normal and shear forces of given values. Let us consider the latter case first. For the sake of uniqueness of the solution of the problem, the distribution functions of the boundary forces are stipulated to be analytic. Stress function yielding internal shell forces is obtained by solving the Cauchy problem

$$\frac{\partial^2 F}{\partial x^2} + \frac{\partial^2 F}{\partial y^2} = 0 . \tag{10a}$$

$$F(x, 0) = \varphi(x), \quad \frac{\partial F(x, 0)}{\partial y} = \psi(x), \tag{10b}$$

where $\varphi(x)$ and $\psi(x)$ are double, and single integrated with respect to x, of the reduced normal, and shear force functions, resp., along the edge. Let function $F_0(x, y)$ be the solution. Now, solution of (10a) under initial conditions

$$F(x, 0) = \varphi(x) + \frac{1}{m^a} \sin mx, \quad \frac{\partial F(x, 0)}{\partial y} = \psi(x) \tag{11}$$

will be function

$$F_1(x, y) = F_0(x, y) + \frac{1}{m^a} \sin mx \cdot \cosh my . \tag{12}$$

A slight change of initial functions $\varphi(x)$ and $\psi(x)$ in (10b) resulting from addition of functions (8) to functions $\varphi(x)$ and $\psi(x)$ may produce a significant change of solution (12) in an arbitrary small neighbourhood of boundary line $y = 0$.

This is also true for a non-zero, analytic surface load $g(x, y)$ of the shell. Namely, let the initial-value problem

$$\frac{\partial^2 F}{\partial x^2} + \frac{\partial^2 F}{\partial y^2} = -g , \tag{13a}$$

$$F(x, 0) = \varphi(x), \quad \frac{\partial F(x, 0)}{\partial y} = \psi(x) \tag{13b}$$

have a solution $F_2(x, y)$. (Functions $\varphi(x)$ and $\psi(x)$ may be zero, then the shell edge corresponding to $y = 0$ is a free one.)

It is easy to see that the solution of the initial-value problem

$$\frac{\partial^2 F}{\partial x^2} + \frac{\partial^2 F}{\partial y^2} = -g , \tag{14a}$$

$$F(x, 0) = \varphi(x) + \frac{1}{m^a} \sin mx, \quad \frac{\partial F(x, 0)}{\partial y} = \psi(x) \tag{14b}$$

will be function

$$F_2(x, y) + \frac{1}{m^{a-2}} \sin mx \cdot \cosh my$$

which can assume rather high values in an arbitrary small neighbourhood of boundary $y=0$, as before.

The above are of importance primarily from computational aspects. Namely, in computation, initial conditions may not be completely satisfied, forcing one to approximation. Approximation of arbitrary accuracy of initial conditions does not result in an approximation of the solution to the same degree.

3. Boundary-value problems in the elliptic case

Let us define first some terms.

1. Be Ω a bounded domain in plane xy, with boundary S. Now, function $u(x, y)$ defined above domain Ω is called *λ-Hölder-continuous* in Ω if there is a constant c with which inequality

$$|u(x_1, y_1)-u(x_2, y_2)| \leqq c\{\rho[(x_1, y_1), \quad (x_2, y_2)]\}^{\lambda}, \quad 0<\lambda\leqq 1$$

holds for every pair of different points $(x_1, y_1), (x_2, y_2)$ in Ω. In the above expression $\rho[(x_1, y_1), (x_2, y_2)]$ denotes the distance between points $(x_1, y_1), (x_2, y_2)$ (p. 1 in [16]). The λ-Hölder continuity may be similarly defined for single-variable functions. For $\lambda = 1$, the Hölder-continuous function becomes Lipschitz-continuous. Hölder continuity is more than ordinary continuity but less than differentiability.

2. Curve S in plane xy is called a *Liapunov curve* (p. 350 in [24]) if

(a) curve S has a definite normal (tangent) at any point;

(b) there is a positive number d such that straight lines parallel to the normal at any point P of curve S intersect part S'_P of curve S inside the circle of centre P, radius d;

(c) for angle $\gamma(P, P')=(n_P, n_{P'})$ subtended between normals $n_P, n_{P'}$ at points P, P' inequality

$$\gamma(P, P')<A\rho^{\lambda}$$

holds, where ρ is the distance between points P and P', A is a constant, and $0<\lambda\leqq 1$.

For an interpretation of closed curves of this type in a different form see e.g. p. 3 in [16] or p. 13 in [4]. The Liapunov property of curve S is more than to be once continuously differentiable but less than to be twice continuously differentiable.

3. Let a direction i (unit vector) assigned to every point of boundary curve S delimiting bounded domain Ω pointing outward from Ω. Now, direction i is called *conormal* of curve S and denoted by ν if after canonic transformation of (1) it passes into normal n of the boundary curve. A more general definition of the conormal valid e.g. in the case where the above-mentioned canonic transformation does not exist is presented on p. 17 in [4].

In the general case, boundary value problems will be interpreted as follows. Let us have a bounded, connected domain Ω in plane xy, with boundary S. Be a direction i given at any point of boundary curve S, such that it is not tangent to edge curve S at that

point, pointing outward from domain Ω. Also, let functions α, $\beta(\alpha^2+\beta^2>0)$, and φ be given on boundary S. Now, let us find a solution of (1) in domain Ω which satisfies condition

$$\alpha\frac{\partial F}{\partial i}+\beta F=\varphi \tag{15}$$

on boundary S, where $\partial F/\partial i$ is the directional derivative of function F in direction i.

The following will be concerned with four special cases of the boundary-value problem under general boundary condition (15).

The *first boundary-value problem* or *Dirichlet problem* is that where $\alpha\equiv 0$, $\beta\equiv 1$ in (15), that is, value of stress function F on the boundary is given.

The *second boundary-value problem* is where $\alpha\equiv 1$, $\beta\equiv 0$ in (15), that is, value of directional derivative of stress function F in direction i on the boundary is given. For $i\equiv\nu$, i.e. direction i coincides with conormal ν, there is a *Neumann problem.*

The *third boundary-value problem* is the one defined by condition (15) itself.

A *mixed boundary-value problem* emerges if in (15) either α or β disappears in each section of boundary S without identically zeroing α or β all along the boundary.

We should mention that publications do not apply uniform denominations for the problems. For instance, the problem called here third boundary-value problem is termed by Miranda [16]—for $i\equiv\nu$—a Neumann problem, by Schiffer [3] a Robin problem, and by Bitsadze [4]—without condition $i\equiv\nu$—a Poincaré problem.

3.1. The first boundary-value problem (Dirichlet problem)

Let Ω be a bounded domain in plane xy, with boundary S. Let stress function F assume values given by function φ along boundary S. Now, the Dirichlet problem

$$\mathscr{L}F=-g\,, \tag{16a}$$

$$F\,|_S=\varphi \tag{16b}$$

has a unique solution in domain Ω provided conditions

(a) domain Ω with boundary S are in the domain of definition of Eq. (16a);
(b) Ω is a simply connected domain;
(c) edge S is a Liapunov closed curve;
(d) $g(x, y)$ is continuous in Ω and S, and λ-Hölder-continuous in Ω;
(e) φ is continuous in S;
(f) $z(x, y)$ is three times differentiable in Ω and in S, and its third partial derivatives are λ-Hölder-continuous

are satisfied (Theorem I, p. 21 in [16]).

It should be noted that condition (c) is always satisfied if S is twice continuously differentiable, condition (d), if $g(x, y)$ is continuously differentiable in Ω, and (f) if $z(x, y)$ is four times continuously differentiable in Ω and on S.

Provided these conditions are satisfied, the solution may be produced by means of integral operators (in potential form). If the Dirichlet problem (16a, b) has a solution without satisfying the above conditions, this is a unique one (Theorem I, p. 5 in [16]).

Unique membrane state of a shell vertically supported all around on a closed (annular) edge beam is provided by boundary condition $F|_S = 0$. This condition is always specifiable and the edge line becomes the funicular curve of arising forces.

Existence of potentials producing the solution is known not to require finiteness of the curvature of boundary curve S at any point of S (p. 350 in [24]). Accordingly, the Dirichlet problem may have a solution even if condition (c) is not fulfilled, that is, boundary S is not a single Liapunov closed curve but it is a union of a finite multitude of Liapunov curve sections joining with knee points. In this case, however, the solution may be singular at the knee points, with infinite normal force values. Singularity occurring at the corners of an elliptic paraboloid shell over a rectangular ground plan, vertically supported along its edge, is common knowlege (see e.g. p. 142 in [14]). In this problem, condition (c) may be met by rounding off the corners with any small (but non-zero) radius, to cease singularity.

For boundary S of straight sections, normal force values may be specified for each section (item 2.2 in [22]). For instance, an elliptic shell over a rectangular ground plan, with no surface load (Fig. 7a) will always be in membrane state if one edge is subjected to normal forces of some distribution $f(x)$, and the shell has to be kept in equilibrium to develop only shear forces all around its edge (Fig. 7b). (The edges are

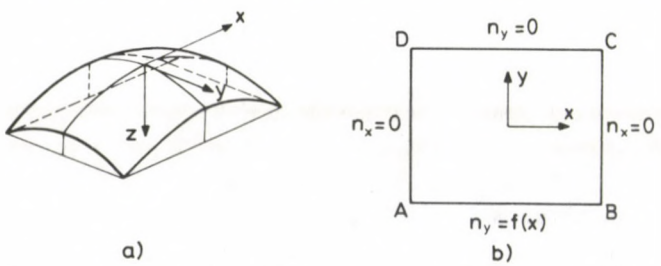

Fig. 7. (a) Elliptic shell. (b) Shell ground plan and boundary conditions

supported both vertically and against displacements in the edge beam planes.) This problem always has a solution, however, not unique in the general case, thus, the problem is statically indeterminate. Namely in the general case, values of stress function F assumed at the edge fit a spatial tetragon, except side AB (Figs 7b and 8). By adding linear and constant terms, however, only two sides of this spatial tetragon can be zeroed, e.g. those above sections CD and DA. Now, the value of the stress function above corner B may still be arbitrarily specified. Since the Dirichlet problem has a unique solution for any value of F at point B, the original problem has an infinity of solutions. The solution needs a further condition to be unique. The problem has a unique solution if e.g. the middle surface of the shell, the edges and function $f(x)$ are

symmetric to the corresponding coordinate planes, thus also the solution is required to be symmetric. The above problem stated for an elliptic shell over an arbitrary triangular ground plan (Fig. 9) has a unique solution. For a polygonal ground plan with more than four sides—just as for a tetragonal ground plan—there is a solution but not a unique one.

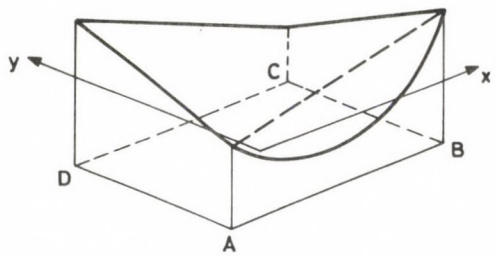

Fig. 8. Boundary curve of stress surface F

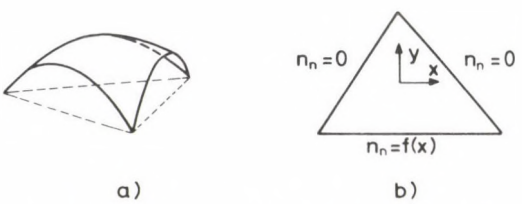

Fig. 9. (a) Elliptic shell over triangular ground plan. (b) The triangular domain and the boundary conditions

Statements similar to the above can be made if all edge sections of the elliptic shell over a polygonal ground plan, loaded on the surface, are exempt from lateral thrust [7], or the normal force value is specified all around the edge.

Special mention is due to shells of translation over a rectangular domain, because of their practical importance. The specification of the reduced normal force value all along the edge of these shells uniquely determines the reduced normal force values n_x, n_y inside the shell. The value of the reduced shear force n_{xy} is, however, uinque only if an additive constant is set apart. The shell is in membrane state in such a way that the shear force can have an inifinity of distributions within it. Namely, now stress function F may be completed, in addition to linear and constant terms, by a term xy, and so the differential equation and the boundary conditions are still satisfied.

Namely, be $z = z_1(x) + z_2(y)$ the equation of the middle surface and be the rectangle sides parallel to axes x and y, so Eq. (1) has the form:

$$\frac{d^2 z_2}{dy^2} \cdot \frac{\partial^2 F}{\partial x^2} + \frac{d^2 z_1}{dx^2} \cdot \frac{\partial^2 F}{\partial y^2} = -g \,. \tag{16c}$$

Let the rectangular domain be bounded by straight lines with the equations $x = \pm a$, and $y = \pm b$. For the sake of simplicity, let the shell be exempt of lateral pressure, a

requirement expressed by boundary conditions

$$n_x = \frac{\partial^2 F}{\partial y^2} = 0, \text{ on straight lines } x = \pm a,$$

$$n_y = \frac{\partial^2 F}{\partial x^2} = 0, \text{ on straight lines } x = \pm b. \tag{16d}$$

These boundary conditions may be formulated also in an integrated form, so that the F values produce a spatial tetragon above the boundary. It is easy to demonstrate that if F satisfies Eq. (16c) and conditions (16d) then so does function $F_1 = F + C_1 + C_2 x + C_3 y + C_4 xy$, where C_1, C_2, C_3, C_4 are arbitrary constants. Also the reduced shear forces n_{xy} obtained from F and F_1 differ from each other by constant C_4. Arbitrary constants C_1, C_2, C_3, C_4 permit to zero F all around the boundary. Irrespective of that, the reduced shear force n_{xy} is not uniquely determined else but ignoring an additive constant. The same is true for the reduced normal force value if specified all around the edge to be non-zero.

This polyvaluedness of the reduced shear force is similar to the case of vault shells over a rectangular domain if one side is parallel to the characteristics, and the value of the reduced normal force is given along the sides normal to the characteristics [23].

Dirichlet problem (16a, b) has a unique solution even if domain Ω is multiply connected. Let edge S consist of $m+1$ closed disjoint sections, i.e. let $S = \bigcup_{j=0}^{m} S_j$ where $S_j (j = 0, 1, 2, \ldots, m)$ is twice continuously differentiable, and let the bounded domain limited by curve S_0 contain the other m curves S_j (Fig. 10a). Let the value of stress

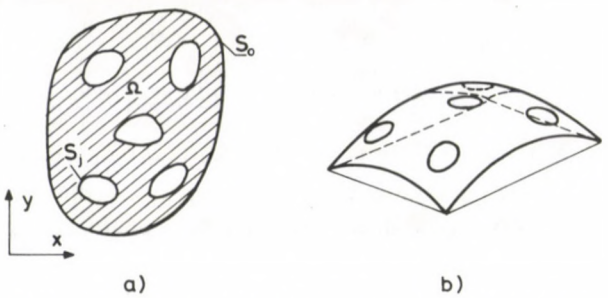

Fig. 10. (a) Multiply connected domain. (b) Elliptic shell over a multiply connected domain

function F be given on curves S_j as $\varphi_j (j = 0, 1, 2, \ldots, m)$. If φ_j is continuous, then problem (16a, b) has a unique solution. Mikhlin (p. 167 in [15]) presents the solution process for the case where Eq. (16a) is of canonic form and homogeneous.

Let every edge of the elliptic shell over a multiply connected domain be bordered by an edge beam resisting only tension and compression (Fig. 10b). Let us specify the values of the stress function above every closed boundary S_j to form there a closed

plane curve (in a different plane for every boundary). Under this condition the shell is in membrane state and the edge beam can be made to develop only tension and compression, that is, edge curves will be funicular curves of the arising forces. Then, however, the edge beams have to be exposed to vertical external forces of the proper distribution to safeguard the equilibrium of the shell and its edge beams as well as the "funicularity" of the edge beam axes also in space. For specified edge planes of the stress surface, the state of stress of the shell, hence the distribution and the value of the vertical forces to be applied on the edges, can be determined. Specifying as the only boundary condition that vertical external forces act on the edge beams (edge curves be funicular curves of the arising forces), the shell is in membrane state, but not in a unique one, since the boundary forces of the stress surface may lie in arbitrary planes. (A shell subjected to a fixed surface load may be in membrane state under a variety of edge loads. Accordingly, the state of stress of the shell will be different.) Under such a boundary condition, the shell is statically indeterminate and the mean value of e.g. the vertical edge load acting on the inner shell edges can also be specified. The distribution function of the edge load cannot, however, be arbitrarily specified, since it is correlated with the membrane forces acting on the edge beam. ([9] presents this relationship for e.g. a circular skylight opening in a paraboloidal shell of revolution.) This type of shell with a doubly connected domain was analyzed by e.g. Csonka [8]. A similar problem under somewhat different conditions was studied e.g. in [10, 11].

Vekua [26, 27] also dealt with membrane shells over multiply connected domains. His examinations, however, do not rely on the Pucher equation but on complex analysis. He found the existence and uniqueness of the solution of the problem, and the type of boundary values to be also related to the so-called index number of the problem which is not be considered here. His results will be outlined in Chapter 4.

3.2. The second boundary-value problem

Be Ω a bounded domain with boundary S in plane xy. Let a direction i (unit vector) pointing outward from Ω be assigned to every point of edge curve S (Fig. 11) and let the directional derivative of the stress function F in direction i on edge S be given by a function φ. Now, let us consider the second boundary value problem:

$$\mathscr{L}F = -g\,, \tag{17a}$$

$$\left.\frac{\partial F}{\partial i}\right|_S = \varphi\,. \tag{17b}$$

The second boundary value problem (17a, b) has a solution that is unique except for an additive constant if conditions are satisfied:

(a) domain Ω with boundary S is in the domain of definition of Eq. (17a);
(b) Ω is a simply connected domain;
(c) edge S is a Liapunov closed curve;

(d) direction i is not tangent to curve S at the point where direction i is indicated;
(e) direction i λ-Hölder-continuously varies along curve S;
(f) $g(x, y)$ is continuous on Ω and S, and λ-Hölder-continuous on Ω;
(g) φ is continuous on S;
(h) $z(x, y)$ is twice differentiable on Ω and S, and its second partial derivatives are λ-Hölder-continuous;
(i) compatibility condition

$$-\int\int_{\Omega} g(x, y)\,\mathrm{d}x\,\mathrm{d}y - \int_{S} \varphi(s)\,\mathrm{d}s = 0 \tag{18}$$

(where s is arc length of curve S) is satisfied.

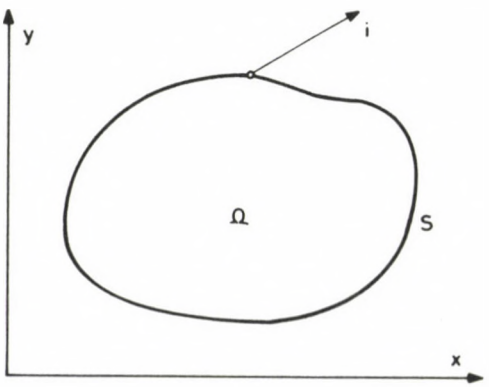

Fig. 11. Simply connected bounded domain

If these conditions are satisfied, the solution can be produced by means of integral operators (in potential form).

It should be mentioned that conditions (e), (f) and (h) are always satisfied if they are assumed to be continuously differentiable rather than to be λ-Hölder-continuous.

Let n be the normal (unit vector) pointing outward from Ω at an arbitrary point P of edge S, and t the direction (unit vector) of the tangent of edge S at point P (Fig. 12). Let $i \equiv n$.

Let us consider an elliptic shell over a polygonal ground plan, subjected to a vertical surface load of arbitrary distribution (Fig. 13a). Let the polygon have m sides, of lengths $a_1, a_2, \ldots, a_m$ (Fig. 13b). Be the shell supported so that its boundary sections $S_j (j = 1, 2, \ldots, m)$; $S = \bigcup_{j=1}^{m} S_j$ are exempt from shear all around. Exemptness from shear of a straight boundary section is known to be provided by the condition $\partial F/\partial n = \text{constant}$ [22]. Thus, actually, the boundary condition becomes:

$$\left.\frac{\partial F}{\partial n}\right|_{S_j} = b_j, \quad b_j = \text{constant} \ (j = 1, 2, \ldots, m). \tag{19}$$

A term of the form $Ax + By$, where A and B are constant can be added to stress function F without affecting the state of stress of the shell. Suitably choosing A and B, two of constants b_j can be zeroed. Be e.g. $b_1 = b_2 = 0$. Now, (19) is replaced by:

$$\left.\frac{\partial F}{\partial n}\right|_{s_j} = b_j, \quad \begin{cases} b_j = 0 & \text{if} \quad j = 1, 2 \\ b_j = \text{const.} & \text{if} \quad j = 3, 4 \ldots, m. \end{cases} \tag{20}$$

Function φ in condition (17b) becomes now a step function, with jumps at the knee points of boundary S. Thus, neither condition (c) nor (g) are satisfied at the knee points of boundary S. Corners are therefore rounded off by circles of radii ε small enough, and discontinuities of function φ are eliminated by connecting function values b_j and b_{j+1} at the end points of the circular arc by means of a section linearly varying along the arc. Thereby conditions (a) to (h) can be satisfied. (Solution of the original problem will be defined as limit transition $\varepsilon \to 0$.) But also compatibility condition (18) awaits to be satisfied, becoming

$$-\iint_{\Omega} g(x, y)\, dx\, dy - \sum_{j=3}^{m} a_j b_j = 0. \tag{21}$$

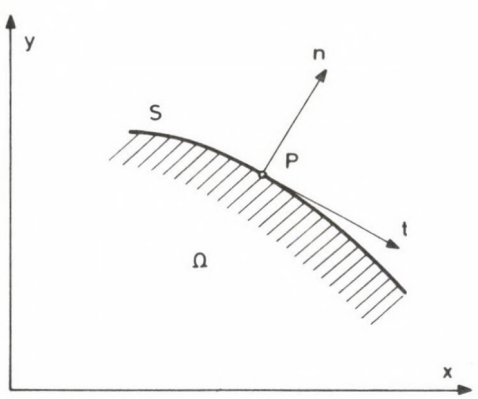

Fig. 12. Normal and tangential unit vectors of the boundary line at a point

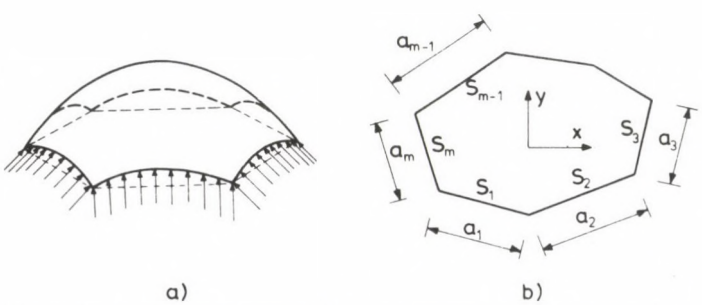

Fig. 13. (a) Elliptic shell over polygonal ground plan, with edges normally supported. (b) The polygonal domain

From $m > 3$, condition (21) is seen to be satisfiable in infinitely many ways, namely all b_j values but one are arbitrary. Any system of constants b_j satisfying (21) determines a given condition (17b) under that the boundary-value problem (17a, b) has a solution, unique except for an additive constant. Since constants b_j have an infinity of systems satisfying (21), also this problem has an infinity of solutions. For $m = 3$, constant b_j is uniquely defined by condition (21), hence also condition (17b) is a unique one, accordingly, the problem has a unique solution except for an additive constant. The additive constant is, however, known not to affect the state of stress of the shell.

In final account, the above permit the statement that an elliptic shell over a polygonal ground plan will always be in membrane state if its edge is exempt from shear forces all around. For a triangular ground plan, the problem is a statically determinate one, and the shell cannot be but in one kind of membrane state. For a tetragonal or polygonal ground plane, however, the problem is a statically indeterminate one, letting the shell to be in a variety of membrane states.

The case where the value of the reduced shear force n_{nt} is specified all along the shell edge is quite analogous to the above.

Our results relying on a mathematical theory can also be achieved by structural considerations. Let us consider the ground plan of the shell treated above with edges exempt from shear (Fig. 13b). Be point P the projection on the ground plan of the

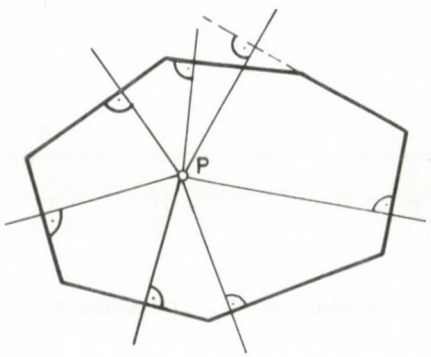

Fig. 14. Influence lines of side-wise partial resultants of reduced normal forces along the boundary

application point of the resultant of surface forces $g(x, y)$ loading the shell (Fig. 14). P needs not to be inside the polygon. Since each edge section is acted upon only by normal forces, the resultant of these normal forces is section-wise normal to the given polygon side. At the same time, the shell as a rigid body may be in equilibrium if e.g. influence lines of the resultants of the normal forces acting on the edge sections intersect at one point on the influence line of the external load resultant. On the ground plan all the influence lines of the partial resultants cross point P (Fig. 14). The possibility for the partial resultants to intersect also in space at one point is provided by the fact that the vertical plane section of an elliptic surface is never straight and so a normal force system

can always be defined on the section curve, with a resultant crossing at a desired height z the section plane forming the curve. Since for spatial forces with a common point of intersection, a force can be balanced uniquely by forces of given influence lines only if there are three influence lines, only the elliptic shell with a no-shear edge, over a triangular ground plan, can be in unique membrane state.

3.3. The third boundary-value problem

Be Ω a bounded domain with boundary S in plane xy. Let a direction i (unit vector) be assigned to every point of the boundary curve S (Fig. 11), and let functions α, β and φ be given on boundary S so that $\alpha > 0$ hold at any point of boundary S. Now, let us consider the third boundary-value problem

$$\mathscr{L}F = -g\,, \tag{22a}$$

$$\left(\alpha \frac{\partial F}{\partial i} + \beta F\right)\Big|_S = \varphi\,. \tag{22b}$$

Let conditions

(a) domain Ω with boundary S is within the domain of definition of Eq. (22a);
(b) Ω is a simply connected domain;
(c) edge S is a Liapunov closed curve;
(d) direction i is not tangent to curve S at the point where it is given;
(e) direction cosines of i differentiably vary along S, so that derivatives are λ-Hölder-continuous;
(f) $g(x, y)$ is continuous on Ω and S, and λ-Hölder continuous on Ω;
(g) β is continuous on S;
(h) φ is continuous on S;
(i) $z(x, y)$ is three times differentiable on Ω and S, and its third partial derivatives are λ-Hölder-continuous

be fulfilled.

Now,—the Pucher operator $\mathscr{L}$ being self-adjoint (p. 12 in [16])—the third boundary-value problem (22a, b) has the following alternatives (Theorems 22, I; 22, III; 23, I; 23, II; 23, VII in [16]):

Homogeneous problem

$$\mathscr{L}F = 0\,, \tag{23a}$$

$$\left(\alpha \frac{\partial F}{\partial i} + \beta F\right)\Big|_S = 0 \tag{23b}$$

associated to problem (22a, b) has either a unique solution $F = 0$, then problem (22a, b) has one and only one solution for arbitrary functions g and φ (producible by means of

integral operators); or the homogeneous problem (23a, b) has p linearly independent solutions $F_1, F_2, \ldots F_p$, and in this case problem (22a, b) can only be solved if for every $F_j (j=1, 2, \ldots, p)$ the compatibility condition

$$-\int\int_{\Omega} g(x, y) F_j(x, y)\, dx\, dy - \int_S \varphi(s) \cdot F_j(s)\, ds = 0\,, \tag{24}$$

where s is arc length parameter of curve S, is satisfied. If condition (24) is satisfied for every $F_j (j=1, 2, \ldots, p)$ problem (22a, b) has an infinity of solutions, and if F_0 is one of them, then all the others are of the form $F_0 + \Sigma c_j F_j$ where c_j is an arbitrary constant. For $\beta > 0$, problem (22a, b) has one and only one solution.

The physical meaning of the third boundary value is known for a circular domain. Be $i \equiv n$, where n is the outer normal to circular line S. Be R the radius of the circle. The specification of the value of the reduced shear force n_{nt} all around the boundary by a function χ leads to the condition [22]:

$$\frac{1}{R} F - \frac{\partial F}{\partial n} = \int \chi\, ds + \alpha\,, \tag{25}$$

where s is the arc length parameter of the circular arc, and a is a constant. Exemptness from shear forces of the edge is expressed by

$$\frac{1}{R} F - \frac{\partial F}{\partial n} = a\,. \tag{26}$$

The possibility for an elliptic shell over a circular ground plan to be in membrane state or not under boundary condition (25) or (26), and in the positive case, whether these boundary conditions uniquely determine the internal forces of the shell or not, can be ascertained according to the alternative theorem above.

Let us consider a simple example. Let us take a shell of paraboloid of revolution subjected to vertical surface loads. Let the equation of the middle surface be

$$z = \frac{1}{2}(x^2 + y^2)\,.$$

Be the shell edge with the equation $x^2 + y^2 = R^2$ exempt from shear forces. Now, the shell balances external loads solely by normal forces in its edge (Fig. 15). Now, the boundary condition is (26). Let this equation be multiplied by -1 to statisfy condition $\alpha > 0$. In this way we arrive at the boundary value problem:

$$\frac{\partial^2 F}{\partial x^2} + \frac{\partial^2 F}{\partial y^2} = -g\,, \tag{27a}$$

$$\left(\frac{\partial F}{\partial n} - \frac{1}{R} F\right)\Big|_S = -a\,, \tag{27b}$$

where a is a constant. In condition (27a), $\alpha \equiv 1, \beta \equiv -1/R$. Load function g is required to satisfy condition (f). Thereby every precondition of the alternative theorem is satisfied.

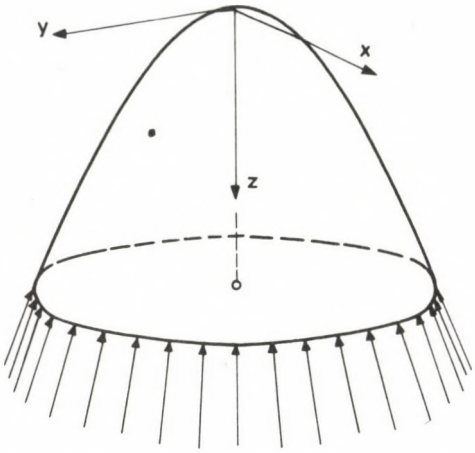

Fig. 15. Paraboloid shell of revolution with normally supported edges

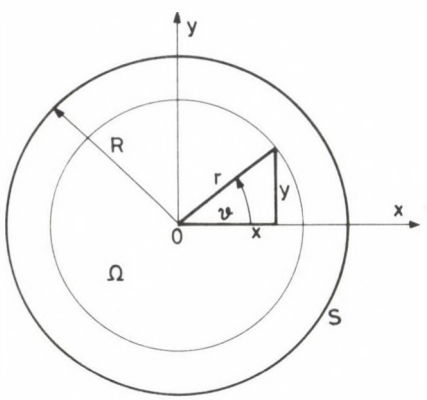

Fig. 16. The shell ground plan and the coordinate systems

Let us examine where this shell is in membrane state. For $\beta > 0$, problem (27a, b) would have a unique solution. In the actual case, however, $\beta < 0$, and so the alternative theorem has to be applied.

Let us turn to polar coordinates by transformation

$$x = r \cdot \cos \vartheta, \quad y = r \cdot \sin \vartheta \tag{28}$$

(Fig. 16). Thereby problem (27a, b) becomes:

$$\frac{\partial^2 F}{\partial r^2} + \frac{1}{r}\frac{\partial F}{\partial r} + \frac{1}{r^2}\frac{\partial^2 F}{\partial \vartheta^2} = -g\,, \tag{29a}$$

$$\left(\frac{\partial F}{\partial r} - \frac{1}{r}F\right)\Bigg|_{r=R} = -a\,. \tag{29b}$$

Let us consider now the homogeneous problem

$$\frac{\partial^2 F}{\partial r^2} + \frac{1}{r}\frac{\partial F}{\partial r} + \frac{1}{r^2}\frac{\partial^2 F}{\partial \vartheta^2} = 0, \tag{30a}$$

$$\left(\frac{\partial F}{\partial r} - \frac{1}{R}F\right)\Big|_{r=R} = 0 \tag{30b}$$

associated to problem (29a, b). A substitution easily demonstrates that the boundary condition (30b) is satisfied by every function of the form $\bar{F} = r \cdot f(\vartheta)$. Substituting $\bar{F}$ into (30a) yields the ordinary differential equation

$$\frac{d^2 f}{d\vartheta^2} + f = 0 \tag{31}$$

with the linearly independent solutions $f_1 = \sin \vartheta$ and $f_2 = \cos \vartheta$. Thus, problem (30a, b) will have the following two, linearly independent solutions:

$$F_1 = r \cdot \sin \vartheta, \quad F_2 = r \cdot \cos \vartheta. \tag{32}$$

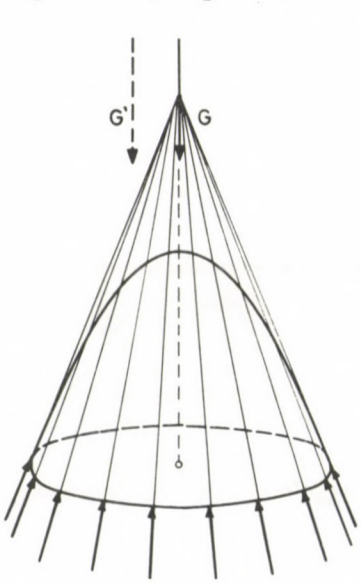

Fig. 17. Forces on a shell

Let us see now whether the compatibility condition (24) is satisfied for functions (32) or not. Since in this case $\varphi = -a$ (a is a constant), substituting F_1 and F_2 into (24) and taking (28) into consideration we obtain

$$\iint_{\Omega} g \cdot y \, dx \, dy = 0, \quad \iint_{\Omega} g \cdot x \, dx \, dy = 0 \tag{33}$$

expressing the moment of surface load g about both axes x and y to be zero. Thus, resultant G of the surface loads has to cross the origin of the coordinate system, i.e. the centre of the basic circle, the common intersection point of influence lines of reduced normal forces along the edge. Now the shell is in membrane state but the internal forces are not uniquely determined. The problem in this case is a statically indeterminate one.

If the load function g fails to satisfy Eqs (33), that is, the resultant of load g does not cross the centre of the basic circle, then the shell cannot be in membrane state.

As a matter of fact, compatibility equations (33) are equilibrium conditions of the shell as a rigid body. The shell concerned can only be in equilibrium if the influence line of resultant G of the surface load g crosses the common intersection point of the influence lines of the normal forces along the edge (Fig. 17). If the resultant of the surface load does not cross the common intersection point (this position of the resultant is shown by vector G' in Fig. 17) the shell cannot be in equilibrium, hence neither in membrane state.

It should be pointed out that similar statements can be made for cones supported in the direction of the generatrices [23].

A number of cases of the mode of supporting discussed above were also analysed by Gol'denveiser (pp. 186 and 202 in [12]; [12a]).

3.4 The mixed boundary-value problem

As we have introductorily mentioned in Chapter 3, by a mixed boundary-value problem referring to Eq. (1) we understand the one where in the boundary condition:

$$\alpha \frac{\partial F}{\partial i} + \beta F = \varphi \tag{34}$$

α or β vanishes in a section of boundary S without being identically zero all along the complete boundary.

For a simply connected bounded domain Ω, and for $\beta = 0$ in some sections of boundary S, the possibility of solving this mixed problem can be ascertained according to the alternative theorem in Section 3.3.

The problem is much more difficult where the bounded domain Ω is simply connected, and in some sections of boundary S, $\alpha = 0$. [16] offers some references on the possibility of solving mixed boundary-value problems of this type (see pp. 233 to 235 in [16]).

If Ω is a doubly connected bounded domain limited by boundaries S_1 and S_2 with no common part ($S = S_1 \cup S_2$, $S_1 \cap S_2 = \varnothing$), and the function F we are looking for is given on boundary S_1, while function (34) on edge S_2 (provided $i \equiv \nu$), F may be written in potential form, permitting to consider the existence of a solution for the problem (p. 233 in [16]).

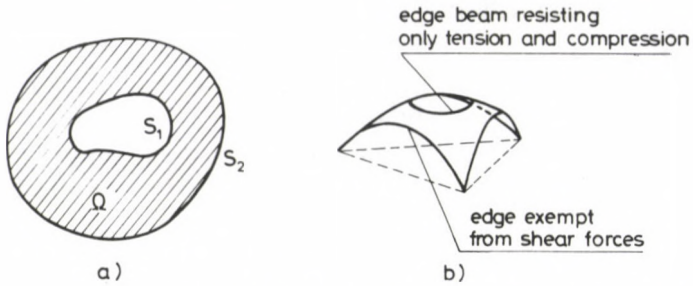

Fig. 18. (a) Doubly connected domain. (b) elliptic shell with a sky-light opening over triangular ground plan

Thus e.g. Eq. (1) of canonic form has always a solution in the domain seen in Fig. 18a if values F and $\partial F/\partial n$ are specified for boundaries S_1 and S_2, respectively [20]. Accordingly, a shell of paraboloid of revolution with a sky-light opening over a polygonal ground plan may always be in membrane state if the opening is bounded by an edge beam resisting only tension and compression, and the outer edge of the shell is exempt from shear forces. Obviously, the edge of the sky-light opening has to be acted upon by a suitable vertical edge load. Such a shell over a triangular ground plan is seen in Fig. 18b.

4. Boundary conditions for the system of the equilibrium equations of elliptic membrane shells

Discussions above relied on the Pucher differential equation of membrane shells. At last—even if as a reference—let us talk about another way of discussion.

Another way of discussing membrane shells is by applying a system of differential equations written for the internal forces (p. 106 in [12]). In these equations the internal forces are unknown, permitting boundary conditions to be given directly with the expressions of the internal forces. Let us consider the tangent plane of an elliptic shell at a point P of the shell edge $\bar{S}$. Let us define directions in the tangent plane, normal to, and tangent to the edge curve at the tangential point. Be N_n the normal force, N_{nt} the shear force in tangential direction. Let us give a direction i in the tangent plane at the tangential point, with an angle $\sigma(\tau)$ between the normal and i (Fig. 19). Now, in the general case, the following boundary condition can be specified for the edge curve (p. 201 in [12], p. 81 in [26]):

$$N_n \cos \sigma(\tau) + N_{nt} \sin \sigma(\tau) = \gamma(\tau), \qquad \tau \in \bar{S}. \tag{35}$$

This condition includes two important cases:

1. for $\sigma(\tau) = 0$, $N_n = \gamma(\tau)$,

2. for $\sigma(\tau) = \dfrac{\pi}{2}$, $N_{nt} = \gamma(\tau)$.

Thus, for $\gamma(\tau)=0$, the shell edge may be required to be exempt from lateral pressure or from shear force.

The boundary-value problem of membrane shells is also interpreted for simply and multiply connected domains, and so is of course the mixed problem. Let us have e.g. a doubly connected shell. Let edge $\bar{S}$ consist of two curves with no common part: $\bar{S}=\bar{S}_1 \cup \bar{S}_2$. Now, $N_n=\gamma_1(\tau)$ on $\bar{S}_1$, and $N_{nt}=\gamma_2(\tau)$ on $\bar{S}_2$ may be specified.

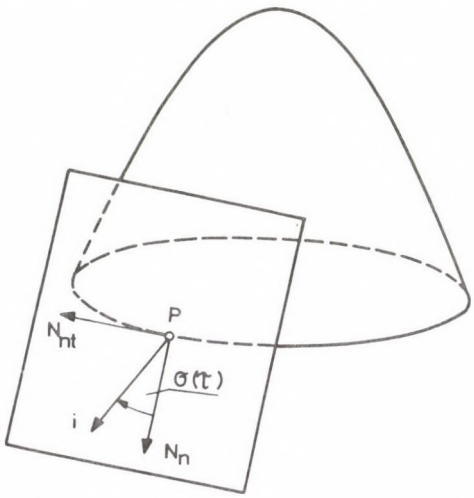

Fig. 19. Preferential directions belonging to the edge curve in a tangent plane of the shell

Vekua [26, 27] gives an analysis of the existence of a solution for these problems, by means of functions of complex variable. Special consideration was made for the case of specifying the distribution of the normal force N_n along the shell edge. According to his analyses, under such a boundary condition, an elliptic shell over a simply connected domain can only be in membrane state if certain integral conditions of form (18) are satisfied. The same statement holds for doubly connected domains. The shell over three or more times connected domain is always in membrane state, but this is not a unique one since if the domain is $m+1$ times connected, then the expression for the internal forces includes $3m-3$ real constants of arbitrary value.

Acknowledgement

The author is greatly indebted to Dr. Lajos Kollár for having raised his interest in the problem of boundary conditions and for his valuable advice forwarding this tripartite paper.

References

1. Beckenbach, E. F.: Modern Mathematics for the Engineer. McGraw–Hill Book Company, New York, Toronto, London 1956, (Chapter 6)
2. Beles, A. A., Soare, M. V.: Das elliptische und hyperbolische Paraboloid im Bauwesen. VEB Verlag für Bauwesen, Berlin; Akademie-Verlag, Bukarest 1971, (S. 238)
3. Bergman, S.—Schiffer, M.: Kernel Functions and Elliptic Differential Equations in Mathematical Physics. Academic Press, Inc., New York 1953
4. Bitsadze, A. V.: Boundary Value Problems for Second Order Elliptic Equations. North-Holland Publishing Comp., Amsterdam 1968
5. Csonka, P.: Apse-like formed paraboloid shells of revolution. Acta Techn. Hung. 32 (1961), 39–52
6. Csonka, P.: Membrane shells with perfectly free edges. Acta Techn. Hung. 40 (1962), 151–167
7. Csonka, P.: The boundary line of the stress surface of calotte shells. Acta Techn. Hung. 48 (1964), 203–209
8. Csonka, P.: Paraboloid shell of revolution with an eccentrical skylight opening. World Conference on Shell Structures October 1–4, 1962 San Francisco, California. National Academy of Sciences-National Research Council, Washington, D. C. 1964, pp. 501–508
9. Csonka, P.: On the internal edge beam of paraboloidal shells of revolution having a circular skylight opening. Acta Techn. Hung. 49 (1964), 219–231
10. Csonka, P.: Regular polygon based paraboloid shells of revolution having a circular skylight opening. Acta Techn. Hung. 79 (1974), 73–91
11. Eibl, J.: Zur Anwendung konformer Abbildungen in der Membrantheorie bei Schalen nach Flächen 2. Ordnung mit positiver Gauss-Krümmung. Werner-Verlag, Düsseldorf 1969
12. Gol'denveizer, A. L.: The Theory of Thin Elastic Shells (in Russian). Gos Izd. Tekhniko-Teor. Lit., Moscow 1953

12a. Gol'denveiser, A. L.: The Theory of Thin Elastic Shells. 2nd. Ed. (in Russian). Izd. Nauka, Moscow 1976

13. Hadamard, J.: Le problème de Cauchy et les équations aux dérivées partielles linéaires hyperboliques. Ed. Herman, Paris 1932
14. Menyhárd, I.: Analysis and Construction of Shell Structures (In Hungarian). Műszaki Kiadó, Budapest 1966
15. Mikhlin, S. G.: Integral Equations and their Applications to Certain Problems in Mechanics, Mathematical Physics and Technology (In Russian). 2nd Edition. OGIZ, Moscow–Leningrad 1949
16. Miranda, C.: Partial Differential Equations of Elliptic Type. 2nd ed. Springer-Verlag, Berlin, Heidelberg, New York 1970
17. Miranda, C.: Private communication to the author
18. Petrovskii, I. G.: Lectures on Partial Differential Equations (In Russian). Gos. Izd. Fiziko-Mat. Lit., Moscow 1961
19. Pflüger, A.: Elementare Schalenstatik. Springer-Verlag, Berlin, Göttingen, Heidelberg 1957
20. Sneddon, I. N.: Elements of Partial Differential Equations. McGraw–Hill, Book Company, New York, Toronto, London 1957
21. Szmodits, K.: Statik der Schalenkonstruktionen. B. G. Teubner Verlagsgesellschaft, Leipzig 1966
22. Tarnai, T.: Existence and uniqueness criteria of the membrane state of shells. I. Hyperbolic shells. Acta Techn. Hung. 91 (1980), 81–110
23. Tarnai, T.: Existence and uniqueness criteria of the membrane state of shells. II. Parabolic shells. Acta Techn. Hung. 92 (1981), 67–88
24. Tikhonov, A. N.—Samarskii, A. A.: Partial Differential Equations in Mathematical Physics (In Russian). Izd. Nauka, Moscow 1972
25. Tolotti, C.: Sul problema di Cauchy. Atti della Reali Accademia Nazionale dei Lincei. Rendiconti Classe di Scienze fisiche, matematiche e naturali. Serie 6ª, Vol. XXIX. (1939), 119–125
26. Vekua, I. N.: Systeme von Differentialgleichungen erster Ordnung vom elliptischen Typus und Randwertaufgaben mit einer Anwendung in der Theorie der Schalen. VEB Deutscher Verlag der Wissenschaften, Berlin 1956
27. Vekua, I. N.: Über die Bedingungen der Verwirklichung des momentenfreien Spannungsgleichgewichtes von Schalen positiver Krümmung. IUTAM. Proceedings of the Symposium on the Theory of Thin Elastic Shells. North-Holland Publishing Comp., Amsterdam 1960, pp. 270–280

Acta Technica Academiae Scientiarum Hungaricae, 96 (1—4) pp. 87—105 (1983)

ON THE CYCLIC LOADING BEHAVIOUR OF SAND

W. F. VAN IMPE*

[Received: 28 February 1984]

The problem of liquefaction of watersaturated sand samples subjected to vertical cyclic loading in undrained conditions has been investigated in many types of laboratory tests. In simple shear and conventional triaxial test equipment, cyclic loading leads to very important compliance due to membrane penetration and end-bearing plates, resulting in unconservative deviations of the measured pore-pressures during these tests. At the laboratory of Soil Mechanics of the Ghent State University, the author developed a model test for cyclic vertical loading of large scale samples without any membrane supply. In this paper, results of a lot of large scale vertical cyclic loading tests and the interpretation of it with respect to the state-of-the art at the moment will be shown.

1. Introduction

It is well known that the dilatation and/or compaction phenomena in a non-cohesive and saturated soil are responsible for internal pore pressure development during very quick loading such as some types of cyclic loading.

Of course the draining conditions around and the permeability of the sand itself must be influencing such pore pressure development. One can feel that they moreover do influence in a very determinate way the deformation characteristics of the soil skeleton.

2. Cyclic triaxial loading tests

(a) A lot of research work has been done over the last two decades in the field of cyclic loading of saturated sand, mainly in consolidated and undrained cyclic triaxial loading conditions. One can refer to the work of Seed and Lee and a lot of other scientists.

One can resume, all of the mentioned research work ends up by describing, after a few loading cycles, a phenomenon called liquefaction of the triaxial sand sample, whatever its relative density.

Indeed, even for dense sand, a few loading cycles at a given stress level can be sufficient to make at a given moment the pore water pressure (Δu) rising up to the initial consolidation stress (σ_c), (Fig. 1).

* Prof. Dr. ir. W. F. VAN IMPE, Laboratorium voor Grondmechanica, B-9710 Zwijnaarde, Grotesteenweg-Noord 2, Belgium

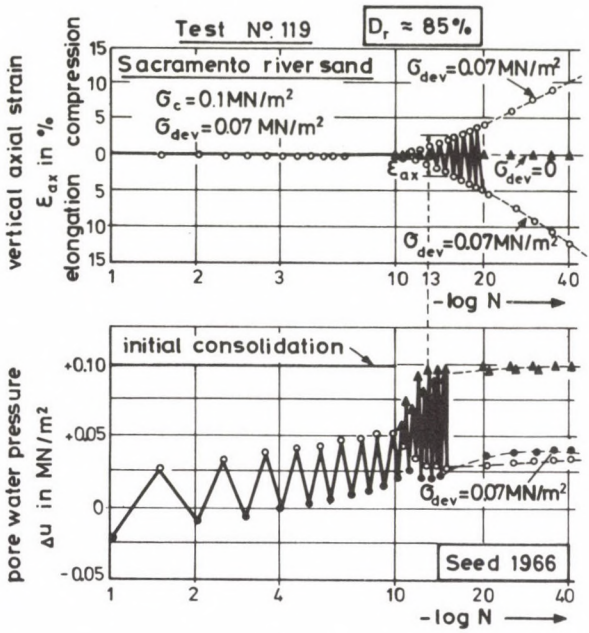

Fig. 1

Be aware although that for dense saturated sand samples:

1. the $\Delta u = \sigma_c$-condition is only very temporary and is produced at low deviatoric stress
2. at higher deviatoric stress Δu is diminishing again
3. axial deformation of the sand sample is developing only relatively slow, even after reaching $\Delta u = \sigma_c$ conditions
4. pore pressures are measured at the top of a completely enclosed small saturated sample.

Moreover, from this test results it became clear the number of loading cycles needed to obtain the first condition of zero effective stress $\Delta u = \sigma_c$ at given conditions of relative density and of deviatoric stress level, is rising with increasing mean effective stress. In literature one at the beginning so suggested that due to cyclic loading on a saturated sand at given relative density, the liquefaction potential is decreasing with increasing mean effective stress.

Such conclusion is opposite to our common knowledge and is contradicted by all practical cases.

(b) The contradictions do find their origin in the word "liquefaction" misused for the description of the phenomena seen in the cyclic triaxial loading.

In the case of a monotonic increasing deviatoric stress (Fig. 2) the term "liquefaction potential of a sand mass" is dedicated to the value of the hydraulic gradient developed at a given density of the sand mass by such deviatoric stress, (value

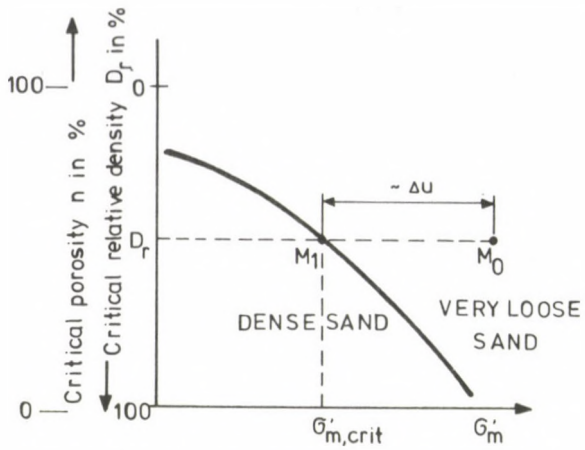

General relation between the spherical stress σ'_m and the critical relative density

Fig. 2

of $M_0 - M_1$). Of course such liquefaction potential rises as the effective spherical stress at stat σ'_m is increasing.

In the case of cyclic deviatoric loading on the contrary the term "liquefaction potential" only is indicating: the chance to bring up pore-water pressure at a given moment and place, to the effective spherical stress value at that point. It is clear that this chance is diminishing if such effective spherical stress at the start of the test is increased. Thus one needs the more loading cycles, the higher the spherical effective stress.

The expression "liquefaction" so only should be used for the collapse of a non-cohesive very loose non-cohesive soil skeleton due to increasing deviatoric stress and satisfying two conditions (Fig. 3):

1. the collapse is developing at very high deformation speed
2. the deformation speed ends up at a rather high level as long as the external loading on the sand mass keeps constant.

It seems that this happens for sands below or at critical density and at constant external loading.

Therefore in the cases 4 and 5 of Fig. 3 there is no liquefaction to be mentioned.

Deformation speeds such as shown in curve 5 are the characteristic results from cyclic triaxial tests on dense sand samples. Some authors therefore now prefer speaking about "cyclic mobility" of dense saturated sand rather than to use the liquefaction-term.

(c) Although, even if the contradictions in terminology can be clarified, one still has to state that the cyclic triaxial results indicate (locally and temporarely) very high pore water pressures Δu even in very dense sand masses. The main researchwork of the past five years in the Soil Mechanics Laboratory of Ghent State University turned

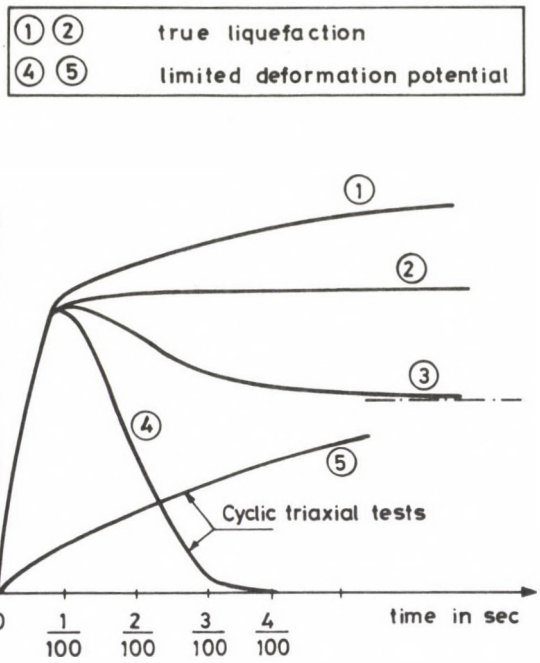
① ② true liquefaction
④ ⑤ limited deformation potential
speed of deformation v
①
②
③
④
⑤
Cyclic triaxial tests
0
1/100
2/100
3/100
4/100
time in sec

Fig. 3

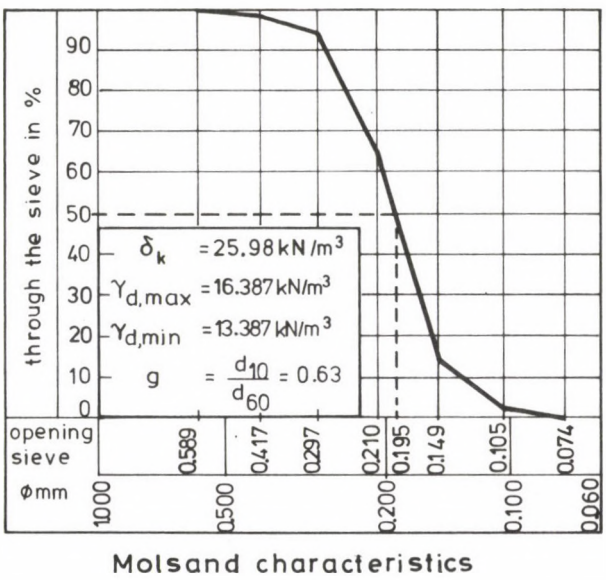
through the sieve in %
90
80
70
60
50
40
30
20
10
0
δk = 25.98 kN/m3
γd,max = 16.387 kN/m3
γd,min = 13.387 kN/m3
g = d10/d60 = 0.63
opening sieve φmm
1.000
0.589
0.500
0.417
0.297
0.210
0.200
0.195
0.149
0.105
0.100
0.074
0.060
Molsand characteristics

Fig. 4

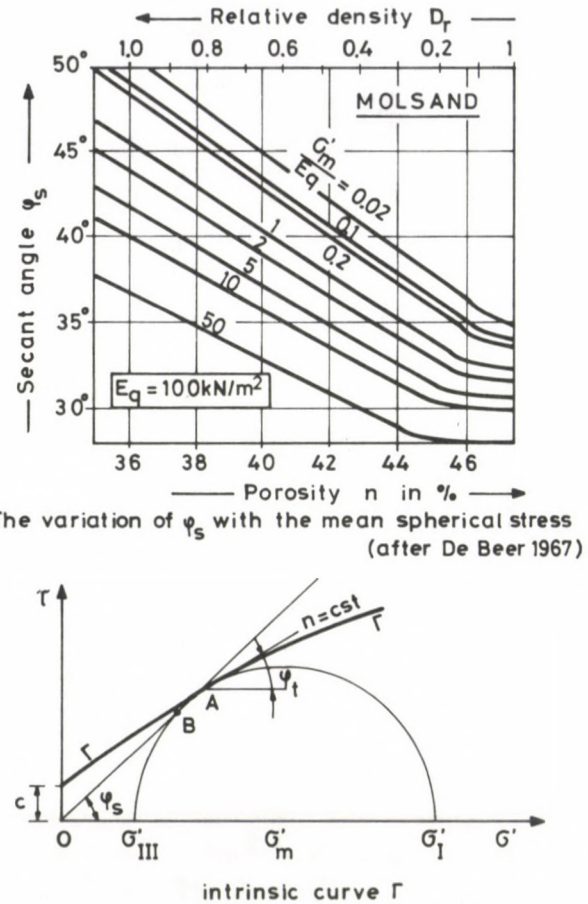

Fig. 5

about the differences in saturated sand of pore pressure development and deformation behaviour during cyclic loading, depending on the way of testing itself [15, 16, 19].

Starting this research a lot of consolidated undrained cyclic triaxial tests were carried out on saturated samples of Molsand, a tertiary sand with well-known characteristics (Figs 4 and 5).

From these test results, some findings are made leading to some criticism on the classical way of interpretation and use of the cyclic triaxial test results, [18]. The interpretation of such triaxial cyclic loading tests is normally based on the idea of constant stress level $s_l = \sigma_{dev}/2\sigma_c$ and constant relative density of the sand throughout the whole cyclic loading test and over the full height of the sample (Fig. 6).

1. One of the findings, that can also be made from a review of the test results in literature, contains the lowering of the cyclic vertical load as soon as axial deformation

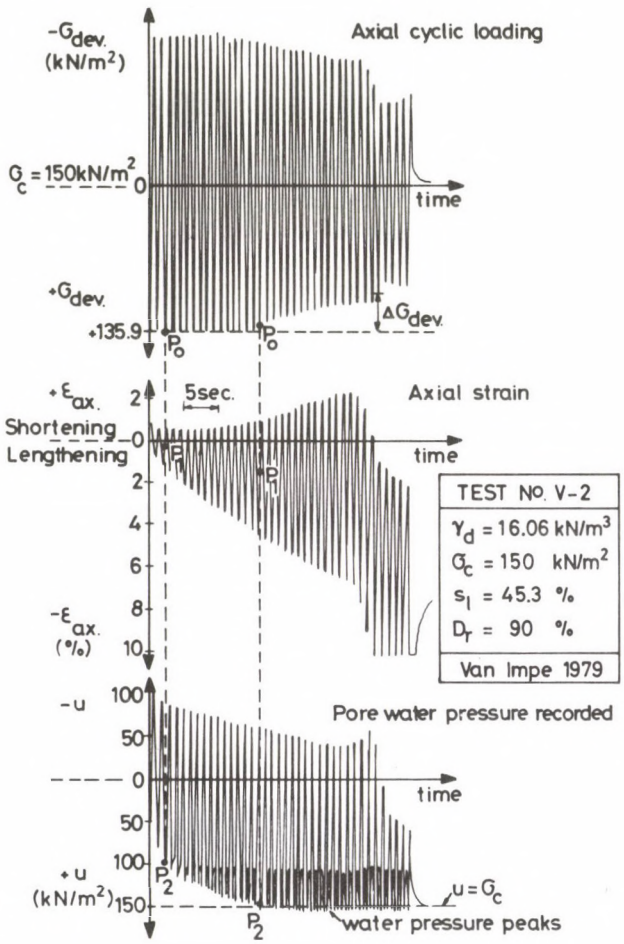

Fig. 6

ε_{ax} of the sample becomes more important. The loading piston in the triaxial equipment no longer follows the sample deformation.

The numerical value of lowering of the axial loads depends on the type of hydraulic system, on the type of bushings of the triaxial cell and on the frequency of the applied cyclic loading. In the interpretation of test results (Fig. 7) the 5% or 10% axial strain level often is used putting the number of cycles needed for this axial strain ε_{ax} versus stress level s_l, supposed to be constant all over the test.

Nevertheless, it should be taken into consideration that such axial strain ε_{ax} in most of the test results appears while the loading piston on the sample ceases to strictly follow the vertical deformations of the sample. As the recorded axial strain always is a measure of the displacements of the loading piston, the expression of the stress level s_l at

the start of the test needed to obtain a given axial strain of the sample mostly only can be a rough assumption.

2. Another finding is that the axial strain level, represented in the conventional diagrams, is put in without a sign. As evident from the test results (Fig. 6), a considerable number of samples however show an axial lengthening during the vertical cyclic loading; such lengthening, more or less pronounced, was found in cyclic triaxial

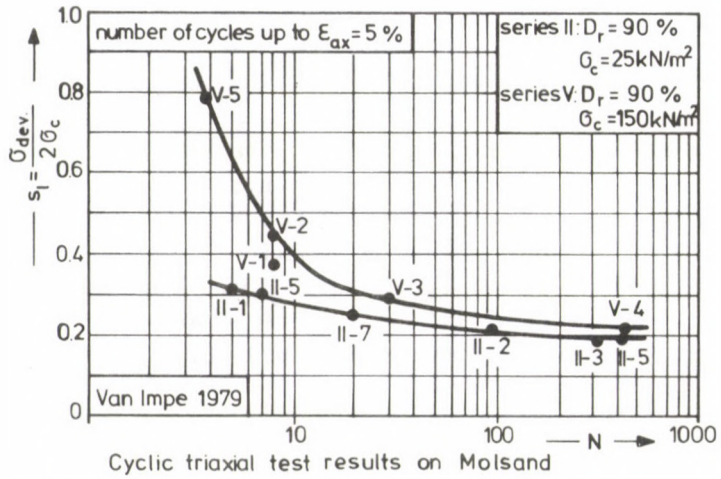

Fig. 7

loading tests on samples of Molsand of relative density $D_r \geqq 70\%$. At $D_r \leqq 40\%$, on the other hand there always exists a positive double strain amplitude (shortening). It therefore, can be expected that there are "critical" combinations of σ_c and D_r above which vertical cyclic loading in triaxial tests leads to lengthening and necking of the sample which does not at all appear in nature. As a cause of the lengthening effect of very dense sand samples in cyclic triaxial tests, one can assume the extreme non-uniformity of the stress distribution leading to the redistribution of pore water in the sample, oversaturating the upper part of it.

(d) Mainly due to the boundary conditions of the sample, the mentioned non-uniform stress distribution is introduced causing non-uniform changes in relative density. Unfortunately, the test results are always interpreted without taking this into account. Triaxial test results under a monotonously rising deviatoric stress are not so much affected by the boundary conditions; moreover they are normally expressed in terms of ultimate stress. In such conditions non-uniform stress distribution has a much more limited influence. In cyclic triaxial tests, on the contrary, the boundary conditions (membrane, and bearing plates) seem to affect the test results in a much more important way.

3. Model tests of vertical cyclic loading on a footing

(a) Instead of making an attempt to perform cyclic triaxial tests in uniform stress conditions, which must be rather impossible, one could try to make cyclic loading model tests; for example with model footings on large sand samples, in which the stress distribution is very similar to that under cyclically and vertically loaded footings. In this way the cyclic loading tests create a heterogeneous stress field, in which, stressed and pore pressures can be measured as they arise at selected locations. From such model tests it is possible, with due consideration of scale effects, to draw better qualitative conclusions concerning the studied cyclic loading problem in nature.

(b) Starting from the mentioned point of view a research program was set up, to study the behaviour of a saturated sand mass of about 0.6 m^3 in well defined drainage conditions, under a vertical cyclic loading transmitted through a stiff circular plate of 120 mm of diameter in the center of the top of the sample (1.06 m × 1.06 m × 0.55 m of height) (Fig. 8). The sample has a well-defined uniform density and is fully consolidated under a given consolidation stress p_c throught a rubber bag filled with pressurized water. The set up of the testing equipment, the way of preparing the sample and the running of the cyclic loading tests have been discussed before [15, 16].

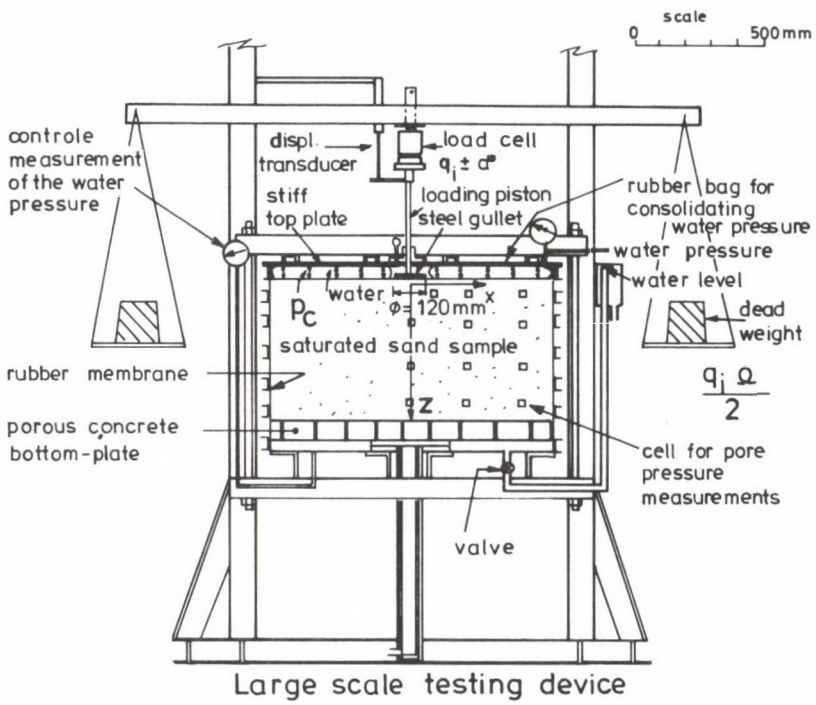

Fig. 8

The dynamic loading tests (at 3Hz) have been performed both on saturated (S) and on dry (D) sand samples. The vertical overburden consolidating pressure p_c on the sample surface, the effective unit weight (γ) of the sample after consolidation, the value of the static starting unit load q_i on the circular model footing and the value of the half-amplitude of cyclic loading a^* are chosen in each of the tests. From these initial test conditions of the Molsand, the unit ultimate bearing capacity of the footing q_r was calculated from earlier research work [1].

The vertical unit cyclic load with amplitude $\pm a^*$ is superimposed on the permanent static unit load q_i on the footing. So the maximum unit load on the footing is

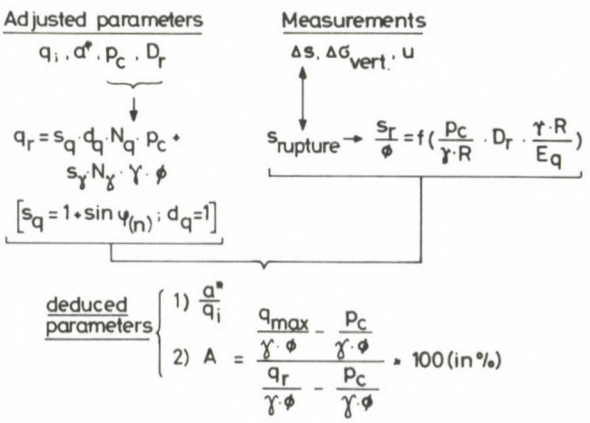

Fig. 9

$q_i + a^* = q_{max}$, the minimum load is $q_i - a^*$; $(a^* < q_i)$. The test results are proposed to be analysed using two dynamic parameters: a^*/q_i and A, where A is given by the expression:

$$A = \frac{\frac{q_{max}}{\gamma \cdot \phi} - \frac{p_c}{\gamma \cdot \phi}}{\frac{q_r}{\gamma \cdot \phi} - \frac{p_c}{\gamma \cdot \phi}} \cdot 100 \quad (\text{in } \%)$$

(ϕ represents the footing diameter).

The measured values represent the vertical deformation of the footing Δs, the developing pore water pressures Δu at different locations and the vertical loading pressures $\Delta\sigma_{vert}$, (Fig. 9).

From earlier research work [1], the settlements s_r at rupture loading q_r for different types of footings in Molsand, depending on the bearing capacity parameters of the sand, are known (Fig. 10).

The values of these parameters for the large scale tests performed, are summarized in Table I.

(c) In the case of saturated sand samples, pore water pressures cells are placed inside the sand mass (Fig. 11).

Alternative drainage conditions were obtained by changing the boundary conditions around the steel ring or the water pressure cell itself.

The test tank with saturated sand with the rubber bag under water pressure p_c and surrounding water at the footing, is entirely closed (undrained condition). In the

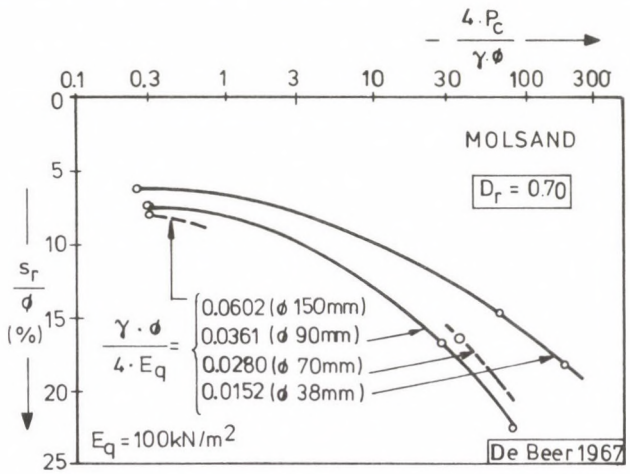

Fig. 10

formation of type (*A*) (Fig. 11), the water around and above the steel ring is in free contact with the pore water of the sand; in the case of type (*B*) the drainage of the free water around the loading steel footing is prevented. In the type (*C*) test, there is no free water volume around the loading plate.

The pore pressure cells also can be put in, in three different ways (Fig. 11).

The first solution (a) consists in introducing bare cells in the saturated sand mass; in the second set-up (b) the water pressure cells are covered by membrane strips of about 300 mm of diameter at some interval. Finally in some tests one or even several pressure cells totally are enclosed in a rubber bag (type c) containing also a saturated sand sample at the same relative density as the surrounding sand mass. As the dimensions of the pore pressure cells cannot be neglected, the measured pore water pressure are to be interpreted as relative numerical values. The compressibility of both the surrounding sand mass and the pressure cell usually is too divergent. To minimize the effect of the differences in compressibility, the cells are wrapped up in smooth strip adapted to the compressibility of the sand sample. Special saturation techniques were developed to assure a minimum degree of saturation of 97% after consolidation of the sample at chosen vertical stresses of q_i and p_c on the scale-footing and on the surrounding surface of the sample.

Table I

Test No.	Sand cond. D or S	$\frac{a^*}{q_i}$	q_r kN/m²	A %	$\frac{p_c}{\gamma \cdot R}$	$\frac{s_r}{\varnothing}$ %	$N_{s=s_r}$	$N_s=$ 10% $\varnothing$	$N_s=$ 50% s_r	$\frac{s_u}{\varnothing}$ %	N_u
A1	S	0.60	477	49.12	9.9	12	–	1250	680	10.0	1300
A2	S	0.60	559	82.08	16.5	14	8	5	3	47.5	1100
A3	S	0.60	4804	1.00	327.7	>35	–	–	–	0.1	500
A4	S	0.60	1438	30.01	98.5	23	–	–	–	4.2	900
A5	S	0.60	414	53.86	6.6	12	–	400	–	2.5	500
A6	S	0.60	534	71.39	9.8	12	110	38	3	15.0	300
A7	S	0.60	729	44.44	33.0	17	–	–	–	1.7	800
A8	S	0.60	197	70.04	1.3	8	85	150	12	15.0	800
B1	S	0.60	354	33.20	35.0	24	–	–	–	0.7	590
B2	D	0.60	566	54.46	43.6	26	–	245	373	13.4	500
B3	D	0.61	756	32.95	65.4	28	–	–	–	4.0	1000
B4	S	0.60	569	64.81	69.8	22	790	95	570	35.0	1000
B11*	S	0.60	353	65.47	35.1	23	–	28	110	11.7	130
C1	S	0.60	394	26.83	72.6	>35	–	–	–	1.7	600
C2	D	0.60	237	51.29	22.8	>30	–	300	–	13.4	1700
A9	S	0.80	120	93.37	0.7	7	2	3	1.2	70.0	500
A10	S	0.80	669	38.89	16.4	14	–	–	–	0.4	400
A11	D	0.80	913	38.77	20.4	15	–	630	580	10.0	1100
A12	D	0.80	913	41.90	20.4	15	–	180	160	10.0	700
A13	D	0.80	880	37.40	20.4	15	–	–	840	8.0	1000
A14	S	0.80	750	18.97	33.0	17	–	–	–	2.0	700
A15	D	0.80	713	44.77	10.2	13	–	–	–	1.0	600
A16	S	0.80	845	40.71	49.1	19	–	500	900	12.5	1000
B5	S	0.80	232	38.02	17.5	20	–	–	–	2.2	600
B6	S	0.80	353	28.86	35.0	23	–	–	–	6.2	1300
B7	S	0.81	232	68.85	17.5	20	10	4	3	27.5	220
B8	D	0.81	462	38.27	32.8	23	–	130	–	11.7	700
B9	S	0.80	538	35.24	70.2	27	–	520	–	10.3	550
C3	S	0.80	382	56.56	72.9	>35	15	7	10	38.3	60
C4	D	0.80	237	35.24	22.8	>30	–	–	–	50.0	900
C5	S	0.81	529	47.31	98.3	>40	–	150	–	12.5	500
C6	S	0.80	549	48.00	108.9	>40	–	70	460	27.0	1000
A17	D	0.42	835	59.29	20.4	15	–	–	–	2.7	1000
A18	S	0.40	435	72.49	6.6	12	–	450	–	10.0	500
A19	D	0.40	267	68.58	0.8	8	550	590	330	16.7	900
A20	D	0.40	735	23.06	10.2	13	–	–	–	2.0	900
A21	S	0.40	754	33.58	32.8	17	–	–	–	1.0	500
A22	S	0.40	687	69.88	16.4	14	–	610	380	11.7	1000
B10	D	0.40	555	63.04	43.7	18	–	–	–	6.7	700
B12	D	0.40	381	98.83	21.7	21	–	1.3	2	17.5	165
B13	D	0.40	783	65.76	65.1	27	–	370	740	20.0	2100
B14	S	0.40	290	65.97	27.9	22	–	290	420	11.2	450
C7	D	0.40	237	91.06	22.8	>35	–	2	–	14.2	400
C8	S	0.40	549	59.63	108.9	>40	–	–	–	1.4	500
C9	D	0.40	237	72.60	22.8	>30	–	24	–	11.7	800
C10	D	0.40	253	62.22	22.6	>30	–	–	–	2.0	600

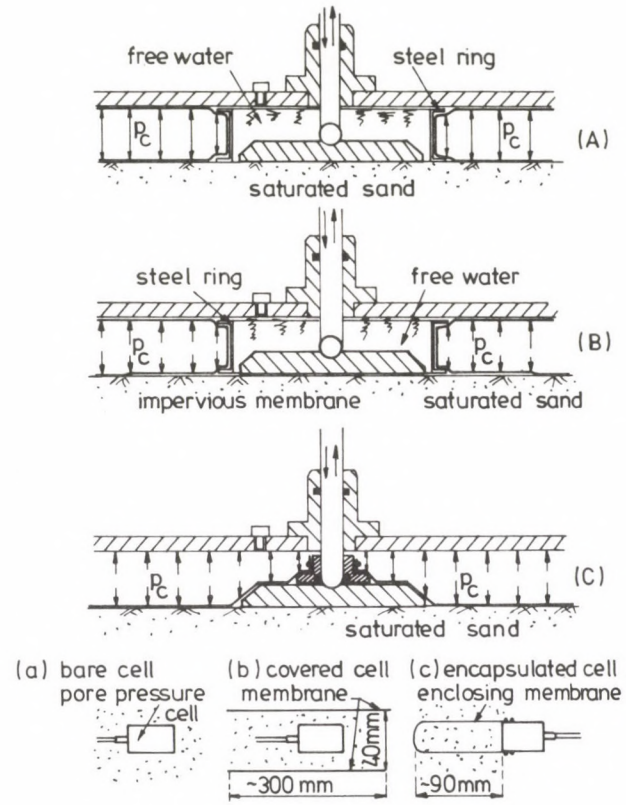

Fig. 11

All tests were performed on samples with relative density above the critical density (Fig. 12).

(d) Analysing the results of the pore pressure measurements, the main conclusions, discussed in detail before [17], can be summarised as:

1. In the mentioned testing procedure and in the case of a set-up of type (*A*) with bare cells (Fig. 13) no considerable residual pore pressure could be measured, irrespective of the values of the dynamic parameters a^*/q_i and A_0. Continuously recorded pore pressures in different points of the sample indicated that there exist pore pressure gradients towards the vibrating footing on the sand surface.

2. In the case of type (*A*) and pore pressure cells covered partially by membranes, the results are showing very small residual pore pressures Δu. The building up of Δu at partially covered pressure cells remains at a rather small level after a sufficient number of loadings. The pore water pressures under this cyclic loading seem to be compensated at some level by the existing drainage conditions.

A typical example of such cyclic loading test is given in Fig. 13 for a saturated sand sample of about $D_r = 25\%$ relative density after consolidation.

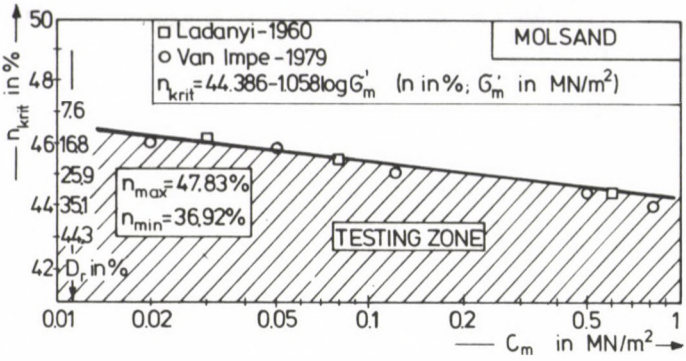
□ Ladanyi-1960
○ Van Impe-1979
MOLSAND
n_{krit}=44.386-1058logG'_m (n in%; G'_m in MN/m²)
n_{max}=47.83%
n_{min}=36.92%
TESTING ZONE
n_{krit} in %
D_r in %
50
48
46
44
42
7.6
16.8
25.9
35.1
44.3
0.01
0.02
0.05
0.1
0.2
0.5
1
C_m in MN/m²

Fig. 12

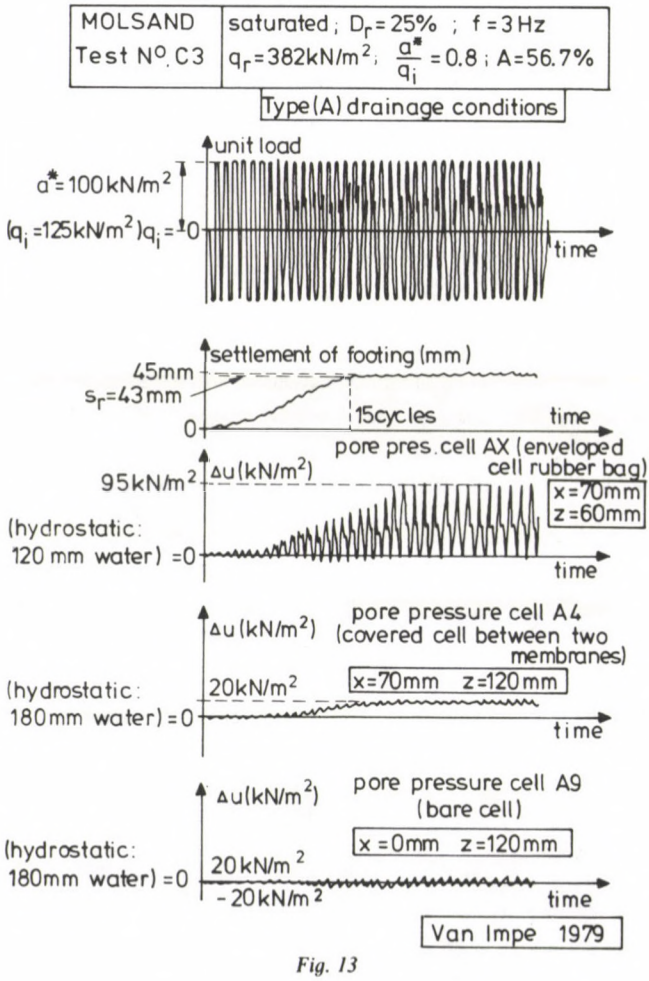
MOLSAND
Test N°. C3
saturated; D_r=25% ; f=3Hz
q_r=382kN/m²; $\frac{a^*}{q_i}$=0.8; A=56.7%
Type(A) drainage conditions
unit load
a^*=100kN/m²
(q_i=125kN/m²) q_i
time
settlement of footing (mm)
45mm
s_r=43mm
15cycles
time
pore pres. cell AX (enveloped cell rubber bag)
95kN/m²
Δu(kN/m²)
x=70mm
z=60mm
(hydrostatic: 120 mm water) =0
time
Δu(kN/m²)
pore pressure cell A4 (covered cell between two membranes)
(hydrostatic: 180mm water) =0
20kN/m²
x=70mm z=120mm
time
Δu(kN/m²)
pore pressure cell A9 (bare cell)
x=0mm z=120mm
(hydrostatic: 180mm water) =0
20kN/m²
-20kN/m²
time
Van Impe 1979

Fig. 13

As can be seen in this figure, in the case of a pore pressure cell totally enveloped in a rubber bag filled with saturated sand of the same density as in the rest of the sample, rather high pore pressure were measured. Conditions of cyclic mobility of the sand inside the rubber bag occurred while almost no pore pressure existed in the surrounding saturated sand in the type (a) setup of the cyclic loading tests. This condition of cyclic mobility inside the closed rubber bags is very similar to the well-known phenomenon of "liquefaction" observed in cyclic triaxial test results on dense saturated sand.

3. In the case of limited drainage conditions around the loading plate of the type (*B*) or (*C*), even for bare pore pressure cells some build-up of pore pressure could be measured in the sand mass nearby the loading plate (Fig. 14). At a certain level, equilibrium is reached and no more build-up could be recorded.

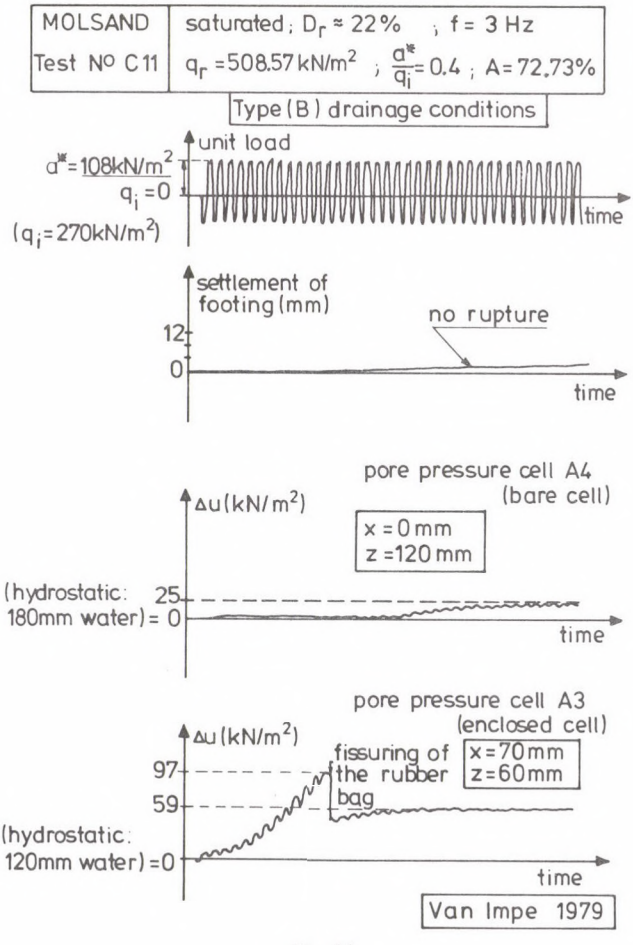

Fig. 14

The remaining pore pressure was even more important in the case of covered cells. Pressure cells enclosed with a rubber bag were always showing the same cyclic mobility phenomenae.

A typical result of a cyclic loading test in the type (B) or (C) set-up is given in Fig. 14. The sudden drop of the pore pressure Δu, measured with the enveloped cell A3, down to a much lower level of remaining pore pressure, was due to an observed rupture of the rubber bag at the connection of the bag to the cell.

(e) Concerning the measured pore pressures in the saturated sand mass under vertical cyclic loading in the center and at the top of the sample, it can be concluded that each way of drainage of the pore pressure gradients is predominant. In the relatively big and fully saturated sand mass of constant total volume, each individual unit volume can change in volume as long as all volume changes compensate each other. So an "internal" way of drainage and the redistribution of the relative density reduce the building up of the pore pressures. Due to the excessive boundary conditions in small triaxial test samples such "internal" drainage cannot occur, leading to unexpected high values of the pore pressures even in very dense sand samples.

(f) Analysis of the measured settlements of the cyclically loaded circular footing. As mentioned before, the settlement s_r (depending on the values of E_q, q_c, γ and diameter $\varnothing$ of the footing) for Molsand was given in an earlier research program on the rupture-settlements for a variety of model footings (Fig. 10).

In the large scale cyclic tests, three rupture criteria were used for comparing the results due to cyclic loading (Table I): (1) footing settlament equal to s_r; (2) a settlement $s = 50\%\, s_r$ and (3) the criterion of $s = 10\%\, \varnothing$. Large-scale dynamic loading tests are made on saturated or on dry sand mass as indicated in Table I. The values given in columns 8, 9, 10 in Table I show the number of loading cycles needed to satisfy a corresponding rupture criterion.

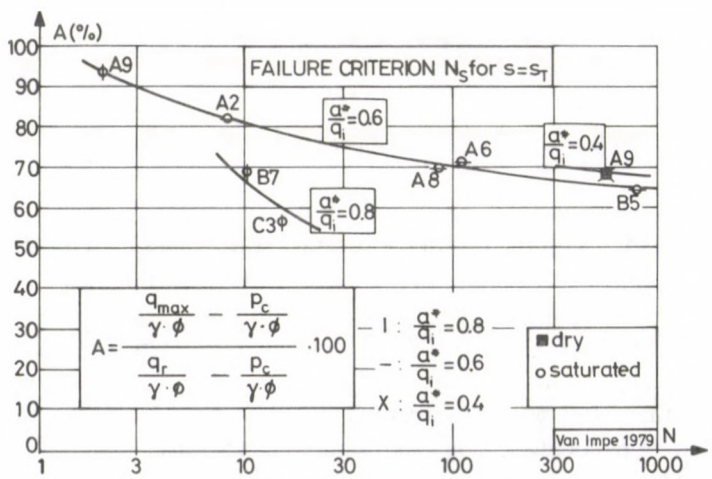

Fig. 15

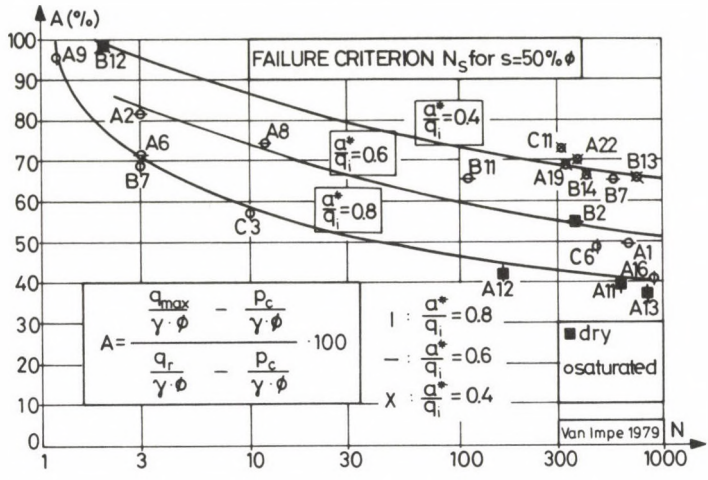

Fig. 16

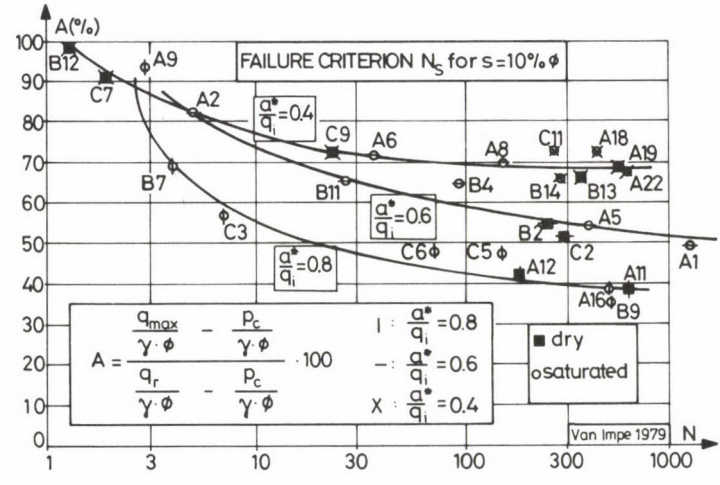

Fig. 17

During settlements due to consolidation or cyclic loading, underneath the rubber bag or underneath the footing, a constant water pressure p_c in the rubber bag, and a constant loading on the footing q_i were maintained throughout.

From all results it is apparent that cyclic loading tests at a given value of a^*/q_i can be fitted by a simple curve (Figs 15–17). In this technique of dynamic loading there is no substantial difference in the settlement behaviour between test results obtained in dry or in fully saturated samples; the results are conditioned only be the mentioned dynamic loading parameters. For given sample conditions:

(i) the value of A needed to reach the selected rupture criterion in terms of loading cycles increases as a^*/q_i decreases.

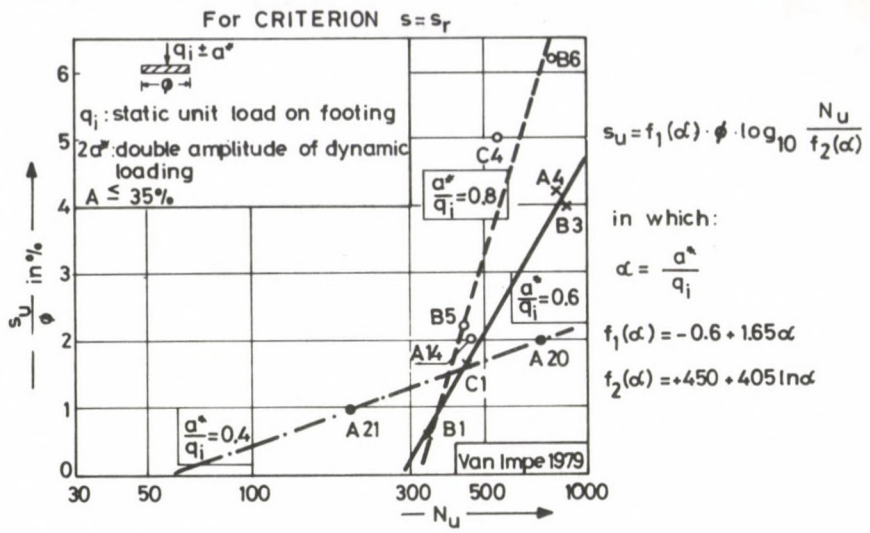

Fig. 18

(ii) for the same a^*/q_i-value, the number of loading cycles needed to reach rupture increases as A decreases.

(iii) for the $s = s_r$ criterion, there exists a lower boundary of A-values for which no rupture can be achieved, at least within a few thousands of loading repetitions.

The final remaining settlement s_u observed after a few thousands in all the tests are recorded (Table I).

The mentioned lower boundary of $A(A_{min})$ underneath which settlements under repeated loading are stabilized seemed to be about 35% in the case of this cyclic loading condition of Molsand.

Analyzing these final remaining settlements s_u of the footings in tests showing only elastic deformation behaviour after a number of cycles N_u [2] one can expect there should exist a relationship between such an ultimate plastic settlement s_u reached after N_u cycles and the parameters A^*, a^*/q_i and $\varnothing$. For all the tests in which rupture was not reached, it is obvious interest to express the possible relation between these "final" settlement, the dynamic test parameters A, a^*/q_i and the dimension $\varnothing$ of the footing. Such a relationship could be found for the test conditions here mentioned at values of $A < 35\%$, for which pore water pressures were insignificant.

For the test results on Molsand obtained, this can be represented in the analytical way as:

$$s_u = f_1(\alpha) \cdot \varphi \cdot \log_{10} \frac{N_u}{f_2(\alpha)},$$

in which:

$$\alpha = \frac{a^*}{q_i},$$

$$f_1(\alpha) = -0.6 + 1.65\,\alpha,$$
$$f_2(\alpha) = +450 + 405 \ln \alpha.$$

4. Conclusions

From the $c-u$-cyclic triaxial tests on Molsand, it was found the stress level, initially applied to the sample, strictly does not remain constant during the test. Axial lengthening of the triaxial sand samples appears above some combination of σ_c and D_r, making the interpretation of such type of cyclic test results rather useless with respect to behaviour in nature.

From results of a large scale model test and concerning the pore pressure building up, it seems the boundary drainage conditions at the loading plate and for the pore pressure cell itself are predominant.

In the case of this testing procedure on Molsand and with relative densities larger than the well known critical density at given values of consolidation stress, there is no difference in the deformation behaviour of dry or saturated sand. Two dynamic loading parameters A and a^*/q_i are defined, with which it was found that the settlements of the dynamic loaded footing can be plotted in a best fitting curve with respect to this loading parameters and the logarithm of number of cycles, for different rupture criteria.

As the loading parameter A is limited for Molsand up to about $A < 35\%$, there exists a rather simple relationship between the final plastic settlement and the number of loading cycles.

References

1. De Beer, E.: Proefondervindelijke bijdrage tot de studie van het grensdraagvermogen van zand onder funderingen op staal—Bepaling van de vormfactor s_b. Tijdschrift Openbare Werken van België No. 6, (1967), No. 1. (1968) No. 4 (1968). No. 5 (1968), No. 6 (1968), 1–183
2. Holzlöhner, U.: Residual settlement in sand due to repeated loading. Proceedings International Symposium on Dynamical Methods in Soil and Rock Mechanics, **2,** (1977) Karlsruhe
3. Ladányi, B.: Etude des relations entre les contraintes et les déformations lors du cisaillement des sols pulvérulents. Annales des Travaux Publics de Belgique No. 3, (1960), 42–59
4. Ladd, R. S.: Preparing test specimens using undercompaction. Geotechnical Testing Journal Vol. **1,** No. 1, March, 16–23
5. Lade, P. V., Hernandez, S. B.: Membrane penetration effects in undrained tests. Journal of the Geotechnical Engineering Division, ASCE Vol. **103,** No. GT2, Proc. Paper 12758, February, (1977) 109–125
6. Lee, K. L., Seed, H. B.: Cyclic stress conditions causing liquefaction of sand. Journal of the Soil Mechanics and Foundation Division, ASCE Vol. 93, No. SM1, Proc. Paper 5058, January, (1967), 47–70
7. Lee, K. L.—Seed, H. B.: Dynamic strength of anisotropically consolidated sand, Journal of the Soil Mechanics and Foundation Division, ASCE Vol. 93, No. SM5, Proc. Paper 5451, September, (1967), 169–191
8. Lee, K. L.—Fitton, J. A.: Factors affecting the cyclic loading strength of soil.—Vibration effects of earthquakes on soils and foundations, ASTM, American Society for Testing and Materials STP 450, (1969), 71–95
9. Lee, K. L.: Fundamental considerations for cyclic triaxial tests on saturated sand, Boss'76. Proceedings, International Conference on the Behaviour of Offshore Structures. Trondheim, August, (1976) 355–391
10. Martin, G. R., Finn, W. O. L., Seed, H. B.: Effects of system compliance on liquefaction tests, Journal of the Geotechnical Engineering Division, ASCE Vol. 104, No. GT4, Proc. Paper 13667, April (1978), 463–479

11. Raju, V. S., Sadasivan, S. K.: Membrane penetration in triaxial tests on sand. Journal of the Geotechnical Engineering Division, ASCE Vol. 100, No. GT4, April (1974), 482–489
12. Seed, H. B., Lee, K. L.: Liquefaction of saturated sands furing cyclic loading. Journal of the Soil Mechanics and Foundation Division, ASCE Vol. 92, No. SM6, Proc. Paper 4972, November (1966), 105–134
13. Seed, H. B., Martin, Ph. P., Lysmer, J.: Pore-water pressure changes during soil liquefaction. Journal of the Geotechnical Engineering Division, ASCE Vol. 102, No. GT4, Proc. Paper 12074, April (1976), 323–346
14. Seed, H. B., Idriss, I. M.: On the importance of dissipation effects in evaluating pore pressure changes due to cyclic loading. Proceedings, International Symposium on Soils under Cyclic and Transient Loading. Vol. 2, 7–11 January (1980), Swansea, pp. 569–570
15. Van Impe, W. F.: A test equipment for large scale vertical cyclic loading tests on saturated sand. Proceedings, International Symposium on Soils under Cyclic and Transient Loading. Vol. 1, 7–11 January (1980), Swansea, 97–107
16. Van Impe, W. F.: Laboratory vertical cyclic loading tests on sand. Proceedings, Tenth International Conference on Soil Mechanics and Foundation Engineering. Vol. 1, June (1981), Stockholm, 815–818
17. Van Impe, W. F.: Studie van het vervormingsgedrag van Molzand onder cyclisch wisselende belastingen. Proefschrift ter verkrijging van de graad van doctor in de Toegepaste Wetenschappen, April, (1981), deel 1: 1–332, deel 2: fig. I–VII, deel 3: fig. VIII–IX
18. Van Impe, W. F.: Interpretatie van cyclische belastingsproeven op zand. Huldeboek Prof. em. Dr. ir. E. De Beer, oktober (1982), 273–279
19. Van Impe, W. F.: Proeven met cyclisch wisselende belastingen—Vervormingsgedrag van zand, PI/Civiele Techniek, jaargang 37, nr. 11, november (1982), 28–37
20. Vesic, A.: Etude expérimentale de la capacité portante du sable sous des fondations directes établies en surface, Annales des Travaux Publics de Belgique, No. 3, (1958)

Acta Technica Academiae Scientiarum Hungaricae, 96 (1—4) pp. 107—117 (1983)

EFFICIENT SECURIZATION OF TRANSMISSION NETWORKS

G. SALLAI*

[Received: 5 January 1984]

The paper presents planning methods to find efficient combinations of various securization techniques for protecting the telecommunications transmission networks against component failures taking the extra cost and the benefits into account. The efficient number of disjoint routes, the optimal degree of the overdimensioning of the multi-routed subgroups, and the optimal application of a rearrangeable standby network are derived for each pair of nodes under various securization conditions and requirements. A computer-aided procedure is also presented for the global transmission network securization problem and design charts and consequences are drawn.

1. Introduction

Expanding and digitalizing telecommunication networks, the protection of the service against traffic overloads and network component failures, is more intensively required. To derive benefits from the new transmission technologies, traffic should concentrate on transmission routes having larger capacity. However, the larger, more efficient circuit groups are far more sensitive to overloads and failures. For securizing the network preventive and curative approaches are distinguished, they may be used in both transmission and switching networks. The optimal combination of various securization techniques are extensively investigated, e.g. [1–6]. The paper presents optimization methods to find an efficient solution for the securization of a transmission network taking the extra cost and the benefits into account.

A transmission network is modelled by a graph, representing each line section by an edge, each transmission node by a graph node. The vulnerability of a transmission network, the component failures are represented by deleting the concerned edges and nodes from the graph.

To secure a transmission network against component failures the multi-routing of circuits (preventive method) and the establishment of a rearrangeable standby network (curative method) are combined. The multi-routing of the circuits implies the division of a circuit group into subgroups having geographically disjoint transmission routes between the concerned pair of nodes. Forming edge-disjoint routes on the graph, the connectivity survives under any line section breakdown, constituting node-

* G. Sallai, 1126 Budapest, Brassai S. u. 14, Hungary

disjoint routes, protection is provided against any node or line section breakdown. By overdimensioning the disjoint subgroups the protection may be improved. A standby protection network is established from reserve systems and link permuters, which are available to form emergency connections when a cable or a microwave link is cut. The standby network is usually planned to provide the specified security level to the circuit groups for which multi-routing would be too expensive.

With an appropriate qualification index including the protection provided under worst-case single breakdown and extra costs required by multi-routing of circuits and use of standby network, the efficient number of disjoint routes and the efficient degree of the use of the standy network can be derived for each pair of nodes. Criteria and charts developed can contribute to finding an optimum combination of techniques for securizing a transmission network. Criteria are extended to take into account impact of the overdimensioning of the multi-routed subgroups and the capacity limits of the standby network as well as the desired security level. Principles for designing efficient standby network are also presented. Finally a computer-aided procedure is shown, which is available to provide both a cost-efficient solution and a specified security-level solution to the global transmission network securization problem

2. Efficiency of multi-routing

The efficiency of multi-routing depends on the topology of the concerned networks and is influenced by the cost of the standby network. The efficient number of disjoint routes is calculated separately for each pair of nodes.

Let R be the number of the possible disjoint routes between a pair of nodes, and denote by $r \leqq R$ the concerned number of disjoint routes, and $c_i^{(r)}$ $(i=1, 2, \ldots r)$ the unitary cost on route i, and let $c_1^{(r)} \leqq c_2^{(r)} \ldots \leqq c_r^{(r)}$. Dividing the demand (given in a certain unit of circuits) into r portions in the ratios of $\mu_1 : \mu_2 : \ldots \mu_r \left(\sum_{i=1}^{r} \mu_i = 1 \right)$, and routing portion i over the route i, it may be assumed, that $\mu_1 \geqq \mu_2 \ldots \geqq \mu_r$. Let a portion μ_s be protected by the standby network with a unitary cost c_s. Then assuming the worst-case single breakdown, security level is calculated as $S = 1 - \max_i \mu_i + \mu_s = 1 - \mu_1 + \mu_s$, where $\mu_1 \geqq 1/r$; the index to qualify the efficiency of the multi-routing securization is defined as

$$Q(r; \{\mu_i\}) = \frac{S}{C} = \frac{1 - \mu_1 + \mu_s}{\frac{1}{c_1}\left[\sum_{i=1}^{r} \mu_i c_i^{(r)} + \mu_s c_s\right]} \tag{1}$$

where C is the total cost in relation to c_1, the unitary cost on a one-path route. We shall consider two extreme cases. In case A let $\mu_s = \mu_1$, i.e. we provide full protection under

single breakdown with the aid of a standby network; in case B let $\mu_s = 0$, i.e. only multi-routing securization is available.

Assuming a uniform division of the circuit group, the Busacker's minimum cost flow algorithm [7] can be used for finding minimum cost (node or edge) disjoint routes on the representing graph. The r-th step of the algorithm provides minimum cost r disjoint routes with a cost of

$$\frac{1}{r}\sum_{i=1}^{r} c_i^{(r)} = \frac{1}{r}\sum_{i=1}^{r} \Delta c_i$$

where $\Delta c_i \geqq c_i^{(i)}$ is the increment of the sum of the unitary costs in the i-th step. Obviously $\Delta c_1 = c_1^{(1)} = c_1$. Substituting $\mu_i = 1/r$ into (1), the qualification index is given as

$$Q(r; \{1/r\}) = \frac{c_1 \cdot (r - 1 + \delta)}{\sum_{i=1}^{r} \Delta c_i + \delta \cdot c_s} \tag{2}$$

where $\delta = 1$ in case A, $\delta = 0$ in case B. Henceforth $Q(r; \{1/r\})$ is abbreviated by Q_r.

Finding the maximum of Q with respect to r and $\{\mu_i\}$, it may be shown by analyzing the derivates of Q, that if

$$\Delta c_{r_0} < \frac{\sum_{i=1}^{r_0-1} \Delta c_i + \delta c_s}{r_0 - 2 + \delta} \quad \text{and} \quad \Delta c_{r_0+1} \geqq \frac{\sum_{i=1}^{r_0} \Delta c_i + \delta c_s}{r_0 - 1 + \delta} \tag{3}$$

then the optimum distribution of circuits is $\mu_1 = \mu_2 = \ldots \mu_{r_0} = 1/r_0$, $\mu_{r_0+1} = \ldots = \mu_R = 0$, and $\max Q = Q_{r_0}$, i.e. the uniform distribution of circuits, splitting the circuit group into r_0 (r_A or r_B, respectively) subgroups optimum. Since $c_1 \leqq \Delta c_2 \leqq \Delta c_3 \ldots$, therefore, one and only one maximum exists, where $Q_{r_0-1} < Q_{r_0} \geqq Q_{r_0+1}$. Note, that in case of non-uniform splitting of circuits the maximum of Q is generally given at r, not less than r_0 [4].

Analyzing the two cases we obtain that if $c_1/c_s < Q_r^{(B)}$ at any r, then $c_1/c_s < Q_{r_A}^{(A)} < Q_{r_B}^{(B)}$, $r_A \geqq r_B \geqq 2$, i.e. the use of standby network is not efficient. If $c_1/c_s > Q_{r_B}^{(B)}$, then $c_1/c_s > Q_{r_A}^{(A)} > Q_{r_B}^{(B)}$, $1 \leqq r_A \leqq r_B$, i.e. c_s is cheap enough to provide full protection. It can be seen, that the cost-efficient protection method out of A and B is, that which has the smaller efficient number of disjoint routes.

In case of $c_i^{(r)} = c_i^{(r-1)}$, i.e. the establishment of a new route does not modify the previous ones, we have $\Delta c_i = c_i^{(i)}$ $(i = 2, 3 \ldots r)$, and denoting $c_i^{(i)}$ by c_i (3) is written as

$$c_{r_0} < \frac{c_1}{Q_{r_0-1}}; \quad c_{r_0+1} \geqq \frac{c_1}{Q_{r_0}}. \tag{4}$$

Under such conditions a universal decision diagram may be given which indicates the efficient protection combinations versus c_s/c_1 and c_2/c_1 (Fig. 1). The decision marked with a query depends on c_3, c_4, etc. When $c_3 \geqq c_1 + c_2$, then $r_A = r_B$

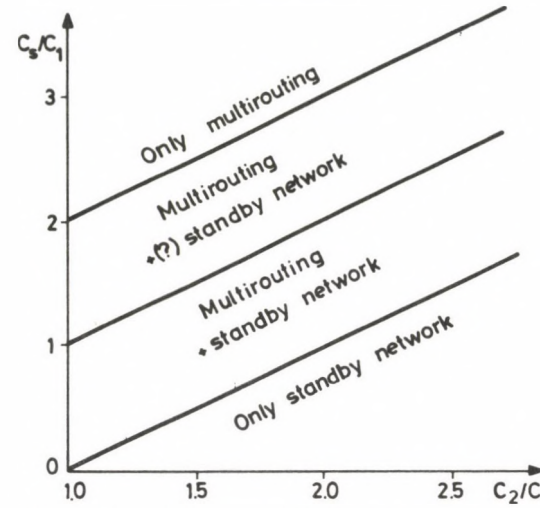

Fig. 1. Universal diagram of efficient protection combinations

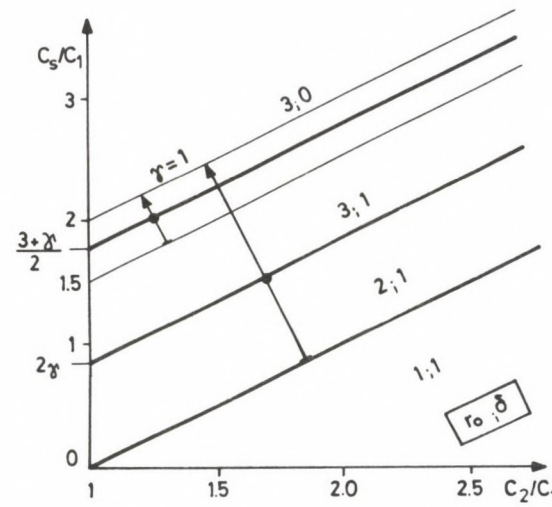

Fig. 2. Efficient protection combinations, if $c_3 = c_2 + \gamma c_1$, $0 \geqq \gamma < 1$; $R = 3$

$= 2$ (the route 3 is inefficient) and the use of the standby network is efficient in its entirety of the marked domain. Figure 2 gives the efficient combinations of r and δ, if $c_3 < c_1 + c_2$ assuming that $R = 3$.

If $c_i = c_1 \cdot q^{i-1}$, $i = 1, 2 \ldots 5$ is a geometric series with parameter $q = c_2/c_1 \geqq 1$, then the decision diagram indicating the efficient combinations of r and δ is shown on Fig. 3.

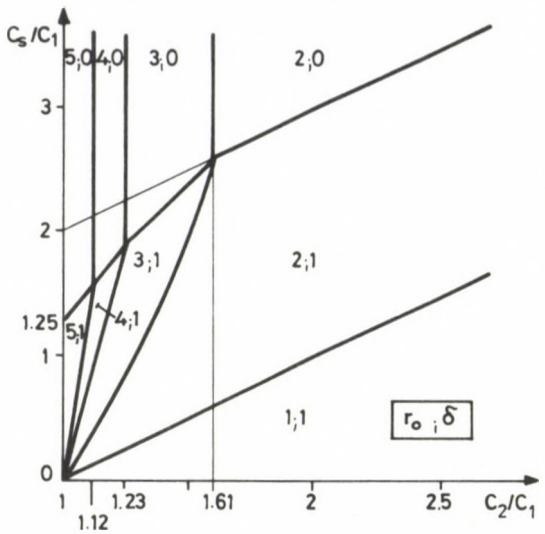

Fig. 3. Efficient protection combinations, if $c_{i+1}/c_i = c_2/c_1$, $R=5$.

3. Overdimensioning of multi-routed subgroups

The efficient security level is always 1 in case A, and $S=1-1/r_B \geqq 0.5$, in case B, which latter may be less than a desired minimum security level S_m.

Therefore, we consider the case C, where an addition to the multi-routing of circuits (case B), a "fixed standby network" is established by overdimensioning the r-path routed subgroups. If $S<S_m$, then a portion

$$\mu_f = S_m - S = S_m - \left(1 - \frac{1}{r}\right) \tag{5}$$

should be available, when any route is cut out of r routes. Thus,

$$Q_r^{(C)} = \frac{c_1 \cdot S_m}{\left(\frac{1}{r} + \frac{\mu_f}{r-1}\right) \sum_{i=1}^{r} \Delta c_i}. \tag{6}$$

Substituting (5) into (6) we obtain

$$Q_r^{(C)} = \frac{c_1 \cdot (r-1)}{\sum_{i=1}^{r} \Delta c_i} = Q_r^{(B)},$$

i.e. the efficiency of the case C is independent of S_m, and equal to the efficiency of the original r-path routing (case B). Consequently $r_C = r_B$, and the relations recognized, between the cases A and B, are valid between the cases A and C. The universal decision

diagram shown on Fig. 1 is completed by the overdimensioning technique if and only if exclusively multi-routing protection is proposed and the security level provided by the multirouting is unsatisfactory.

4. Efficiency of the application of a standby network

In case A, we assumed full protection using the rearrangeable standby network with a unitary cost c_s in a degree $\mu_s = \mu_1$. Now we generalize this model in two steps. Firstly we consider the case D, when the standby network has a capacity limit μ_0 between the examined pair of nodes and the desired maximum security level $S_M < 1$, e.g. $S_M = 0.8$. Thus, the possible values of μ_s are:

$$0 \leqq \mu_s \leqq \min(\mu_0 ; \mu_1 + S_M - 1) \leqq \mu_1 .$$

Derivating (1) with respect to μ_s we obtain, that if

$$c_s \geqq \frac{\sum_{i=1}^{r} \mu_i c_i^{(r)}}{1-\mu_1} = \frac{\sum_{i=1}^{r} \Delta c_i}{r-1} \qquad (7)$$

$$\uparrow$$

$$\mu_i = 1/r$$

the choice of $\mu_s = 0$ is efficient, case D goes into case $B(r_D = r_B)$. Otherwise, as high as possible use of the standby network is efficient. It means that when case A—assuming maximal μ_s—is more favourable than case B, then case D with any value of $\mu_s > 0$ is also, and so is $r_D = r_A$. However, if

$$r_A \geqq R_M = \left\lceil \frac{1}{1-S_M} \right\rceil \qquad (8)$$

the use of the standby network is not required, and $r_D = \min(r_B, R_M)$. As a consequence on Fig. 1 that if the network topology does not preclude (8), i.e. $R \geqq R_M$ the standby network is queried in both intermediate domains, and the decision is also dependent on S_M. Specially, if $S_M \leqq 0.5$, then the standby network is deleted in the entirety of the concerned domains. Figure 4 shows the universal decision diagram to the solution of optimum protection combination taking into account S_m and S_M, the parameters of the desired security level and R, the number of possible disjoint routes (assuming that $\mu_0 \geqq S_M$).

In general, the unitary cost c_s is a function of μ_s. Assuming a monotonous increasing step-wise function with cost parameters $c_{s_1} < c_{s_2} < \ldots c_{s_L} < \ldots$ in the form of

$$c_s(\mu_s) = c_{s_L} \text{ if } \mu_{0,L-1} < \mu_s \leqq \mu_{0,L}$$

with $\mu_{0,0} = 0$ (case E), the qualification index for an r uniform path routing is denoted by $Q_r^{(E)}(\mu_s)$.

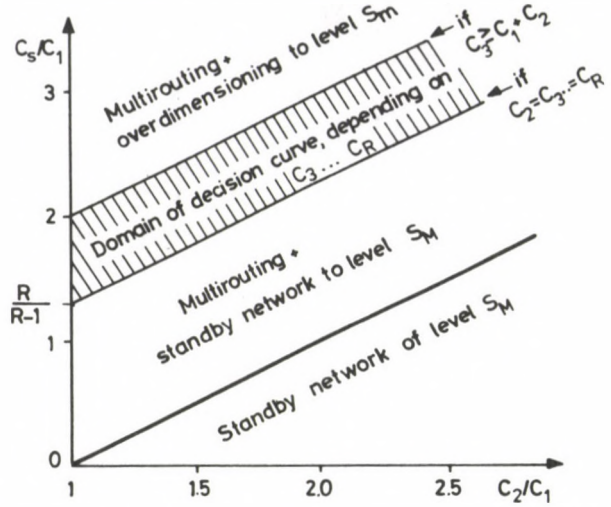

Fig. 4. Universal diagram of optimum protection combinations with an (S_m, S_M) security level

Finding maximum of $Q_r^{(E)}(\mu_s)$ with respect to r and μ_s, we can state that:

(a) instead of μ_s we may consider L, the number of steps (conclusion of case *D*); consequently it is sufficient to find the maximum of

$$Q_{r,L}^{(E)} = c_1 \frac{1 - \frac{1}{r} + \mu_{0,L}}{\frac{1}{r}\sum_{i=1}^{r} \Delta c_i + \sum_{j=1}^{L} (\mu_{0,j} - \mu_{0,j-1}) \cdot c_{s_j}}$$

with respect to r and L.

(b) a step L is to be taken into account only if

$$c_{s,L} < \frac{c_1}{Q_{r_B}^{(B)}}, \quad \text{where} \quad Q_{r_B}^{(B)} = \max_r Q_{r,0}^{(E)};$$

(c) an efficient number of disjoint routes $r_E \leqq r_B$; specially $r_E = r_B$ if

$$c_{s,1} > r_B \cdot \Delta c_{r,B} - \sum_{i=1}^{r_B} \Delta c_i$$

(d) if $\max_L Q_{r_1,L}^{(E)}$ is given at L_1, and $r_2 < r_1$, then $\max_L Q_{r_2,L}^{(E)}$ is given at $L_2 \geqq L_1$.

A simple procedure based on these statements to find the optimum combination of r and L, additional features, supplements and case studies are shown in [8].

5. Planning efficient standby routes

For estimating c_s, the unitary cost of the use of the rearrangeable standby network, a standby network model is used, which also provides design principles.

We assume, that the permissible topology of the standby network is identical to the topology of the transmission network to be protected and the unitary cost of a standby circuit is proportional to the unitary cost of a normal circuit between the same pair of nodes by a factor $\alpha > 1$ as well as a standby circuit is used by $n(\mu_s)$ relations as an average.

To minimize standby network cost the standby requirement $\mu_s = S_M - 1 + 1/r$ is to be divided among many routes, thus denoting by $r_s (r \leqq r_s \leqq R)$ the number of standby routes the total cost in relation to c_1 can be written, as

$$C = \frac{\sum_{i=1}^{r} \Delta c_i}{r \cdot c_1} + \frac{\alpha}{n(\mu_s) \cdot c_1} \frac{\sum_{i=1}^{r_s} \mu_{s,i} c_i^{(r_s)}}{(\mu_s - \mu_{s,1})/\mu_s} \qquad \text{if } r > 1$$

where

$$\sum_{i=1}^{r_s} \mu_{s,i} = \mu_s, \quad \mu_{s,1} \geqq \mu_{s,2} \geqq \ldots \geqq \mu_{s,r_s},$$

and we have taken into account that in case of the breakdown of a normal route, the corresponding standby route is also cut.

Minimization problem of C with respect to r_s and $\{\mu_{s,i}\}$ is, it is recognized, identical with the minimization problem of Case *B* discussed in Sect. 2. Accordingly, we obtain that the optimum solution is to divide μ_s into r_B uniform portions, i.e. the optimum number of standby routes is equal to the efficient number of disjoint routes in case *B*, and $\mu_{s,1} = \mu_{s,2} = \ldots = \mu_{s,r_B} = \mu_s / r_B$. Introducing $w(\mu_s) = \alpha / n(\mu_s)$, we can then write:

$$C = \frac{\sum_{i=1}^{r} \Delta c_i}{r \cdot c_1} + \mu_s \cdot w(\mu_s) \cdot \frac{\sum_{r=1}^{r_B} \Delta c_i}{(r_B - 1) \cdot c_1}, \qquad \text{for } r > 1. \tag{9a}$$

If $r = 1$, the routes $2, 3 \ldots r_B$ are assumed to be standby routes, thus

$$C = 1 + S_M \cdot w(S_M) \cdot \frac{\sum_{i=2}^{r_B} \Delta c_i}{(r_B - 1) \cdot c_1}, \quad \text{for} \quad r = 1. \tag{9b}$$

For general cases $c_s(\mu_s)$ can be identified from equations (9). To obtain an estimation for c_s, we unify (9), simplifying the function $w(\mu_s)$ on the basis of decreasing attribute of $n(\mu_s)$ as follows:

$$w(\mu_s) = \begin{cases} W & \text{if} \quad r > 1 \\ W \cdot \left(1 + \dfrac{c_1}{\sum_{r=2}^{r_B} \Delta c_i} \right) & \text{if} \quad r = 1 \end{cases}$$

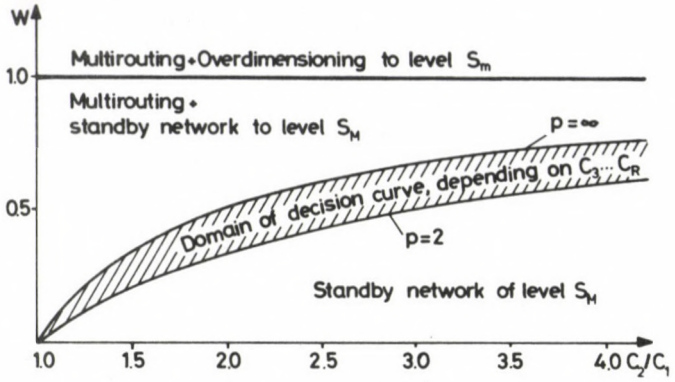

Fig. 5. Optimum protection combinations versus W and c_2/c_1

where W is an appropriate approximating constant. Thus, the estimation for c_s is:

$$c_s = W \cdot \frac{\sum_{i=1}^{r_B} \Delta c_i}{r_B - 1}. \tag{10}$$

Comparing c_s to the inequality (7), we have that if $W < 1$, then the use of standby network is proven to be efficient. Substituting (10) into (3), in case of $W \to 0$ we obtain $r_A \to 1$; in case of $W \to 1$, then $r_A \to r_B$.

Figure 5 shows a transformed form of the decision diagram on Fig. 4, also taking into account the condition $\Delta c_i = c_i$ and the lower and upper limits of (10) in the form of

$$W \cdot \left(\frac{c_1}{R-1} + c_2 \right) \leqq c_s \leqq W \cdot (c_1 + c_2).$$

The equation of the bounds of the shaded domain is given as

$$W = \frac{(x-1) \cdot (p-1)}{1 + x \cdot (p-1)}$$

where $x = c_2/c_1$, $p = 2$ for the lower bound, $p \geqq r_B$ for the upper bound. We can state from Fig. 5 that if the security level is generally higher, then n can enhance and the establishment and use of a standby network is preferred.

6. Computer-aided planning of transmission networks under security constraints

Usually the transmission networks are planned to provide a security level $S_o (= S_m = S_M)$ specified for each relation so that the multi-routing of circuits is applied with a permitted cost λc_1 ($\lambda > 1$) and the standby network is planned to satisfy the

residual security requirements [1, 2, 6]. To find a sub-optimal planning compromise, various sets of S_o and λ should be tested.

Using the above efficiency principles and criteria a favourable planning procedure may be constructed which directly provides an optimal combination of the various protection techniques. The flow chart of the proposed procedure is outlined on Fig 6. The procedure is available to provide (a) cost-efficient solution by an internal

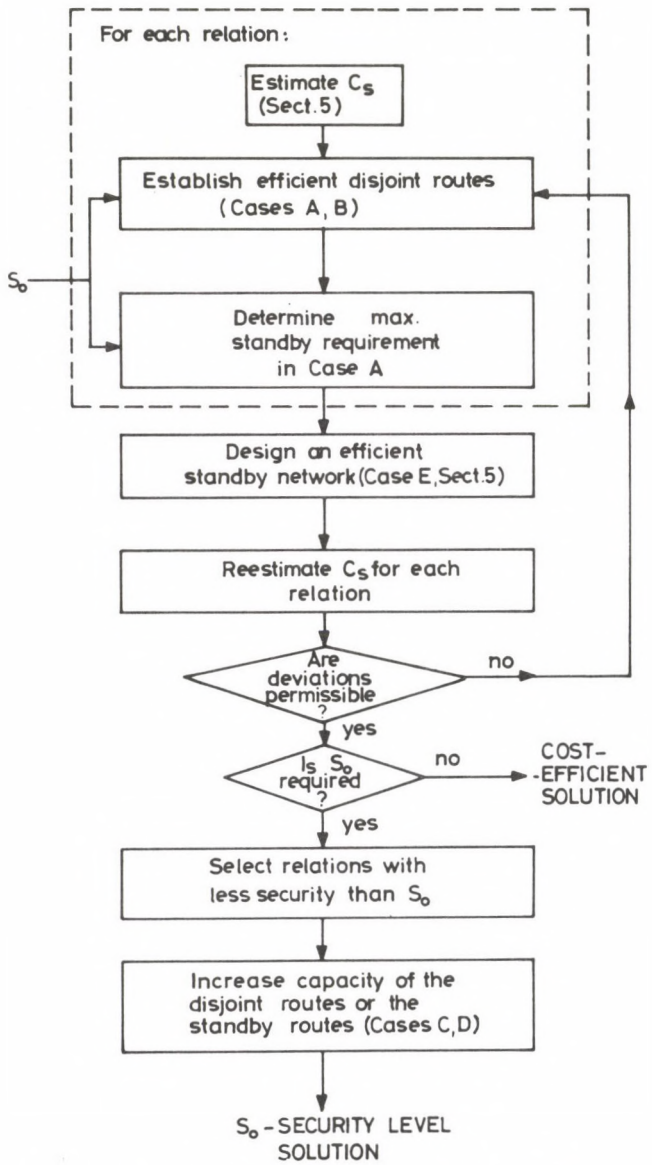

Fig. 6. Computerized procedure for optimal security planning of transmission networks

iteration and (b) specified security-level solution applying supplementary steps. The procedure is presently incorporated into the computer-program system developed by the Research Institute of Hungarian PTT for planning metropolitan and long-distance telephone networks.

7. Conclusions

The paper presented criteria and a computerized procedure for finding the optimal combination of the securization techniques of the transmission networks: multi-path routing of circuits, overdimensioning of disjoint subgroups, use of rearrangeable standby network. The efficient multi-routing has no more than r_B uniform disjoint routes, where r_B is a topological attribute of the graph of the network, the efficient number of disjoint routes without standby network in the concerned relation. It is found, that the overdimensioning is not included in cost-efficient solutions, but it may be favourable for reaching a specified security level. The application of a standby network is efficient if the standby routes serve many relations and it is optimal if r_B uniform standby routes are used. Under higher security requirements the use of the standby network is preferred.

References

1. Berdineau, J., Guerineau, J. P.: Security of telecommunications networks: application in the area of Ile-de-France. Proc. of Networks' 80, Paris, September 1980
2. Pereira de Almeida, C.: Long-distance transmission network planning improving reliability at reduced costs, ibidem
3. Haenschke, D. G., Kettler, D. A., Oberer, E.: Network management and congestion in U. S. telecommunications networks. IEEE Trans. on Comm. Vol. 29. April (1981), 376–385
4. Sallai, G.: Efficiency aspects in network securization. Proc. of Networks' 83, Brighton, England, March 1983
5. Gunnarsson, S., Qvarfort, L.: Alternative route policy, ibidem
6. Lindberg, P., Mocci, U., Tonietti, A.: A procedure for minimizing the cost of a transmission network under service availability constraints in failure conditions. Proc. of 10th ITC, Montreal, June 1983
7. Busacker, R. B., Saaty, T. L.: Finite Graphs and Networks. Mc Graw Hill Book Co., New York 1965
8. Sallai, G.: Cost-effective security planning of transmission networks. Report of Research Institute of Hungarian PTT (in Hungarian), Budapest, January 1983

Acta Technica Academiae Scientiarum Hungaricae, 96 (1—4) pp. 119—137 (1983)

FLUID MECHANICAL ANALYSIS OF THE EXHAUST TURBINE OF THE TURBOSUPERCHARGER UNDER NON-STEADY FLOW CONDITIONS

E. PÁSZTOR* and Y. DIB

[Recieved: 15 March 1983]

The experimental and theoretical evaluation of the efficiency of the exhaust turbine of pulsating (non-steady) flow, i.e. the establishment of the difference between efficiencies of the turbines of steady and non-steady flow is dealt with. The authors constructed a test equipment in which the frequency and the amplitude of the pulsation could be varied within the actual limits existing in a Diesel-engine. The theoretical and experimental investigations ascertained that because of the shock and separation losses taking place in the impeller, under the effect on the pulsation, the efficiency of the turbine of pulsating (non-steady) flow is always lower than that working at the same mode of operation but under steady conditions. It is demonstrated how the different parameters which define the non-steady flow, influence the efficiency of the turbine of non-steady flow.

1. Introduction

The small radial exhaust turbines serving for turbosupercharging the automobile engines has aroused great interest in recent years. Several researchers studied the characteristics relating to the efficiency and performance of the turbines at non-steady (pulsating) flow conditions.

The working conditions of the exhaust turbines of the turbosupercharged internal combustion engines are strongly characterized by non-steady processes. The investigation of this circumstance is significant, among others, from the point of view of the development of the change of the charge, however, it is of crucial importance in connection with the cooperation of condenser and the turbine of the turbosupercharger because at the non-steady flow working; the variation of the efficiencies of both units cannot be neglected.

This paper is intended to contribute to the investigation of this problem or, more exactly, to the analysis of the reduction of the efficiency of the exhaust turbosupercharger taking place at the non-steady (pulsating) flow working mode, as well as to find out how to prevent the diminishing of the efficiency.

* E. Pásztor, H—1221 Budapest, Honfoglalás u. 48/b, Hungary

2. Setting-up and definition of the problem

By investigating in every possible way the performance and efficiency of the exhaust gas turbine of the turbosupercharger the non-steady (pulsating) working conditions should be considered.

Under the effect of the pulsation (Fig.1) the exhaust gas flows out from the stationary vane ring of the turbine with an absolute velocity c_1 of variable value but

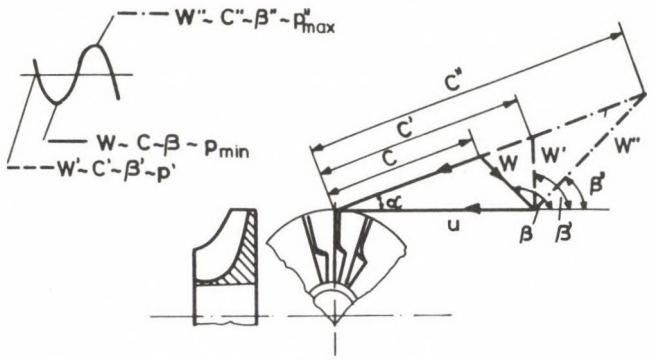

Fig. 1. Flow conditions in the runner of a turbine of radial vane system: c_1 = absolute velocity, w_1 = relative velocity, u_1 = peripheral velocity, p_{max} = maximum pressure, p_{min} = minimum pressure, p' = average pressure, α_1 = entrance angle of absolute velocity, β_1 = entrance angle of relative velocity

having nearly the same direction ($\alpha_1 \sim$ constant). Accordingly, not only the value of the relative velocity w_1 but also the direction (β_1) of the gas entering in the runner varies because the peripheral velocity u_1 of the runner, due to he rather high value of the moment of inertia, remains constant.

As is to be seen in Fig. 1 the variable angle β_1 induces shock (separation, turbulence, throttle, etc.) losses at the suction edge of the runner and practically in the whole runner. This shock loss reduces the available capacity and, consequently, also the efficiency of the turbine. From that said above it follows that for the purpose of an exact evaluation of the performance and efficiency of the turbine, it is the non-steady working state which is to be taken into account.

In such a case the flow characteristics cannot be considered to be constant or of mean value because the neglect of the periodic variation under the pulsation could lead to a non-permissible error in the evaluation of the characteristics or the working conditions of the exhaust turbine. A further consideration which permits to construct such a non-steady (pulsating) test as well as to develop the theoretical (mathematical) model is that the variation of the absolute velocity c_1 at the outflow of the stationary radial vane ring, induced by the pulsation, results in the reduction in efficiency of the exhaust gas turbine. The purpose was to evaluate the reduction of the efficiency caused by the pulsation and how this reduction could be minimized.

For varying the absolute velocity c_1, that is, to produce pulsation, a rotary valve, turned by an electric engine (Fig.2, designed by No 12) has been arranged in front of the exhaust turbine of the automatic turbosupercharger. In that way the non-steady working state has been established which resulted in reducing the efficiency in the

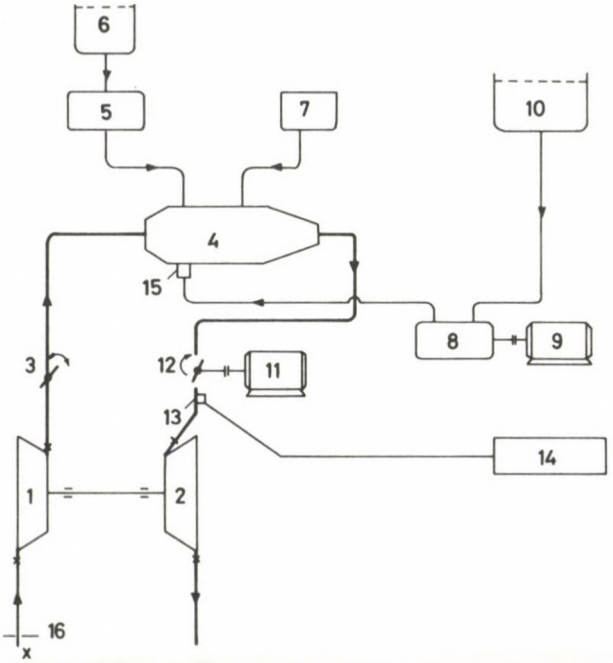

Fig. 2. Working scheme of the test equipment: 1. Condenser, 2. turbine, 3. throttle valve, 4. combustion chamber, 5. starting fuel pump, 6. starting fuel tank, 7. equipment producing ignition spark, 8. head fuel pump, 9. driving motor of fuel pump, 10. fuel tank, 11. driving motor of rotary valve, 12. rotary valve, 13. piezoelectric sensor (signaller), 14. pressure signal recorder 15. injection nozzle, 16. measuring orifice, *X*. measuring points of pressure and temperature

turbine. From the test results also the reduction of the efficiency of the turbine could be evaluated.

The program of the theoretical investigation and the calculation were built up in a way that at the same time also the variation of the absolute velocity c_1 at the entrance of the runner as well as that of the variation of the value of the relative velocity w_1, the flow direction (β_1) and the gas flowing in the runner have been taken into account.

The theoretical calculation is built up on the basic values found from the test results, thus simulating these latter ones.

3. Test set up and method applied at the present investigation, test results

3.1. Test set up

The tests had been performed by making use of a turbosupercharger type JAFI I which was made into a run automatic (so becoming an idle running gas turbine). The turbine of the turbosupercharger contained a radial-flow impeller, a total inflow stationary vane ring and an inflow volute chamber.

The special equipment serving for this purpose (Fig. 2) had been built by the Institute for Vehicle Engineering of the Technical University Budapest. The construction of the equations may readily be followed on the diagramatical layout of Fig. 2, therefore, no detailed description of it is given here. During the test procedure particularly great care was taken to make an exact measurement of the thermal characteristics of the turbine, since the reduction of the efficiency of the turbine had been established from the performance equilibrium of the condenser and the turbine. At each measuring point two or three thermoelements had been arranged (at spacing from

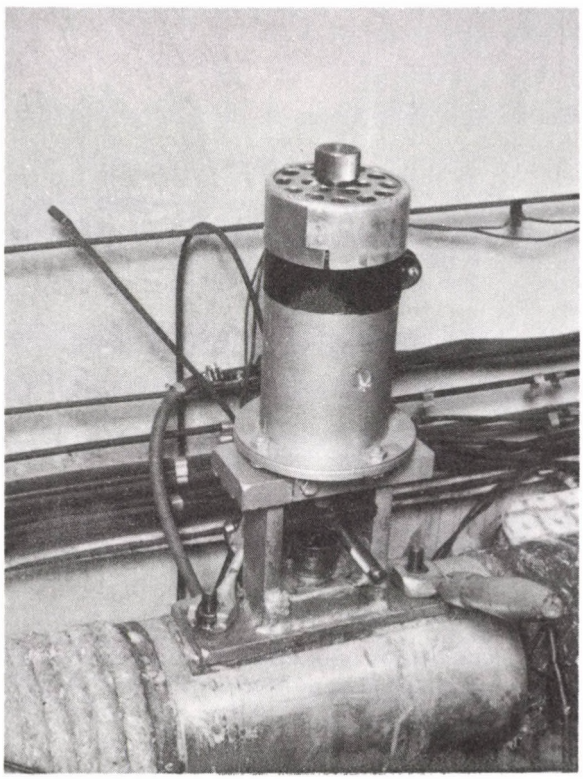

Fig. 3. Photograph of electric engine in a mounted state

180° to 120°, and produced the average of the measurement values. The entrance and outflow pressures of the condenser and the turbine had also been measured at two or three operating points, and the pressure gauges were also placed to spacings 180° to 120°. For the measurements of the pressures mercury and water pressure gauges were used. The inlet air was taken from the surroundings within the laboratory, the temperature of which was sensibly constant. The r.p.m. of the turbosupercharger was measured with the aid of an electric tachometer.

The working ratio of the turbosupercharger had been investigated by r.p.m. between 30 000 and 55 000. The steady working states of different loadings served as basis for the measurements (in such cases the rotary valve did not work or cause throttling) had been produced by an appropriate position of the throttle valve (Fig. 2, No. 3) arranged behind the condenser, while the non-steady (pulsating) working state was produced by inserting a rotary valve (Fig. 2, No. 12 and Fig. 4) revolved by an electric engine (Fig. 2, No. 11 and Fig. 3) of variable r.p.m. arranged before the turbine. The supply tube fitted in front of the turbine in which the rotary valve had been arranged (Fig. 4) had a diameter 120 mm; the diameters of the rotary valves were by

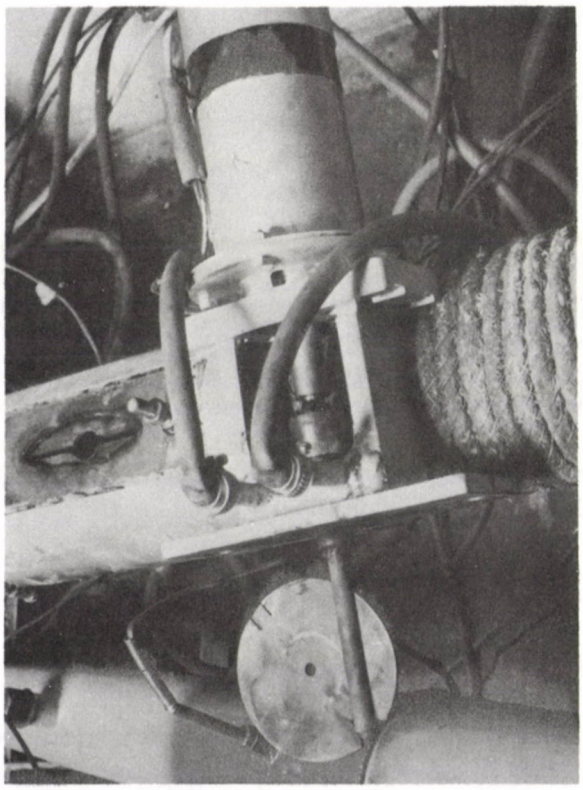

Fig. 4. The demounted rotary valve with its electric engine and cutout serving for the encasement of the rotary valve in the conduit before the turbine

order of succession 110, 113, 115, 118 and 119 mm in order to produce the pulsations of different amplitudes. The frequency of the flow pulsation of the gas produced by the rotary valve of variable r.p.m. was 25, 40, 60 Hz, respectively.

The pulsating pressure before the turbine varying with time was measured with the aid of a piezoelectric pressure intensifier (13). The electric signals was recorded on a special tape-recorder (14).

3.2. Measurement procedure, test program

(a) Steady flow (non-pulsating) operation

After re-examining all units of the test equipment, in order to obtain exact measurement results, the characteristics of the automatic turbosupercharger at the three positions (0, 1, 2) of the throttle valve (Fig. 2, No. 3) and with standstill of the rotary valve (12) was established. The measurement had been initiated with an open (0) rotary valve. The rotary valve in position (2) produced the greatest possible throttle at which the system could still be operated.

By raising the r.p.m. of the turbosupercharger between 30 000 and 55 000 gradually by 5 000 r.p.m. of all these r.p.m., all measurable thermal hydrodynamical characteristics were measured.

(b) Non-steady flow (pulsating) operation

For the purpose of checking, first the characteristics of the turbocharger was measured from the zero position of the throttle valve being at standstill, at a given r.p.m of the turbocharger. Then, the electric engine was switched on which controlled a rotary valve of given diameter and produced succesively the pulsations 25, 40 and 60 Herz. Hereafter, the same characteristics were again measured at higher r.p.m. by raising it by 5 000 successively, until the highest value, that is, 55 000 r.p.m. was attained. Then, a rotary valve of larger diameter was arranged before the turbine, and the entire measurement procedure was repeated by varying meanwhile the r.p.m. of the turbine and the frequency of the pulsation.

3.3. Processing and evaluation of test results

(a) Procedure and basic results of the steady state evaluation

The thermal-flow characteristics of the test set up was measured in a steady state manner except the frequency and amplitude of the pulsation frequency, therefore, the procedure of the basic evaluation practically was the same both in the steady and non-steady cases.

The basic relationship used for the evaluation may be found in refence [1].

The rotary valve having been arranged immediately in front of the turbine to a sufficient distance from the condenser (Fig. 2), no such high pulsation was noticed in the course of the measurements and their evaluation which would have resulted in the worsening of the measurable value. The characteristics, i.e., characteristic curve of co-working of the condenser of the turbosupercharger is depicted in Fig. 5 for different static throttlings and for different diameters of the rotary valve. On the variation of the amplitude and frequency of the pulsation no measurable change of the characteristic curve could be observed due to the circumstances mentioned above, wherefore, in this

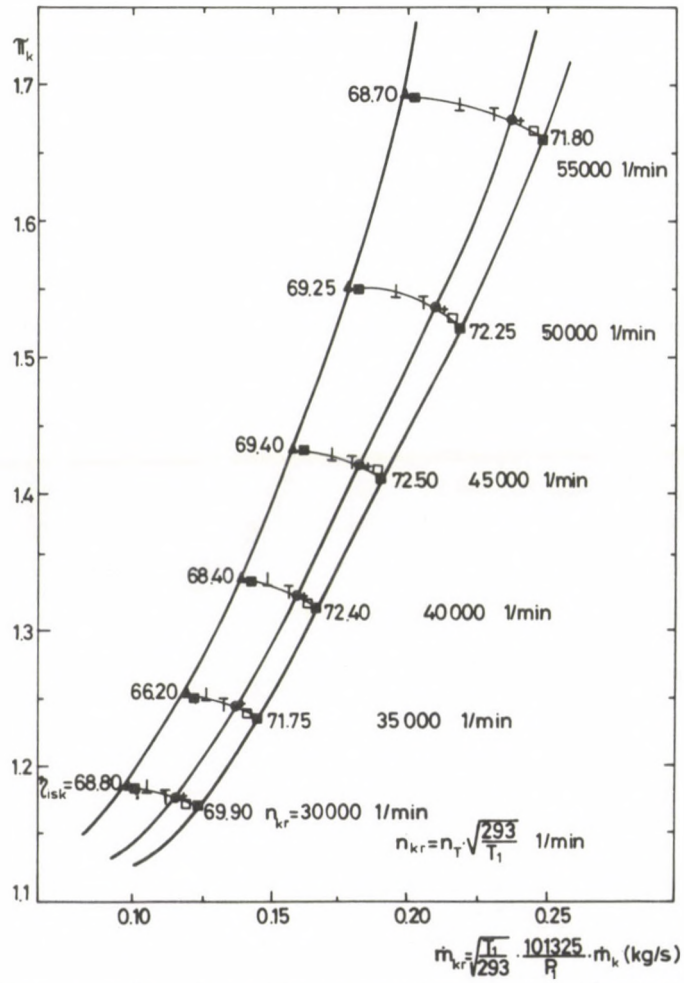

Fig. 5. Characteristic curve of the condenser of the turbosupercharger: $x=0$ throttling, $0=1$ throttling, $\Delta=2$ throttling, 0 = valve ∅ 110 mm, $+$ = valve ∅ 113 mm, $\top$ = valve ∅ 115 mm, $\perp$ = valve ∅ 118 mm, ■ = valve ∅ 119 mm

figure the steady and the pulsating flowe are represented together. In the figure also the values of efficiency (η_{isk}) of each operating point are given which are equally valid both for the steady and the non-steady flows.

In Fig. 6 the characteristic curves of the turbine of the turbosupercharger and their co-working curves are to be seen for the case of different throttlings and rotary valve diameters. The values of the efficiency (η_{ist}) at several points of operation are also indicated here. As a matter of course, these efficiency values were related only to steady working. The variation of the frequency of the pulsation affected the turbine characteristic curve to such a slight extent, the efficiency excepted, that to avoid the overcrowding of the figure the pulsation frequency is not indicated here.

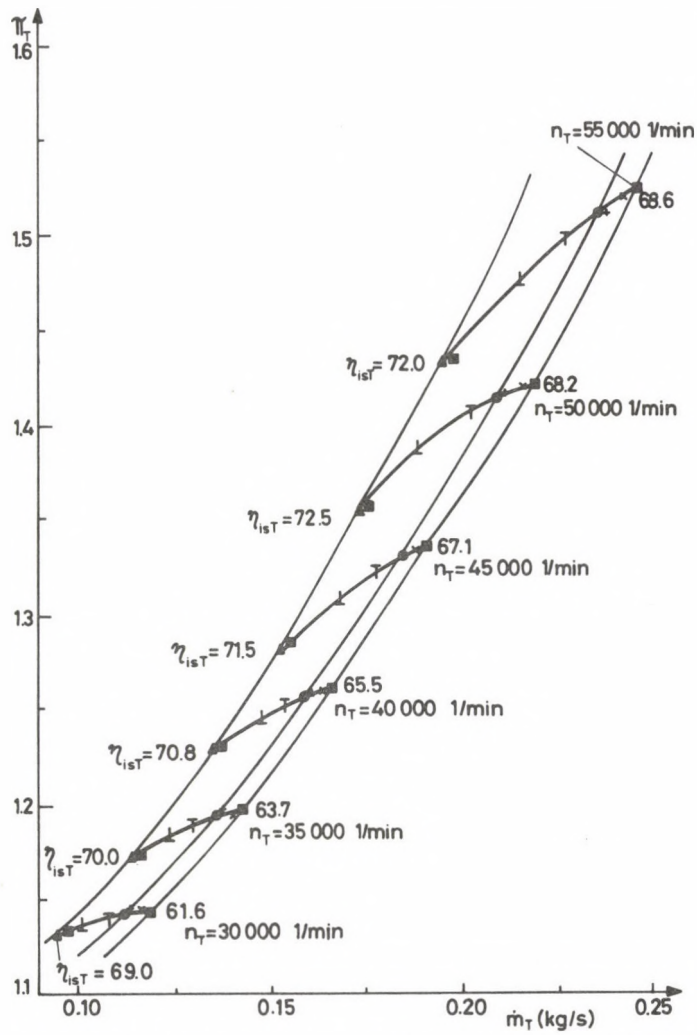

Fig. 6. Characteristic curve of the turbine of turbosupercharger (Notation applied is the same as that in Fig. 5)

(b) Evaluation of the turbine of non-steady flow and its basic results

The procedure of the evaluation of the non-steady (pulsating) test results was as follows (in the figures the values of the test results are designated with the subscript "exp."):

Every operating point of pulsating flow actually measured was identified and, at the steady-flow working, searched for that one at which, from the point of view of throttling, was identical with that of the non-steady flow (Fig. 6). Then the value of the isentropic turbine efficiency (η_{isT}) of each operating point was evaluated. From the value (η_{isT}) the value of the non-steady (pulsating) isentropic turbine efficiency ($\eta_{inst\,T}$) was subtracted, the difference having been denoted with ($\Delta\eta$); that is, $\Delta\eta = \eta_{isT} - \eta_{inst\,T}$. Making use of this method, the ratio $\Delta\eta/\eta_{ist}$ was calculated, that is, the deviation

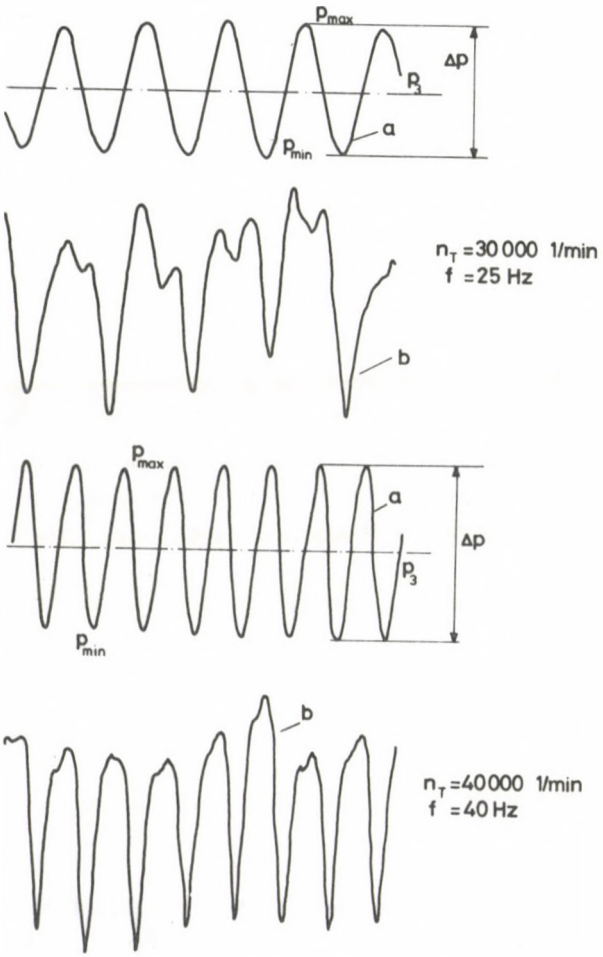

Fig. 7. Shapes of the pressure waves immediately before the turbine. *a* = filtered waves; *b* = non-filtered waves

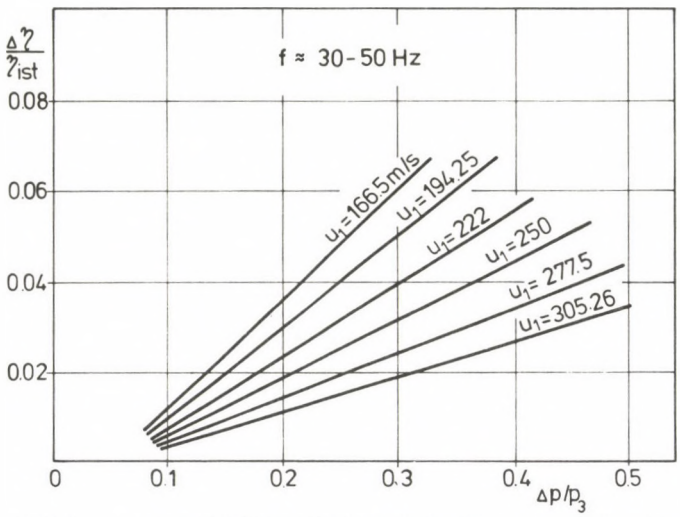

Fig. 8. Variation of $(\Delta\eta/\eta_{ist})_{exp}$ versus $\Delta p/p_0^*$ according to the tests within a given region of frequency in case of different peripheral velocities u_1 measured.

(decrement) of the efficiency caused by the pulsation. The pressure waves recorded on the special tape (Fig. 7) was played back. After filtering out the external disturbing signals, the frequency (Hz) and amplitude ($\Delta p = p_{max} - p_{min}$) as well as the ratio $\Delta p/p_0^*$ was determined wherein

$$p_0^* = \frac{p_{max} + p_{min}}{2},$$

i.e., braked (measured) entrance pressure in turbine.

Thus, the values $\Delta p/p_0^*$ and $\Delta\eta/\eta_{isT}$ associated with the very same operating point have been determined and the connected functions $p/p_0^* = f[\Delta\eta_{isT}]$ plotted for different r.p.m. and frequencies. According to the measurements the variation of the frequency hardly affected the efficiency of the turbine, therefore, as a final result, the variation of $\Delta\eta/\eta_{isT}$ is represented as a function of $\Delta p/p_0^*$ in Fig. 8 for different peripheral speeds. The measurement values are valid between the limits of frequencies 30 Hz and 50 Hz.

4. Theory of development of the shock loss taking place in the impeller and its determination

4.1. Shock losses on a plane vane system

Consider first an incompressible working fluid which, in the simplest case, flows through a plane vane system. The flow enters into the plane vane system, which is composed of straight vanes, at an angle β_1 (Fig. 9) and separates on the inlet edge of the

vanes. Under the effect of the internal friction the flow direction becomes identical with that of the vane system at a given point, that is, the flow will be equalized.

The shock loss caused by the impact of the incompressible working fluid through the vane system, can be calculated as follows.

Let the outline abcd (Fig. 9) considered as a checking surface. Let us assume that in the cross-section cd (which has been assigned in an arbitrary distance to the inflow

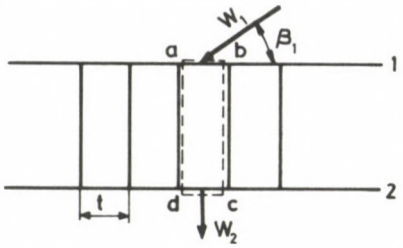

Fig. 9. Flow scheme in plane vane system

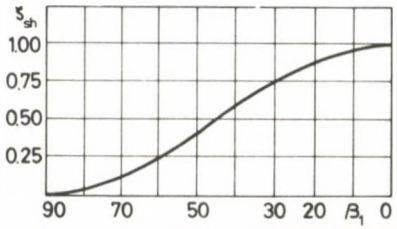

Fig. 10. Shock losses ζ_{sh} in the plane vane system plotted versus angle β_1

profile ab) the disturbance induced by the vane system has been fully equalized, and its direction coincided with that of the vane system. With the aid of the continuity equation related to the outline abcd and the pulse equation the loss coefficient [1]; [2]

$$\zeta = \frac{p_1^* - p_2^*}{\frac{1}{2}\rho w_1^2} = \cos^2 \beta_1$$

wherein ρ = density

p_1^*, p_2^* = braked pressure of inflow and outflow gas, respectively.

From the above equation it is clear that if the gas flows into the runner at an angle $\beta_1 = 90°$ (Fig. 10) then no shock loss occurs, while the shock loss linearly increases with the increase or decrease of the entrance angle of the gas (in the figure only the half of the symmetrical curve is depicted).

4.2. Development of the shock loss on a vane ring

One extends the simplest conclusions deducted in the preceding paragraph to the (circular) vane ring, so significant difficulties arise which are associated with the pulse equation related to the relative velocity as well as with the Coriolis and centrifugal forces (Fig. 11). The most significant ideas for the solution are dealt with on the basis of

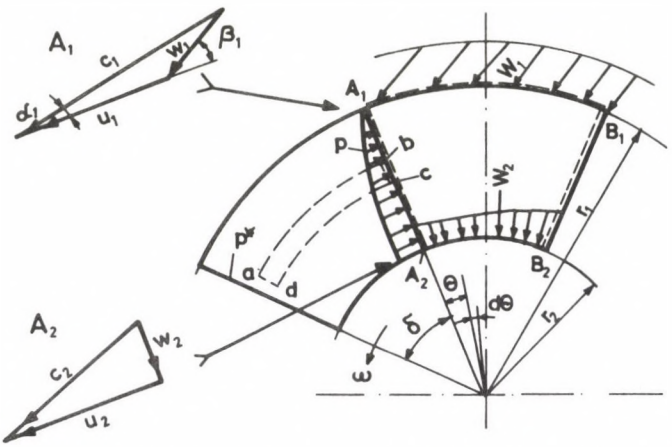

Fig. 11. Flow scheme of vane ring: A_1 = velocity triangle at point A_1, A_2 = velocity triangle at point A_2

reference [1]. For the evaluation of the coefficient of the shock loss in the vane ring, the relative radius of the equalization ($\bar{r}$) has to be known which can be calculated with the following relationship

$$\sin\beta_1 \cdot \cos\beta_1 \cdot \delta = (1-\bar{r}^2)\left[\frac{(\sin\beta_1 + \bar{u}\cdot\delta\bar{r}^2)^2}{4\cdot\bar{r}^2} - \bar{u}\sin\beta_1\delta\right]$$

wherein $\delta = 2\pi/z$, pitch of vane ring,

$\bar{u} = u_1/w_1$, dimensionless peripheral velocity,

$\bar{r} = r_2/r_1$, relative radius of equalization.

In case of $\beta > 90°$, the above relationship may be written in the following form

$$\sin\beta_1' \cdot \cos\beta_1' \cdot \delta = (1-\bar{r}^2)\left[\frac{(\sin\beta_1' + \bar{u}\cdot\delta\cdot\bar{r}^2)^2}{4\bar{r}^2} + \bar{u}\sin\beta_1'\cdot\delta\right]$$

with $\beta_1' = 180° - \beta_1$

In Fig. 12 the variation of $\bar{r}$ is plotted versus β_1 and α_1.

Here $\delta = 2\pi/z = 2\pi/11$, since in this case the number of the blades of the runner was 11.

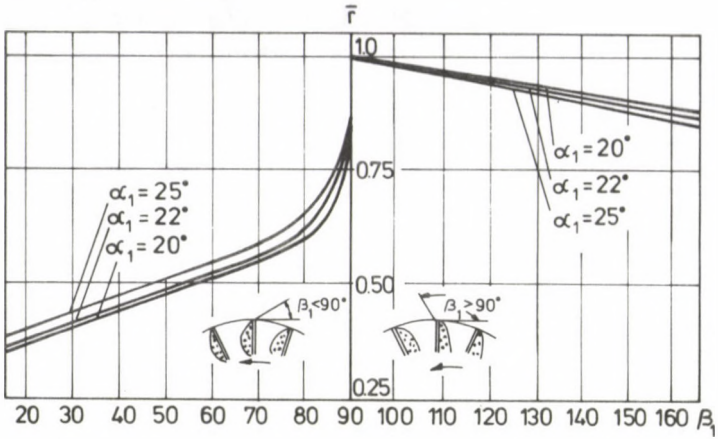

Fig. 12. Variation of the relative compensation radius ($\bar{r}$) as a function of angles β_1 and α_1

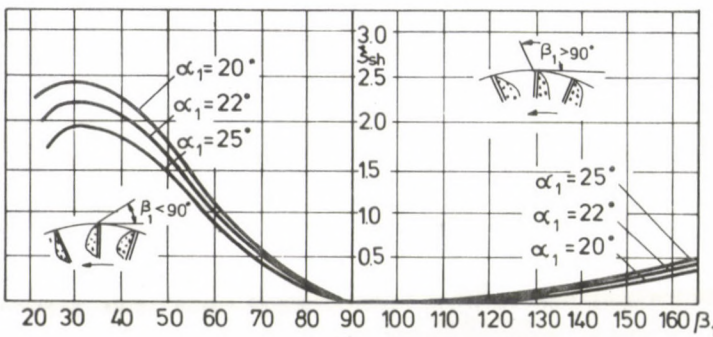

Fig. 13. Variation of the shock loss ζ_{sh} in dependence of angles β_1 and α_1

Eventually, the value of the coefficient of the shock loss ζ_{sh} is given by the following equation:

$$\zeta_{sh} = \frac{1}{\bar{r}}(1-2\sin^2\beta_1) + \frac{\sin^2\beta_1}{\bar{r}} - \frac{1-\bar{r}}{2\bar{r}^3}(\sin\beta_1 + \bar{u}\cdot\delta\cdot\bar{r}^2)^2 +$$

$$+ \frac{\bar{u}}{\bar{r}}\left[4(\cos\beta_1+\bar{u})(1-\bar{r}) \pm \frac{(\sin\beta_1+\bar{u}\cdot\delta\cdot\bar{r}^2)^2}{\bar{r}^2\cdot\delta\cdot\sin\beta_1}\left(1-\bar{r}-\frac{1-\bar{r}^3}{3}\right) - \right.$$

$$\left. - 4\bar{u}\frac{1-\bar{r}^3}{3}\right]$$

The minus sign is used in the case of $\beta_1 < 90°$.

In Fig. 13 the values of the coefficient of the shock loss ζ_{sh} are indicated according to the calculations with angles $\alpha_1 = 20°; 22°; 25°$.

In the case of the turbine investigated the value of the angle α_1 was 22° and that of $\delta = 0.5712$.

5. Calculation of the efficiency of the turbine of non-steady flow, calculation results

5.1. Calculation of the efficiency of the turbine of non-steady flow

On the basis of the coefficients of gas dynamics and the test results obtained, the angle β_1 of the gas entering in to the runner and, consequently, from Fig. 13, also the value of ζ_{sh} have been evaluated.

The value of the pressure loss caused by the shock was:

$$\Delta p_v = \frac{1}{2} \zeta_{sh} \rho w_1^2$$

Let us now examine how to fit the pressure loss brought about by the pulsation (Fig. 14) into the process investigated.

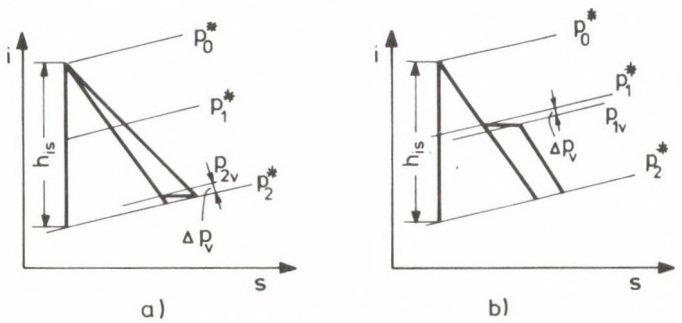

Fig. 14. Expansion process of the turbine and the shock loss caused by the impact

Two methodes have been worked out in the course of this investigation:

— The actual pressure at the outflow edge of the runner (p_{2v}) may be evaluated by adding the pressure difference (Δp_v) brought about by the pulsation to the pressure p_2^* measured after the turbine (Fig. 14a):

$$p_{2v} = p_2^* + \Delta p_v$$

— Considering that the pressure loss caused by the shock is practically brought about at the entrance of the runner of the turbine (p_{1v}), the calculation may be carried out by subtracting the pressure difference Δp_v caused by the pulsation from the entrance pressure p_1^* (Fig. 14) which yields

$$p_{1v} = p_1^* - \Delta p_v .$$

By examining both cases, the difference between the results of both methods is insignificant.

With the calculation program the first of the above methods has been considered (assuming that the shock pressure loss takes place at the outflow of the runner) because the calculation theory and the computer program itself also become simpler and easier to survey.

After evaluation of the pressure loss caused by the pulsation the calculation should be repeated by considering p_{2v} in lieu of p_2^* in evaluating the pressure ratio of the turbine.

5.2. The main results of the calculation

The results of the calculation of the efficiency of the turbine was obtained with the aid of a computer specially developed for this purpose at the centre of computation of the Technical University, Budapest. The results are detailed by the work referred to under [1].

In the course of the experiment the pressure waves recorded on the magnetic tape was played back and after filtering out the external disturbances (Fig. 7) each of the pressure waves had been distributed into twenty sections in this way obtaining twenty efficiencies to a wave length. The average of twenty efficiencies obtained along a wave

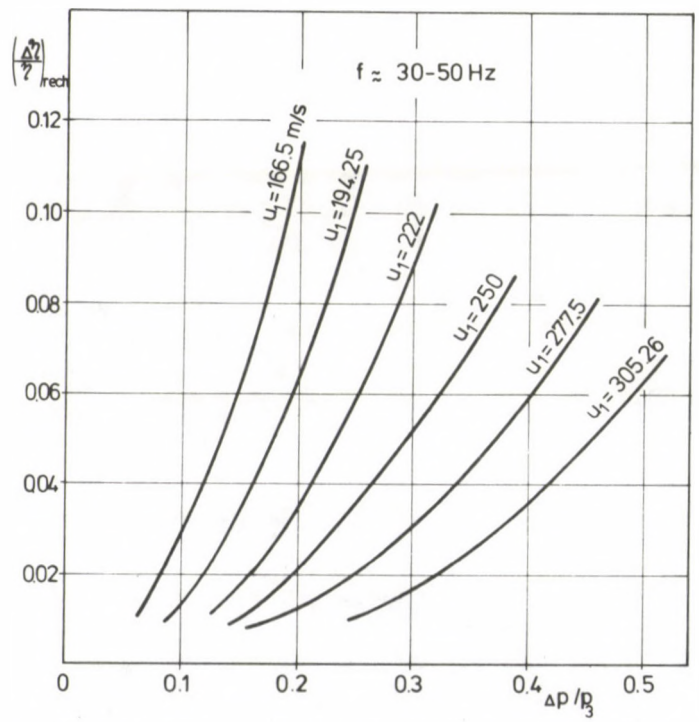

Fig. 15. Variation of the values $(\Delta\eta/\eta_{ist})_{rech}$ as a function of $\Delta p/p_0^*$ calculated in a given range of frequency for different peripheral velocities

has been denoted with ($\eta_{inst\,T}$) and the efficiency obtained at the mean value of the wave with (η_{isT}).

After that the values $\Delta\eta = \eta_{ist} - \eta_{inst\,T}$ and $\Delta\eta/\eta_{ist}$ as well as $\Delta p/p_0^*$ were established by following the procedure applied at the experiment.

The functions $\Delta p/p_0^* = f(\Delta\eta/\eta_{isT})$ associated in this way have been determined in a given range of frequency for different peripheral velocities. The results are indicated in Fig. 15. In the figures the calculation results are designated with the subscript *rech.*

6. Correlation of the experimental and theoretical (calculation) results

In order of the correlation of the results obtained at the experiment and with the aid of the theoretical calculation, the final results obtained by making use of both methods have been plotted in a diagram (Fig. 16).

From the figure it is to be seen that the calculation resulted in a larger reduction of the efficiency, mainly in case of lower peripheral velocities. This reduction in the efficiency was much smaller in the case of higher peripheral velocities. By evaluating

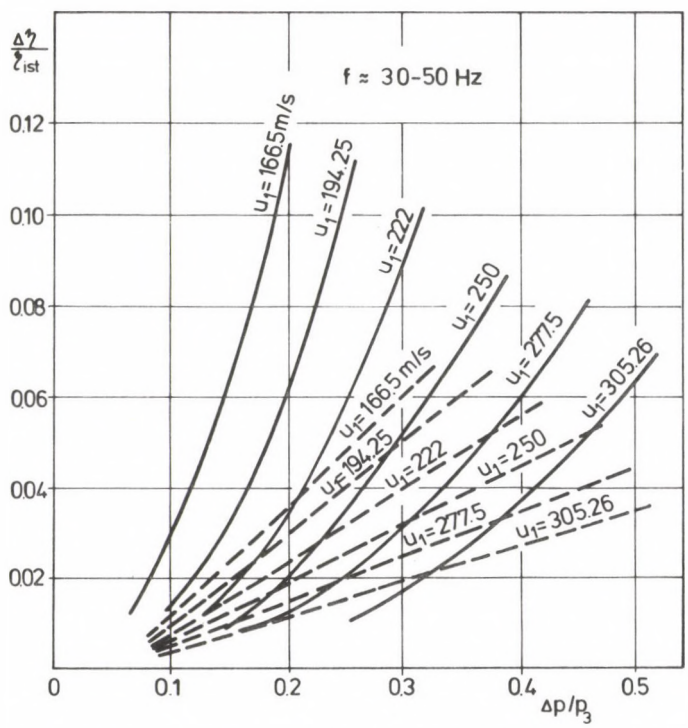

Fig. 16. Variation of the values measured and calculated ($\Delta\eta/\eta_{isT}$) plotted versus $\Delta p/p_0^*$ for different peripheral velocities within a defined region of frequency; —— calculated; - - - - measured

these results it is to be taken into account that the pulsation occurred immediately at the pipe stub of the turbine and, according to the calculation method used the pulsation was not damped in the parts of the turbine. The value of the coefficient of the shock loss has been defined by using quasi-stationary method, the loss caused by the separation between the rotor blades and by the shock is practically of less value than that defined by the quasi-stationary procedure.

Let us now examine the the differences between the experimental and calculation results. For this purpose the ratio of the reduction of the efficiencies obtained by the experiments $(\Delta\eta/\eta_{isT})_{exp.}$ and by the calculations $(\Delta\eta/\eta_{isT})_{rech.}$ which has been designated with D:

$$\frac{(\Delta\eta/\eta_{isT})_{exp}}{(\Delta\eta/\eta_{isT})_{rech}} = D\,.$$

In Fig. 17 the pairs of the values u_1 and $\Delta p/p_0^*$ associated with the same D values at the frequencies $f \cong 30$ to 50 may be seen. In the figure, above the parameter $D = 1$ the curves of parameter $D > 1$, and below those of parameter $D < 1$ are to be found. Since actually with the increase of the loading of the Diesel-engine supercharged not only the value of u_1 but also that of $\Delta p/p_0^*$ increases, in varying the working stage of the Diesel-engine the value of D is by close approximation considered constant.

The connected values u_1, $\Delta p/p_0^*$ of the existing, actually operating Diesel-engines are grouped in the immediate vicinity of the curve of $D \approx 1$ parameter, it might be stated with a rather good approximation that in the actual working stages the calculated and measured values approximate each other well.

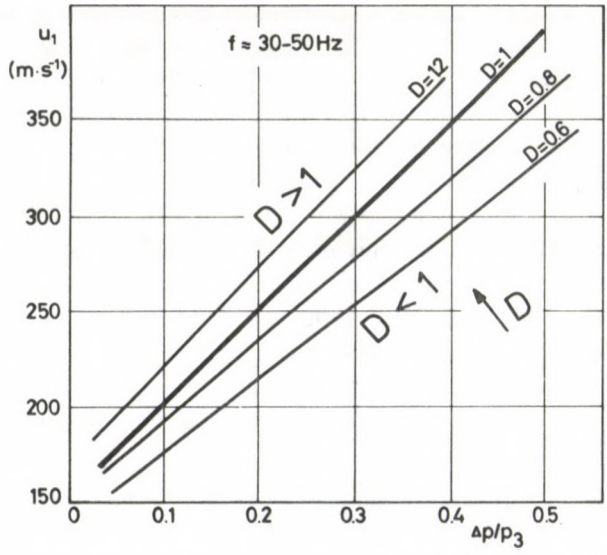

Fig. 17. Variation of the values of ratio D as function of the peripheral velocity and $\Delta p/p_0^*$ in a defined region of pulsation frequency

At actual working stages near the maximum, the $\Delta p/p_0^*$ — value before the exhaust turbine seldom exceeds 0.5, its average lies between 0.4 and 0.5 [3]; [4]; [5]. In such cases, the peripheral velocity of the turbine of the turbosupercharger under actual working conditions is 330 to 360 m/s, consequently, the actual working conditions could well be realized with the test equipment.

7. The results obtained

In the following the issues obtained by the work of the authors are outlined briefly.

1. A test equipment was set up with the aid of which a pulsation which approached the actual one before the turbine, therefore, the test equipment was suitable for the investigation of the working of the pulsating turbine.

2. According to measurements performed of the pulsation before the turbine, it did not bring about measurable change in the values of compressor characteristics. There, the pulsation presented itself only in the form of throttling. This has been attained by arranging a large damping tank between the turbine and the condenser.

3. According to the measurements and calculations performed, the efficiency of the pulsating gas flow turbine was always worse than that of the steady flow turbine. According to the tests, in the entire investigation range the reduction of the efficiency measured was 1 to 4%, according to the calculations, on an average, it was 0.5 to 11%.

4. At a given peripheral velocity and at a given frequency of pulsation the efficiency of the turbine of non-steady flow was unequivocally worsening with the increase of the ratio $\Delta p/p_0^*$, while in case of $\Delta p/p_0^* \approx 0.5$ at the maximum peripheral velocity ($u_1 \cong 300$ m/s) which could be obtained, the experimental reduction of the efficiency was about 3.5%, and the calculated one 6% or so.

5. The efficiency of the non-steady turbine had been influenced by the pulsation frequency only in a negligible way according to both the tests and the calculations.

6. According to the tests the increase of the peripheral velocity at a constant ratio $\Delta p/p_0^*$ and constant frequency unequivocally decreased the values $(\Delta\eta/\eta_{ist})_{exp}$, i.e. the turbine became relatively more and more favourable. In case of the value to be produced within the whole range of the periphieral velocity $(\Delta p/p_0^*) \approx 0.2$ the average change of the value $(\Delta\eta/\eta_{ist})_{exp}$ was about 2.3 to 2.5 per cent, and according to the calculations about 9.5 to 10.5 per cent.

7. By a final summary of the measurement results a good approximate relationship was established for determining the reduction of the efficiency of the non-steady working turbine:

$$\left(\frac{\Delta\eta}{\eta_{isT}}\right)_{exp} = \left[0.34 - 0.27\left(\frac{u_1}{u_{1\,max}}\right)^{0.8}\right]\frac{\Delta p}{p_0^*}$$

with $u_{1\,max}$ = highest peripheral velocity in the course of the tests.

The limiting values of validity of the relationship are as follows:

$$\Delta p/p_0^* \approx 0 \text{ to } 0.5; \quad u_1 \approx 150 \quad \text{to} \quad 300 \text{ m/s}.$$

The tests were performed with full inflow (i.e. not partial inflow) turbine, further, only the pressure of the entering medium but not its pulsation, therefore, the validity of the above relationship is strictly restricted to the case treated.

8. For the significant part of the actual working stages the calculation and test results are in close agreement; this particularly holds true to the working stages approaching that of full loading. During the studies, authors established a factor D which showed to what degree the calculation and measurement results agree with each other in the different ranges of loading.

9. The coefficient of the shock loss ζ_{sh} increases with the decrease of β_1 between the angles 90° and 30° and grows to the value 2.5, however, in case of $\beta_1 > 90°$ it increases slower with the decrease of β_1, hardly exceeds 0.5, and with $\beta_1 = 90°$ the value of ζ_{sh} is zero.

10. The shock loss factor (ζ_{sh}) is also the function of the entrance angle α_1, in case of $\beta_1 < 90°$ decreases with the increase of α_1, whereas in case of $\beta_1 > 90°$ increases at a negligibly slow pace. However, the reduction ζ_{sh} taking place in the range $\beta_1 > 90°$ does not compensate the increment of the outlet loss caused by the growth of α_1, thus, in such instances efficiency of the turbine is worsening both at the steady flow and non-steady flow cases.

11. In order to increase the efficiency of the turbine at a non-steady flow working state it is convenient to select the average value of the angle β_1 under the pulsation between 90° and 120° because within such range of angle the coefficient of the shock loss is, at an average, of minimum value.

References

1. Dib Y.: Variation of the efficiency of the exhaust turbine of the turbosupercharger under non-steady flow (pulsating) conditions. Thesis. Budapest, 1982
2. Митрохин, В. Т.: Выбор параметров и расчет центростремительной турбины на стационарных и переходных режимах. Москва, машиностроение, 1974
3. Wallace, F. I., Adgey, J. M., Blair, G. P.: Performance of inward radial flow turbines under non-steady flow conditions. Proc. Instn. Mech. Engns. 1969–70 (1984), (Pt. 1)
4. Arndt, P.: Analyse instationärer Strömungsvorgänge beim Ladungswechsel eines Mehrzylinder-Ottomotors and eines aufgeladenen Dieselmotors. Diss. TH., Aachen 1977
5. Pfost, H., Neubauer, H.: Strömungsvorgänge in Zentripetalturbinen von Abgasturboladern bei instationärer Beaufschlagung. MTZ 42 (1981), 6

Acta Technica Academiae Scientiarum Hungaricae, 96 (1—4) pp. 139—153 (1983)

FUNDAMENTAL RELATIONSHIPS BETWEEN GRINDING PARAMETERS

I. KALÁSZI*

[Received: 4 January 1983]

The author extends the application of the parameters of grinding ability suggested by Lurje and supplies proof of their importance higher than expected. Beside comparison they may also be integrated mathematically for the grinding time and the values thus obtained simultaneously represent also the volume of the metal ground during this time. These values offer the pssibility to determine the parameters with iteration using the metal volume ground as measured at two points of time, without the need of measuring radial force. By the method described the parameters are suitable for production planning as well. Namely, by the help of the wheel life constant introduced, the metal volume ground by the grinding wheel during the wheel life may be determined. The calculation accuracy exceeds that required for the practice as proved by the author experimentally.

1. Introduction

The parameters which could be measured on grinding are limited to the following:

Δr_{sz} = radial change in size of grinding wheel [mm]
W_{sz} = wheel volume worn [mm^3]
G_f = metal removal [mm^3]
F_t = tangential force [N]
F_r = radial component of cutting force [N]
K = grinding ratio
n_t = revolution per minute of the workpiece [1/min]
n_{sz} = revolution per minute of the grinding wheel [1/min]
R_a = roughness of the ground surface [μm]

These have to be used to form further parameters for the comparison of various grinding processes under different conditions.

The first parameter which is also applied in the practice of our days:

$$K = \frac{G_f}{W_{sz}} \left[\frac{mm^3}{mm^3}\right]$$

This parameter is, however, not reliable, because at the grinding time $t = t_{kr}$ it reaches its definite value and as a ratio it might give the same values for wheels with

* I. Kalászi, H-1118 Budapest, Villányi u. 83—85, Hungary

different diameters in spite of the differences between the metal removal outputs. The ratio $F_r:F_t$, depending on the time t, is often used for evaluation.

Neither K nor $F_r:F_t$ is adequate in technological designs.

Hahn [1], recognizing these anomalies, introduced the Λ chip removal parameter [mm²/kp] by which it may be written:

$$F_r = \frac{B \cdot v_e}{\Lambda}(1 - e^{-\frac{S}{B}\Lambda t}) \text{ [kp]}$$

where B = the width of wheel, [mm]

$v_e\left[\frac{\text{mm}}{\text{sec}}\right]$ = radial infeed speed

S = stiffness of the system [kp]

t = grinding time [min]

The member in brackets on the right side of the function, continuously increases the value of $B \cdot ve/\Lambda$ from 0 to some seconds. Λ refers to the efficiency of chip removal, the equation is selective, can be applied for comparison but not suitable for technological design.

In Hungary, the method suggested by Lurje was tried out. Lurje [2] proposed to use the grinding parameter K_{f2} [mm³/min, kp] and the exponent λ for the comparison of the grinding abilities of various wheels. The author and his research team tested the efficiency of a number of grinding lubricants with the help of these parameters [3]. The relationship between the parameters by Lurje is expressed by the equation

$$K'_{f2} = K_{f2} e^{-\lambda t}\left[\frac{\text{mm}^3}{\text{min, N}}\right] \tag{1}$$

where K_{f2} is the complex parameter for grinding ability to be calculated for the time $t = 0$; thus, at least two measurings are required for the determination. It is evident from the dimension that the metal removal, the time and radial force have to be measured. Assumably, this apparent difficulty might be the reason why no further reports have been published on new trials made in Hungary. This paper, also summarizing the measuring data in other publications, is intended to stimulate the researches to be continued. It points out the possibility of the extended application of parameters; explains the integral of equation (1) comparing it with practical experiences and suggests a method for the calculation of wheel life as the metal removal between two truings of wheel. Last of all, for the determination of λ and K_{f2} a new iteration process is suggested which is based on the metal removals measured at two points of time.

The paper applies the symbols accepted in the *Journal of Technology* [4] and the values expressed earlier in K_{f2} [mm³/min, kp] converts to K_{f2} [mm³/min, N]. The desk calculators are adequate for rapidly processing the data obtained by measuring. The author used for his calculations the Type HP-97 with programs previously set up by himself.

2. Theoretical considerations

2.1. Definition of K_{f2}

The *Journal of Technology* defines K_{f2} as follows [4]: "Complex grinding ability parameter by Lurje. It expresses the metal volume pro minute in mm^3 which can be removed by 1N radial grinding force with 1 mm length of the width of wheel, measured just after the truing of wheel. It offers the advantage that the change of grinding ability characteristic of the grinding process might be written in form of a logarithmical equations in function of time; the exponent λ represents the selective measure of the change. The applications of K_{f2} has been extending for some years. For grinding of steel its value varies between 10 and 45 [mm^3/min, N] depending on the grinding tools and the method of grinding."

In the paper already referred to [2] Lurje reports on experiments on a large scale. Their main result was the conclusion that K_{f2} to be calculated under given conditions changed, depending on time subject to the function λ. Different values of K_{f2} will be obtained at various radial forces, hardness of wheel or feeds pro revolution per minute.

λ is also dependent on conditions. As measured by Lurje, it may be $\lambda = 0.08$–0.16 for internal grinding and $\lambda = 0.05$–0.15 for external grinding. The way of wheel truing, the grinding characteristics, the sizes and characteristics of wheel etc. also influence λ. The extent of change is assimptotic to the axle x and more rapid by for higher values of λ. The lower this value, the more favourable are the properties of the wheel. The dependence of λ on the grinding lubricants has been studied by the Institute of Production Engineering of the Technical University Budapest [3].

The values λ and K_{f2} are to be calculated from two measured points. Namely, from equation (1) it may be written:

$$t = \frac{1}{\lambda} \ln \frac{K_{f2}}{K'_{f2}}. \tag{2}$$

Using $K'_{f2} = K_1$ measured for t_1 and $K'_{f2} = K_2$ for t_2 the following relationship will be obtained:

$$\lambda = \frac{\ln \dfrac{K_1}{K_2}}{t_2 - t_1} \quad \text{and/or} \quad K_{f2} = \left[\frac{K_1^{t_2}}{K_2^{t_1}}\right]^{\frac{1}{t_2 - t_1}}. \tag{3}$$

Knowing the values λ and K_{f2} and using equation (1) the points of the curve describing the change may be calculated, i.e. the curve may be plotted against the grinding time t. Figure 2 gives some examples.

2.2. Metal removal as integral of the area below the curve (suggestion of the author)

The slope of the curve of equation (1) in function of time is dependent on the exponent $-\lambda t$ of the natural logarithm e. This equation may easily be integrate according to t. Thus, we shall have the function:

$$Q = \int K'_{f2}\,\mathrm{d}t = \int (K_{f2} e^{-\lambda t})\,\mathrm{d}t \tag{4}$$

The definite integral of equation (4) in the interval $0-t$ gives the total metal volume Q_t [mm^3/N] which is removed under the given conditions with 1 mm width of the wheel, unit of radial force and during the time t. The definite integral of equation (4):

$$Q_t = \int_0^t (K_{f2} e^{-\lambda t})\,\mathrm{d}t = \left[-\frac{1}{\lambda} K_{f2} e^{-\lambda t} \right]_0^t = \frac{K_{f2}}{\lambda}(1 - e^{-\lambda t}). \tag{5}$$

Thus, if the constants of equation (1) are known, the metal volume which is removed from the unit width of the workpiece with the unit of radial force can be calculated for any period of time. The radial force F_r, as being dependent on the working parameters, has to be known for the given case. $F_{r\,\mathrm{spec}}$, referred to 1 mm width, is generally lower than 1.

Its decrease is combined with a lower value of K_{f2}. Lurje, on basis of the graphical analyses of his curves, stated that $K_{f2} = C_k (F_{r\,\mathrm{spec}})^{0.16}$. For example, for wheals of moderate hardness and moderate graining $C_k = 24$. If $F_{r\,\mathrm{spec}} = 5$ [N/mm], then $K_{f2} = 24.5^{0.16} = 31$ [mm^3/min, N]. Using the relationship the value corresponding to the given wheel and the working conditions to be set up may be substituted into equation (5). In this way the integral will give the real metal removal. By calculating the total metal removal it becomes possible to determine the number of workpieces to be produced between two wheel truings.

2.3. $C_T \cdot K_{f2}$ and the belonging T as criteria of wheel life

As explained, the complex grinding ability parameter decreases in function of time. In certain cases this decrease might reach even 1/3 of the original value (to be discussed in Section 3). It would be unreasonable to use wheels which have already suffered such a considerable loss of grinding ability. It is suggested to introduce the wheel life criterion belonging to the grinding time

$$[K_{f2}]_{\max} \leqq C_T K_{f2}\,. \tag{6}$$

The wheel life constant is in the range $C_T = 0.6$–0.9 and thus in accordance with equation (2) wheel life may be expressed by

$$T = \frac{1}{\lambda} \ln \frac{K_{f2}}{C_T K_{f2}} = \frac{1}{\lambda} \ln C_T\,. \tag{7}$$

For example, one of the measurings carried out by Korcsak [5] (see Table 1 and curve 1 in Figure 2), gave the results $K_{f2}=28$ and $\lambda=0.07$. If $C_T=0.5$ is chosen (column 5 in Table 1), then it will be

$$T=\frac{1}{0.07}\ln\frac{1}{C_T}=9.91\ [\text{min}].$$

That means that the grinding ability parameter after 9.91 minutes is: $K_{f2}=14$ [mm^3/min/N]. The integrated total metal volume removed at the unit length during this time amounts to: $Q_t=200$ [mm^3/N], provided that the radial force is $F_r=1$ N. Korcsak applied the value $F_{r\text{spec}}=6$ [N/mm] for his measurings, thus the metal volume actually removed—taking into consideration the calculation technics used for measuring—is described by the function

$$Q_{\text{val}}=F_{r\text{spec}}\cdot Q_t=6\cdot 200=1200\ [\text{mm}^3].$$

The number of the workpieces to be ground during the wheel life is given by the quotient of the real value of "Q_{val}" and the metal volume to be removed on basis of the stock allowance (Q_{mdb}), i.e.

$$n_{mdb}=\frac{Q_{\text{val}}}{Q_{mdb}}. \tag{8}$$

2.4. Iteration to determine λ and K_{f2} (as suggested by the author)

If the total metal volume is known which is removed from the unit width of the workpiece with the unit force at two points of time during one single grinding process, λ and K_{f2} might be calculated. Assuming that the total metal removal at the time t_1 is Q_{t1} and at t_2 it is Q_{t2}, then using equation (5) the result will be:

$$Q_{t1}=\frac{K_{f2}}{\lambda}(1-e^{-\lambda t}) \quad \text{and} \quad Q_{t2}=\frac{K_{f2}}{\lambda}(1-e^{-\lambda t}). \tag{9}$$

As quotient it may be written:

$$\left[\frac{Q_{t1}}{Q_{t2}}\right]=\frac{(1-e^{-\lambda t_1})}{(1-e^{-\lambda t_2})}. \tag{10}$$

In equation (10) λ is the only unknown value. If λ' is continuously increased from a low value properly chosen, the two sides will be equal at a given value of λ'. In this case λ will be equal the value to be obtained. By substituting this value in either form of equation (9) K_{f2} will be calculable. When using a desk calculator, each step of iteration takes some seconds and 5 or 6 steps are sufficient to come to result provided that the increase of λ' is not chosen to be too low. Increase by 0.005 or 0.01 is reasonable. Proof is supplied by the data obtained by the author and his colleagues with conventional methods of λ and K_{f2} determinations (3).

3. Measuring results

Measuring can be carried out in different ways:

— Force components at every time interval and the metal removal are measured; the research group of the Institute for Production Engineering applied this method [3].

— The radial force F_r is set, the slide holding the workpieces is pressed to the grinding wheel with weights to be put on and the measuring is limited to the time and metal removal. The measurings of Korcsak [5] were made in this way (Fig. 1).

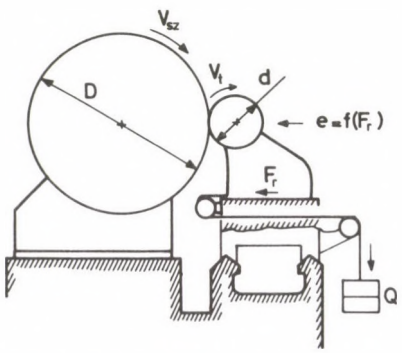

Fig. 1. Experimental device of Lurje

— The values of Q_1 and Q_2 are measured only, while F_{rspec} is calculated by the functions explained (suggested by the author).

The evaluation of the measurings suggested by the author is discussed subsections 3.1, 3.2, 3.3 and 3.4.

3.1. Evaluation of the measurings performed by the research group of the Institute for Production Engineering [3]

One of the results of the measurings reported in [3] is that when using unalloyed carbon steel (HB = 200 ± 10) and wheel KA 32 I 11 KE as well as ISO basic fluid for plane grinding, $K_{f2} = 44.1$ and $\lambda = 0.007$ (see Table 2 of the paper [3] published].

According to equation (5) the integral of the area below the curve by Lurje, if $t = 10$ minutes, the result will be

$$Q_t = \frac{K_{f2}}{\lambda}(1 - e^{-\lambda t}) = \frac{44.1}{0.007}(1 - e^{-0.007 \cdot 10}) = 440 \left[\frac{\text{mm}^3}{\text{N}}\right].$$

As found at the measurings the mean radial force at 10 mm width of the workpiece amounts to 69.5 N. I.e. the real metal volume removed from 1 mm width of the

workpiece may be expressed by the function:

$$Q_{val} = F_{rspec} \cdot Q_t = 6.95 \cdot 440 = 3060 \left[\frac{mm^3}{mm}\right].$$

The value measured is 2980. Deviation between the value measured and the value calculated: 3%. The measured force F_r is supervized by a known empirical relationship. The first step is to calculate value F_t, because formulas are available for this only; by multiplying these values with the quotient $F_r:F_t$ the radial force is obtained. The quotients of the radial forces F_r and those of the tangential forces F_t are indicated in Table I (measured by the author in [3]).

Table I

$t_{[min]}$	$F_r:F_t$	Mean
1	1.68	
2	1.74	
3	1.66	
4	1.65	
5	1.64	
6	1.68	1.69
7	1.69	
8	1.68	
9	1.72	
10	1.73	
11	1.75	
	Σ 18.62	

Thus, the mean value $F_r:F_t \cong 1.7$ is to be seen from Table I. Lurje suggests for this value the quotient 1.8→2.5 [6]. In Hungary, force values were measured by Tóth [7] and Tutsek [8]. For usual grinding, the quotients of the forces measured by them are within the range suggested by Lurje. In this case, let we chose the value 1.7.

It is to be discussed to which extent the empirical formula by Masslov [9] may be used for the determination of F_t. If $v_t = 10$ m/min, $s = 10$ mm and $f = 0.03$ mm/double stroke, the formula by Masslow will lead to the following function:

$$(*)F_t = 21 v_t^{0.7} s^{0.7} f^{0.6} = 67.4 \text{ [N]} \quad \text{(measured: 41.1)}.$$

The deviation between the measured and calculated values was obtained with an accuracy of 64%. Consequently, if for any K_{f2} and λ given in literature the value of F_r is unknown, it will be possible to calculate it with sufficient approximation by applying this empirical formula as the product of F_t and the constant 1.7. Explanation is given by a sample in the next item.

* Note: s [mm/rev] ≙ table speed/work piece revolution; HKF = grinding fluid

3.2. Evaluation of the measurings by Iliász

Iliász [10] has been engaged in comparing the effects of the binding materials of grinding wheels. He used the conventional wheal marked "20", carbon steel $C=0.6\%$ (HB $260 \div 280$) for internal cylindrical grinding under the test conditions: $v_{sz}=28$ m/s, $v_t=39$ m/min, $s=8$ mm/rev, $f=0.004$ mm/Kl, HKF*: 2.5% emulsion. Now, using the relationship by Lurje, as referred to by Iliász, the integrated and real value of Q_t as well as the life—chosing the life constant $C_T=0.5$—is to be determined by the method suggested by the author. Iliász gave for the wheel "20" the values $\lambda=0.12$ and $K_{f2}=24.2$.

As to equation (5), choosing the life constant $C_T=0.5$, the wheel life will be

$$T=\frac{1}{\lambda}\ln\frac{1}{C_T}=\frac{1}{0.12}\ln\frac{1}{0.5}=5.77\ [\text{min}]$$

rounded 6 minutes. Accordingly, Q_t is calculated by:

$$Q_t=\frac{K_{f2}}{\lambda}(1-e^{-\lambda t})=\frac{24.2}{0.12}(1-e-^{0,12.6})=102.8\left[\frac{\text{mm}^3}{\text{N}}\right].$$

To calculate Q_{val} the force $F_{r\ \text{spec}}$ must be known. This is, however, not indicated by Iliász. Using the Masslov equation for the calculation of F_t we shall have:

$$F_t=C_w v_t^{0.7} s^{0.7} a^{0.6}=44.6\ [\text{N}].$$

If $F_r : F_t=1.7$ is chosen, the radial force will be

$$F_r=1.7\cdot F_t=1.7\cdot 44.6=75.9\ [\text{N}].$$

The radial force is operative at 8 mm, thus

$$F_{r\ \text{spec}}=\frac{75.9}{8}=9.5\left[\frac{\text{N}}{\text{mm}}\right]$$

and

$$Q_{\text{val}}=F_{r\ \text{spec}}Q_t=9.5\cdot 102.8=976.6\ [\text{mm}^3]$$

During a grinding time of $t=6$ minutes the author of the paper [10] measured $Q_{\text{val}}=2190$ mm^3, i.e. the deviation from the calculated value amounted to 55%. At the same time, Figure 7 by Iliász [10] shows starting intensity of the wheel wear between $t=6$ and $t=8$ minutes, thus redressing is really advisable at $t=6$ minutes as has already been calculated above. As to the deviation of 55% it was assumed that for taking up the curves $t-Q$ and $K'_{f2}=f(K_{f2})$ not the same data should have been used. For our studies the iteration process was applied (with [mm^3/min, Kp] dimension), to be to good comparison).

The results obtained by iteration were $\lambda=0.1$ and $K_{f2}=71.1$ [mm^3/min, kp], thus

for $t=4$

$$Q_t=\frac{K_{f2}}{\lambda}(1-e^{-\lambda t})=\frac{71.14}{0.1}(1-e^{-0.1\cdot 4})=234.6\left[\frac{\text{mm}^3}{\text{kp}}\right]$$

and

$$Q_{val} = Q_t \cdot F_{r\,spec} = 0.95 \cdot 234.7 = 223.02\ [mm^3]$$
measured: 213 [mm³]
deviation: +10.02; $\Delta H = 4.5\%$

for $t = 8$

$$Q_t = \frac{K_{f2}}{\lambda}(1 - e^{-\lambda t}) = \frac{71.14}{0.1}(1 - e^{-0.1 \cdot 8}) = 391.3 \left[\frac{mm^3}{kp}\right]$$

and

$$Q_{val} = Q_t \cdot F_{r\,spec} = 0.95 \cdot 391.3 = 371.7\ [mm^3]$$
measured: 363 [mm³]
deviation: −8.7; $\Delta H = 2.4\%$

It is thus proved that the two curves were taken up with different data (assumed failure of Iliász).

3.3. Evaluation of the measurings by Korcsak

Korcsak [5] tested 19 various kinds of steel and in Table 15 of his paper [5] the values of K'_{f2} are given. These are the only values indicated, but for all the kinds of steel, for the grinding times $t = 5$ and $t = 15$ minutes. In this way it was possible to calculate the constants by Lurje. Korcsak used for infeed grinding a cylindrical grinding machine specially modified where 1 cm width of wheel was exposed to 8 N radial force. The conditions of the grinding process were: $v_{sz} = 35$ m/s and $v_t = 20$ m/min, width of the workpiece 36 mm. The chip removal occurred by itself because of the constant value F_r and varied between 0.036 and 0.009 mm. For the calculation the value of $F_{r\,spec}$ is needed. F_t is calculated for the average $f = 0.02$ mm/rev. according to the method as explained above:

$$F_t = C_w v_t^{0.7} s^{0.7} f^{0.6} = 210.4\ [N].$$

Radial force:

$$F_r = 1.7 \cdot 210.5 = 357.8\ [N].$$

This force is operative at 36 mm width, consequently

$$F_{r\,spec} = \frac{357.8}{36} = 9.9 \left[\frac{N}{mm}\right].$$

The wheel used by Korcsak for grinding was of moderate graining and moderate hardness (PP350 × 40 × 127, 3924 ClK, according to GOSZT). A part of his measurings was evaluated with the method suggested by the author. From two points λ and K_{f2} values were calculated and used for plotting in diagram some data of measurings obtained for each characteristic group of metals (see: Table II and Fig. 2). Table II also shows the integrated values of Q_t for $t = 5$, $t = 10$ and $t = 15$ minutes. The values of $T$and Q_T belonging to the life criterion $0.5 \cdot K_{f2}$ are also given. Table II clearly indicates that

Table II. Conversion of the data obtained by Korcsak as suggested by the author

No.	K_{f2}		λ	K_{f2}	$\frac{T}{C_T=0.5}$ [min]	$\frac{K_{f2}}{\lambda}$	Q_T [mm³/N]	$Q\left[\frac{mm^3}{N}\right]$ $t=5$	$Q\left[\frac{mm^3}{N}\right]$ $t=10$	$Q\left[\frac{mm^3}{N}\right]$ $t=15$	Remark
	$t=5$	$t=15$									
1	2		3	4	5	6	7	8	9	10	11
1	19.6	9.6	0.070	28.0	9.9	400	200.0	120	200.0	260.0	C=0.3% steel, sorbite structure
2	15.4	9.1	0.052	20.0	13.33	384	192.3	188	157.6	207.6	C=0.22% chromium-vanadium steel, magnesite structure
3	12.5	7.8	0.047	15.8	14.75	336	168.0	70	124.3	171.6	C=0.5% nickel-chromium steel, sorbite structure
4	10.8	6.0	0.050	14.4	13.86	288	144.0	63	112.3	152.7	C=0.67% carbon steel, troostite structure
5	7.7	4.2	0.060	10.4	11.55	173	86.2	45	77.9	102.2	C=0.12% austenite steel, austenite, carbide structure
6	4.3	2.0	0.77	6.3	9.12	82.8	41.4	26	43.9	51.3	W=16% high-speed steel, martensite structure

(a) Column 2: Measuring data given by Korcsak; columns 3–10: values calculated by the method as suggested by the author; column 6: constant of $Q = \int K'_{f2}\,dt$; columns 7–10: integrated values of Q_t at various points of time; column 11: characteristic of the metal processed as given by Korcsak

(b) Characteristics of grinding Wheel PP350 × 40 × 127, 3925C1K (GOSZT), $v_{sz}=35$ m/sec, $v_t=20$ m/min, $a_{average}=0.02$ mm/rev, $D_{mdb}=36$ mm

(c) Curves: see Fig. 2.

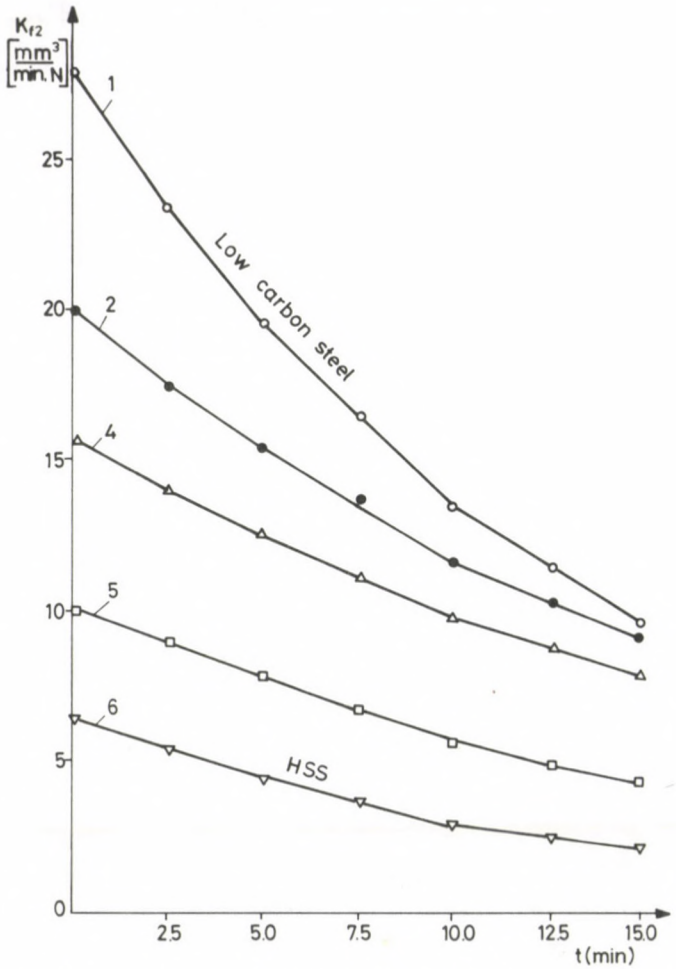

Fig. 2. Measurings by Korcsak evaluated according to Lurje (see Table II)

after reaching the value $0.5 \cdot K_{f2}$ it would not be reasonable to continue grinding. For example, in the case indicated in the first line the metal removal is 120 [mm^3/N] in the first five minutes, while in the 5.1. minute after T life time it is not more than 60 [mm^3/N]. This fact supplies a proof of the rapid decrease of the grinding ability of the wheel and emphasises the necessity of redressing after $t = 9.9$ minutes.

The test run marked 1 gives information about the grinding of standard carbon steel. If $T = 9.9$ min and the grinding conditions are the same as at the experiments made by Korcsak, then the real value Q_{val} will be the product of $Q_T = 200$ [mm^3/N] and $F_{r\,spec} = 9.9$ [N/mm], i.e.

$$Q_{val} = F_{r\,spec} \cdot Q_T = 9.9 \cdot 200 = 1980 \text{ [mm}^3\text{]}.$$

It is assumed that from the cylinder of a workpiece produced from this steel an allowance of 0.5 mm has to be ground off to ∅100 mm. In this case the metal volume to be removed from 1 mm width of the workpiece is

$$Q_{\text{mdb}} = D\pi \cdot 1 \cdot 0.5 = 157 \ [\text{mm}^3] .$$

The number of workpieces which might be produced between two truings:

$$n = \frac{Q_{\text{val}}}{Q_{\text{mdb}}} = \frac{1980}{157} = 12 .$$

The other data in Table II., connected with various kinds of metal, are also suitable for similar use.

4. A new conception for evaluating the test results

The use of the values K_{f2} and λ has been limited so far, although with successful results, but for comparison only. But it is evident from Section 3 that by applying the relationship introduced by Lurje essential technological parameters can be calculated. The tests discussed in Chapter 3 point to the physical importance of this function. In the knowledge of the constants *it is possible to calculate the metal volume to be removed from the unit length of the workpiece during the grinding time t*. Knowing this value and using the metal removal given in the drawing the number of the workpieces which can be ground during the wheel life might be calculated, similar to the method described in the Manual of the Fortuna Works [11] (See Table III).

Regarding the fact that λ depends on the conditions and K_{f2} on the wheel and metal, it would be advisable to determine both values for each grinding wheel, grinding method and all kinds of metal to be ground; Korcsak carried out such determinations with the same wheel, measuring the values K_{f2} at 19 materials at two points of time each.

Concerning the ratio $F_r : F_t$ our knowledge is also rather limited, although the calculations would require extended knowledge. For F_t more than one empirical formulas are known which, as has already been explained, offer successful use. The more exact knowledge of this ratio might help to determine the radial force F_r with higher accuracy and from this the value $F_{r\,\text{spec}}$; this modifies the metal removal Q_t [mm³/N] belonging to $F_{r\,\text{spec}} = 1$ [N/mm] which can be calculated from the relationship by Lurje.

5. Conclusions

The importance of the parameters by Lurje λ and K_{f2} is higher than was believed to be so far. For comparisons both parameters have already been proved successful earlier. Lurje himself has also examined the effects of several changes of properties by

Table III. Determination of λ and K_{f2} by means of Q_1 and Q_2 measured at two points of time, with iteration process.

(For comparison the values are given in [mm³/min, kp])

Symbol	Q_1 $\left[\frac{mm^3}{kp}\right]$	Q_2 $\left[\frac{mm^3}{kp}\right]$	t_1 [min]	t_2 [min]	K_{f2} for Q_1	K_{f2} for Q_2	K_{f2} mean	λ	K_{f2} at t_1	K_{f2} at t_2	Remark (researcher)
1	760	1260	5	20	208.6	187.6	198.1	0.14	98.3	12.05	Korcsak
2	664	1176	5	20	200.4	198.6	199.3	0.16	89.6	8.12	Korcsak
3	403	1050	5	20	107.4	112	109.7	0.08	73.5	22.15	Korcsak
4	294	672	5	20	81.6	80.96	81.3	0.10	49.3	11.0	Korcsak
5	213.3	363	4	8	71.1	71.18	71.14	0.10	47.7	32	Iliász, $v_t = 39$ m/min
6	216.7	396.94	4	8	60.19	60.11	60.15	0.05	49.25	40.3	Iliász, $v_t = 56$ m/min
7	213.5	371.7	4	8	62.27	60.51	61.00	0.07	46.10	34.0	Iliász, $v_t = 78$ m/min

(a) 1, 2, 3, 4, Q_1, Q_2 by Korcsak: Obrabatyvaemosty stalej pri shlifovanii krugom raznoj kharakteristiki. Veszt. Mashinostroenie (1962), No. 2. 62–66 Grinding conditions: wheel EB 36 SZT1K, $v_{sz} = 50$ m/s, $v_t = 10$ m/min, $e = f$ ($F_r = 12$ kp). Workpiece: 1: steel 45; 2: steel 50 G; 3: 20 × N3A; 4: 33 × CA (GOSZT) External grinding.

(b) 5, 6, 7, Q_1 and Q_2 by Iliász [4]. Grinding conditions: see in the text. Internal grinding.

these constants. The author of this paper has come to the conclusion that the integral of this relationship presents a practical value and offers the possibility of calculating a new life criterion: the metal volume to be removed between two dressings. This provides an essential contribution to the technological design. Some relationships F_r/F_t need further research to clarify and to achieve higher accuracy in the calculations, but the relationships already known help to achieve an accuracy of $3 \div 50\%$ in design.

References

1. Hahn, R. S.: On the mechanics of the grinding process under plunge cut conditions. Trans. of ASME No. 65 *Prod.* 7 (1965)
2. Lurje, G. B.: Kriterii otsenki rabotospasobnosty shlifovalnyh krugov. Vestnik Mashinostroenia 4 (1967)
3. Kalászi, I., Iliász, D., Tóth, I.: Performance and evaluation of grinding fluids. *SME* MR 72–213 Technical paper, 1972 Chicago
4. Review of grinding in Hungary, 60/1, 65–66
5. Korcsak, S. N.: Proizvoditelnosty protsessa slivovaniya stalnih detalej. Masinostroenie, Moscow 1974
6. Lurje, G. B., Komiszarzsevszkaja, V. N.: Slifovalnüe sztanki i naladka. Vüszsaja Skola, Moscow, 1976, p. 188
7. Tóth, I.: Wear of grinding wheel. Gép, (1973), No. 2. (in Hungarian).
8. Tutsek, J.: Einfluß der Bindungscharakteristik auf die Schnittkräfte bei Schleifscheiben verschiedener Fabrikate. Schleifen und Trennen Folge **55**, (1970), 9–15, Kundenschrift der Tirolit Werke
9. Masslow, E. N.: Grundlagen der Theorie des Metallschleifens. Vlg. Technik, Berlin 1952
10. Iliász, D.: Effect of ceramic binding material on the characteristics of grinding. Review of Grinding in Hungary. 1970/71, 27–35 (in Hungarian)
11. Fortuna Works AG: Cylindrical Grinding. Műszaki Könyvkiadó, Budapest 1967, p. 75. (in Hungarian)

APPENDIX

Accuracy on the determination of the constants by Lurje

(A) General considerations

When determining the values K_{f2} and λ the accuracy to be achieved depends on the test conditions. Determinations are generally made by measuring the metal volume V which is removed from the unit width of the workpiece during the time Δt, thus the value

$$Q_{t_i} = \frac{V}{\Delta t}\left[\frac{\text{mm}^3}{\text{mm, min}}\right]$$

will be obtained, where Q_{t_i} is the specific value referred to the point of time t_i. When measuring the specific radial component of grinding force, $F_{r\,\text{spec}}$, at the point of time t_i, the parameter by Lurje at this point of time will be

$$[K_{f2}]_i = \frac{Q_{t_i}}{F_{r\,\text{spec}}}\left[\frac{\text{mm}^3}{\text{min, N}}\right].$$

Q_{t_i} can be determined with high accuracy. At cylindrical grinding by using a micrometer the diameter of the workpiece d_t can be measured with an accuracy of ± 0.005 mm. That means that in accordance with the relationship $(d_t \pm 0.005)\pi \cdot 1 = d_t \pm 0.015$ an accuracy of $\pm 0.015\ \text{mm}^3$ can be achieved on determining the metal volume V which, if $d = 100$ mm, will present a deviation of $\pm 0.004\%$.

As to the determination of force, the deviations might depend on the conditions. Assuming a measuring system of average quality the error amounts to $\pm 5\%$. In general, when taking a force $F_{r\,spec} = 10$ N/mm and an average real value $Q_t = 200$ [mm^3/mm, min] the extremes of the measured value might be

$$[K_{f2}]_{t=10} = 200/9.5 = 21.05$$

and

$$[K_{f2}]_{t=10} = 200/10.5 = 19.05\,,$$

thus $\Delta H = 2.2$ and/or 1.7, i.e. the deviation varies between $+11\%$ and -9%.

If on measuring force the deviation exceeds $\pm 5\%$, it will be reasonable to determine the constants λ and K_{f2} from the coherent "i" pair of points. In such cases the value $i = 4 \div 6$ provides an accuracy sufficient for the practice. By applying the known process of the Gaussian method the exact values can be obtained from the "i" pair of points.

(B) Determination of the constants by Lurje from "n" pair of points

The relationship $[K_{f2}]_t = K_{f2}e^{-\lambda t}$ is transformed to the next form:

$$\log [K_{f2}]_t = \log K_{f2} - (\log e)\lambda t \tag{1}$$

where K_{f2} and λ are the unknown values.

Introducing the following symbols from equation (1)

$$\log [K_{f2})_t = Y,$$
$$\log K_{f2} = B\,,$$
$$\lambda(\log e) = A\,,$$

we shall have

$$\bar{Y} = B + A\bar{t} \tag{2}$$

where the relationship obtained by the Gaussian method:

$$A = \frac{\sum_i^n t_i Y_i - n\bar{t}_i \bar{Y}_i}{\sum_i^n t_i^2 - n\bar{t}_i^2} \tag{3}$$

and

$$B = \bar{Y}_i - A\bar{t}\,. \tag{4}$$

In knowledge of A and B the values to be obtained are:

$$K_{f2} = \text{num log} B\,,$$

$$\lambda = \frac{-A}{\log e}\,.$$

The overlinings refer to mean values such as: $\bar{Y} = \dfrac{\sum_i^n Y}{n}$, etc.

Acta Technica Academiae Scientiarum Hungaricae, 96 (1—4) pp. 155—167 (1983)

FLUCTUATION OF PHYSICAL CHARACTERISTICS IN THE FLAME OF LOW CAPACITY OIL BURNERS

K. REMÉNYI*

[Received: 27 September 1983]

The analysis of the fluctuation of the physical characteristics of flames is highly assisting in the better understanding of the combustion process and the operation of the firing equipment. By means of up-to-date instruments the spectrum of the fluctuation in pressure, temperature and electric conductivity can readily be measured and is suitable for frequency analysis. The analysis offers useful information on the turbulent mixing and the reactions in the flame.

Notation

ρ — density of flowing medium
u — axial flow velocity
v — velocity perpendicular to axis
x, y — axial and radial coordinates
c — concentration
m — component in unit volume
c_p — specific heat at constant pressure
t — temperature
t' — mean temperature pulsation
h — specific enthalpy
r — radius perpendicular to axis of flow
α — degree of burnout
H — enthalpy
B — fuel flow
D — diameter of burner outlet
T_u — degree of turbulence
v' — mean pulsation of velocity
e — electric conductivity
e' — mean pulsation of electric conductivity
p — pressure
p' — mean pulsation of pressure

1. Introduction

Because of the complexity of the physics-chemical processes in industrial firing equipment, the knowledge of flame characteristics, that feature the quality of firing and can be simply determined by up-to-date measuring methods, is of great significance. A

* K. Reményi, H-1014 Budapest, Uri u. 38, Hungary

lot of information about the quality of firing is given by the fluctuation of different physical characteristics, for which the most frequent frequency of the fluctuation detected in the wave length range observed is usually called "flame frequency". Flame parameters that can be subjected to frequency analysis are brightness, pressure, temperature and electric conductivity of the flame, the composition of different components, etc. Direct correlations can be found between the individual physical characteristics and certain characteristics of the flame, e.g. pressure fluctuation results in the "noisiness" of the flame and, with an increase in fluctuation the firing equipment may become unstable, etc.

The hydrocarbon flames of industrial firing equipment are generally of turbulent diffuse nature. Since the fuel oil and the combustion air are introduced into the burner outlet separately, to a great extent combustion will depend on the process which determines the creation of the combustible mixture. Mass-, pulse-, and heat transport, furthermore the chemical reactions take place simultaneously in the flame. The balance equations (1) of the time mean values of the variable for axisymmetrical turbulent jet are as follows:

(a) Momentum equation (pressure distribution and buoyant force are neglected)

$$\frac{\partial\overline{\rho u^2}}{\partial x}+\frac{1}{y}\frac{\partial\overline{y\rho uv}}{\partial y}=0\,.$$

(b) Mass conservation equation for the individual components

$$\frac{\partial\overline{\rho uc_i}}{\partial x}+\frac{1}{y}\frac{\partial\overline{y\rho vc_i}}{\partial y}=m_i$$

(c) Energy equation (adiabatic conditions are assumed)

$$\frac{\partial\overline{\rho uc_pt}}{\partial x}+\frac{1}{y}\frac{\partial\overline{yvc_pt}}{\partial x}=\Sigma m_ih_i$$

These correlations give no information about the turbulent nature of the flame. The balance equations represent an ordering principle, but the "turbulent diffusivity" parameters are unknown, so the system of equations cannot be solved. The isothermal turbulent jet model of Reichardt [2] and the mathematical models for turbulent flame [3, 4, 5]—representing the developed version of the Reichardt model—assume that in the flame the velocity, concentration and temperature distributions in the individual axial sections are universal and of the Gauss type. The diffusivity factors are determined from the distribution of the time mean values of the individual variables.

The diffusivity factor of the momentum exchange is:

$$\varepsilon_j=\frac{v\partial v/\partial x}{2\partial^2 v/\partial r^2}$$

The mass exchange factor is:

$$\varepsilon_M = \frac{v\partial c/\partial x}{2\partial^2 c/\partial r^2}$$

This mathematical model can be used in general with swirl-free flow and gas firing [6].

For turbulent diffuse natural gas flames Lenze and Günther [7] elaborated a testing method meeting the practical demands, with a burner of simple construction, where fuel leaves the burner outlet through a round section while O_2 oxidizer leaves through an annular section.

They assumed for flames burning both in open space and in closed space that the flame front was the surface determined by the time mean value of the stoichiometric concentration.

They determined the burnout of the fuel in the individual axial sections by measuring the fuel concentration.

The degree of burnout is:

$$\alpha = 1 - \frac{2\pi \int_0^y H_u u_y \, dy}{B_0 H_{u0}}.$$

For the description of variation of the burnout along the axis they adopted Heiligenstaedt's correlation [8] which says:

$$\alpha(x) = 1 - \exp\left[-a(x/D_0)^b\right]$$

and where a and b are constants determined by experiments. It could be assumed that concentration profiles in the flame were alike. Using this assumption they could define not only the local values but the mean values of the reaction density (energy developed in a unit volume) for the axial sections as well. In this way reaction density and its fluctuation can be determined along the flame axis which, in turn, characterize the accelarating and decaying phases of the reaction very well.

2. Experiments with oil flames

Based on what has been said above it can be stated that for the flame type of our experiment the diffusivity factors characterizing the turbulent momentum, mass and heat exchange cannot be determined from the time mean values. In the state of turbulency the value of state characteristics changes as a function of place and time. Turbulency is characterized by two fundamental facts. First, the movement has numerous different, but simultaneously existing variants. Second, there is a constant exchange of energy among the different variants. The theory of turbulance should establish correlations describing the simultaneously existing variants and the energy

exchange among them. In flames the mechanism of turbulence is even more complicated since the generation of turbulence has many ways, e.g. thermal instability. (Thermal instability was observed for example with oxygen poor burning of oil drops.)

The swirls generated by turbulence receive energy at a constant rate and pass it on to smaller and smaller swirls and in stationary state energy dissipates in the system. In stationary state the rate of energy dissipation is equal to that of the energy input generating the big swirls.

Turbulence in flames is usually examined on the basis of Taylor's "free path length" theory. The degree of turbulence, T_u is determined from velocity fluctuation measurements using the following formula:

$$T_u = \frac{\sqrt{\overline{u'^2}}}{\bar{u}} \equiv \frac{u'}{u},$$

or is directly measured by an instrument. The macro- and micro-scales characteristic of the size of the big and small swirls are determined by frequency analysis.

With the measuring equipment developed for these experiments we could measure the fluctuation of static pressure, temperature and electric conductivity, furthermore the "turbulence factors" T_t of temperature and T_e of conductivity. T_t and T_e are defined in a way analogous to T_u [9].

3. Introduction of the experimental apparatus

The schematic drawing of the experimental apparatus is shown in Fig. 1. For the examination of the impeller type burners generally used for lower heat requirements we used a Priofect block oil burner, with the following specification;

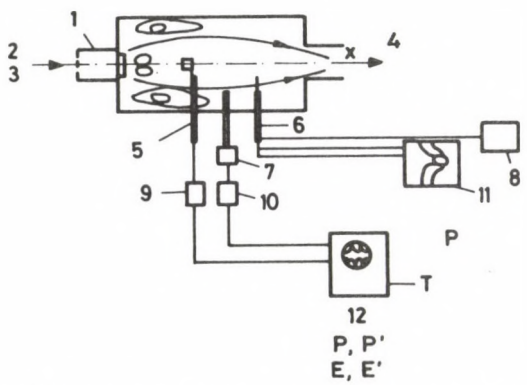

Fig. 1. Schematic diagram of the experimental apparatus. 1. burner; 2. oil; 3. air; 4. flue gas; 5. conductivity sensor; 6. combined probe; 7. pressure sensor; 8. CO_2 measuring instrument; 9. electric circuitry; 10. oscillator; 11. compensograph; 12. oscillograph

burner outlet diameter:	90 mm
impeller outer diameter:	70 mm
impeller inner diameter:	30 mm
impeller blade angle:	45°
atomizing pressure:	686.5 kPa
flow rate	8 – 6.3 *kg*/h
cone angle	80° – 60°

of the Danfoss nozzles used.

Burner capacity was set 94.5 kW and 74.5 kW (340 MJ/h and 268 MJ/h) for the first series, 58 kW and 70 kW for the second one. The fuel used was a kind household fuel oil marked TH 20/50.

Before commencing the measurements the burner was adjusted is such a way that the soot and carbon monoxide content of the flue gases comply with the technical regulations currently in force. Air flow in the burner was slightly swirly. Under isothermal conditions the swirl factor S_x (the moment of momentum and the momentum multiplied by the burner outlet diameter) has the value of 0.2 at the axial section $x/D=0.5$ and this value decreases to its half by the axial value $x/D=4$.

For the burner experiments a watercooled cylindrical furnace of 400 mm inner diameter was used. Measurements could be carried out in the whole flame cross section.

Temperature was measured by $PtRh_{10}$—Pt thermocouples. They were used without protective tubes, the combustion catalyzing effect of platinum was eliminated by an appr. 10 μ thick aluminium-chloride layer chrystallized on it. The probe parts used for the evaluation of the static and total pressure and for taking gas samples were made of 1.6/0.8 mm diameter ceramic tubes. A Schiltknecht made pressure transducer with a measuring range of 0–10 and 0–500 Pa was connected to the probe.

Gas analysis was performed by a Siemens-Ultramat CO_2 and SO_2 analyzer. The electric conductivity of the flame was measured by a sensor and electric circuitry developed at our Institute [10]. The measurements were carried out spot by spot in the axial cross section of the flame and the time mean value of the variables was determined from signals registered by an oscillograph.

For pressure pulsation measurements a DISA Pu 2a type capacitive pressure sensor with 220 mm channel length and 01 mm thick steel membrane was used.

A device connected to the pressure sensor ensured frequency modulation, demodulation and amplification. The probe was suitable for measuring the static and dynamic pressure of gases. The boundary of the reaction zone, the "edge of the flame" was determined form the signal of the electric conductivity ($e \rightarrow 0$).

4. Evaluation of the experimental results

For studying the progress of combustion process we determined the mean values of the individual parameters [11]. The change in the degree of burnout of the fuel gives information on the combustible content and the change in the electric conductivity on the intensity of the reaction in the flame and on the completion of the combustion. The temperature conditions characterize the degree of heat dissipation and heat development. These parameters are summarized in Fig. 2, which we used here exclusively for the determination of the flame dimensions and reaction conditions, adopting the results of [11].

For a flame with 94.5 kW capacity Fig. 2 presents an empirical function describing the change of the degree of burnout along the axis, by the following function;

$$F\left(\frac{x}{D}\right) = \int_0^{x/D} \lambda^2 \frac{x}{D} \exp\left(-\lambda \frac{x}{D}\right) \mathrm{d}x$$

where the value of parameter λ was found 0.86. Whether or not this type of function is generally applicable or what the range is within which the parameter varies must be determined from further measurements. The evaluation of the research work [11] will be presented by the author.

As the first step in the evaluation of the pulsations generated in the flame, the pulsations of the pressure of the air jet leaving the burner outlet were measured along the axis. This is shown in Fig. 3. The change due to combustion is illustrated in Fig. 4. From the figures it can be stated that due to the turbulent flow in the case of isothermal jets at the value of $x/D = 1.1$ a vigorous pulsation exists, but for $x/D = 6.6$ this pulsation

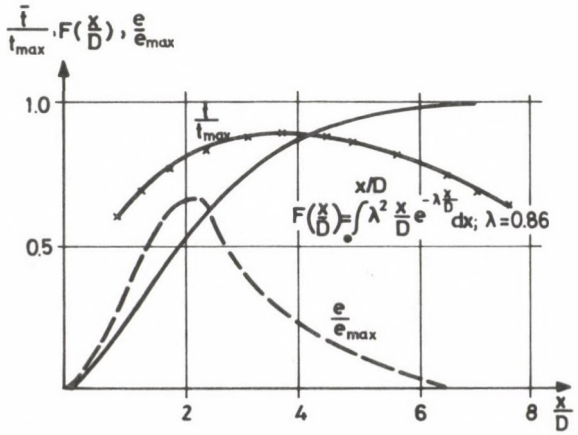

Fig. 2. Variation of the degree of burnout, $F(x/D)$ (———) electric conductivity, e'/e_{max} (– – –) and temperature, t/t_{max} (– x – x – x –) as a function of the distance x/D along the axis [1]. Burner capacity: 94.5 kW

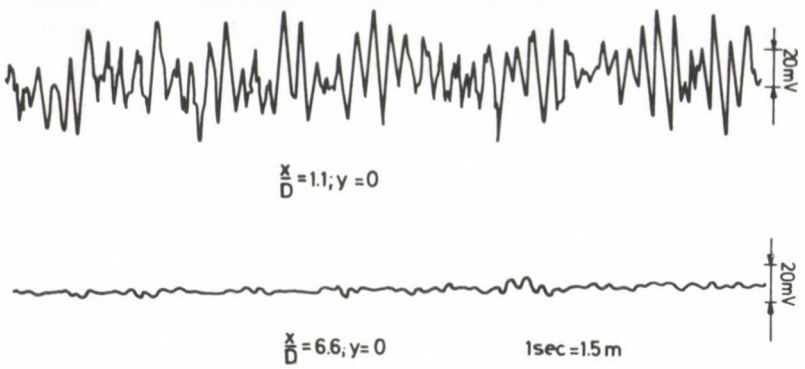

Fig. 3. Pressure fluctuation at two points of the axis of the isothermal jet. 1. film speed: 1.5 m/s

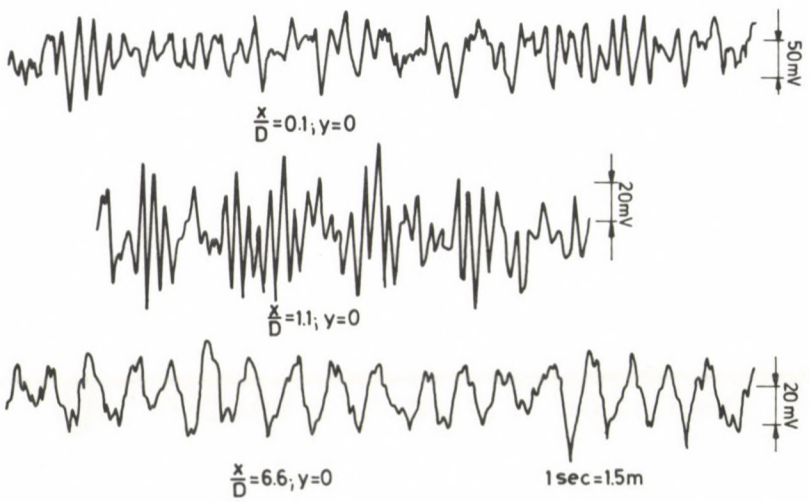

Fig. 4. Pressure fluctuation at three points of the axis of the oil with 94.5 kW capacity. 1. film speed: 1.5 m/s

ceases. In the case of combustion, even at the distance of $x/D = 6.6$, meaning practically the flame effect a significant pressure pulsation arises.

For the characterization of the pulsating values, the mean value y and the standard deviation referring to the time period t are commonly used, as shown in Fig. 5. The value of the standard deviation was determined on the basis of photos with area equalization, i.e. it was characterized by $|\bar{y}'|$. For values $y > 1$ somewhat lower standard deviation values are obtained. The mean pulsation values in the cross section were plotted against the average of the mean values as percentage values. In the flame with 94.5 kW capacity the combustion zone shifts to the edge of the flame as the distance from the burner outlet increases along the axis and, consequently, greater fluctuation is

observed here. Comparing flames of 74.5 kW capacity with 1.04 to 1.2 excess air factor it can be stated that with higher excess air—in compliance with the greater burnout—the relative fluctuations are higher at the beginning of the flame and lower in its second half. Combustion will be more intensive at the edge of the flame. This character was also demonstrated by the concentration distribution.

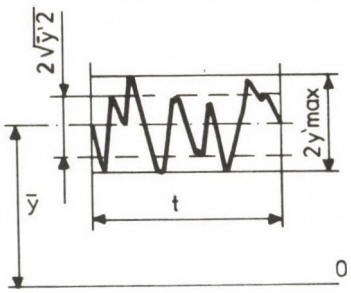

Fig. 5. Auxiliary diagram for evaluating the pulzation of the flame characteristics [1]

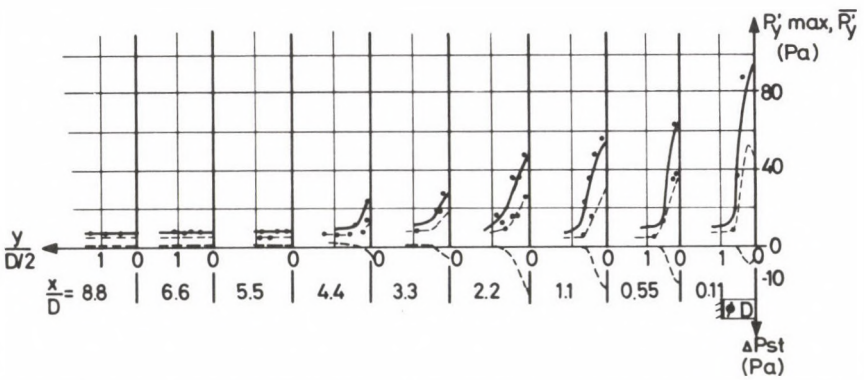

Fig. 6. Static pressure (–.–), pressure pulzation $\bar{p}'_y$ (– – –) and amplitude maximum of pulzation (———) $p'_{y\,max}$ in different x/D axial sections in isothermal air jet [1]

As a rule we can state that the mean value and the pulsation jointly characterize the combustion process as follows:

— uniform, intense combustion is characterized by high mean values of conductivity and low relative fluctuation.

— if the combustion takes place in those regions of the flame, where it is in contact with reaction products, (in the boundary region of the external or internal recirculation zone), due to the intense turbulent transport processes, fluctuation of great amplitude and high mean value occurs, mostly at an extremely low mean value (value of e' is high).

We carried out pressure fluctuation measurements in various axial cross sections of the flames, in directions perpendicular to the axis. The fluctuation distributions

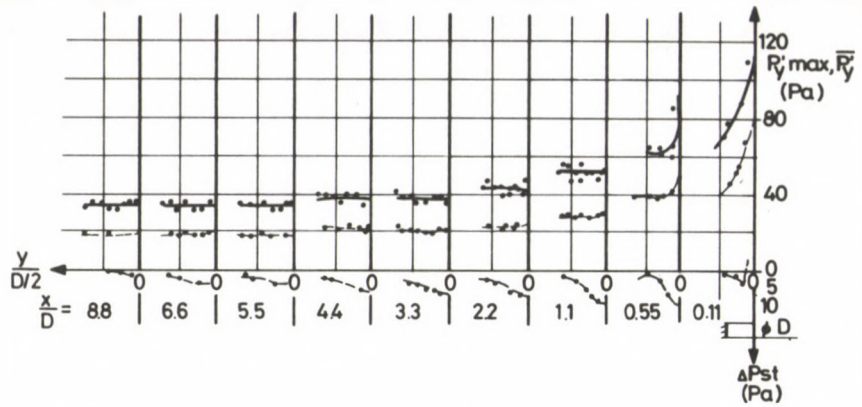

Fig. 7. Static pressure (–.–), pressure pulsation $\bar{p}'_y$ (– – –) and amplitude maximum of pulsation $p'_{y\,max}$ (———) in different axial sections x/D. Burner capacity: 94.5 kW. Cone angle of atomization: 80°

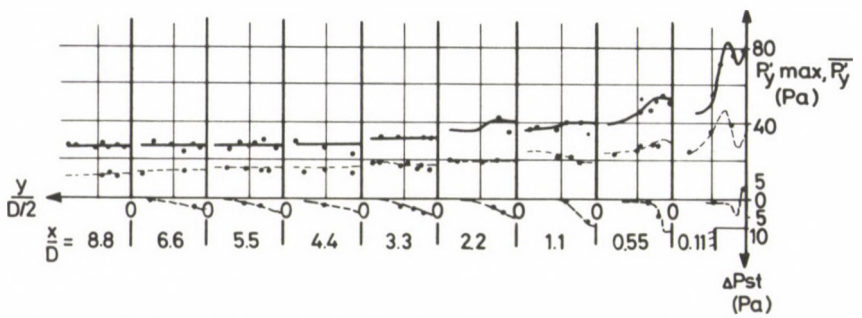

Fig. 8. Static pressure (–.–), pressure pulsation $\bar{p}'_y$ (– – –) and amplitude maximum of pulsation $p'_{y\,max}$ (———) in different axial sections x/D [1]. Burner capacity: 74.5 kW. Cone angle of atomization: 60°

measured in the isothermal jet and the flame were compared in order to establish the extent of role which the turbulence of flow vs the combustion play in generating the pressure fluctuation observed in the flame. In Fig. 6. the values of the static pressure P_{st} the amplitude of the medium and maximum fluctuation (p'_y and $p'_{y\,max}$, resp.) measured in various axial sections of the isothermal jet are shown. (p'_y was similarly determined as e'.) For values $x/D > 5$ all three values show uniform distribution, and also the velocity and the static pressure can be considered uniform.

Figures 7 and 8 show the distribution of p_{st}, p'_y and $p'_{y\,max}$ flames with higher or lower capacity. The figures show that damping of the fluctuations takes place after the first 25% of the flame length for the flame with higher capacity and already after 15% of the flame length for the lower capacity flame. The velocity and pressure fluctuation decay at the end of the flame, at a value $x/D > 8$. In the flame the magnitude of the fluctuations as well as their distirbution in space differ considerably in character from those experienced in the isothermal jet. Fluctuation characteristics in the flame also

depend—through the spatial distirbution of the fuel—on the spatial intensity distribution of the combustion.

We have come to the conclusion that combustion, i.e. the chemical reactions, is in interaction with the turbulent flow structure of the flame. Fig. 9 shows the variation of the mean aplitude of the pressure fluctuation along the axis, indicating the jet region with nearly uniform fluctuation. In this region, for burners of similar nature it is sufficient to examine the pressure fluctuation in one spot only to determine its

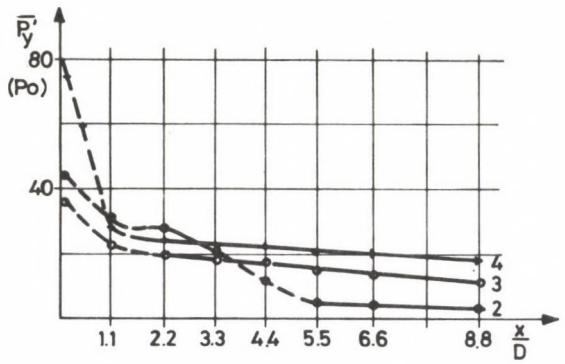

Fig. 9. Variation of the mean amplitude of pressure pulsation as a function of x/D [1]. 1. ——— region of uniform fluctuation; 2. isothermal jet; 3. 74.5 kW burner capacity; 4. 94.5 kW burner capacity

character with satisfactory approximation. On the basis of our measurements we have concluded that a change of a multiple of 10 Pa in the combustion chamber pressure resulted only in a negligible influence on the fluctuation values.

Analysing the frequency distribution of the pressure fluctuations we found that higher chamber pressures brake the high frequencies and the great-amplitude low-frequency pressure fluctuation leads to unstable combustion. (The flame does not ignite at the given chamber pressure, or pressure waves are generated.) Figure 12 gives a good illustration of the effect of the combustion on the distribution of the pressure fluctuation. At a distance of 1–2 burner diameter from the burner outlet presumably the flow and mixing processes are determinant, the curves converge, though with higher burner capacities the retroaction of the combustion extends up the burner outlet. At the end of the flame, at a distance of 6–8 burner outlet diameter, on the surface of the flame there is considerable difference between the conditions of the isothermal flow and the flame. With an increase in the burner capacity—as a result of combustion—fluctuation will ever increase at a given constant distance from the burner outlet.

The further experiments conducted at 58 and 70 kW burner capacities aim at comparing the fluctuations in temperature, electric conductivity and pressure. The distribution curves of the temperature and conductivity fluctuations are shown in Figs

10 and 11. Inside the flame the fluctuation of the conductivity is high, and gives information on the chemical reaction. At the edge of the flame temperature fluctuation increases. This indicates the end of the combustion process since the combustible volume parts igniting occasionally on the edge lead to a highly inhomogeneous zone.

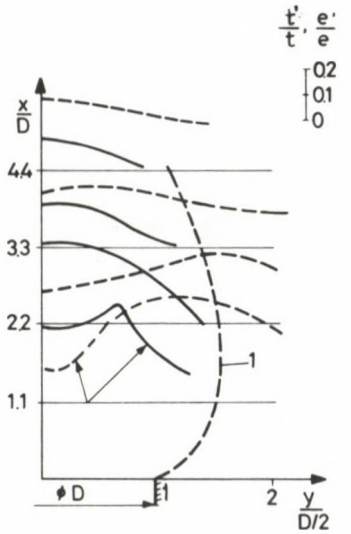

Fig. 10. Variation in temperature t'/t (– – –) and electric conductivity e/e' (———) fluctuation as a function of the distance x/D along the axis [1]. Burner capacity: 58 kW. Excess air factor: $m = 1.1$. 1. Boundary zone of chemical reactions

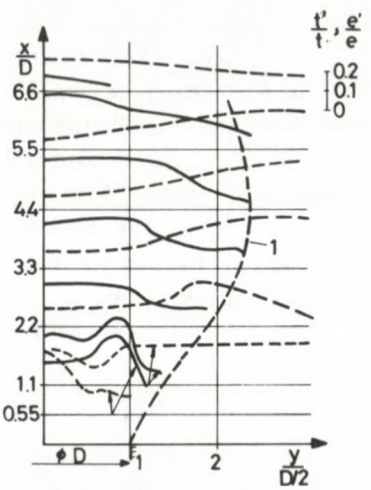

Fig. 11. Variation in temperature t'/t (– – –) and electric conductivity e'/e (———) fluctuation as a function of the distance x/D along the axis [1]. Burner capacity: 70 kW. Excess air factor: $m = 1.05$. 1. Boundary zone of chemical reactions

With increasing distance from the edge of the flame the rate of fluctuation decreases to the rate of the fluctuation caused by the flow. Of course no temperature fluctuation can be observed in isothermal flow where pressure fluctuation is characteristic of the flow. The relative temperature fluctuations t'/t are consistently greater in the outer zone of the flame. At the edge of the flame temperature and the time mean value of the electric

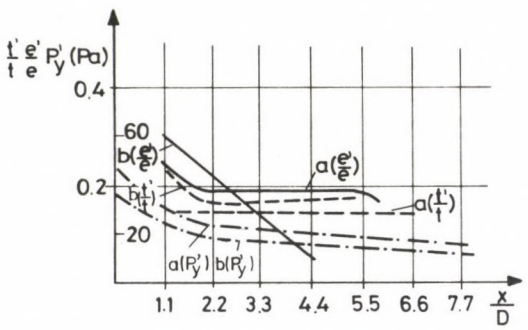

Fig. 12. Variation in the average temperature fluctuation. t'/t (– – –), electric conductivity fluctuation; e'/e (———) and pressure fluctuation p'_y (–.–) in the oil flames examined [1]. a — burner capacity: 70 kW; b — burner capacity: 58 kW

conductivity depending on the reaction intensity decreases. The higher fluctuations are a result of the mass and momentum exchange of the flame and the recirculation zone.

The fluctuations e'/e of the electric conductivity correspond to the reaction intensity. The fluctuations of static pressure, p' occur in the recirculation zone at the axis.

In Fig. 12 the average fluctuation values of p', e'/e and t'/t are indicated for flames with 58 and 70 kW capacity. The average level was determined from the distributions in the individual sections. After the first part of the flame the temperature and pressure fluctuation values are nearly constant, the fluctuations in conductivity depend considerably on the mixing of the fuel and the air. Better flue gas characteristics were experienced with the flame in which conductivity fluctuation dropped suddenly from a nearly constant value in the flame to zero at the edge of the flame.

For the flame with 70 kW capacity the Fourier analysis of the fluctuation signals t and e recorded at two points ($x/D = 0.01$, $R = 0$ and $x/D = 0.44$, $R = Q$) indicate that the load level of the pulzation continuously decreases with increasing frequency.

References

1. Mrs. Balogh, L.: Szénhidrogén lángokban a tüzelőanyag kiégés és egyes lángjellemzők ingadozásának vizsgálata. (Examination of the burnout rate and the fluctuation of some flame characteristics in hydrocarbon flames), VEIKI Report (1977) Budapest
2. Reichardt, H.: Gesetzmässigkeiten der freien Turbulenz. VDI-Forschungsheft 414 (1942).
3. Baron, T.: Reactions in turbulent free jets. Chem. Ing. Progr. 50 (1954), 273–276
4. Eichoff, H.: Änlichkeit und einfache Modellgesetze freibrennender und eingeschlossener Strahlflammen. Verfahrenstechnik 5, (1971), 118–122
5. Lenze, B.: Turbulenzverhalten und Ungemischkeit von Strahlen und Strahlflammen. Thesis, Karlsruhe 1971
6. Mrs. Balogh, L.: Szénhidrogénláng és villamos vezetőképesség energiacsere-viszonyainak kapcsolata (Connection between the energy exchange relations of hydrocarbon flame and electric conductivity). VEIKI Report (1976) Budapest
7. Lenze, B., Günther, R.: Ausbrand und Wärmeentwicklung in Erdgas—Diffusionsflammen. BWK 27 (1975), 10, 387–394
8. Heiligenstaedt, W.: Wärmetechnische Rechnungen für Industrieöfen. Springer Verlag Berlin, Heidelberg 1966
9. Reményi, K.: On flame frequency. Acta Techn. Hung. 74, (1973), 215–226
10. Mrs. Balogh L.:—Borbényi I.: Szénhidrogén lángokban az égés és a villamos vezetőképesség kapcsolata (Connection between combustion and electric conductivity in hydrocarbon flames). Energiagazdálkodás 10 (1977), 432–436
11. Mrs. Balogh, L.: Az áramlási viszonyok és a cseppelosztás hatása a kiégésre olajlángokban (The effect of the flow conditions and the drop size distribution on the burnout rate of oil flames). VEIKI Report (1978) Budapest
12. Lenz, W., Günther, R.: Measurements of fluctuating temperature in a free-jet diffusion flame. Combustion and Flame 37 (1980), 63–70

Acta Technica Academiae Scientiarum Hungaricae, 96 (1—4) pp. 169—178 (1983)

DEFLECTION OF PARTIALLY PRESTRESSED REINFORCED CONCRETE BEAMS UNDER SHORT TIME LOADS

L. GARAY* and S. D. JABOU

[Received: 15 March 1983]

The short time flexural rigidity of partially prestressed reinforced concrete beams is influenced by the average crack distance in the tension flange. Formulae available for the calculation of the maximum crack distance cannot be applied directly for the calculation of the average one. Considering, that (*i*) the crack distribution is the result of the loading process, and (*ii*) cracking can be initiated by chance in each embedding concrete area of each bar or tendon, it is assumed, that the cracking process follows stochastic rules, governed by the number of the bars. So the average crack distance can be derived from the maximum one according to the rule of the "Drunkard's Walk". Test results support this assumption.

1. Subject

A large mass (~ 1 million per year) of prestressed reinforced concrete beams is used in Hungary. To control the serviceability limit state their deflections must be calculated. The manufacturing technology of the beams significantly influences the measure of deflections, and the different codes prescribe various models for calculation, so the experimental control appears to be reasonable.

We investigated the bigger type of the mass produced beams. For control of the calculation model we also used some specially reinforced beams produced on the same manufacturing line as the typical ones.

2. Tests and results

The constant parameters of test beams were:

crossection	32 500 ($\pm 1\%$) mm^2
height	290 ($\pm 1\%$) mm
span	4 200 ($\pm 5\%$) mm
cube strength ($200 \times 200 \times 200$ mm^3)	54.5 (± 2.5) N mm^{-2}

* L. Garay, H-1115 Budapest, Tétényi u. 34/a, Hungary

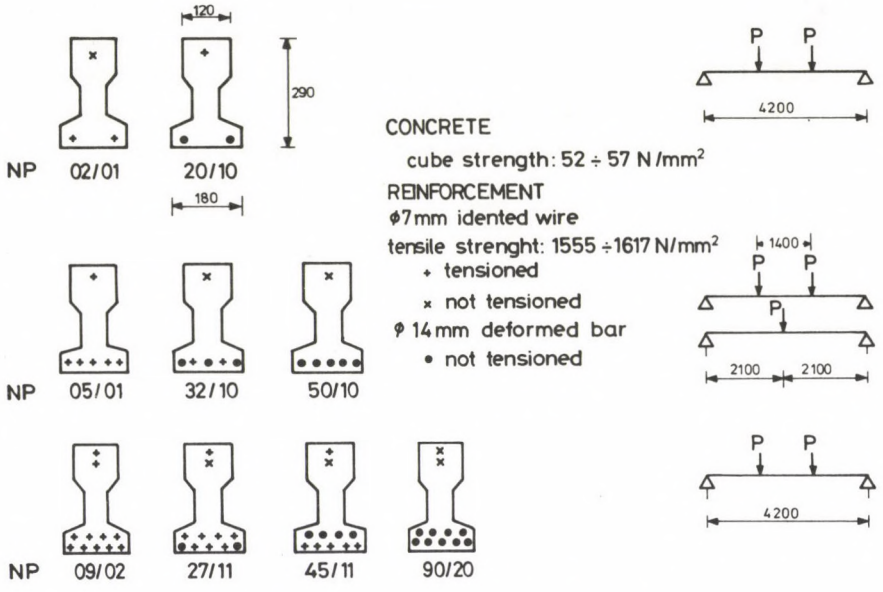

Fig. 1. Test specimens and arrangement of loading

The beams represented 3 levels of load carrying capacity with 9 types of reinforcements. The reinforcement ratio varied between $p=0.24$ and $p=4.5\%$. The diameter of indented high-tensile wires was 7 mm and the tensile strength were between 1555 and 1617 N mm^{-2}. The diameter of the deformed bars was 14 mm and the nominal yield/tensile strength was 400/600 N mm^{-2}. Fig. 1. shows

— the measures of the crossection;
— the various arrangements of the reinforcement in the cross-section;
— the symbols of the types and
— the arrangement of loading.

Four specimen beams were manufactured of types with 2 and with 9 reinforcing members each and 3 specimen beams were manufactured of types with 5 reinforcing member each. Thus altogether 42 beams were tested.

The beams were first loaded till their service moment. In case of prestressed beams this moment was above their cracking moment. After deloading the beams were loaded up to the same level. The results of this second loading were evaluated. We measured:

— the deflections of the middle and the loaded cross-sections,
— the strain of the tensile and compression fibre with deformeters of 254 mm basis length on the 1400 mm long middle portion of the beams,
— the maximum crack width
— the number of cracks and their distribution at the design load level.

The load reached its maximum value roughly in two hours.

The stress/strain diagrams of reinforcing members were linear in the region of interest. The variance of the concrete strength did not show a difference at 5% significance level, according to the Bartlet's test. The effective prestressing force was calculated from the secondary cracking moment. These calculations were made on the basis of the moment/deflection and moment/tensile strain diagrams. The evaluation shows, that the moment/deflection diagrams announce retardatively the appearence of the first crack. So the decompression moment must be verified from the data of the moment/tensile strain diagrams. These values were used for the calculation of the deflection.

The differences in the values and in the variances of the prestressing force were higher than was expected. According to data of the 28 prestressed beams the average prestressing force was 72% of the calculated one and the normalized range of scatter was between 0.34–1.39. The beams prestressed with two wires show higher variances than the beams prestressed with five or more wires. In the group of beams prestressed with 2 wires the average value of the prestressing force was 61% of the calculated one, and the normalized scatter was between 0.34–1.39. The same issue appeared in the group of 18 beams with five of more prestressed wires, was 79% and 0.58–1.11, respectively. This shows that the uncertainties are higher in case of a small prestressing force. The reason of this is that the prestressing device is designed for 10 wires, and the relative deviation in case of two wires is higher than in case of 5–10 wires. This problem is not as important in the practice as the numbers show, namely, the beams prestressed with two wires were made only for the test programme and the low value of effective prestressing force did not reduce the ultimate load carrying capacity of the beams.

Figures 2 and 3 show the measured and the calculated deflections of the beams with two point loading. The darkened fields represent the regions of measured deflections. All diagrams show the possible extremities of deflections. These are calculated from the rigidity of the homogeneous (stage I) and of the cracked (stage II) crossection, respectively. The diagrams show that the deflections calculated according to various fomulae and on the basis of the measured effective prestressing force are higher than the measured ones.

The differences in the calculated and measured deflections are considerably less in case of non-prestressed beams than in case of prestressed ones. The values of the formers practically do not differ, but in case of prestressed beams the differences considerably depend on the prescriptions. The values calculated according to the CEB-FIP recommendations are the closest to the measured ones.

Figure 4 represents the deflections of the one point loaded beams, and for comparison in the same scale the deflections are given of similar beams loaded with two forces. The evaluation of the diagrams shows that the difference of the calculated and measured values is higher in case of one point loading. The reason of this is that the used formulae are based on the rigidity of the cracked cross-section and on the moment diagram of equally distributed load. Thus, the model of calculation and of test differs more in case of a one point loading.

To investigate the average rigidity of the sectionally cracked beam first the reliance of the average strain in the tension fibre was evaluated. The CEB-FIP recommandations contain such data. Figure 5 shows the results. The data of this evaluation can be divided into two groups. The first group includes data of beams reinforced only with prestressing wires (marked with x).—The second group includes data of beams where the reinforcement contains deformed bars independently of whether these bars were combined with prestressing wires or not. The deviations in the first group are considerably higher than in the second one. The values of the second group are very similar to the range of the CEB-FIP recommendations. The reason for this is that the surface of deformed bars and an indented wire differs considerably. In the presence of deformed bars, the distribution of the cracks is more equal.

In the second step we compared the measured average crack distance depending on the ratio of the average tensile strain to the calculated maximum steel strain. (All

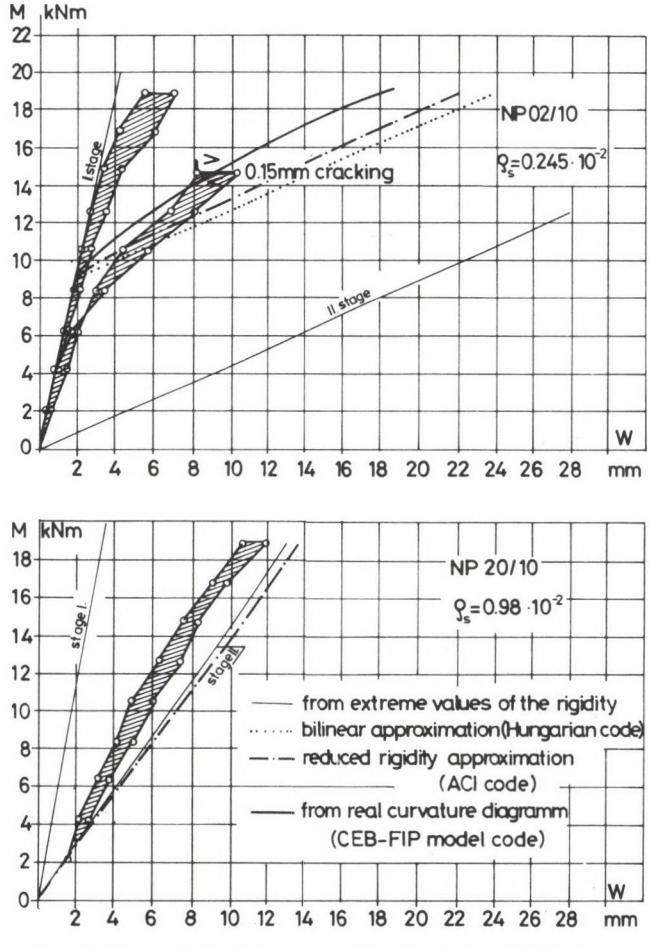

Fig. 2. Comparison of the measured and calculated deflection

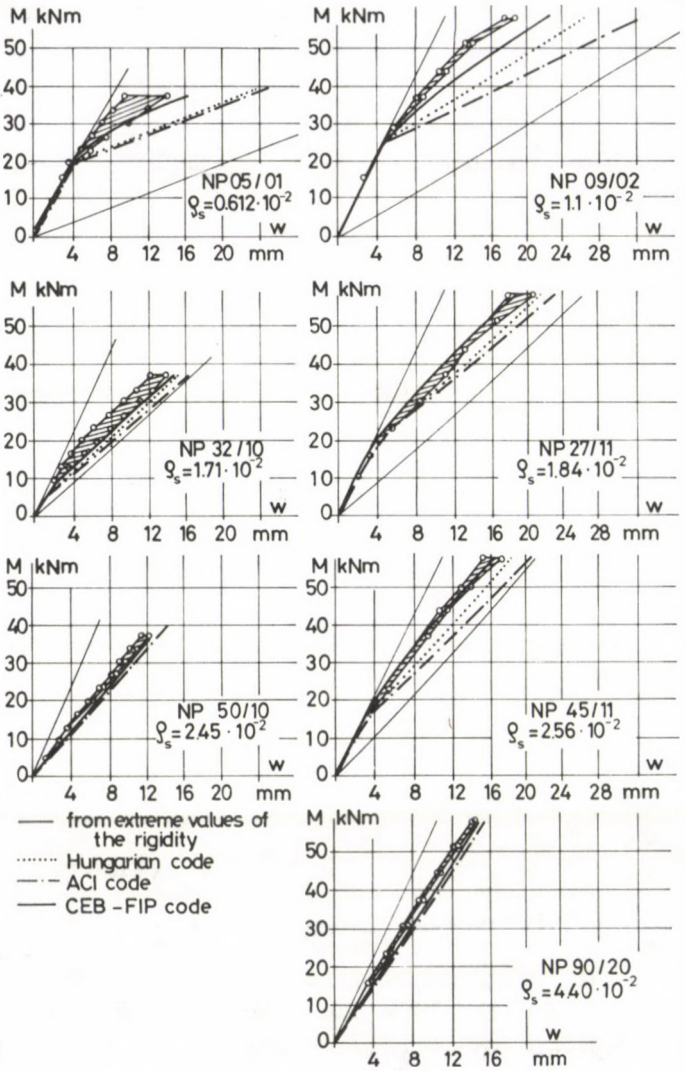

Fig. 3. Measured and calculated deflection

values correspond to the maximum working moment and to the middle part of the beam loaded with constant bending moment.) Figure 6 gives the result of this comparision. The linear interdependence is a good approximation. It is remarkable that the regression line does not intersect the $\varepsilon_{sa}/\varepsilon_{s\,max}$ axis at the unity. The reason of this can be that at the edges of the cracks slips or movements occur between concrete and the embedded reinforcement. The slip length is 52 mm. That means, that if the crack distance does not exceed 52 mm, the concrete block between the cracks does not

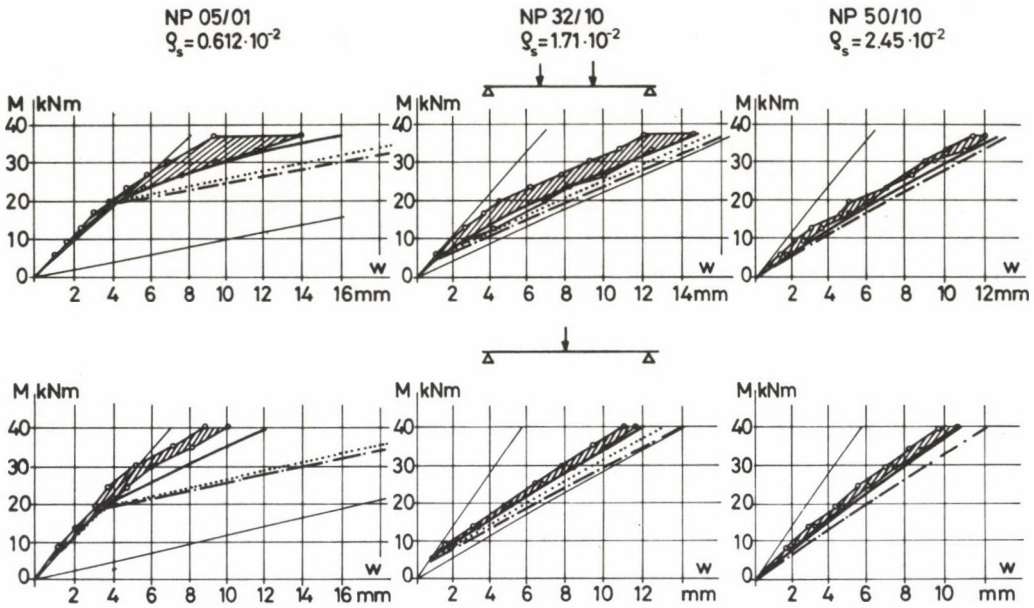

Fig. 4. Comparison of the measured and calculated deflection by one and two point loading

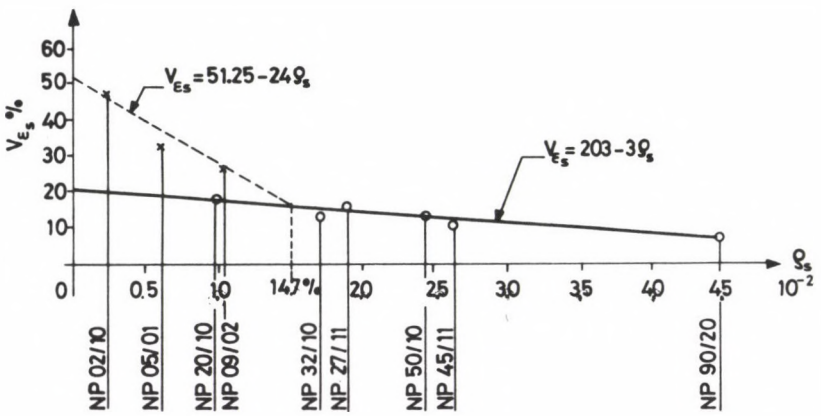

Fig. 5. Relationship of coefficient of variation in measured tension strain and reinforcement ratio

increase the rigidity of the beam, consequently in such cases the rigidity calculated from the cracked cross-section rules the phenomena of the deflection.

In the third step we investigated the possibility of calculating the average crack distance. The CEB-FIP recommendations assume a knowledge of the average crack distance. The litterature seldom deals with the calculation of the average crack distance, but it deals for more with the maximum distance for the calculation of the

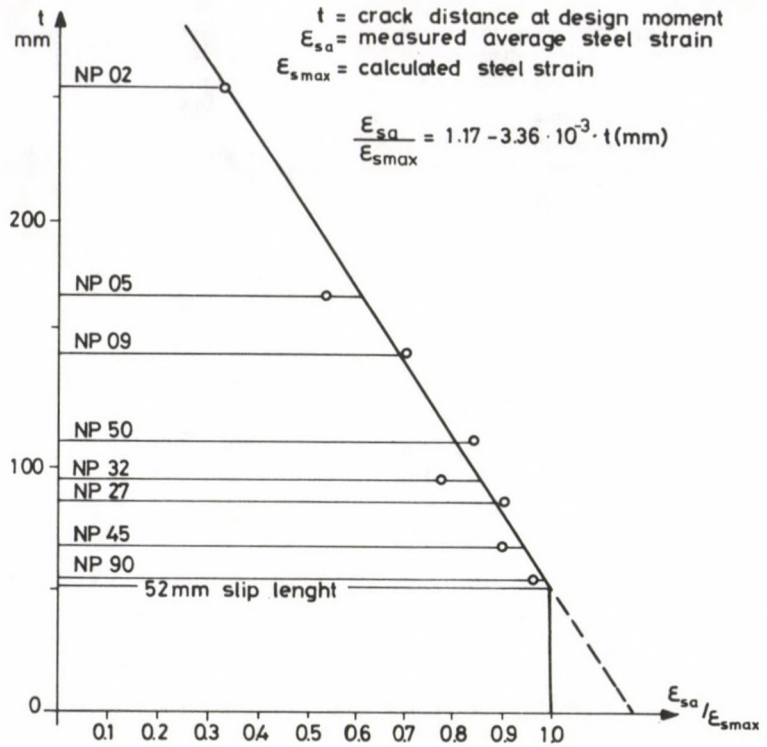

Fig. 6. Relationship of average crack distance and steel strain ratio

maximum crack width. The question was whether the formula of the maximum crack distance can be adapted for the calculation of the average crack distance. For this reason we reduced the measured average crack distances of the beams with the quotient of the reinforcement ratio to the average diameter of the reinforcement. The basis of this reduction was the well-known formula of the maximum crack distance in the tensioned reinforced concrete bar which was established by Saliger. This reduction did not bring the expected result. As the upper diagram of Fig. 7. shows, the scatter of these values was very large. The evaluation of the results shows that the reduced values form groups according to the number of the reinforcing members, and the average values of these groups decrease with the increasing number of the reinforcing members. The decrease is not linear.—Looking for physical reasons of this finding we came to the conclusion that the cracking should be handled as a stochastic process. In case of a tension bar reinforced with one single member the cracks will develop, probably at about the possible maximum distance. Increasing the number of the reinforcing members, each member can initiate cracks by chance, and the probability of a coincidence in the cracks is small. The cracks are going through the embedding concrete, so it is evident that the more reinforcing members are embedded in the

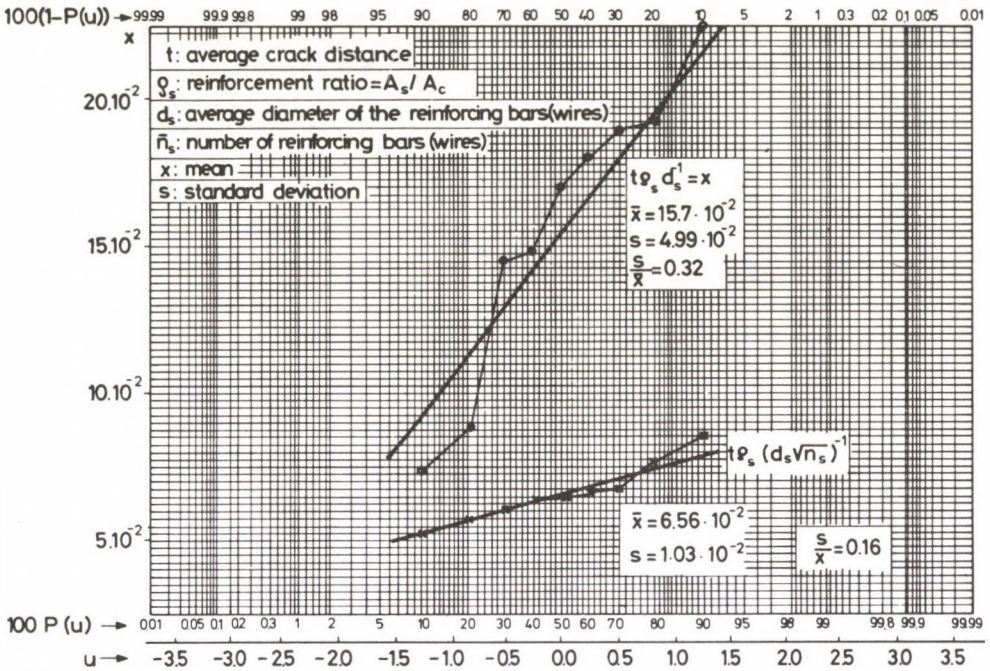

Fig. 7. Statistical analysis of the reduced crack distances (each point represents the mean crack distance measured on one type of specimens)

tensioned bar, the closer will the cracks in the bar occur. Consequently the average crack distance will depend on the number of the reinforcing members. According to this consideration it was obvious that with good probability the well-known rule for the average quadratic distance can be used for the demonstration of the average crack distance. Accordingly, we reduced the formerely mentioned values with the square root of the number of the reinforcing members. The result of this reduction was, that all data gathered around one average value within an acceptable scatter (characteristic for concrete). The lower diagram of Fig. 7. shows the result.

Only this one experiment cannot satisfactorily support the generalization of the explained assumption, but this is a good opportunity to turn the attention to the stochastic character of the process of the cracking. The described model can be used for the evaluation of other experiments. This mentality gives new aspects for the calculation of the maximum crack width, namely, instead of the possible maximum crack width the width occuring with a prescribed small probability can be the basic assumption for the crack-width analysis.

3. Conclusion

The experiments show that:

3.1. The technological circumstances determine the scatter of the effective prestressing force.

3.2. The value of the effective prestressing force also depends on the technological circumstances. In our case this was about 80% of the calculated one, so the losses are higher than was calculated.

3.3. The lower value of the prestressing force did not influence the ultimate strength of the beams, but it considerably influenced the calculation of deflection and crack width.

3.4. The investigated formulae err in favour of safety (see Figs 2 and 3), if the real prestressing force is taken into account. The magnitude of the error depends on the shape of the moment diagram, too (see Fig. 4). Exception is the CEB-FIP recommendation, which does not give formulae but prescribes a correct model for the calculation. The reliance of this calculation depends on the scatter caused by the technological circumstances and on the accuracy in the estimation of the average crack distance.

3.5. In case of indented wire reinforcement the coefficient of variation which characterize the uncertainity of the calculation, in our case was considerably higher, than given in the CEB-FIP recommendations (Fig. 5).

3.6. On the calculation of the average strain of the tension fibre—even in case of a short time loading—one has to calculate with the slip (movement) of one part of the embedded reinforcement. According to our experiment this was independent of the diameter and surface property of the reinforcement. Thus, probably this is determined only by the strain increase of the reinforcement which occurs because of the loading (Fig. 6).

3.7. The average crack distance in the tension fibre depends on the reinforcement ratio, on the average diameter of the reinforcement, and in addition on the number of the reinforcing members, too. The average crack distance decreases proportionally with the square root of the number of the reinforcing members following the rules of stochastic processes.

4. Acknowledgement

The authors express their thanks to the Hungarian Concrete and Reinforced Concrete Works (BVM) for the technical and financial support of the experiments.

References

1. Saliger, R.: Stahlbetonbau. Deuticke Verlag, Wien, 1949
2. Myrlea, T. D.: Deflection of reinforced concrete members. Progress Report of ACI Committee 307, ACI Journal, Proceedings, V. 27 (1931), 351

3. Deflection of Reinforced Concrete Flexural Members. – ACI Committee 435, ACI Journal Proceedings, V. 63, No. 6, June 1966, 637–674
4. Beeby, A. W., Taylor, H. P. J.: Cracking in Partially Prestressed Members.—Paper presented at the Sixth International Congress of the FIP, Prague 1970
5. Deák, Gy., Tassi, G.: Estimation of deformations of prestressed concrete beams. Paper presented at the Eighth International Congress of the FIP, London 1978 (Manuscript)
6. Bennett, E. W., Veerasubramanian, N.: Behaviour of nonrectangular beams with limited prestress after flexural cracking. ACI Journal, Proceedings V. 69, No. 9, September (1972), 533–542
7. Branson, D. E.: Design procedures for computing deflections ACI Journal, Proceedings V. 65, No. 9, September (1968), 730–742
8. MSz 15022/2–72. Építmények teherhordó szerkezeteinek erőtani tervezése. Feszített vasbeton szerkezetek
9. International recommendations for the design and construction of concrete structures. CEB-FIP Bulletins No. 5 117 and 120, Paris 1977
10. Building Code Requirements for Reinforced Concrete. ACI Committee 318–63, Ditroit. American Concrete Instutite, 1963
11. Deflection of Reinforced Concrete Members. Bulletin ST-70. London. Portland Cement Association, 1947
12. Building Code Requirements for Reinforced Concrete. ACI Committee 318, Ditroit. American Concrete Institute, 1971
13. Albandar, F. A., Mills, F. M.: The prediction of crack widths in reinforced concrete beams. Magazine of Concrete Research V. 26, No. 88, September (1974), 153–160
14. Beeby, A. W.: A note on an aspect of the variability of deflections. Magazine of Concrete Research V. 26. No. 88, September (1974), 161–168
15. Broms, B. B.: Crack width and crack spacing in reinforced concrete members. ACI Journal, Proceedings V. 62. No. 10, October (1965) 1237–1256
16. Nawy, E. G.: Control of flexural cracking in reinforced concrete. ACI Journal. December (1972) 728–732
17. Jabou, S. D.: Short time deflection of partially prestressed flexural concrete beams under serviceability load conditions. Thesis, Budapest 1979

IN MEMORIAM S. D. JABOU

Died 1982. The war in the Middle East deprived science of a talented man and our country of a true friend.

BOOK REVIEW

L. IMRE: *Hőátvitel összetett szerkezetekben* (Heat Transfer in Composite Devices) Akadémiai Kiadó, Budapest 1983. pp. 689.

In the monograph written in Hungarian the author deals with the physico-mathematical modelling of the thermal processes taking place in combined constructions, as in machines and equipment assembled of different parts, as well as with the methods for solving mathematical problems, in connection with the subject in question. In a part of complex constructions, as a condition or a result of their operation, sources of heat arise. The external or internal heat sources might have the most different origins (internal heating, losses transformed into heat in the course of different processes, heat introduced with streaming fluids, etc.). The heat streams of heat sources bring about, either directly or indirectly, calefaction of parts in the construction. The structural units are in thermal interaction both with each other and with the surrounding of the construction. The knowledge of the temperature field developed, is in most cases significant from the point of view of two circumstances: either the unfavourable heating should be circumvented or, precisely the distribution of the temperature needed to produce favourable working conditions should be realized. Earlier, the evaluation by calculation of the temperature fields developed in the complex constructions could only be carried out, mainly with the help of empirical relationships, applying rough neglects, resulting in heavy uncertainties. Although the analytic solution of the differential equation of the heat conduction to homogeneous solids, in linear cases and under well defined boundary conditions has been known for a long time, nevertheless, the structural units of the combined constructions are in most cases of irregular form, frequently non-linear couplings occur; the temperature dependence of the structural parts cannot always be neglected, nor the boundary conditions developed as a result of the thermal interaction of the structural parts can in advance be clarified. Therefore, due to the thermal interaction of the structural elements the determination of the temperature fields of the structural parts with appropriate exactness, their separation from each other and detachment from their thermal connections is, so to say, hardly realizable.

It seems to be particularly difficult to resolve problems in connection with which the thermal conditions of the construction are determined by several transport processes being in close interaction with each other and, therefore, the simultaneous consideration of all these processes is necessary. Complex constructions should be simulated and described as thermal systems.

The monography helps research and designing engineers engaged in studying complex heat engineering problems, in constructing physical and mathematical models, as well as in university and high-school education of engineers by presenting new, effective procedures. Starting from the basic knowledge acquired by university studies, the author treats the theory of heat transfer, the theoretical bases of the heat flow network modelling methods, the methods of finite differences and finite element analysis, by presenting simple examples of application, and reviews the basic mathematical knowledge needed for practical applications.

Since the computerization of the established mathematical model may be realized in several ways, the book does not deal with these details because of its restricted size, however, it gives several references to the professional literature to be used in connection with the subject matter treated in this book.

With this comprehensive monograph the reader engaged in resolving intricate thermal problems, receives an excellent aid to his work.

PRINTED IN HUNGARY

Akadémiai Kiadó és Nyomda, Budapest

NOTICE TO CONTRIBUTORS

Papers in English* are accepted to the condition that they have not been previously published or accepted for publication.

Manuscripts in two copies (the original type-written copy plus a clear duplicate one) complete with figures, tables, and references should be sent to the

Acta Technica
Münnich F. u. 7. I. 111A
Budapest, Hungary
H-1051

Although every effort will be made to guard against loss, it is advised that authors retain copies of all material which they submit. The editorial board reserves the right to make editorial changes.

Manuscripts should be typed double-spaced on one side of good quality paper with proper margins and bear the title of the paper and the name(s) of the author(s). The full postal address(es) of the author(s) should be given in a footnote on the first page. An abstract of 50 to 100 words should precede the text of the paper. The paper should not exceed 25 pages including tables and references. The approximate locations of the tables and figures should be indicated on the margin. An additional copy of the abstract is needed. Russian words and names should be transliterated into English.

References. Only papers closely related to the author's work should be referred to. The citations should include the name of the author and/or the reference number in brackets. A list of numbered references should follow the end of the manuscript.

References to periodicals should mention: (1) name(s) and initials of the author(s); (2) title of the paper; (3) name of the periodical; (4) volume; (5) year of publication in parentheses; (6) number of the first page. Thus: 5. Winokur, A., Gluck, J.: Ultimate strength analysis of coupled shear walls. American Concrete Institute Journal 65 (1968), 1029.

References to books should include: (1) author(s) name; (2) title; (3) publisher; (4) place and year of publication. Thus: Timoshenko, S., Gere, J.: Theory of Elastic Stability. McGraw-Hill Company, New York, London 1961.

Illustrations should be selected carefully and only up to the necessary quantity. Black-and-white photographs should be in the form of glossy prints. The author's name and the title of the paper together with the serial number of the figure should be written on the back of each print. Legends should be brief and attached on a separate sheet. Tables, each bearing a title, should be self-explanatory and numbered consecutively.

Authors will receive proofs must be sent back by return mail.

Authors are entitled to 50 reprints free of charge.

* Hungarian authors should submit their papers also in Hungarian.

Periodicals of the Hungarian Academy of Sciences are obtainable at the following addresses:

AUSTRALIA
C.B.D. LIBRARY AND SUBSCRIPTION SERVICE
Box 4886, G.P.O., *Sydney N.S.W. 2001*
COSMOS BOOKSHOP, 145 Ackland Street
St. Kilda (Melbourne), Victiria 3182

AUSTRIA
GLOBUS,Höchstädtplatz 3, *1206 Wien XX*

BELGIUM
OFFICE INTERNATIONAL DE LIBRAIRIE
30 A venue Marnix, *1050 Bruxelles*
LIBRAIRIE DU MONDE ENTIER
162 rue du Mindi, *1000 Bruxelles*

BULGARIA
HEMUS, Bulvar Ruszki 6, *Sofia*

CANADA
PANNONIA BOOKS, P.O. Box 1017
Postal Station "B", *Toronto, Ontario M5T 2T8*

CHINA
CNPICOR, Periodical Department, P.O. Box 50
Peking

CZECHOSLOVAKIA
MAD'ARSKÁ KULTURA, Národní třida 22
115. 66 Praha
PNS DOVOZ TISKU, Vinohradská 46, *Praha 2*
PNS DOVOZ TLAČE, *Bratislava 2*

DENMARK
EJNAR MUNKSGAARD, Norregade 6
1165 Copenhagen K

FEDERAL REPUBLIC OF GERMANY
KUNST UND WISSEN ERICH BIEBER
Postfach 46, *7000 Stuttgart 1*

FINLAND
AKATEEMINEN KIRJAKAUPPA, P.O. Box 128 *SF-00101 Helsinki 10*

FRANCE
DAWSON-FRANCE S. A., P. 40, *91121 Palaiseau*
EUROPÉRIODIQUES S. A., 31 Avenue de Versailles, *78170 La Celle St. Cloud*
OFFICE INTERNATIONAL DOCUMENTION ET
LIBRAIRIE,48 rue Gay-Lussac
75240 Paris Cedex 05

GERMAN DEMOCRATIC REPUBLIC
HAUS DER UNGARISCHEN KULTUR
Karl Liebknecht-Straße 9, *DDR-102 Berlin*
DEUTSCHE POST ZEITUNGSVERTRIEBSAMT Straße der Pariser Kommüne 3 4, *DDR-104 Berlin*

GREAT BRITAIN
BLACKWELL'S PERIODICALS DIVISION
Hythe Bridge Street, Oxford OX1 2ET
BUMPUS, HALDANE AND MAXWELL LTD.
Cowper Works, *olney, Bucks MK46 4BN*
COLLET'S HOLDINGS LTD., Denington Estate *Wellingborough, Northants NN8 2QT*
WM. DAWSON AND SONS LTD., Cannon House *Folkstote, Kent CT19 5EE*
H. K. LEWIS AND CO., 136 Gower Street
London WC1E 6BS

GREECE
KOSTARAKIS BROTHERS INTERNATIONAL
BOOKSELLERS, 2 Hippokratous Street, *Athens-143*

HOLLAND
MEULENHOFF-BRUNA B. V., Beulingstraat 2,
Amsterdam
MARTINUS NIJHOFF B.V.
Lange Voorhout 9 11, *Den Haag*
SWETS SUBSCRIPTION SERVICE
347b Heereweg, *Lisse*

INDIA
ALLIED PUBLISHING PRIVATE LTD., 13/14
Asaf Ali Road,*New Delhi 110001*
150 B-6 Monunt Road, *Madras 600002*
INTERNATIONAL BOOK HOUSE PVT. LTD.
Madame Cama Road, *Bombay 400039*
THE STATE TRADING CORPORATION OF INDIA LTD.,
Books Import Division, Chanralok 36 Janpath, *New Delhi 110001*

ITALY
INTERSCIENTIA, Via Mazzé 28, *10149 Torino*
LIBRERIA COMMISSIONARIA SANSONI, Via Lamarmora 45, *50121 Firenze*
SANTO VANASIA, Via M. Macchi 58
20124 Milano
D. E. A., Via Lima 28, *00198 Roma*

JAPAN
KINOKUNIYA BOOK-STORE CO. LTD.
17-7 Shinjuku 3 chome, Shinjuku-ku, *Tokyo 106-91*
MARUZEN COMPANY LTD., Book Department, P.O. Box 5050 Tokyo International, *Tokyo 100-31*
NAKUA LTD. IMPORT DEPARTMENT
2-30-19 Minami Ikebukuro, Toshima-ku, *Tokyo 171*

KOREA
CHULPANMUL, *Phenjan*

NORWAY
TANUM-TIDSKRIFT-SENTRALEN A.S., Karl Johansgatan *41 43, 1000 Oslo*

POLAND
WEGIERSKI INSTYTUT KULTURY, Marszalkowska 80, *00-517 warsawa*
CKP-I W, ul. Towarowa 28,*00-958 Warsawa*

ROUMANIA
D.E.P., *Bucuresti*
ILEXIM,Calea Grivitei 64-66, *Bucuresti*

SOVIET UNION
SOJUZPECHAT IMPORT, *Moscow*
and the post offices each town
MEZHDUNARODNAYA KNIGA, *Moscow G-200*

SPAIN
DIAZ DE SANTOS, Lagasca 95, *Madrid 6*

SWEDEN
GUMPERTS UNIVERSITETSBOKHANDEL AB
Box 346, *40125 Göteborg 1*

SWITTZERLAND
KARGER LIBRI AG, Petersgraben 31, *4011 Basel*

USA
EBSCO SUBSCRIPTION SERVICES
P.O. Box 1943, *Birmingham, Alabama 35201*
F.W. FAXON COMPANY, INC.
15 Soutwest Park, *Westwood Mass. 02090*
READ-MORE PUBLICATIONS, INC.
140 Cedar Street, *New York,N.Y. 10006*

YUGOSLAVIA
JUGOSLOVENSKA KNJIGA,Terazije 27, *Beograd*
FORUM,Vojvode Mišića 1, *21000 Novi Sad*

HU ISSN 0001-7035 Index: 26.025